UNIVERSITY OF SOUTHAMPTON

FACULTY OF NATURAL AND ENVIRONMENTAL SCIENCES

Ocean and Earth Sciences

Volume 1 of 1

Unravelling high frequency and sub-seasonal variability at key ocean circulation 'choke' points: a case study from glider monitoring in the Western Mediterranean Sea

by

Emma Heslop

Thesis for the degree of Doctor of Philosophy

February 2015

UNIVERSITY OF SOUTHAMPTON

ABSTRACT

FACULTY OF NATURAL AND ENVIRONMENTAL SCIENCES

Ocean and Earth Sciences

Doctor of Philosophy

UNRAVELLING HIGH FREQUENCY AND SUB-SEASONAL VARIABILITY AT KEY OCEAN CIRCULATION 'CHOKE' POINTS: A CASE STUDY FROM GLIDER MONITORING IN THE WESTERN MEDITERRANEAN SEA

By Emma Elizabeth Heslop

A quiet revolution is taking place in ocean observations: in the last decade new multi-platform ocean observatories have been progressively implemented in forward looking countries with ocean borders of economic and strategic importance. These developments are designed to fill significant gaps in our knowledge of ocean state and ocean variability through long-term science and society led monitoring. These new ocean observatories are now delivering results, not only the headline results of single issue experiments, but careful and systematic improvements in our knowledge of ocean variability, and thereby, increasing ocean forecast skill, the ability to link physical process to ecosystem response and to detect the impact of future climatic change.

This PhD has used data from a recently initiated glider monitoring program to characterise variability in key components of the Mediterranean circulation that act through the Ibiza Channel. The Ibiza Channel is a key 'choke' point in the Mediterranean basin scale circulation and governs an important north/south exchange of different water mass that is known to impact regional ecosystems, in a zone of high biodiversity. The quasi-continuous glider sampling at this critical location has enabled important sub-seasonal to seasonal variability to be captured, and models to be developed to characterise the previously described 'complex' pattern of exchange. For the first time, glider monitoring revealed high frequency variability in the transport of water mass, of the same magnitude as the previously characterised seasonal cycle, but occurring over timescales of days to weeks. Although previous ship surveys had noted high cruise-to-cruise variability, they were insufficient to show that in fact water volumes exchanged through the Ibiza Channel vary on 'weather' timescales. Using the glider data in combination with an 18-year record of ship missions, long-term seasonal cycles in the north/south exchange were characterised. New month-by-month patterns were defined for the southward transport, while generally held views regarding the seasonality of the northward transport were revised. The pattern of the exchange was further characterised by 4 proposed seasonal 'modes', which reflect an annual interplay between vigorous mesoscale and basin scale dynamics.

Restricted 'choke' points between our ocean basins are critical locations to monitor water transport variability, as they constrain the inter-basin exchange of heat, salt and nutrients. The Ibiza Channel is one such location. In addition to characterising key components of the regional circulation, this PhD also provides insight into use of glider monitoring at such critical locations, which can be used to inform multi-platform ocean observation strategy. This study is part of the quiet revolution.

Table of Contents

List of tables

List of figures

DECLARATION OF AUTHORSHIP

I, Emma Heslop

declare that this thesis and the work presented in it are my own and has been generated by me as the result of my own original research.

Unravelling high frequency and sub-seasonal variability at key ocean circulation 'choke' points: a case study from glider monitoring in the Western Mediterranean Sea

I confirm that:

1. This work was done wholly or mainly while in candidature for a research degree at this University;
2. Where any part of this thesis has previously been submitted for a degree or any other qualification at this University or any other institution, this has been clearly stated;
3. Where I have consulted the published work of others, this is always clearly attributed;
4. Where I have quoted from the work of others, the source is always given. With the exception of such quotations, this thesis is entirely my own work;
5. I have acknowledged all main sources of help;
6. Where the thesis is based on work done by myself jointly with others, I have made clear exactly what was done by others and what I have contributed myself;
7. Part of this work has been published as:
   Heslop, E. E., S. Ruiz, J. Allen, J. L. López-Jurado, L. Renault, and J. Tintoré (2012), Autonomous underwater gliders monitoring variability at "choke points" in our ocean system: A case study in the Western Mediterranean Sea. Geophys. Res. Lett., 39, L20604.

Signed: 

Date: 01/02/2015

Acknowledgements

This research was partially funded by the European Union FP7 Projects, MyOcean, PERSEUS and JERICO. The glider data were collected under a monitoring program operated by ICTS SOCIB (Balearic Islands Coastal Ocean Observing and Forecast System) with in-kind support from IMEDEA (Instituto Mediterráneo de Estudios Avanzados , CSIC-UIB). Ship-based CTD data were provided by IEO (Instituto Español de Oceanografía), the Catholic University of Valencia and SOCIB. The SST data from GRHSST (Group for High-Resolution Sea Surface Temperature), were made available by IFREMER (L'Institut Français de Recherche pour l'Exploitation de la Mer) under the MyOcean Project. The SRTM30Plus data set is freely available from several sources, e.g. ftp://topex.ucsd.edu/pub/srtm30_plus/srtm30/data/

A big thank you is extended to my supervisors for their advice during my research. This is a significant commitment and I am grateful to Prof. Harry Bryden, Dr. Simón Ruiz, Dr. John Allen and Prof. Joaquín Tintoré for all their support.

The 'canales' glider missions completed during the timeframe of this PhD already represent an important regional oceanographic record, which is a credit to the SOCIB team, in particular our main glider operator Mr. Marc Torner, the ETD Field Team and the Data Centre. I would also like to thank IEO-COB, in particular José Luis López-Jurado, who provided access to the IEO's ship data.

This thesis is dedicated to my great friend Peter Wilson (1968 – 2013).

Definitions and Abbreviations

ADCP	Acoustic Doppler Current Profiler
AMOC	Atlantic Meridional Overturning Circulation
AW	Atlantic Water
AWo	Atlantic Water old - of longer residence in the Mediterranean
AWr	Atlantic Water recent - of more recent Atlantic origin
BALOP	BALearic OPerational Forecasting System
BC	Balearic Current
CTD	Conductivity Temperature Depth
CSIC	Consejo Superior de Investigaciones Científicas
DWF	Deep Water Formation
EGO	Everyone's Glider Observatory
EKE	Eddy Kinetic Energy
EMT	Eastern Mediterranean Transit
EOF	Eigen Orthogonal Functions
GHRSST	Group for High-Resolution Sea Surface Temperature
GROOM	Gliders for Research Ocean Observation and Management
IC	Ibiza Channel
IEO-COB	Instituto Español de Oceanografía - Centre Oceanogràfic de Balears
IFREMER	L'Institut Français de Recherche pour l'Exploitation de la Mer
IMEDEA	Instituto Mediterráneo de Estudios Avanzados
JERICO	Joint European Research Infrastructure network for Coastal Observatories
LIW	Levantine Intermediate Water
MC	Mallorca Channel
NAO	North Atlantic Oscillation
NC	Northern Current
PERSEUS	Policy-oriented marine Environmental Research for the Southern European Seas
ROMS	Regional Ocean Modelling System
SOCIB	Sistema d'observació i predicció costaner de les Illes Balears
SST	Sea Surface Temperature
UIB	Universidad de las Islas Baleares
WIW	Western Mediterranean Intermediate Water
WMDW	Western Mediterranean Deep Water

CHAPTER 1: Introduction

1.1 Variability in ocean circulation

Characterising variability in ocean circulation, at a variety of temporal and spatial scales, is a current key hot topic and oceanographic challenge, in the Mediterranean and in the global ocean (Bryden et al. 2012, Malanotte-Rizzoli et al. 2013).

The RAPID array[1], a mooring array extending across the North Atlantic Ocean at 26.5°N which has been monitoring the Atlantic Meridional Overturning Circulation (AMOC) since 2004, observed only recently a 30% drop in the average strength of this overturning circulation (McCarthy et al. 2012). The AMOC is responsible for transporting over a million gigawatts of heat north from the tropics, primarily in the Gulf Stream, and cooler waters south, at depth, in the Deep Western Boundary Current, thus any significant change in the AMOC water volume transport will have a profound effect on heat distribution in the Atlantic Ocean (Bryden et al. 2005, McCarthy et al. 2012, Bryden at al. 2014). Prior to the RAPID array observations, ocean models did not exhibit such high variability in AMOC strength, variability that influences the seasonal weather pattern across northwestern Europe and the intensity of the hurricane season (Bryden at al. 2014). This anomaly lasted over a year and has indicated significant gaps in our understanding of the drivers and variability of a fundamental component of the global ocean circulation and heat distribution system (Hall and Bryden 1982, Rahmstorf 2003, Bryden et al. 2014). Both weather and ocean models have yet to integrate the full impact of this event (Bryden at al. 2012). In addition to this headline observation, the RAPID array has identified seasonal signals in the transport associated with the various components of the AMOC, enabling interannual trends to be seasonally adjusted, sparse historical observations to be placed in context (Cunningham et al. 2007, Meinen et al. 2010) and now a long-term decline in AMOC strength to be detected (Smeed et al. 2014).

[1] For more information visit http://www.rapid.ac.uk/rapidmoc/

Without careful long-term observations of ocean circulation the detection of future climatic change, including both natural oscillations and that brought about by human-induced changes in atmospheric composition, will be difficult (Delaney and Barga 2010), the modelling of our ocean/atmosphere climate system simplistic (Mote et al. 2011), and our seasonal weather forecasts lacking an important ocean based component (Bryden et al. 2014). In fact, since the detection of the 2009 - 2010 anomaly two additional AMOC monitoring arrays have been proposed (Nature News May 2013), and are now in operation (Nature News May 2014).

Such changes in circulation are not limited to the Atlantic. The Mediterranean Sea can also be considered a small-scale global ocean (Malanotte-Rizzoli et al. 2013), with areas of active deep water formation, driving a basin scale cyclonic thermohaline circulation that is sensitive to changes in atmospheric modes (Josey et al. 2011, Schröeder et al. 2013), and modulated by vigorous mesoscale activity, complex topography and extreme atmospheric events (Tintoré et al. 1991, Tintoré et al. 1990, Mertens and Schott 1998, Vargas et al. 2012). Twenty years ago the Mediterranean was viewed as a stable environment, however an abrupt shift in sites of deep water formation in the Eastern Mediterranean (after 1988, termed the Eastern Mediterranean Transit, Theocharis et al. 1992, 2002), followed by the production of new and significantly warmer saltier and deep water in the Western Mediterranean (from 2005, termed the Western Mediterranean Transit, López-Jurado et al. 2005, Smith et al. 2007, Shröeder et al. 2010), indicated that the Mediterranean is a region of active change, sensitive to atmospheric and anthropogenic changes (Rohling and Bryden 1992, Josey 2003, Josey et al. 2011). Observations here have relevance to our understanding how the global ocean circulation functions. The Western Mediterranean Transit (WMT) has been linked to the Eastern Mediterranean Transit (EMT), through hydrographic change (Shröeder et al. 2010), further illustrating that variability in the ocean interacts across a range of temporal and spatial scales, and is not simply affected by atmospheric forcing (Bryden et al. 2014). Careful and systematic observations are required in order to unravel these interactions.

Variations in the strength of ocean currents not only affect the transport of heat and salt, but also influence the distribution of biological nutrients and marine organisms. Ocean circulation patterns are one of the base building blocks defining the extent and connection between bio domains (Rossi et al. 2013) and are fundamental to ecosystem variability (Ruiz

et al. 2013, Reglero et al. 2013, Micheli et al. 2013). Physical processes still need to be defined at many key locations in the ocean system at temporal scales of days-weeks in order to better understand ocean variability and to better constrain our modelling of physical and biogeochemical processes (Sun and Frank 2010, Bryden et al. 2012). This is particularly important in areas of high biodiversity combined with high population density and therefore high pressure on marine resources, such as the Mediterranean Sea (Bianchi & Morri 2000, Myers et al. 2000, Micheli et al. 2013).

In summary, although ocean circulation exhibits significant variability across a range of scales, this has yet to be well characterised. It is important to unravel this variability in order to enhance our model forecast skill, to link physical process to biogeochemical and ecosystem response, and for the detection of climatic change. This is particularly important for the Mediterranean, where human interaction with the marine environment is high and the circulation is sensitive to atmospheric and anthropogenic change. Observations of variability in the Mediterranean circulation system have relevance to our understanding of global ocean circulation and are key to the improved modelling and management of regional ecosystems (Ruiz et al. 2013, Reglero et al. 2013, Micheli et al. 2013).

Over the last twenty years much work has been undertaken to define mean global circulation, in programs such as WOCE and Argo. The challenge now is to characterise the underlying variability, which interacts across sub-seasonal to decadal timescales to influence this mean pattern. In this study, gliders, an emerging technology for long-term, high-resolution ocean monitoring (Testor et al. 2010), are used to quantify circulation variability across the Ibiza Channel, an important 'choke' point in the basin scale circulation of the Western Mediterranean Sea. Characterising the variability in the exchange of water mass through the Ibiza Channel will increase our understanding of the basin scale circulation, improve our regional model forecast capability, and help link ocean processes to observed biological variability. Insight gained here in the use of gliders and in the patterns of ocean circulation variability at 'choke' points will inform monitoring elsewhere in the global ocean.

1.2 Mediterranean Sea circulation

The Mediterranean is a semi-enclosed sea, connected to the Atlantic through the restricted Straits of Gibraltar (width 14 km, sill depth 300 m) and separated into two basins, linked through the Strait of Sicily (Astraldi et al 1999, Millot 1999, Millot and Taupier-Letage

2005), see fig. 1. The Mediterranean is an evaporation basin, warmer less saline surface waters inflow from the Atlantic through the Strait of Gibraltar (~1 Sv, Millot and Taupier-Letage 2005) and more saline waters outflow at depth. The inflows balance the energy lost to the atmosphere in the Western and Eastern Mediterranean basins through high rates of evaporation and strong winter cooling events. These drive two major circulation components, an upper layer open cyclonic circulation cell and deep thermohaline circulation cells in both the Eastern and Western basins, driven by dense water formation and analogous to those existing in the polar regions of the Atlantic, which operate and integrate with the surface water pathways (Malanotte-Rizzoli et al. 2013). This basin scale circulation is overlain by continuous and vigorous mesoscale activity that modulates the surface and intermediate flows.

The lower salinity Atlantic Water (hereafter AW) inflow initially forms an intense and unstable current, the Atlantic Jet, which passes along the north coast of Algeria, spawning eddies and a pattern of sub-basin gyres, of the order of 100 – 200 km in diameter (Font et al. 1988a, Renault et al. 2012, Malanotte-Rizzoli et al. 2013), see fig. 1. The end of the Alboran Sea gyre pattern is marked by the Almería-Oran Front, which lies to the east of the two main gyres, the semi-permanent Western Alboran gyre and the intermittent Eastern Alboran gyre.

The surface AW then continues as the Algerian Current along the north coast of Africa and either follows a cyclonic path around the Eastern Mediterranean basin or branches southwest of Sicily to flow north along the coast of Italy (Millot and Taupier-Letage 2005). To the north of Corsica the two branches of the surface flows converge to form the Northern Current (hereafter NC), which then flows west, following the shelf break. The NC passes from the Ligurian Sea, through the Gulf of Lion and the Balearic Basin, before flowing out into the Algerian Basin, thus completing the surface cyclonic circulation of the Western Mediterranean (Millot and Taupier-Letage 2005), see fig. 1.

In the Eastern Mediterranean high air-sea flux exchanges in winter cause the surface AW to cool and sink to form the relatively saline Levantine Intermediate Water (hereafter LIW), which then follows the same cyclonic pathway around the Eastern and Western Mediterranean basins, below the surface AW at depths between 300 to 1000 m. LIW plays an important role as the return flow of intermediate water that finally exists through the

Strait of Gibraltar into the Atlantic (Millot 1999, Millot and Taupier-Letage 2005) and forming the open upper layer thermohaline cell (Malanotte-Rizzoli et al. 2013). The influence of this salty intermediate layer can be detected across the Atlantic and northwards into the polar region, where it could play a role in pre-conditioning before dense water formation (Candela 2001, Malanotte-Rizzoli et al. 2013).

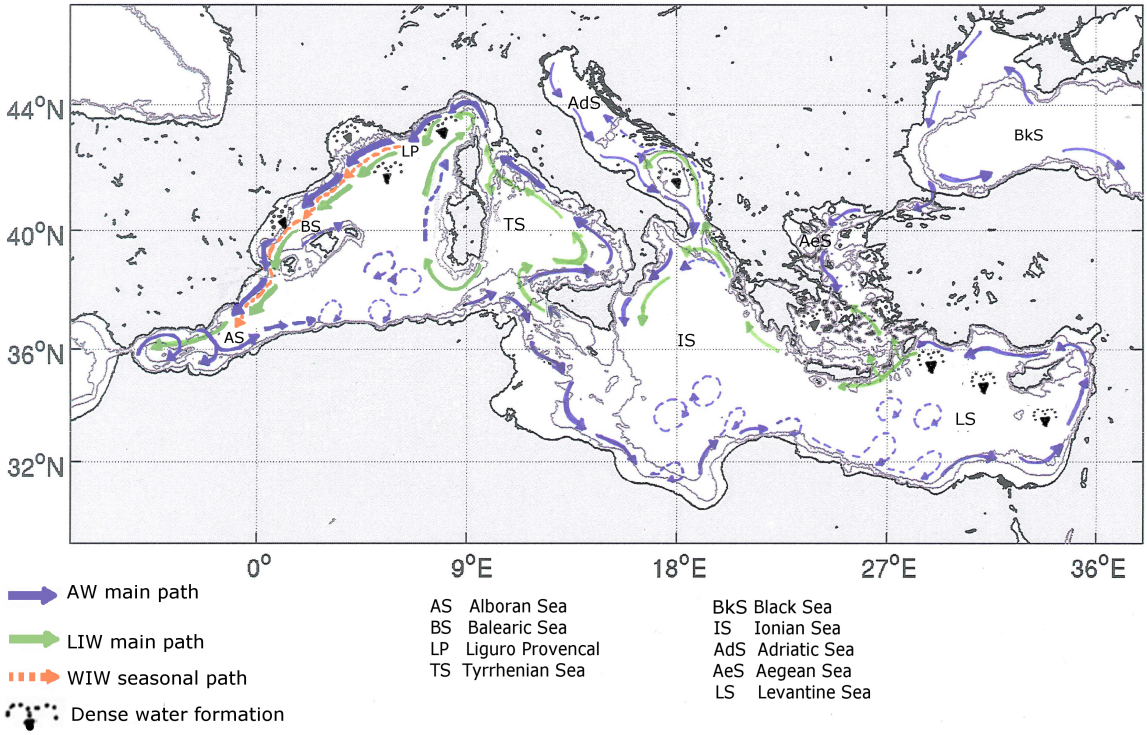

Figure 1. Mediterranean Sea general circulation, surface and intermediate waters.
The circulation path surface and intermediate waters are shown, of AW (blue), WIW (orange) and LIW (green), see inset for abbreviations and water mass characteristics, the 200 m and 1000 m isobaths are also marked (grey lines). This figure is adapted from Millot and Taupier-Letage (2005) and Poulain et al. (2012).

Notwithstanding this potential global dimension, LIW plays an important preconditioning role in deep water formation (here after DWF) in the Western Mediterranean. Western Mediterranean Deep Water (hereafter WMDW) is formed during extreme winter weather events in the Gulf of Lion where intense winter cooling causes stratification to break down, leading to deep convection (MEDOC 1970, Font et al. 1988b, Leamen and Schott, 1991, Mertens and Schott, 1998, Marshall and Schott 1999). WMDW has also been observed forming in the Ligurian Sea and northeast of Menorca (López-Jurado et al. 2005, Smith et al. 2008, Malanotte-Rizzoli et al. 2013). From these sites of formation WMDW spreads south at depths below 1000 m, its path constrained by bathymetry. Winter formation of WMDW is 'pre-conditioned' by the speeding up of the Gulf of Lion gyre (Leamen and Schott, 1991, Mertens and Schott, 1998, Marshall and Schott 1999), which

increases upward 'doming' and contributes to faster breakdown of stratification. Salty intermediate LIW is also believed to play a key role in aiding the breakdown of stratification (Shröeder et al. 2010). Western Mediterranean Intermediate Water (hereafter WIW), characteristically cold and fresh, is also formed during strong winter cooling events when fresher surface waters cool and mix to reach buoyancy equilibrium between AW and LIW. This regional winter water mass then forms a patchy temperature minimum layer that flows south with the NC at variable depths above LIW. WIW is fresher and cooler than LIW (fig. 3 and table 1) due to its formation on-shelf and/or proximity to major rivers, and has been observed cascading down shelf canyons in the Gulf of Lion and the Balearic Basin (Durrieu de Madron et al. 2005, Canals et al. 2006).

The Balearic Sea is one of the four main sub basins of the Western Mediterranean Sea, see fig. 1, all of which are governed by distinct dynamic processes (García et al. 1994, Millot 1999). Open to the north, the Balearic Sea connects to the Ligurian-Provençal region with a generally accepted northern limit of 42° 30' N. To the south and east it is bounded by the Balearic Islands, Ibiza, Mallorca and Menorca, see fig. 2. Between these islands lie the Balearic Channels, the Ibiza Channel (hereafter IC), the Mallorca Channel (hereafter MC) and the more shallow and northerly Menorca Channel. Flows between the sub-basins are significantly constrained by the narrow IC (800 m deep and 80 km wide) and to a lesser extent by the MC (600 m deep and 70 km wide). On the western side of the IC the Northern Current (NC), part of the cyclonic circulation, flows south out of the Balearic Sea, whilst on the eastern side, Atlantic Water (AW) of more recent Atlantic origin (warmer and fresher) flows in from the Algerian Sea to the south. The IC therefore plays an important role in governing a north/south exchange of different water masses and the Balearic Sea an important 'transition' zone between the different sub-basins to the north and south. To the north lies the Liguro-Provençal region, dominated by atmospheric forcing and dense water formation events, and to the south the Algerian Sea, dominated by the inflows of AW through the Strait of Gibraltar and intense mesoscale activity (García et al 1994, Millot 1999, Renault et al. 2012).

1.3 The Ibiza Channel 'choke' point

Early ship based surveys, with a relatively coarse (20 km) resolution, initially described a simple circulation pattern in the Balearic Basin; defining a wind driven basin scale cyclonic gyre with a central doming of isopycnals, similar to that found in the Gulf of Lion (Ovchinnikov 1966, Font and Miralles 1978). In the 1980's studies with a higher spatial

resolution (8 km) and undertaken using new technologies (ADCP and Neil Brown CTD) revealed a more complex system, identifying two frontal structures and their associated geostrophic fluxes (Font et al 1988, Font et al. 1988b, Salat & Font 1987, Castellón et al 1990): the Catalan Front on the continental side of the Balearic Sea, marked by a salinity gradient and following the shelf break down to 400 m with transport of 1 Sv, and the Balearic Front following the Balearic shelf break, not reaching below 300 m, with transport of 0.5 Sv and primarily defined by a temperature gradient. Satellite IR imagery confirmed the permanent existence of these two fronts (La Violette et al. 1990) and associated currents, the Northern Current (NC) and Balearic Current, and also significant mesoscale activity, with eddies, meanders and filaments during periods of stronger inflow (Font et al., 1988b, La Violette et al. 1990, Pinot et al. 1994, Lopéz Garcia et al. 1994). A splitting or branching of the NC north of the IC was noted, typically occurring during the spring/summer period and causing a reduction in flows south and a branching or re-circulation of the NC north-eastward (fig. 2), to strengthen the Balearic Current (Font 1986, Salat & Font 1987, Font 1988, López-Jurado and del Río 1994, García et al. 1994).

The Balearic Current was identified as being fed by AW inflowing through the Ibiza and Mallorca Channels (Font 1974, Font and Miralles 1978), the Balearic Front thus separating the fresher, warmer AW inflowing from Algerian Sea from the comparatively colder and more saline AW of longer residence in the Mediterranean that flowed south with the NC. In the Balearic Basin it is possible to distinguish between these two types of AW, see table 1 and fig. 3, more saline AW of longer residency in the Mediterranean, with typical surface salinities of ~37.8 (here AWo) and AW of more recent Atlantic origin, with typical surface salinities of ≤ 37.5 (here AWr). The salinity front, AWo/AWr, where these two watermasses meet has been identified as the preferred spawning location for Atlantic bluefin tuna once a temperature threshold is reached (Alemany et al. 2010, Reglero et al. 2010).

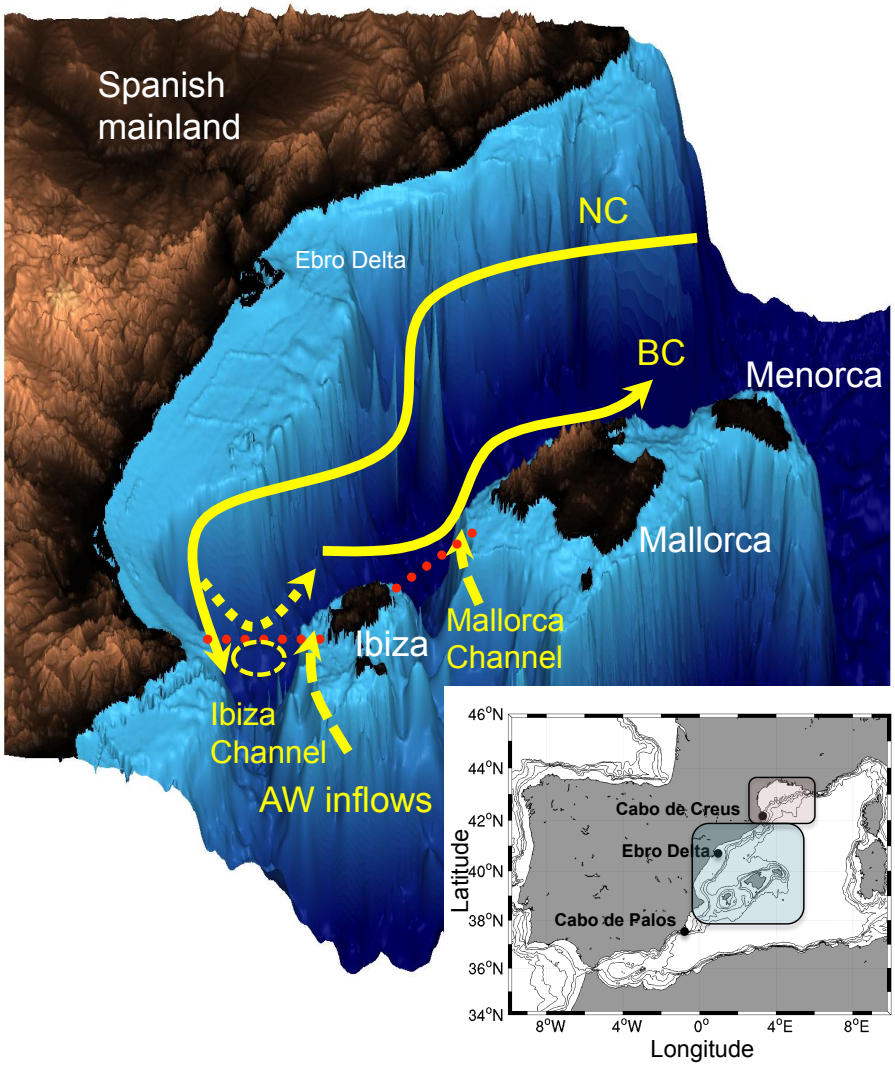

Figure 2. Balearic Sea circulation, with main currents and channels.
The Northern Current (NC), Balearic Current (BC) and AW inflows are marked, as is the intermittent re-circulation of the NC (dashed line) above an IC ' blocking' eddy (dashed circle). The Ibiza and Mallorca Channels are marked, as is the approximate location of the glider transects (red dots). The inset shows the location of the Balearic Basin (blue) and the Gulf of Lion (pink) in Western Mediterranean Sea, and coastal locations mentioned in the text. Adapted from Heslop et al. (2012).

The branching of the NC was linked to the presence of eddies in the IC that 'blocked' or impeded the NC flow, in particular to anticyclonic eddies with cores of the cold winter Western Mediterranean Intermediate Water (Millot 1991, Font 1988, López-Jurado and del Río 1994, García et al., 1994, Pinot et al., 1994), see inset for a summary of the water masses present in the Balearic Sea. A scheme with two patterns for the Balearic Basin spring/summer circulation has been proposed, relating the circulation pattern to the strength of the previous winter (Monserrat et al. 2008); in strong winters, WIW 'blocking' eddies are present in the IC in spring/summer causing a recirculating of the NC and no AW inflows, in milder winters no 'blocking' eddies form and there is a south flowing NC

with AW inflows. The IDEA index (Monserrat et al. 2008), using sea surface pressure in the Gulf of Lion as a proxy for WIW formation, has been suggested as a means of identifying the circulation pattern for years with no observations. By extension, the presence of WIW in the Balearic Channels has been used as an indicator of AWr inflows and thus the location of the AWr/AWo front, and bluefin tuna spawning grounds, north or south of the Balearic channels (Balbín et al. 2014).

Levels	Description	θ / S	Depth (m)	Abbreviation
Surface	Atlantic Water of longer residence in the Mediterranean	θ ≥ 13.0 37.5 < S < 38.35	0 to 300	**AWo**
	Atlantic Water of more recent Atlantic origin	θ ≥ 13.0 S ≤ 37.5	0 to 100	**AWr**
Intermediate	Western Mediterranean Intermediate Water, formed in the northwestern Mediterranean during intense winter cooling events	θ < 13.0 S ≤ 38.45	0 to 300	**WIW**
	Levantine Intermediate Water, formed in the Eastern Mediterranean during in winter cooling events	θ ≥ 13.0 S ≥ 38.35	300 - 1000	**LIW**
Deep	Western Mediterranean Deep Water, formed in the Gulf of Lions during extreme winter events	θ < 13.0 S > 38.45	>1000	**WMDW**

Table 1. Characteristics of water masses present in the Balearic Basin.
Water mass definitions follow Pinot and Ganachaud (1999), Pinot et al. (2002) and López-Jurado et al. (2008) and names follow the nomenclature agreed at 36th CIESM Congress, Monte Carlo, 26th Sept 2001, with a subdivision adopted by Heslop et al. (2012) to denote Atlantic Water of 'longer residency in the Mediterranean' (AWo) and Atlantic Water of 'more recent Atlantic origin' (AWr).

The Ibiza Channel is an important 'choke' point in the basin scale circulation of the Western Mediterranean Sea, which governs an inter-basin exchange of water masses that is known to affect local ecosystems of global interest, specifically the abundance and distribution of Atlantic bluefin tuna larvae (Alemany et al. 2010). It can be blocked by eddies linked to a regional winter mode water, WIW, and represents the last constricted 'choke' point in the upper layer basin scale circulation before the return flow finally exits, through the Strait of Gibraltar, into the Atlantic. In this region a complex interplay of oceanographic processes affects the circulation, an interplay that is concentrated through the Ibiza Channel. Although it has been argued that 'choke' points are not optimal locations for the study of circulation (Wunch 1992) due to the integration of signals from different basin processes, this can also be reason to study circulation at such locations, in order to unravel variability across a range of scales and with differing drivers.

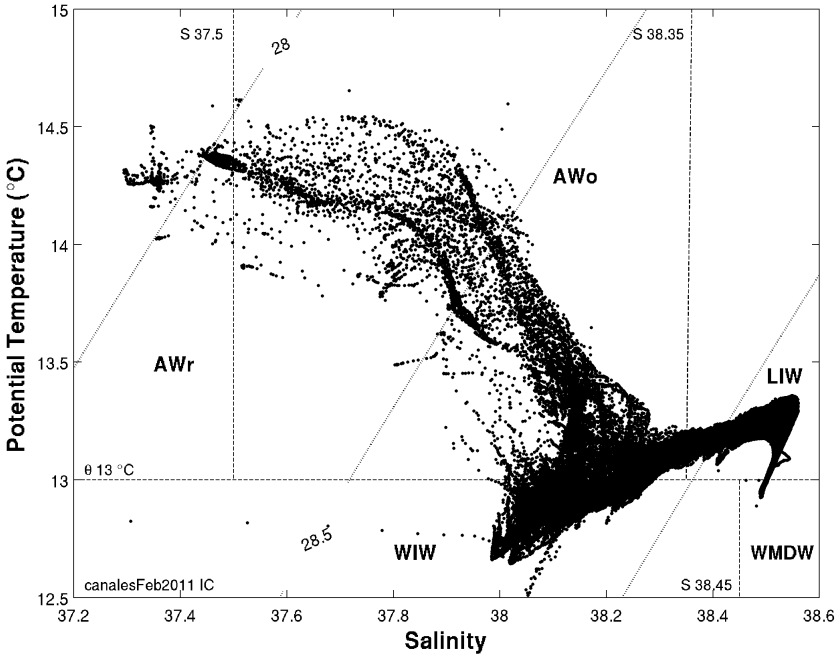

Figure 3. θ/S of key water masses present in the Balearic Basin.

This example is from glider mission canalesFeb2011, the dotted lines are potential density and the dashed lines separate four main regional water masses, also see table 1 above for details.

Summary: Water masses present in the Balearic Basin

Atlantic Water (AW) originates as a comparatively fresh inflow through the Strait of Gibraltar and becomes progressively more saline through interaction with the atmosphere (evaporation) and mixing as it follows the basin scale surface cyclonic circulation. AW therefore exhibits a range of salinities along its path, with salinities ranging from 36.5 near Gibraltar to 38.0 and 38.2 in the northwest Mediterranean (Millot 1999). In the Balearic Basin it is possible to distinguish between two types of AW, more saline AW from the north and of longer residency in the Mediterranean (here AWo) and AW of more recent Atlantic origin that inflows from the south (here AWr), see table 1. At intermediate levels lies the warm and salty Levantine Intermediate Water (LIW), typified by a sub-surface maximum in salinity and temperature and typically occupying a depth range between 200 m to 800 m. Western Mediterranean Intermediate Water (WIW) is a regional winter mode water that lies above LIW with the general characteristics $12.5 < \theta < 13$ °C and $37.9 < S < 38.3$ (Salat and Font 1987, López Jurado et al. 2008, Vargas-Yáñez et al. 2012). This cold and relatively fresh water mass is generally identified as a subsurface temperature minimum ($\theta < 13°$) and is typically visible as an uneven layer located between 50 to 200 m. Western Mediterranean Deep Water (WMDW) lies below LIW, at 1000 m and deeper, and is characterised by $\theta < 12.9°$ (Millot et al. 1999). Two other regional water masses found in the Western Mediterranean Sea, Tyrrhenian Deep Water and Eastern Mediterranean Deep Water, are generally not represented in the Balearic Basin.

1.4 Variability, current view

In the late 1990's, recognising the importance of the Balearic Channels in the regional circulation, IEO (Instituto Español de Oceanografía) undertook a 2.5 year study of the IC and MC to resolve the interannual, annual and mesoscale variability in the exchange through the channels. Called the CANALES experiment (Pinot et al. 2002), this study still stands as a benchmark today and involved ship surveys (13 in total) and moorings. The CANALES experiment identified:

- A seasonal maximum and minimum in the exchange through the IC: a winter (March) peak in southward transport of 1.4 – 1.0 Sv which coincided with weak northward transport, of order 0.2 Sv; a summer (July) maximum in northward transport, of order 0.7 Sv, with a minimum of <0.5 Sv in southward transport
- For the MC a similar but a weaker seasonal cycle, only visible in the net transport
- 'Energetic' inflows of warmer southern waters, driven by Algerian eddies that 'pushed' water through the MC
- Two types of anticyclonic 'blocking' eddies: most had a diameter of 20 to 30 km and slowly funnelled through the IC, but occasional large eddies of ~70 km diameter blocked the IC for months

Arguably CANALES was most successful at defining the seasonal maxima and minima for the meridional exchange through the IC and the role of anticyclonic eddies in causing the NC to branch or bifurcate north of the IC, with an associated impact on the southward transport. The pattern of circulation in the IC was described as 'a highly complex and variable' and interannual variability linked to the DWF driven thermohaline circulation.

Seasonal variability in the NC had already long been identified. Early studies in the south of France noted that the NC became faster, narrower and deeper from October to March and was broader and more shallow during the summer (Astraldi et al. 1989, Millot 1999). A rapid mid-autumn increase in current strength was also observed (Bethoux 1982, Bethoux 1988). Font (1990) also noted a sudden increase in NC strength in October/November in the Balearic Basin (with a decrease in March) and Pinot et al. (2002) observed a sudden and barotropic re-intensification of the NC in November. More recently, satellite altimetry has indicated that peak flows occur in December/January, with a sudden intensification across all sub-basins, and that minimum flows occur in August and vary by location (Birol et al.

2010). In a Balearic Basin study of satellite altimetry the peak mean flow was found to occur in autumn with greatest variability in winter (Mason and Pascual 2013).

In the Balearic Basin, Pinot et al. (2002) suggested that the autumn increase in NC strength was linked to the strengthening of wind activity in the north, although Acoustic Doppler Current Profile (ADCP) data has indicated that the mechanical transfer of energy from wind is not a major driver of circulation (Font 1990, Garcia et al. 1994). The spring/summer strengthening of AW inflows has been linked to the decline in the NC, the period of weak NC flows enabling AW from the south to 'invade' the Balearic Channels (Font et al. 1988b, Millot 1999, Pinot and Ganachaud 1999, Pinot et al. 2002). This pattern is overlain by inflows, related to the presence of strong mesoscale eddies to the south (Pinot et al. 2002, Taupier-Letage and Millot 1988) or to the absence of the Almería-Oran front (García-Lafuente et al. 1995).

The source of interannual variability in the strength of the NC has generally been attributed to DWF in the Gulf of Lion (Madec et al 1991, Millot 1999, Malanotte-Rizzoli et al., 2013). Modelling studies support this theory, indicating that intense DWF leads to intensified inflows of AW into the Gulf of Lion and a strengthening of the NC (Demirov and Pinardi 2007). Primitive equation models have also suggested that wind can play a role as a driver of the cyclonic circulation by contributing to the preconditioning for dense water formation (Herbault et al. 1997). Long-term records of inflows into the Gulf of Lion through the Corsica Channel, used as a proxy for NC circulation strength, have linked these inflows to both wind activity over the northwest Mediterranean (Astraldi and Gasparini 1992) and to the North Atlantic Oscillation (NAO, Vignudelli et al. 1999). Studies of air-sea fluxes (Josey 2003, Josey et al. 2011) also indicate that at decadal scales the frequency and location of deep convection is influenced by large-scale atmospheric modes. More recently the influence of the Eastern Mediterranean Transit (EMT) has also been detected in the hydrographic preconditioning for WMDW formation (Shröeder et al. 2010). The strength of the NC could thus be influenced by a range of atmospheric and hydrographic stimuli, which operate and interact across a broad range of timescales. To date no study has directly linked the interannual variability of DWF to the strength of the thermohaline overturning circulation and this therefore remains an open question (Malanotte-Rizzoli et al. 2013).

Although both cyclonic and anticyclonic eddies have been observed in the Balearic Basin and IC, the majority of eddies present in the IC are anticyclonic (Pinot et al. 2002) and typically range in diameter from 20 to 30 km (the Rossby radius at this latitude is 10 – 15 km), with velocities of 25 to 30 cm s^{-1} and coherent to depths of 400 - 500 m (Font et al. 1988b, Send et al. 1999, Beuvier et al. 2012). Larger eddies have also been observed, with diameters > 50 km (Pinot and Ganachaud 1999, Pinot et al. 2002, Pascual et al. 2002), and it has been speculated that these larger eddies could be generated by the merging of smaller eddies and thus be related to the amount of WIW produced during winter convection (Pinot and Ganachaud 1999). However, although frequently observed in the IC the generation and evolution of the WIW 'blocking' eddies is not fully understood.

Eddies have been observed in the Balearic Basin during the winter/spring periods of stronger NC current flow (Crépon et al., 1982, Font et al. 1988b, Pinot et al. 2002). As noted above, early satellite sea surface temperature studies showed intense mesoscale activity concurrent with strong inflows from the Gulf of Lion and the Algerian Basin (La Violette et al. 1990, Font et al. 1988b, Pinot et al. 1994, Lopéz Garcia et al 1994). Studies suggest these are generated through baroclinic instability (Crépon et al., 1982, Font et al. 1988b, Pinot et al. 2002) and that the location of eddy and filament generation is linked to specific topographic features (Wang et al. 1988, Tintoré et al. 1990, Masó and Tintoré 1991), such as submarine canyons. Modelling studies also indicate that baroclinic eddies are associated with the release of kinetic energy in the NC (Testor and Gascard 2003, Demirov and Pinardi 2007). Some eddies have been observed to form in the Gulf of Lion to the north and migrate south with the NC to the Balearic Basin (La Violette et al. 1994, Pinot et al. 2002, Pascual et al. 2002) and also during the CANALES experiment Pinot et al. (2002) observed anticyclonic vortex eddies in the core of NC meanders. Interestingly in a study of an 18-year satellite altimetry record (merged sea level anomaly data) for the Balearic Basin, Mason et al. (2013) detected eddy kinetic energy (EKE) as highest in autumn and lowest in spring. It has also been suggested that eddies acquire vorticity through wind energy (Pascual et al. 2002, Schaeffer at al. 2011).

Despite the link between WIW and the IC 'blocking' eddies the production of this regional winter mode water is also not yet fully understood (Vargas-Yáñez et al. 2012). Two types of formation have been proposed: shelf/slope (Fieux 1974, Salat and Font 1987, Gasparini, Vargas-Yáñez et al. 2012) and/or patchy open ocean convection (Lacombe and Tchernia

1974, Fuda et al., 2000, Sparnoccia et al. 1995). Most recent studies are of likely on-shelf formation with observations of dense water cascading down submarine canyons in both the Gulf of Lion and the Balearic Sea (Durrieu de Madron et al. 2005, Ulses et al. 2008, and the production of WIW occurring along the length of the Spanish shelf, from Cabo de Creus in the north to Cabo de Palos in the south (see fig. 2), during the strong winter of 2009/10 (Vargas-Yáñez et al. 2012). In addition, Heslop et al. (2012) suggested that the WIW observed in the IC in winter 2010/2011 was formed on the shelf area to the north of the IC, in the region of the Ebro Delta (fig. 2). WIW has also been observed in the Ligurian Sea (Gasparini et al 1999, Sparnocchia et al. 1995) and so formation is likely to be widespread and the variable characteristics the result of patchy formation in response to strong local weather events (Sparnoccia et al. 1995, López-Jurado et al. 1995, Gasparini et al. 1999, Pinot and Ganachaud 1999, Pinot et al. 2002, Vargas-Yáñez et al. 2012). Vargas-Yáñez et al. (2012) found that the winter 2009/10 formation exhibited a larger range of temperature and salinity values than those generally used to define WIW and López-Jurado et al. (1995) speculated that WIW appearing in the IC in early spring could be more local in origin than that appearing later in spring/early summer. The variability of WIW, in its formation sites, annual production volumes and water mass characteristics, is not yet well understood and deserves more research, as shelf to open ocean exchange process that impacts regional circulation.

As outlined above, the dynamic components of the Balearic Basin circulation are complex and interact across a range of timescales. These range from decadal (atmospheric weather patterns influencing DWF events, preconditioning and possibly also climatic change), to inter annual (winter cooling, seasonal wind, deep and intermediate water formation) to mesoscale (eddies, storm events). Many open questions remain about the both the drivers and interaction between these processes. The sub-seasonal variability as a result of this interaction, although frequently noted ('large cruise-to-cruise variability in transport through the channels' García_Ladona et al. 1996, Lopéz-Jurado and Díaz del Río 1994, Pinot and Ganachaud 1999, Pinot et al. 2002), has to date been poorly characterised, with relatively few studies capable of observing variability at sub-seasonal scales. For example, during the benchmark CANALES experiment although 3 moorings with ADCP instruments were deployed in the IC the spatial resolution was not adequate to produce more than a general estimate of the exchange of water mass or to tease out a mechanistic understanding of the variability in the water masses in this complex region.

The measurements from satellites, although continuous, are not sufficient to characterise circulation variability in the channels. For altimetry, the resolution of the data (30 km), the location of the satellite tracks and the proximity to land, make the study of the Ibiza and Mallorca Channels problematic. Sea Surface Temperature (SST) data from infra-red sensors or ocean colour data from higher frequency satellite sensors are limited to observing patterns at the surface and they are also significantly impaired by cloud contamination, and in the case of SST, the strong seasonal surface heating in the Mediterranean.

In the face of such spatial and temporal complexity the glider platform, with its ability to repeatedly monitor transects, across all seasons, was seen as an ideal way to extend our knowledge of the high frequency dynamics of the IC, and the seasonal and ultimately interannual variability.

1.5 New platform, new view

Gliders are becoming established as an important new tool for ocean observations (Rudnick et al. 2004, Testor et al. 2010). They modify their buoyancy, by pumping oil in and out of a pressurised hull, and their centre of gravity by moving internal battery packs fore and aft. The lift provided by small wings then enables them to 'glide' or 'fly' through the water, following a saw-tooth pattern in the vertical, whilst navigating between user-determined surface waypoints in the horizontal (fig. 4). They sample conductivity, temperature, depth (CTD) and other biogeochemical indicators, depending on the vehicle mounted sensor array (Rudnick et al. 2004). They have several key advantages for oceanographic monitoring, they operate autonomously, in all weathers, sample at a higher resolution than traditional ship surveys, for months at a time and at a lower cost than traditional ship surveys.

The high-resolution data gained from gliders has already provided insight into the variability of major coastal currents (Castelao et al. 2008, Todd et al. 2011), the evolution of mesoscale eddy structures (Ruiz et al. 2009, Martin et al. 2009, Baird and Ridgeway 2012, Bouffard et al. 2012, Pelland et al. 2013), and the mixing in the upper ocean and air-sea energy exchanges (Ruiz et al., 2012). Recently they also constituted an important part of the emergency response to the Deepwater Horizon oil spill.

Using gliders to regularly monitor key transects or 'endurance' lines[2] is increasing. They compliment existing infrastructure, such as ship surveys and deep moorings, which are required for full depth and high accuracy ocean profiling, synoptic process studies and the measurements of specific ocean tracers, and significantly expand observing capability. Initially limited by battery life, platform robustness and sensor accuracy, these early operational issues were actively resolved by the glider community (e.g. EU FP7 Project GROOM, Gliders for Research Ocean Observation and Management, and EGO, Everyone's Glider Observatory) and glider manufacturers. For example, most glider operators now use both lithium batteries and pumped CTDs. Gliders are now extending our ocean observing capacity and opening up a new era of higher resolution, lower cost, cross season observing. With the development of an increasing array of new sensors for biogeochemical (e.g. pCO_2, PH), micro turbulence and acoustic parameters, the future for gliders as a key monitoring technology looks bright.

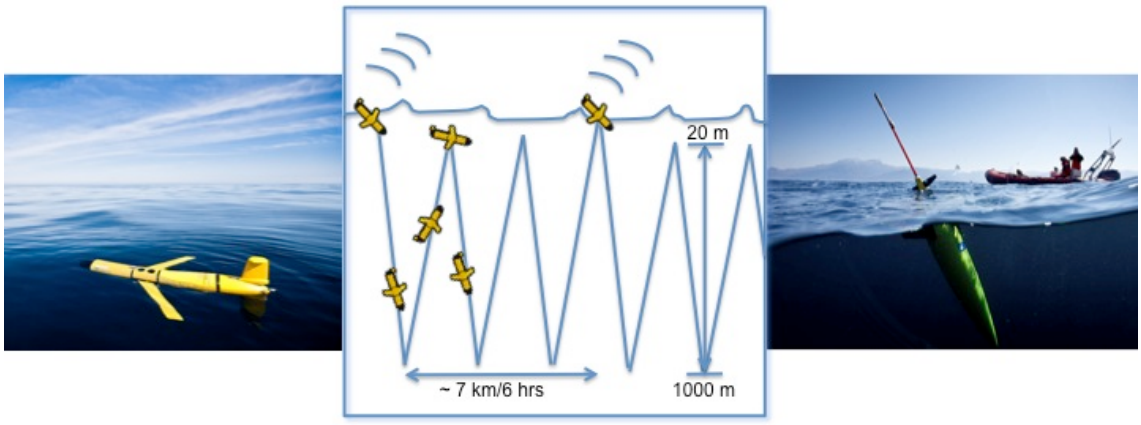

Figure 4. Schema for a glider a flight path.
In the centre is a sketch of the on-mission flight path for a Slocum glider, a Seaglider flight path is similar except they surface and transmit data after every 'V' profile pair rather than after a set period of time. To the left an image of a Slocum Deep glider and to the right an image of a Seaglider, the two glider platforms operated by SOCIB.

1.6 Present study

In this thesis the data from three years of glider monitoring of the Ibiza and Mallorca channels is analysed. In addition, a longer but more sparse record of ship data (1996 - 2013), primarily from IEO-COB, is combined with the glider data to give an 18-year time series, with which to investigate long term mean circulation patterns and interannual variability. The thesis is structured as follows: Chapter 1, contains the introduction to issues

[2] The term 'endurance' line indicates transects where long-term glider monitoring is maintained

raised and the region of study, Chapter 2 provides details on the data and methods, Chapter 3 contains a description of the 3-years of glider missions, a detailed but necessary step that provides insight into the key dynamic features visible in the IC, Chapter 4 is an analysis of the variability in the transport of water mass and the spatial patterns associated with that transport, Chapter 5 is a discussion of the findings, Chapter 6 contains perspectives on the operation of quasi-continuous glider monitoring, and in Chapter 7 the key findings of this PhD are concluded.

CHAPTER 2: Data, methods and analysis

This chapter is organised as follows; first the data and initial quality control and processing steps are described for all datasets used in this analysis, from gliders, ship and satellite (SST) observations. As gliders remain a relatively new platform some space is given in section 2.2 to describing the methods developed during this PhD to deal with the glider datasets, here glider specific processing and quality control methods, including salinity correction and CTD calibration, are described. The aim throughout this work has been to create a robust processing methodology that would work consistently, for profile and transect analysis, across missions and platforms.

2.1 Data

2.1.1 Glider

From 2011 SOCIB, the Balearic Islands Coastal Ocean Observing and Forecasting System (Tintoré et al. 2013), with in-kind support from IMEDEA (CSIC-UIB), has operated regular glider missions in the Ibiza and Mallorca Channels, maintaining a long-term glider monitoring line in the IC, with the objective of no greater than a month gap between missions. Between January 2011 and December 2013 twenty glider 'canales' (meaning channels in Spanish) missions have been undertaken, eighteen of which are used in this analysis[3]. During these 18 missions, 66 transects of the IC and 22 transects of the MC were completed and approximately 13,000 profiles of the water column obtained, see table 2. This represents, by an order of magnitude, more profiles than all the previous hydrography, requiring specific data processing methods to be developed to handle the glider data. The majority of the missions were undertaken using Teledyne Webb Research Inc.'s Slocum Deep gliders, however, Seagliders, from iRobot, and Slocum Coastal gliders were also used, see table 2 for details on the all glider missions.

[3] Two of the missions are not used in this analysis, during canalesJul2011 the CTD unit was switched off and canalesSep2011 was undertaken with a costal glider (maximum sampling depth of 200 m) and was therefore not comparable with the other missions for the calculation of geostrophic transport.

Table 2. Summary of 'canales' glider missions 2011 to 2013.

								Number transects		
Year	**Mission name**	**Glider name**	**Glider type**	**Glider unit**	**Mission start**	**Mission end**	**Number profiles**	**IC**	**MC**	**Mission/data notes**
2011	canalesJan2011	ideep00	Slocum G1	SL184	12/01/2011 12:30	04/02/2011 11:48	876	6	1	IC T6 short in E (1.0E) can see in T and S that northward flows appear, shelf part not captured fully, however sufficient and used in transport analysis.
	canalesFeb2011	ideep00	Slocum G1	SL184	10/02/2011 11:00	04/03/2011 08:00	825	6	1	IC T7 odd profile at approx. 0.88E (50 - 100 m), however next profile similar so not discounted, T6 also looks similar. IC T8 short (0.95E) and can see that northward flows not captured, not comparable for transports and therefore removed before analysis.
	canalesMar2011	ideep00	Slocum G1	SL184	18/03/2011 12:30	11/04/2011 07:50	861	5	1	IC T3 starts higher than usual. T8 is very short, not used as a transect (discarded).
	canalesMay2011	ideep00	Slocum G1	SL184	03/05/2011 12:30	21/05/2011 12:00	1054	3	1	IC T4 problem with CTD suspected in mid transect (something caught in the tube?), salinity not recoverable and so not used as a transect (discarded). Spikes at the surface in IC T3. IC T6 is short (0.9 E), northward flows not captured, not comparable for transports and therefore removed before analysis.
	canalesJun2011	ideep00	Slocum G1	SL184	02/06/2011 14:55	19/06/2011 20:50	734	4	1	IC T6 is short and only to 400m, used for transect analysis but not comparable for transports and therefore removed before analysis.
	canalesJul2011	ideep00	Slocum G1	SL184	06/02/2011 13:00	20/06/2011 10:00	N/A	N/A	N/A	All sensors inadvertently switched off due to changes in mission program/code.
	canalesSep2011	icoast00	Slocum coastal	SL050	20/09/2011 12:00	24/09/2011 00:00	N/A	N/A	N/A	Coastal glider mission, sampled to 200 m depth, not included in the analysis
2012	canalesMar2012	sdeep02	Seaglider	SG538	12/03/2012 09:00	27/04/2012 10:50	744	2	1	1st Seaglider canales mission, some open question about salinity calibration, OK for now, but calibration of other Seaglider missions would help.
	canalesMay2012	ideep02	Slocum G1	SL132	07/05/2012 07:00	01/06/2012 12:00	811	4	1	T8 very short, just shelf, not used as a transect (discarded).
	canalesJul2012	ideep00	Slocum G1	SL184	09/07/2012 18:20	01/08/2012 08:40	743	4	2	MC T8 short (2.0E) , be aware that not all transport northward may be captured, IC T5 spikes in salinity.
	canalesAug2012	ideep00	Slocum G1	SL184	22/08/2012 17:20	16/09/2012 15:20	870	4	2	MC T9 short (1.95E), with just under 1/2 channel missing, not comparable for transports and therefore removed before analysis.
	canalesOct2012	ideep02	Slocum G1	SL132	24/10/2012 13:15	01/11/2012 23:55	394	1	1	Glider fought current N of Ibiza and aborted in IC due to a leak. IC T4 short (0.6°E) useful for visual analysis but not comparable for transports and therefore removed before analysis.
	canalesNov2012	sdeep00	Slocum G2	SL243	27/11/2012 10:00	13/12/2013 12:00	811	2	2	First G2 mission, with pumped CTD
2013	canalesJan2013	sdeep00	Slocum G2	SL243	30/01/2013 10:00	21/02/2013 10:45	545	4	1	IC T6 is short (1.0E), not comparable for transports and thus removed before analysis. Spike in salinity in IC T4. Data is gappy, start of buffer problems?
	canalesMar2013	sdeep01	Slocum G2	SL244	22/03/2013 11:00	15/04/2013 11:00	819	4	1	1st sdeep01 mission. MC T1 trials to 300 m first part channel (1.85E) only 50%, so not comparable for transports and thus removed before analysis. IC T7 has large gap (13/04/2013) due to buffer problem in science bay (7.7 software), not comparable for transports and therefore removed before analysis.
	canalesMay2013	sdeep00	Slocum G2	SL243	21/05/2013 11:30	14/06/2013 10:00	751	4	2	1st mission with lithium batteries and new way points, MC T1 had tests (discarded double section), MC T9 short (2.0E) so use transports northwards with caution. IC T7 spike in salinity in surface. IC T7 is 5 days apart from RADMED calibration transect.
	canalesJul2013	sdeep00	Slocum G2	SL243	15/07/2013 10:00	02/08/2013 07:45	560	4	1	2nd mission with lithium batteries, spike salinity in IC T1. Used thermal lag correction even with pumped CTD due to sharp seasonal thermocline.
	canalesSep2013	sdeep00	Slocum G2	SL243	09/09/2013 10:00	04/10/2013 16:00	715	4	2	Amazing glider tracks, very close together, little current. A drifter in August shows NC is recirculating. Used thermal lag correction even with pumped CTD due to sharp seasonal thermocline.
	canalesNov2013	sdeep00	Slocum G2	SL243	02/11/2013 00:55	11/11/2013 09:40	408	1	1	Mission aborted due to drop in voltage after one IC transect, MC T2 profile 178 odd, replaced with NaN (pump glitch or debris?). Used thermal lag correction even with pumped CTD due to sharp seasonal thermocline, suprising for Nov.
	canalesDec2013	sdeep00	Slocum G2	SL243	03/12/2013 13:50	17/12/2013 17:13	486	4	0	Mission re-started after repairs (03/12), some strange profiles in IC T4. Not able to use thermal lag correction as mission plan no longer includes an upcast/downcast section required for calculation of thermal lag coefficients.
	TOTALS						**13,007**	**66**	**22**	

Gliders follow a saw-toothed flight path through the water column, between the surface and a current maximum depth of 1000 m, while navigating between surface waypoints, see fig. 4. The standard IC transect line is at 39°N, between surface waypoints at 38.99°N, 0.13°E and 38.98°N, 1.10°E, which is approximately perpendicular to the major current flows (fig. 5). The MC transect line is between surface waypoints at 39.22°N, 1.65°E and 39.50°N, 2.18°E, again approximately perpendicular to the major flows. During a typical 'canales' mission a glider is deployed close to Mallorca, navigates across the MC and around the island of Ibiza, then samples 2 to 4 sections of the IC before returning to Mallorca via the same route, see fig. 5. The maximum depth of the channel along the IC transect is ~950 m and the MC ~900 m, thus deep gliders sample to the full channel depth.

Each IC transect is 80 km and takes an average of 3 days to complete, with 2 days for the deep (central) section of the channel (off the continental shelf with depths ≥ 200 m), which is used in the calculations of water volume transport. Transects of the MC, 66 km, were sampled at the start and/or end of each mission, each transect taking an average of 2.8 days to complete, with 1.6 days for the deep ($z \geq 200$ m) section of the channel. The glider profile spacing is dependent on the depth of the glider dive and therefore the bathymetry. Thus profiles are more closely spaced on-shelf (fig. 5). The distance between glider CTD profiles is on average 2.7 km in the deep channel and 300 m on the shelf. The glider flight path is generally close to that of the transect line (the line between the transect way points). On average the distance of the flight path to the transect line was of order of 1.8 km, occasionally however stronger currents can sweep the glider off track (see fig. 5, canalesJan2011), necessitating a real-time adjustment of the navigation instructions.

Thus a typical 'canales' mission takes approximately 24 days to complete and includes 4 transects of the IC and 1 or 2 transects of the MC. The IC and the MC were therefore sampled with different frequencies. During a mission the IC was intensively 'burst' sampled approximately every 3 days and the MC sampled once every 3 – 6 weeks. However as can be seen from table 2 many missions were not 'typical', deployment locations were changed to take advantage of ship missions and weather windows, flight paths altered in response to strong currents, and occasionally missions were cut short or aborted due to battery depletion, leaks or other glider malfunction. The complexity of glider mission operation is not to be underestimated and requires real-time management by the glider operators.

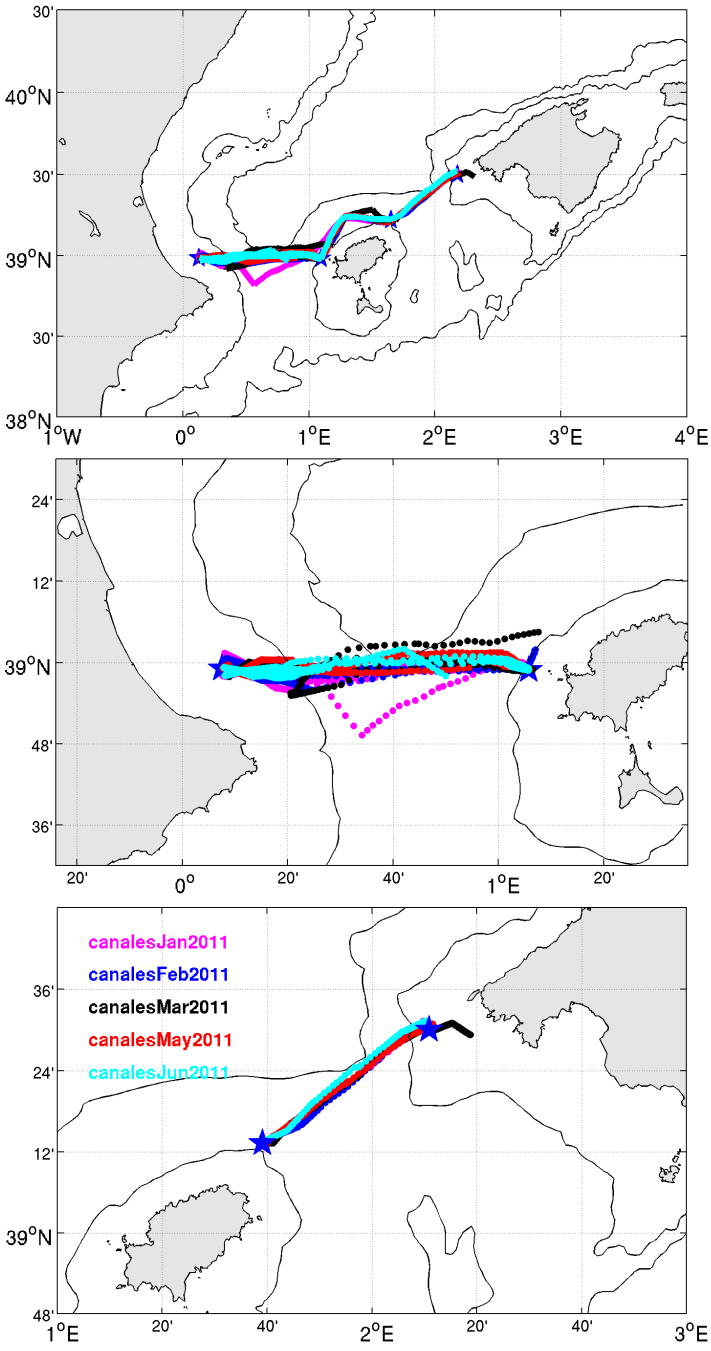

Figure 5. Typical 'canales' mission glider flight paths.

The 'canales' missions in 2011 are used as an example; each mission is a different colour (see legend), (top panel) the complete flight path, (mid panel) the IC section and (bottom panel) the MC section. Each point represents a profile, and the transect waypoints (blue stars) and 200 m and 1000 m isobaths (grey lines) are marked. The glider flight path was generally close to the transect line, occasionally diverging when the glider encountered strong currents, as in canalesJan2011.

Notwithstanding the many issues involved, the now 3-year quasi-continuous record of SOCIB monitoring operations in the IC has delivered a unique dataset.

The approach taken here to process the glider data is incorporated into the operational methodology of SOCIB and the glider processing code freely available for download as a toolbox: http://www.socib.es/~glider/doco/gliderToolbox/index.html

2.1.2 Ship CTD

Data from 18 years of ships missions were provided by IEO-COB, encompassing missions from 1996 to 2013, both directly by J-L Lopéz-Jurado and from the IBAMar 2.0 dataset (Lopéz-Jurado et al. 2014), which includes data from the original 'CANALES' campaign (Pinot et al., 2002). The recently released IBAMar 2.0 dataset is an important hydrographic record for the Balearic region, and it is a credit to the commitment of IEO, in particular of J-L Lopéz-Jurado, that the data have been consistently collected and archived for over 20 years. Weather permitting, the IEO transects of the IC and MC were undertaken at the same stations across different projects and years. Ship data from two recent SOCIB ship campaigns, using the new research catamaran B/O SOCIB, are also included in this analysis (MEDESS092013[4] and SOCIB_Dic13). These missions are important for the later ship to glider data comparisons (see Appendix D). Data from the Catholic University of Valencia June 2011 DERIVA campaign is also included, courtesy of Dr. J. Alcántara. See Appendix A for a full list of the 54 ship campaigns used in this study.

The IEO IC transect is parallel and 15 km to the south of the glider transect and the distance between stations is 10 km, unless more sparsely sampled due to weather, see fig. 6. The IEO MC transect is also parallel and 15 km to the east of the glider transect. During the recent MEDESS092013 and SOCIB_Dic13 ship campaigns the IC was sampled multiple times, again with a station resolution of 10 km. The most northerly transect of the SOCIB ship missions is coincident with the glider transect, the other transects are parallel and at 10 km intervals to the south, as for the MEDESS09 campaign, or 20 km to the south for the SOCIB_Dic13 campaign, see fig. 6.

[4] EU project MEDESS (Mediterranean Decision Support System for Marine Safety), see http://www.medess4ms.eu/ for more details.

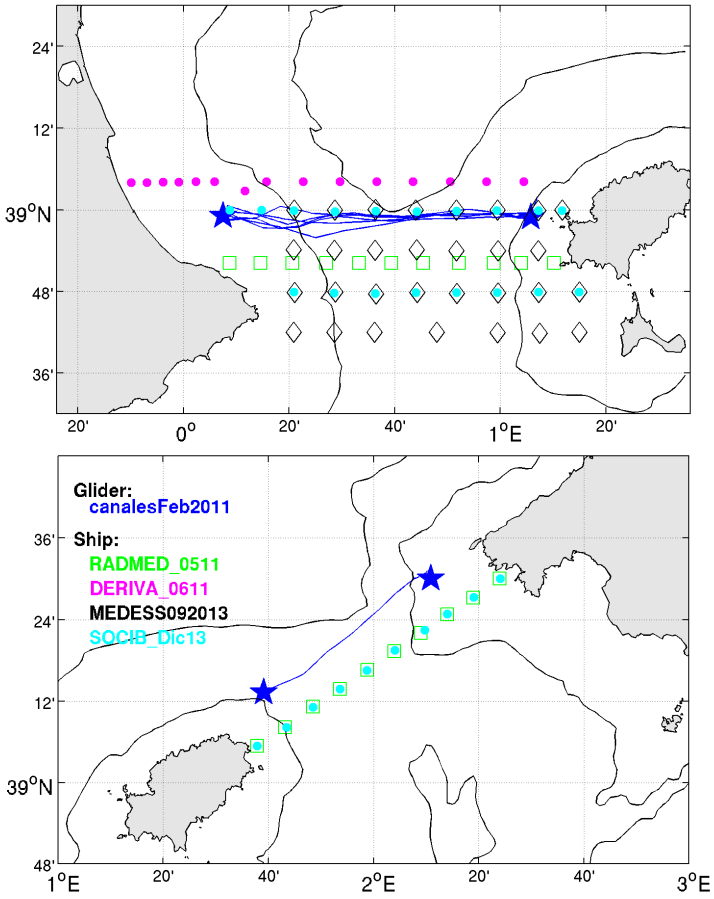

Figure 6. Location of ship transects.

For the Ibiza Channel (top panel) and Mallorca Channel (bottom panel). Different ship missions are marked by colour and marker (see legend), a sample glider mission (canalesFeb2011) is also shown (blue) and the 200 m and 1000 m isobaths (grey lines). Each marker represents a ship CTD profile and the lower resolution of the ship stations is visible in comparison with the glider profiles in fig. 5.

The ship CTD data was sampled at 25 Hz and then post-mission processed using standard Sea-Bird Electronics Inc. software routines. The IEO data was processed in the following sequence; wildEdit, filter, alignctd, celltm, w-filter, derive, binavg and averaged to 1 m bins, and the SOCIB data with the following sequence; wildEdit, filter, alignctd, celltm, loopedit, derive, binavg and averaged to 0.5 db bins. The IEO CTD salinity data was calibrated against in-situ water samples using IAPSO standard seawater and a Guildline 8400A salinometer. The temperature and salinity can be considered accurate to within 0.005 °C and 0.005 PSU (Lopéz-Jurado et al. 2014). The Catholic University of Valencia DERIVA mission was also calibrated and processed by IEO using the same methods and can be considered accurate to the same levels of precision. The SOCIB CTD salinity data was calibrated against in-situ water samples using IAPSO standard seawater, a Guildline

Portasal salinometer and a WOCE standard conductivity ratio correction procedure, and again can be considered accurate to the same levels of precision.

2.1.3 Ship Vessel Mounted Acoustic Doppler Current Profiling

Vessel Mounted Acoustic Doppler Current Profiling (VM-ADCP) data were acquired during the SOCIB_DIC13 ship campaign (02/12/2013 – 05/12/2013) from a 150 kHz RDI VM-ADCP fitted to the B/O SOCIB. During this mission 4 ADCP transects of the IC and 1 of the MC were obtained. Meaningful water velocities are obtained from VM-ADCP instruments once the instruments measurement of water column movement has been corrected for the ship's direction, speed and attitude, removing the ship's motion from the initial velocity estimate. This is not a trivial task as typically a vessel's velocity through the water is between one and two orders of magnitude greater than the ocean currents and therefore these sources of error can easily dominate the signal. There are three potential sources of error, error in the attitude of the VM-ADCP relative to the attitude of the vessel, error in the knowledge of the ship's heading and error in the knowledge of the vessel's velocity through the water. For the attitude error an initial calibration was found following the installation of the ADCP system, in this case an adjustment of -45.5°, then on-mission bottom tracking was employed to further refine the calibration between the ship and ADCP attitude, this secondary calibration was determined to be +1.08° with an amplitude of 1.006. To correct for the ships heading and velocity a new AshTech Trimble ADU800 3D GPS system navigation system was used to provide accurate data on the ships attitude. This system measures the phase difference between incoming satellite signals from which the ship's heading, pitch and roll are determined through ultra short baseline navigation principles.

Finally the ping-by-ping profiles were averaged to 2 minute and 10 minute ensemble profiles, which reduced the positional ship velocity calculation errors by a factor of the square root of the number of pings in the ensemble. The RDI stated accuracy of the VM-ADCP instrument is 1 cm s^{-1}, and with the AshTech Trimble 3D GPS as a source of heading, pitch and roll, the system is able to accurately measure ocean currents of velocity $\geq$ 5 cm s^{-1}.

2.1.4 Satellite Sea Surface Temperature

Satellite Sea Surface Temperature (SST) from two sources was analysed: daily SST from GHRSST (Group for High-Resolution Sea Surface Temperature), a multiple source satellite

product made available by IFREMER (France) as a Level 3 gridded product and night SST from the Modis_A sensor, an L3 single source product available from the NASA OceanColor website, were analysed for 2011. Although the GHRSST dataset has a higher resolution it contains artefacts associated with the mixing of data from multiple satellite sensors and so the single source Modis data was used as an additional comparison, both datasets suffered from significant cloud contamination.

2.2 Glider data processing

Glider data processers face specific issues related to the relatively slow sampling rate of the CTD, the glider flight pattern and the handling of more than one glider platform. Part of the work of the glider community, through EGO (Everyone's Gliding Observatories, a community of glider users, www.ego-network.org), GROOM (Gliders for Research, Ocean Observation and Management, an EU FP Project) and JERICO (Towards a Joint European Research Infrastructure network for Coastal Observatories, an EU FP Project including gliders as one of the key observing platforms), has been to share knowledge and best practice with relation to glider operations and datasets. With specific work packages within the GROOM project dedicated to addressing glider data processing issues.

Below aspects of the glider flight, sampling and processing methods are detailed, as they differ from traditional ship CTD data processing techniques.

2.2.1 Profiles

Glider profiles are assumed vertical, however gliders follow a saw toothed flight path in the vertical such that deep profiles have a horizontal scale of order 1.5 km from surface to the channel floor. The median position, between the start and end of the profile, is here taken to represent the profile location and although this is a common assumption for glider profiles its impact is not often discussed. A visual inspection was undertaken that indicated no difference (steepening) in the noise for those sections that are sampled on downcast and upcast vs. those sampled only on downcast, i.e. those transects with a higher density of profiles showed the same pattern of high frequency variability. In addition, a test was undertaken to assess any difference between the processing of the glider data from glider 'V' flight path directly to a grid rather than the approach taken here, which is to first create a vertical profile before interpolation to a grid. The results of this test are summarised at the end of this chapter, section 2.5, however they indicate that for the scale of features studied this assumption has little impact on the resultant dataset or view of the exchange. It

should however be noted that this may not hold true when gliders are able to dive to greater depths, say 6000 m, and such assumptions may have a far greater impact.

2.2.2 Flight path

In the course of a mission gliders naturally deviate slightly from the intended flight path in response to changes in currents and channel dynamics, generally however they are remarkably on-track, see fig. 5. For the 'canales' missions the mean distance of the glider to the standard glider transect line is 1.7 km and generally not greater than 3 km. A maximum deviation distance of 15 km to the standard transect line was defined for the calculations, which is approximately the Rossby radius at this latitude. Only one transect exceeded this limit, T6 in canalesJan2011, when the glider was swept south by strong currents (fig. 5, magenta). As this was the only example and as only a few profiles in this transect exceeded the limit, these were included in the calculations. Mapping the glider data to the 'standard' endurance line had no detectable impact on the results for the features studies here.

2.2.3 Glider inflexion depth

The SOCIB Slocum gliders were programmed to surface every 6 hours for a GPS position fix and, in between fixes, to inflect at 20 m sub-surface. This means that in the deep channel the gliders generally completed 2 or 3 dives before surfacing, with the result that full 'surfacing' profiles were 4 to 6 km apart. The upper 20 m of the Slocum glider data therefore has a lower sampling resolution than that below 20 m. The surface 20 m was re-constructed by interpolating between the surfacing profiles, a method that generally works well, however when the inflexion point is at a similar level as the strong summer/autumn thermocline, the surface interpolation shows the affects of this sub-sampling. This is seen as a banding in temperature, salinity and subsequently geostrophic velocity between the surfacing profiles, an example of smearing of signals where small-scale variability in the thermocline is sampled as the variability. For an example see glider mission canalesSep2013 in Chapter 3 and in detail in Appendix D. This can produce an apparent disconnect between features above and below the thermocline. Various methods were tested to reduce this effect, however the variability is real and so a component of the banding is also real, in addition similar patterns are also seen in ships CTD sections and so there is also a genuine disconnect above and below the strong summer/autumn thermocline. One possible method is to process the glider 'V' flight path directly to a grid, however this results in greater smoothing. To keep genuine features whilst removing induced banding is not feasible and so the interpolation method used here represented a reasonable option given

the mission programmed inflexion depth of 20 m. Any effect on the calculation of transport is not however anticipated to be significant (see summary at the end of this chapter, section 2.5).

2.2.4 Salinity correction

The application of correction procedures to salinity and other data is a fundamental component of physical oceanographic campaigns. Salinity is calculated from conductivity and temperature, however conductivity is primarily a function of temperature and only secondarily of dissolved salts. Errors in the calculated salinity arise if the water sample being measured by the conductivity sensor is not the same as that being sampled by the temperature sensor, which can occur when sensors are not co-located. The sharp summer thermocline in the Mediterranean (10 °C over 30 m) means that any mismatch in sensor sampling is accentuated. Correcting any misalignment in sensor sampling can be a more or less complicated procedure based on the CTD instrument and the platform. In gliders the problem is fairly complex due to the relatively slow sampling speed of the CTD, the glider flight path, velocity and the flow through the CTD unit.

The CTD package used in Slocum and Seabird gliders is a Glider Payload CTD (GP-CTD), manufactured by Sea-Bird Electronics, and is based on the SBE-41CP supplied with Argo floats. In early gliders this CTD was un-pumped due to power consumption considerations, however after 2012 a pumped version was made available. The correction described below was developed initially to solve issues with the salinity sampling in the un-pumped version of the GP-CTD, however it was also applied to the output from the new pumped glider CTD unit for summer/autumn missions when the seasonal thermocline was strong. In the GP-CTD the temperature sensor and the conductivity sensor are connected by a duct of approximately 10 cm in length, through which, in the earlier un-pumped versions of the CTD, the flow was unknown but generally approximated to be the glider speed through the water (Garau et al. 2011). If the temperature and conductivity sensors are sampling a homogeneous or gradually changing salinity/temperature profile the problem of misalignment is not so apparent. However in regions of fast temperature change spikes of up to 0.3 PSU occur in salinity, due to the mismatch between temperature and conductivity measurements (fig. 7, lower panel). A pattern of hysteresis is also visible between upcast and downcast profile pairs in θ/S, as the recorded temperature change lags the actual temperature change experienced by the conductivity cell, again most evident at the thermocline (fig. 7 upper panel). With a maximum sampling rate of 0.5 Hz there are

also relatively few samples across thermocline, the zone of maximum temperature gradient, which accentuates the issue and limits the performance of the correction procedures. The correction of salinity data from gliders with un-pumped CDTs is therefore particularly problematic and several studies have been undertaken with regard to the application of corrections to this type of dataset (Kerfoot et al. 2006, 2010, Merckelbach et al. 2010, Garau et al. 2011).

There are three possible sources of errors in salinity for the un-pumped glider GP-CTD:

1. **Sensor Response Lag:** This is dependant on the physical characteristics of the thermistor and conductivity cell, from which corrections can be determined following Fofonoff et al (1974):

   $$T = T0 + \tau T * \Delta T \qquad (1)$$

   Where T is the temperature at time t0, T0 is the measured temperature at time t0, τT is the time correction constant for temperature and ΔT is the gradient in temperature.

2. **Physical Separation Lag:** The temperature sensor and the conductivity cell are separated by a Perspex tube, length 10 cm and diameter approximately 1 cm. In a pumped CTD the flow rate is known and a time correction can be applied, however for the un-pumped CTD, the flow rate and the flow dynamics within the tubing are not well defined. An estimation of the order of magnitude of this correction can be made by assuming laminar flow and equating the mean glider surge speed to the mean flow speed through the CTD. This gives a lag of 0.25 s, which is below the 0.5 Hz sampling resolution of the unit.
3. **Thermal capacity lag:** This is commonly termed the thermal lag correction and is due to heat exchange between the tubing and the water passing through the tubing, which means that the temperature measured by the conductivity cell is warmed or cooled on its journey to the sensor depending on whether the glider is descending or ascending through the water column. The correction method for thermal lag in CTD instruments has been analysed by several authors (Lueck 1990, Morison et al. 1994, Johnson et al. 2007, Merkelbach 2009, Garau et al. 2011), and it is generally based on an empirical model derived by Lueck (1990) and enhanced by Morison et al. (1994). Here, following several tests (described below) a method based on Morison et al. (1994) and adapted

for the variable speed of the glider by Garau et al. (2011) was used (see inset for summary of the thermal lag correction).

Test 1: Values were determined for temperature and conductivity sensor response lags using an adapted version of the method (1) above, finding a lag of 1.2 to 1.4 s for temperature and 2.7 to 3.4 s for conductivity. Applying the sensor lag correction reduces the hysteresis between up and down cast (fig. 7 upper panel, light blue), however the result is very spiky. In a similar study with a different glider and dataset, Kerfoot et al. (2010) determined the sensor time lags to be 1.2 s and 0.8 s for temperature and conductivity respectively. Given that both estimates are considerably greater than the manufacturers values, Sea-Bird Electronics suggest 0.5 s for temperature and 0.1 s for conductivity, it seems likely that these calculated sensor time lags also include the effect of the thermal lag.

Test 2: The application of a thermal lag correction alone reduces the hysteresis between the up and downcast and results in a considerably improved profile (fig. 8, red). It can also be seen that the effect of the sensor lag corrections applied pre-thermal the lag correction is to increase the spikiness of the corrected salinity (fig. 8, magenta), whereas the application of the thermal lag correction alone has a smoothing effect on the salinity correction (fig. 8, red). The application of the sensor lag correction followed by the thermal lag correction was also tested, however although the hysteresis is reduced the salinity profile is spikier than with just the thermal lag correction (fig. 7, green and magenta).

The sensor lags are below the 0.5 Hz sampling resolution of the glider data and so difficult to detect with sufficient precision. The tests showed that the application of the thermal lag correction alone provided the most convincing solution to the problem of glider salinity correction.

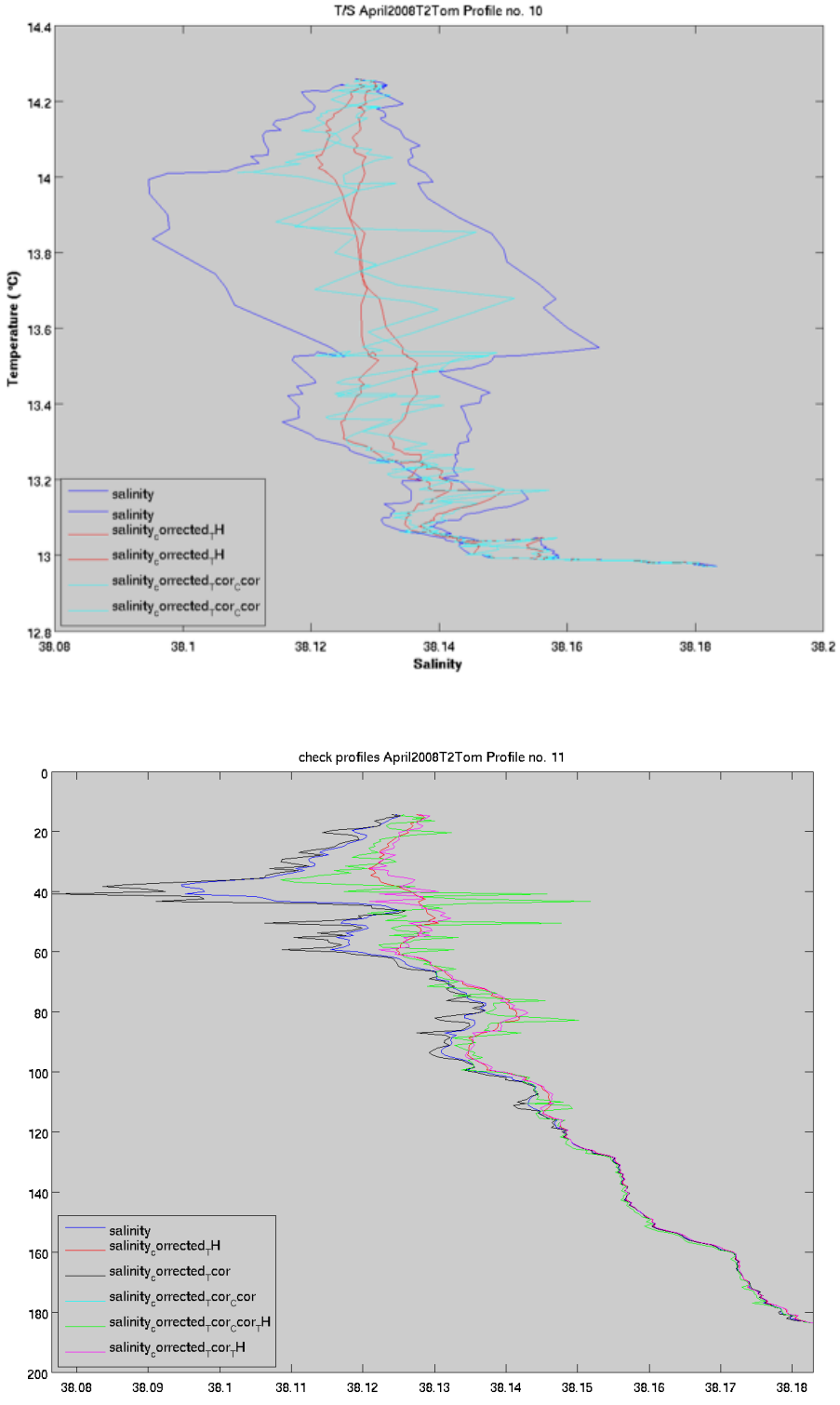

Figure 7. Corrected and uncorrected salinity for a sample glider profile.

In θ/S (upper panel) hysteresis between raw data downcast and upcast profiles is clearly visible (dark blue), after correction for sensor lag only (light blue) reduced, after correction for thermal lag alone (red), significantly improved. A salinity profile (lower panel) with corrections: raw data (dark blue), after correction for sensor lag (light green), after sensor lag correction and thermal lag correction (light green conductivity, magenta temperature) and after the correction with thermal lag alone (red).

Previous authors have also suggested that the error due to thermal lag is considered the likely cause of the largest component of error in salinity and not only in glider data (Johnson et al. 2007, Merkelbach 2009, Garau et al. 2011), this result is therefore consistent with these earlier findings.

Summary: Thermal Capacity or Thermal Lag correction for gliders

The temperature inside the conductivity cell is estimated through an expression, based on a model developed by Lueck (1990), expanded by Morison et al. (1994) and adapted for the glider platform by Garau et al. (2011); by taking into account the variable speed and pitch of the glider in deriving a through cell flow velocity for use with in the Morison et al. (1994) derived expression:

$T_{cor}(n) = -b\, T_{cor}(n-1) + a[T(n) - T(n-1)]$ (1)

$a = 4 f_n \alpha\tau / 1 + 4 f_n \tau$ (2)

$b = 1 - 2a/\alpha$ (3)

Where T is the measured temperature at scan n, T_{cor} the estimated correction, which is subtracted from the temperature to give an estimate of the T inside the conductivity cell at measurement n, fn is the Nyquist frequency (1/2 the sampling frequency), α and τ are the amplitude of the error and the time constant respectively.

Accounting for the variable speed and pitch of the glider, α and τ are derived from:

$\alpha(n) = \alpha_0 + \alpha_s V(n)^{-1}$ (4)

$\tau(n) = \tau_0 + \tau_s V(n)^{-1/2}$ (5)

Where V is the flow velocity in the conductivity duct, α_0 and α_s are the values for offset and slope respectively, similarly for τ. Note: this relationship holds for flow velocities that do not vary too much.

To apply the correction a low-pass filter is applied to the pressure to remove digital noise; using a recursive Seabird Electronics filter (www.Sea-Bird.com, Manuals, SBEDataProcessing_7.21a.pdf, Page 91). The time stamp (e.g. sci_time in Slocum gliders) is then linearly interpolated to provide time for all CTD measurements. τ and α are then found using an objective function that measures the area between the curves of T/t and C/t for a downcast and up cast profile pair and minimises the difference between the paired profiles. The values for α_0, α_s, τ_0 and τ_s, are then derived through a minimisation technique (see Garau et al. 2011 for full description). The corrections are then derived for each profile and the median values applied to the whole dataset. The MATLAB based code to perform the correction is available for download as the GliderToolbox from the SOCIB website at, http://www.socib.es/~glider/doco/gliderToolbox/index.html

The thermal lag correction (see inset for description) assumes that the paired up cast and downcast are sampling the same water profile, which for the features under study (geostrophic currents) is not unreasonable, given that for the deep profiles this separation is of the order of 1000 m and 1.5 hours. Although the assumptions, such as the interpretation of the flow speed of the glider through the water from the measured pitch and vertical velocity, and the type of flow dynamics in the tube could possibly be further refined. There is a limit to the improvements that can be made, given the glider sampling resolution in the vertical. In addition pumped GP-CTD units are now the norm, which significantly reduce the problems associated with the thermal lag effects.

For now, the thermal lag correction developed by Garau et al. (2011) offers the 'best' salinity correction solution available for the processing of un-pumped glider CTD data, and has been used to correct the glider data presented within this thesis. The thermal lag correction was also applied to the data from pumped GP-CTD units when a strong seasonal thermocline was present.

2.2.5 Salinity calibration

SOCIB operates a fleet of 7 gliders and over the 18 'canales' missions a total of 3 different types of glider platform (Slocum Deep G1, Slocum Deep G2 and Seaglider), 5 different glider units (SL184, SG538, SL132, SL243 and SL244), two different types of CTD sensor (pumped and un-pumped) and 6 different CTD units (CTD-SBE_0013, CTD-SBE_0168, CTD-SBE_0129, CTD-SBE_0195, CTD-SBE_0107 and CTD-SBE_0064) were used. CTD units are not unique to a glider, as units are returned to the manufacturer for calibration, are repaired and are swapped between gliders. To calibrate glider salinity data the CTD units need to be tracked from mission to mission, see table 3 below.

For the calibration glider CTD data was compared to contemporaneous ships CTD data using where possible transects sampled within 1 to 2 days of each other. To perform the calibration, potential temperature and salinity from contemporaneous glider/ship transects were plotted on the same θ/S diagram and fig. 8 shows a typical example from glider mission canalesSep2013 transect T3 (black) and ship mission MEDESS092013 transect T1 (magenta). Here it can be seen that the match between the two datasets in terms of water masses sampled is excellent, however there is a small offset in salinity between the two datasets.

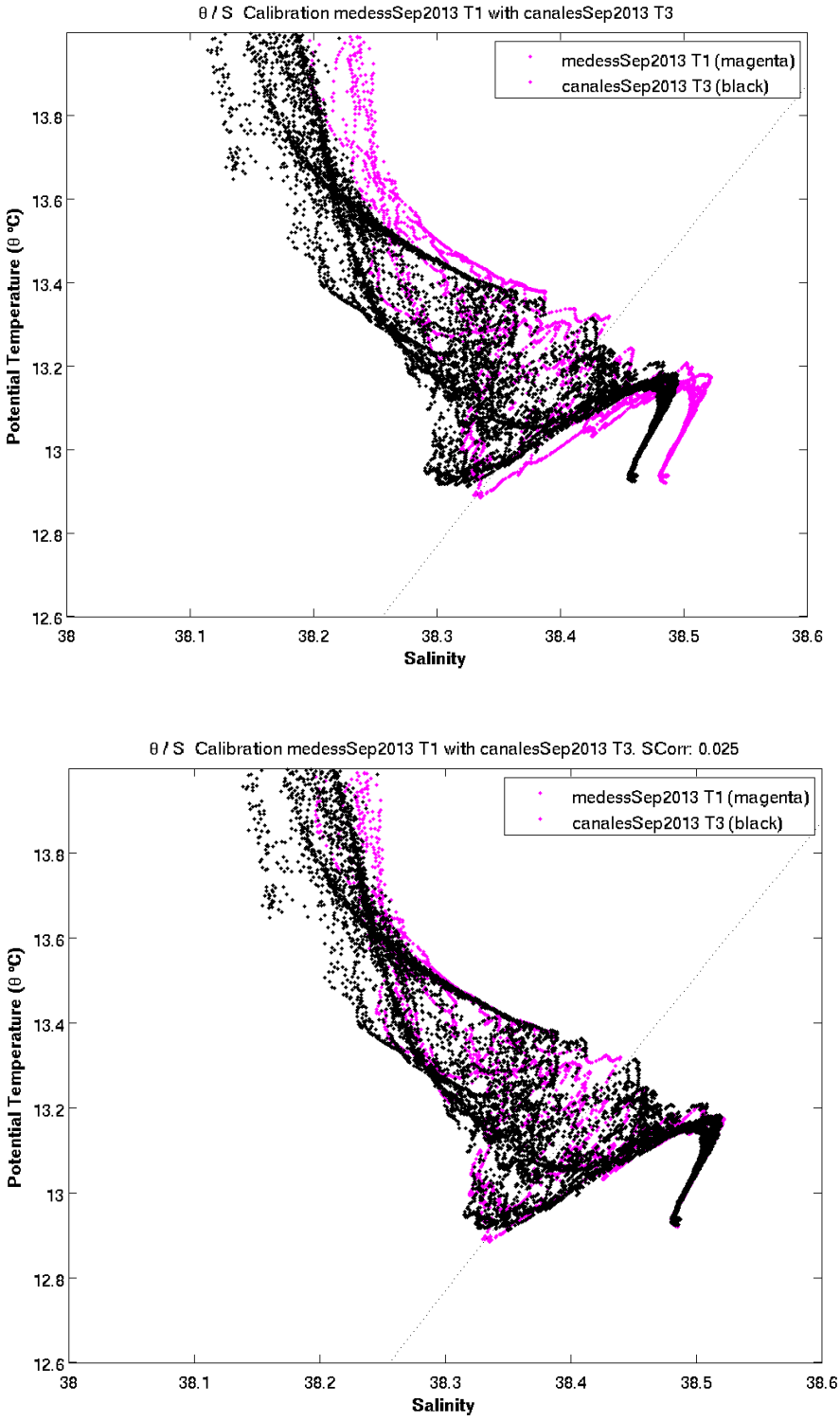

Figure 8. Glider salinity plotted with contemporaneous ship data for calibration.
Ship data from MEDESS092013 T1 (magenta) and glider canalesSep2013 T3 (black) are shown, (top panel) shows the sub-surface section of the water column so that the offset in salinity between glider and ship salinity can be clearly seen, (lower panel) after a +0.025 correction offset has been applied to the glider salinity data.

The ship data were calibrated against in situ water bottle samples and have an estimated precision of 0.003 in salinity[5], and therefore were assumed to be the more precise dataset. The glider salinity was adjusted, by adding small increments to salinity, until the LIW-WMDW section of the two θ/S profiles were coincident (fig. 8, lower plot). This section of the water column was chosen as a focus for the calibration, as the water mass properties remain more stable over the time at depth, however the full water column was also analysed for robustness of fit. As can be seen in the fig. 8 example, the salinity offset was addressed through the addition +0.025 to the (thermal lag corrected) glider salinity data and post calibration the fit between the two datasets is almost exact. Similar analyses were carried out for all contemporaneous ship and glider missions and the offsets in salinity obtained for the individual CTD units found to be relatively consistent through time, see table 3.

Year	Mission	Glider			Calibration			
	name	name	platform	unit	CTD Unit	Comparison	offset obtained	offset applied
2011	canalesJan2011	ideep00	Slocum G1	SL184	CTD-SBE_0013			0.020
	canalesFeb2011	ideep00	Slocum G1	SL184	CTD-SBE_0013	T6 / RADMED_0211 T1	0.019	0.020
	canalesMar2011	ideep00	Slocum G1	SL184	CTD-SBE_0013			0.020
	canalesMay2011	ideep00	Slocum G1	SL184	CTD-SBE_0013	T6 / RADMED_0511 T1	0.021	0.020
	canalesJun2011	ideep00	Slocum G1	SL184	CTD-SBE_0013	T5 / DERIVA_0611 T3	0.020	0.020
	canalesJul2011	ideep00	Slocum G1	SL184	CTD-SBE_0013			
	canalesSep2011	icoast00	Slocum coastal	SL050	CTD-SBE_0041			
2012	canalesMar2012	sdeep02	Seaglider	SG538	CTD-SBE_0168	canalesMay2012	-0.018	-0.018
	canalesMay2012	ideep02	Slocum G1	SL132	CTD-SBE_0129			0.014
	canalesJul2012	ideep00	Slocum G1	SL184	CTD-SBE_0195	canalesMay2012	0.017	0.017
	canalesAug2012	ideep00	Slocum G1	SL184	CTD-SBE_0195			0.017
	canalesOct2012	ideep02	Slocum G1	SL132	CTD-SBE_0129	canalesNov2012	0.014	0.014
	canalesNov2012	sdeep00	Slocum G2	SL243	CTD-SBE_0107			0.025
2013	canalesJan2013	sdeep00	Slocum G2	SL243	CTD-SBE_0107			0.025
	canalesMar2013	sdeep01	Slocum G2	SL244	CTD-SBE_0064	T4 / RADMED_0313 T3	0.016	0.016
	canalesMay2013	sdeep00	Slocum G2	SL243	CTD-SBE_0107	T7 / RADMED_0613 T3	0.025	0.025
	canalesJul2013	sdeep00	Slocum G2	SL243	CTD-SBE_0107			0.025
	canalesSep2013	sdeep00	Slocum G2	SL243	CTD-SBE_0107	T3 / medessSep2013 T1	0.025	0.025
	canalesNov2013	sdeep00	Slocum G2	SL243	CTD-SBE_0107			0.025
	canalesDec2013	sdeep00	Slocum G2	SL243	CTD-SBE_0064	T2 / SOCIB_Dic13 T3	0.007	0.016

Table 3. Summary of missions for salinity calibration.

To check for potential sensor drift, all the data (glider and ship) were compared for the 3 CTD units calibrated in this manner. An example of the resultant plot is shown in fig. 9, for CTD unit CTD-SBE 0013. Note, for simplicity of viewing θ/S data from 800 to 900 m are shown, for the full analysis all data were used however these plots quickly become over crowded and so here the lower section is shown to better illustrate the features present. In

[5] The maximum correction applied during 18 years of missions by the IEO has been +0.007 PSU, most corrections are of order 0.001 – 0.003 (J-L López-Jurado, personal communication)

fig. 9 a spread of values in the glider data from different missions can be seen (fig.9, upper panel, dots), however there is also a similar spread in the data from the contemporaneous ship missions (fig. 9, upper panel, crosses).

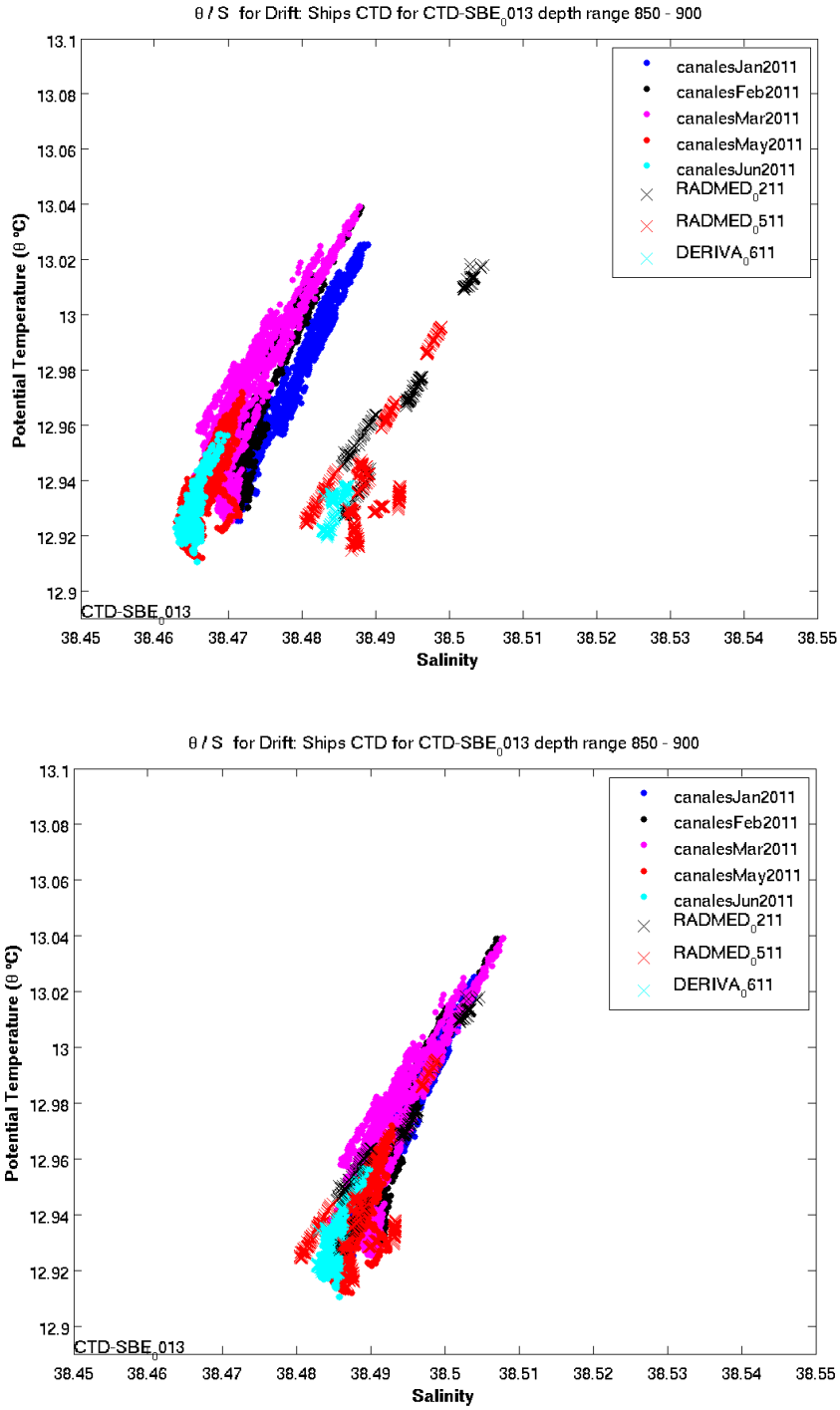

Figure 9. Contemporaneous glider and ship data for CTD-SBE 013 calibration.

For glider CTD unit CTD-SBE 0013 the un-corrected glider data (upper panel) and corrected glider data (lower panel) are plotted with all the contemporaneous ship data. Glider data are dots and ships data are crosses and the contemporaneous missions have the same colour code for easy comparison (see legend).

Similar results were obtained for the other CTD units, and so the conclusion drawn was that the range in values represents real variability, perhaps related to seasonal changes in the depth of water mass. With no detectable drift in the glider sensors, a single correction coefficient was applied to the salinity data from each CTD unit. In the lower panel of fig. 9 is the same example with calibrated glider salinity, the glider and ship data can be seen to cluster together. The spread of values shown in the salinity for these deep waters is of order 0.01 PSU and this indicates the precision to which we can calibrate the glider salinity with this method.

Some of the glider CTD units did not have a mission that coincided with a ship campaign, however the salinity data still required correction. In these cases the CTD units were compared against the closest corrected glider mission to obtain a salinity correction offset value. Again, no apparent drift was found in the sensors calibrated in this manner. See table 3 for the list of all glider-ship and glider-glider calibration offsets applied.

2.3 Initial data processing

In this study the glider data underwent 4 specific data processing and quality control steps prior to analysis and combination with the ship data:

1. Conversion of raw binary data and interpolation to time base: The binary data were converted to physical units and a low-pass filter applied to the pressure to remove digital noise, using a recursive Seabird Electronics filter (SBE Data Processing Manual, Page 91). The timestamp was linearly interpolated to provide time for all CTD measurements. Repeated (i.e. non-updated) GPS fixes were removed and the missing positions linearly interpolated between the 'real' GPS fixes. The inflexion points for the up and down casts were identified from the smoothed pressure signal.

2. Salinity correction: Salinity values outside of $20 < S < 40$ were removed and then the correction parameters for the thermal lag or thermal capacity correction found following the methodology of Garau et al. (2011), as detailed in section 2.2.4. The thermal lag or thermal capacity correction was applied to the conductivity and a new 'corrected salinity' variable generated.

3. Profile creation: The temperature and corrected salinity from each downcast and upcast were assumed to represent vertical profiles, and a mean time and location was

used to represent the profile. Each vertical profile was then interpolated to a 1 m vertical grid, which is approximately the resolution of the dataset and matches vertical resolution of the ships data after initial processing.

4. Salinity data calibration: A CTD specific salinity correction coefficient was determined from comparison with in situ data, see section 2.2.5, and applied to the thermal lag 'corrected salinity' variable.

The SOCIB glider CTD units are calibrated every 2 years and so temperature can be considered accurate to within 0.004 °C[6]. The results from the glider salinity (see section 2.2.5) indicate that the precision achievable for salinity is of order 0.01.

2.4 Methods and analysis

Throughout the analysis potential temperature, and for gliders, thermal lag corrected salinity (hereafter referred to as salinity) were used. For the ship data, 'salinity' refers to the output of the processing tools provided by Seabird Software, see section 2.1.2 for a list of the Seabird Software modules applied to all ships datasets, which includes a thermal lag function.

To create a uniform dataset of glider and ship CTD transects for the analysis it is important to create a set of comparable transects. To do this a series of platform specific procedures were employed to condition the data prior to the calculation of geostrophic velocity:

- For all gliders: profiles (potential temperature and salinity) were mapped to a 'standard' transect line, taken as the line passing through the transect waypoints, at ~39°N
- Slocum gliders only: short profiles due to glider (6h) surfacing pattern were in-filled with nearest neighbour profile temperature and salinity data
- Slocum gliders only: temperature and salinity were interpolated horizontally between surfacing profiles above the inflexion depth of 20 m
- Seaglider gliders only: temperature and salinity data in the surface 3 m were deleted due to spiking caused by the initiation of a pump, to move the batteries and change the glider centre of gravity/pitch, as the glider neared the surface. The temperature and salinity data from 4 m depth were copied to the surface 3 m

[6] Sea-Bird Electronics Inc. stated sensor accuracy for the GP-CTD unit is 0.002 °C per annum for the temperature sensor and 0.002 (equiv. salinity) per annum for the conductivity sensor

- Ship data only: some ship profiles had sections of data replaced by NaN for reasons of quality control, these were in-filled with temperature and salinity from the 'nearest neighbour' profile

Following these conditioning procedures, profiles of potential temperature and salinity profiles were binned to 5 m in the vertical and 2 km in the horizontal and then linearly interpolated to a standard 'grid' of data points. The bins sizes were chosen in order to remove some small scale variability in the vertical and provide an even set of profiles at a resolution approximately equivalent to the spacing of the glider profiles in the deep channel. The 2 km spacing is obviously below the resolution of the 10 km ships data profile spacing, so although 2 km profiles are produced no additional data is available. All profiles across the channel transects were then trimmed to a standard bathymetry, using a standard bathymetry product (SRTM30Plus, Becker et al. 2009), see fig. 10.

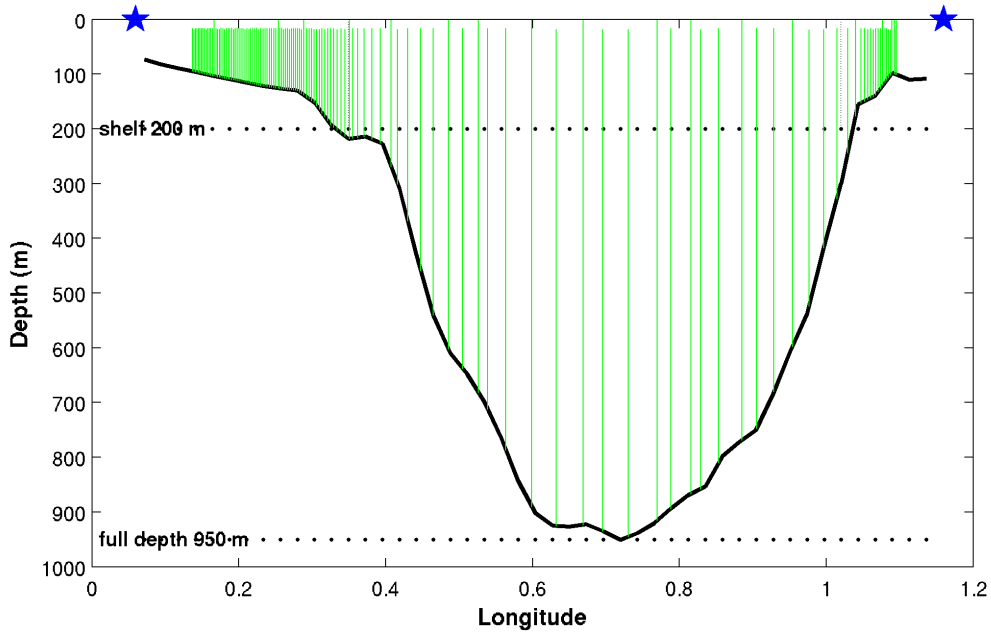

Figure 10. Ibiza Channel cross-section with glider profiles and bathymetry.
The glider transect surface waypoints are marked (blue stars) and a vertical profiles from a sample glider transect (canalesDec2013 T2) is shown to illustrate the density of the glider profiles on-shelf and in the deep (central) section of the channel, the data is cropped to the standard bathymetry.

The output from these procedures is a set of potential temperature and salinity transects with data at standard grid points and cropped to a standard channel bathymetry, for both glider and ship data.

Prior to the calculation of geostrophic velocity a 6 km horizontal moving average smoothing was applied to the potential temperature and corrected salinity, this smoothing window was chosen for the glider data through experiment, in order to smooth the horizontal signal whilst representing the original data distribution. From this smoothed data the geostrophic velocity perpendicular to the transect line was calculated from potential density, using the geostrophic assumption (Pond and Pickard 1983) and using the common deepest depth between each pair of profiles as the reference level of zero velocity.

The volume of water transport was calculated from each geostrophic velocity data point multiplied by the cell area that this represented (5 m x 2 km). The geostrophic transport was analysed by water mass, using regionally accepted values of θ and S to identify the different water masses present (Pinot et al. 2002, Pinot and Ganachaud 1999, López-Jurado et al. 2008).

The deep (central) section of the channel, off the continental shelf and with depths $\geq$ 200 m is used to represent the water volume transport of the section, see fig. 10. This assumption was chosen for 3 reasons. Firstly the geostrophic velocity assumption becomes invalid at shallow depths and on-shelf i.e. the velocity at 200 m are not likely to be zero on-shelf and so the resultant velocities are likely inaccurate. Secondly, for operational reasons, neither glider nor ship transects capture the full on-shelf area (perhaps for this reason amongst others Pinot et al. 2002 employed a box model technique to calculate the transport). Thirdly the flows under study primarily occur in the deep channel section.

In order to test the 'deep channel' assumption a regional configuration of the Regional Ocean Modelling System (ROMS) model (Shchepetkin and McWilliams, 2003, 2005), implemented over the Balearic Sea and developed within the framework of the BALearic OPerational (BALOP) forecasting system (Tintore et al. 2012), was used. A continuous glider mission was simulated across the IC at 39°N and the model output (potential temperature, salinity and absolute velocity, u and v) sampled with a simulated glider transect, with a completion time of 4 days and a profile spacing of 1 km. The profiles from the model (θ, S, u and v) were processed in the same manner as the glider data to produce an estimate of geostrophic velocity.

For the transport analysis the glider and ship datasets are combined to produce long-term means for the transport of water masses in IC and MC. This analysis assumes that the transports from these two different datasets can be combined and treated as equal without, for example, any weighting applied. A detailed study was therefore undertaken of contemporaneous ship and glider missions to understand the impact of the differences in the temporal and spatial sampling resolution and the transect location (Appendix D).

In order to analyse spatial patterns and temporal variability of the spatial patterns an Eigen Orthogonal Functions (EOF) analysis was performed on the geostrophic velocity field of the glider transects of the IC. Firstly, the mean geostrophic velocity field was calculated and removed from each of the 61 complete glider transects of the IC, then the Eigen values and vectors were calculated and from this de-trended (mean removed) dataset and the pattern in geostrophic velocity that the EOFs represented and the amplitude of these EOFs found. Plots were produces to show the EOFs, with the mean amplitude by month, and selected samples of what this might represent at different times of the year, see Chapter 4, section 4.4.

During the sampling, processing and analysis of this, and any oceanographic dataset, a number of assumptions and approximations are made, which can impact the results. For this study these could be summarised as follows:

- The geostrophic velocity derived transports are sufficiently well calculated
- Glider transects can be generally viewed as synoptic
- Ship CTD and glider transects can sensibly be combined for analysis

In order to assess the impact of these assumptions a number of tests and specific studies were performed, details of which can be found in the appendices. For the zero velocity assumption these included, a sensitivity test using assumed values for the base of profile velocities (see Appendix B), a test comparing glider DAV and geostrophic velocity DAV (see Appendix C), a comparison of contemporaneous glider geostrophic velocity and ship VM-ADCP sections (see Appendix D), and the use of the 'deep channel' to represent total transport was tested using the output from a Regional Ocean Modelling System (ROMS) model implemented over the Balearic Sea (Tintoré et al. 2012), as described above. To gain insight into the issue of synopticity in the 'canales' glider sections a specific study was

undertaken to assess the differences in temperature and salinity between consecutive transects of the IC (see Appendix E), insight was also gained from the glider to ship transect comparison (Appendix D). The viability of combining ship and glider data for the transport analysis was assessed through the comparison of three contemporaneous glider and ship missions (see Appendix D).

Finally, as mentioned in section 2.2.1, although not a key assumption, a specific test was performed to assess if any difference was visible in the sections when the glider 'V' flight path was interpolated directly onto a 2D grid, rather than first creating a vertical profile and then interpolating in the horizontal (Appendix F), the method used in this study to process the glider data. The test showed that only minor differences are visible in temperature and salinity and that the more direct glider 'V' to 2D method provides a slightly smoother pattern in geostrophic velocity, likely due to the Delaunay triangulation method of interpolation. The difference seen in transport values is slight, 2% in the transport north and 4% in the transport south, which provides perhaps an indication of the scale of error associated with the choice of basic processing methods.

The results of these tests and influence that this may have on the interpretation of the results are discussed in detail at the end of Chapter 4, section 4.5.

CHAPTER 3: Glider missions 2011 - 2013

In this chapter a brief (~3 page) overview for each glider mission is provided, in order to illustrate the essential characteristics and changing dynamics, within each mission, across missions and across years. Each glider mission is similar in scope to a traditional ships expedition and at one time might have merited a more complete description, or even a paper, however this is not practical for long term glider monitoring and therefore the descriptions below summarise the main features and evolving dynamics, primarily in the IC and to a lesser extent in the MC. Each description starts with the features observed in the IC, followed by those observed in the MC, ending with a short a summary to link the dynamics across transects, missions, channels and years. The novelty of the view presented by the glider missions is highlighted and synthesised at the end of this section. Finally five 'modes' or patterns are proposed to characterise the features observed in the Ibiza Channel over this 3-year period of intensive glider monitoring.

Note: The number and dates provided for each transect, e.g. T1 (13/01), are the sequential transect number and the mean date for the deep central section of the channel (i.e. off the continental shelf and with depths ≥ 200 m), the mean date is used to represent both the water mass transport value and the section. In the following analysis the geostrophic velocity and associated transport southward is denoted as negative and northward as positive. Sections of potential temperature, salinity and geostrophic velocity are provided for the IC in this Chapter and for the MC in Appendix G. The sections presented are essentially viewed as synchronous and the validity of this assumption is discussed at the end of Chapter 4, after the variability in the geostrophic transport of water mass has been explored in more detail.

3.1 Glider missions 2011

canalesJan2011

IC: At the start of the mission a strong NC is visible in the west of the channel, as indicated by the downward tilt of the isopycnals towards the western edge of the IC. In T1 (13/01) it is visible as a broad southward flow in the geostrophic velocity section, extending from just on the shelf at 0.35°E and across the channel to 0.75°E, penetrating to maximum depths of 350 m at around 0.5°E, see fig. 11a. The tilt of the isopycnals associated with the NC is ~6.2 x 10^{-3} (e.g. $\Delta z/\Delta x$ for σ 28.8 kg m^{-3}). In the surface 100 m

the channel is split almost 50:50 between inflows and outflows. The inflows extend from 0.75°E to 1.0°E and to depths of ~100 m. The core of the inflow is ~0.65°E, with associated geostrophic velocities of 25 cm s^{-1}. In the centre of the channel (0.7°E) the NC lies just below the surface and just below the AW inflows. The NC shallows and reduces in extent in T2 (16/01), occupying the western side of the channel from the shelf break to 0.65°E and penetrating to depths of ~275 m, with core geostrophic velocities of 25 cm s^{-1}. The inflows appear as two more shallow streams at 0.75°E and 1.0°E. In T3 (19/01) WIW arrives in the channel for the first time in 2011, and floods south with the NC as a cold fresh water mass (θ 12.9° C, S 38.05) see fig. 11a and b. This causes the isopycnals to steepen and the NC to strengthen and deepen. In T3 (19/01) the westward tilt of the isopycnals associated with the NC is of order 4.1 x 10^{-3} and the current penetrates to ~220 m depth. By T6 (28/01) the isopycnals tilt down with a gradient of order 15.2 x 10^{-3} to the western channel edge and the current penetrates to 400 m depth, and the associated geostrophic velocity has risen to 45 cm s^{-1}, see fig. 11a. In T6 the glider was swept 18 km south by the strong NC flows (see fig. 5 in Chapter 2). In T5 and T6 the isohalines and isopycnals steepen such that the 38.2 halocline and the 28.8 isopycnal breach the surface (previously at depth 70 m). The transport of water mass rises correspondingly from -0.92 Sv in T3 to -1.74 Sv in T6, with an increase of 0.5 Sv between transects T5 and T6 (26/01 to 28/01). Concurrently with this, in the east of the IC, there are strong inflows of fresher and warmer AW (fig. 11a and b), which increase and freshen from T3 to T6, as the transports associated with these inflows rise from +0.16 Sv in T3 to +0.58 Sv in T6. These inflows are visible as 1 or 2 streams and generally across half of the deep section of the channel, from 0.7°E to the transect end and penetrating to a maximum depth of 200 m (fig. 11a). The freshest AW (with salinities in the range 37.4 to 37.7) is visible in the surface 40 to 70 m, deeper in the east and reducing in depth towards the west and the strongest flows are in the surface 100 m (see fig. 11a). The extent of the inflows appears to change in response to the changes in the NC.

In the plots of θ/S, fig. 11b, there is evidence of an inter-basin 'exchange' of water mass, with 2 distinct mixing lines, one from WIW to cooler AWo (θ 13.8 °C, S 38.2) for the waters of northern origin and another from LIW to warmer fresher AW (θ 14.5 °C, S 37.6) inflows from the south. Note that in several transects the fresher AW, visible in the surface inflows in fig. 11a, does not meet the generally accepted definition for Atlantic waters of more 'recent' Atlantic origin (AWr), i.e. S ≤ 37.5.

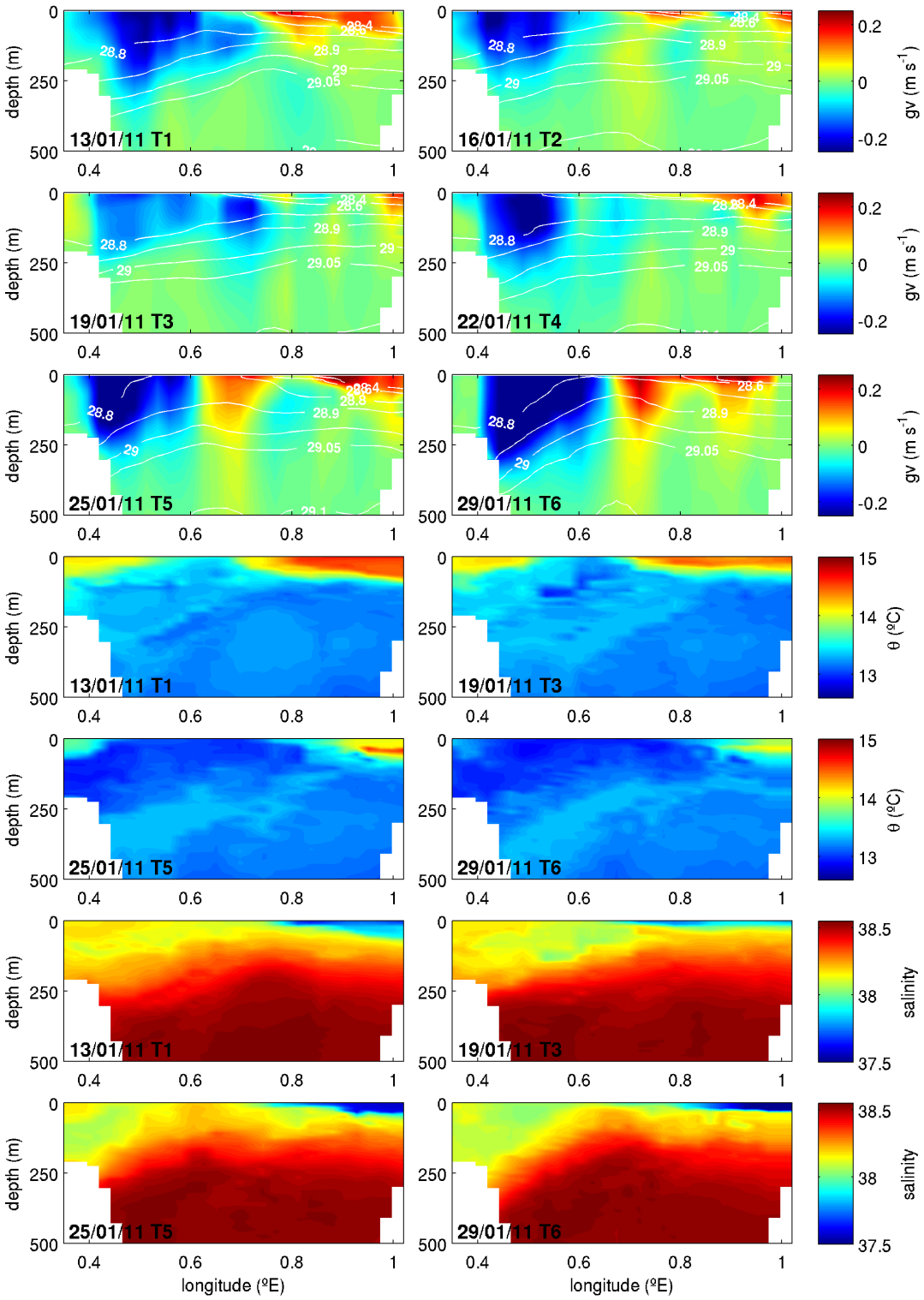

Figure 11a. Geostrophic velocity (gv), potential temperature (θ) and salinity sections for canalesJan2011. The transect numbers and mean date are marked in the bottom left of each panel, geostrophic velocities northward are positive and southward are negative, and selected isopycnals are marked in white.

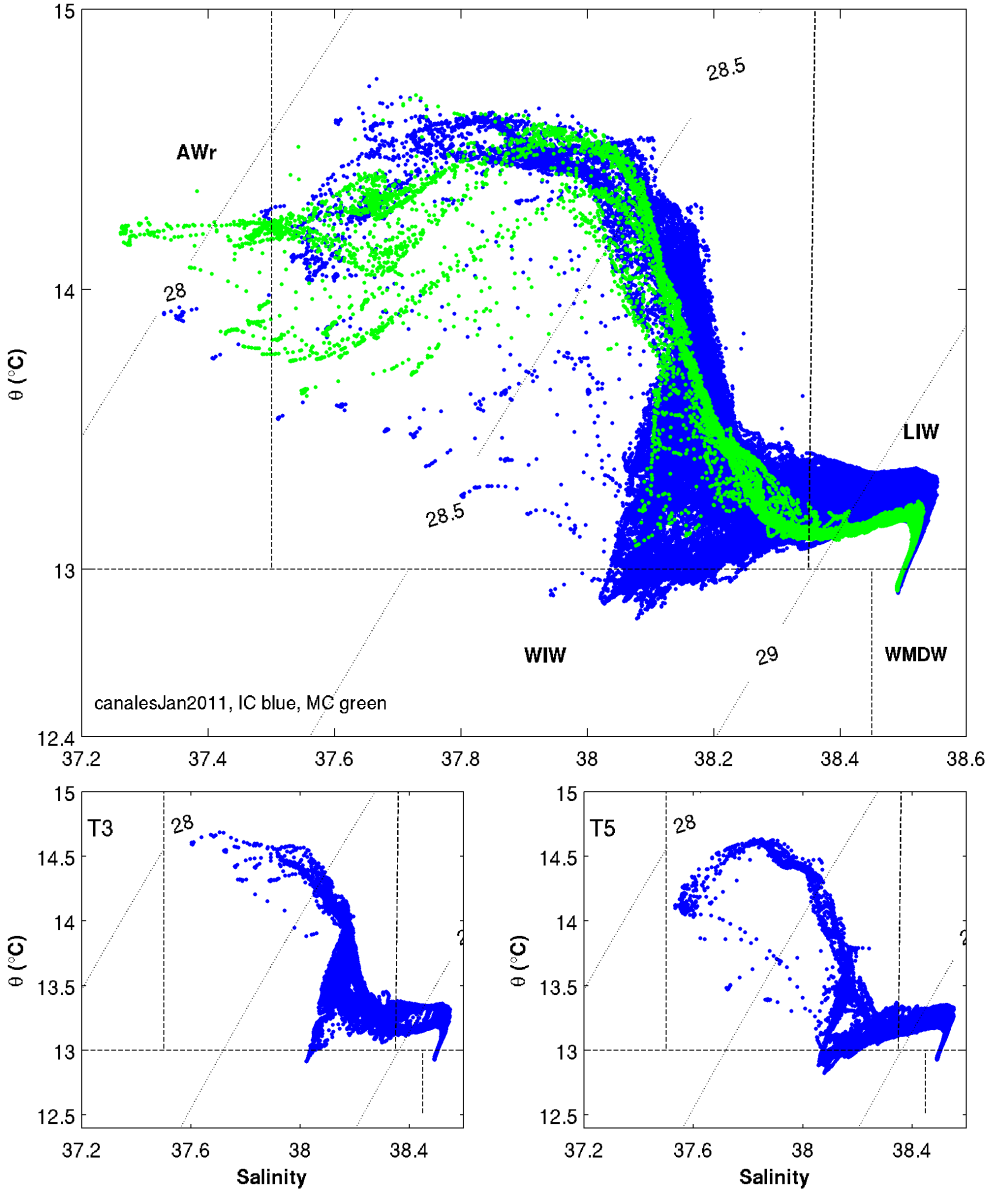

Figure 11b. θ/S plots for canalesJan2011.

The IC transects are marked in blue and the MC transects in green. The lower panels show details of the arrival of WIW to the IC (T3) and the cross-mixing lines (T5).

MC: In T8 (01/02) a fresh AW water mass lies above the thermocline (0 to 70 m) across the width of the MC, with similar properties to that visible in the IC but with a slightly fresher range of salinities, 37.2 – 37.7, see fig. 11b. The layer is freshest in the northeast of the channel (see Appendix G for sections). In geostrophic velocity a weak outflow current is visible in the southwest of the channel with associated transports of -0.24 Sv and stronger inflows are visible in the northeast associated with transports of +0.55 Sv. The

outflow below the thermocline has the general character of waters from the north (S 38.0 to 38.1 and with lower temperatures), whilst above the thermocline the outflows are of a less saline AW. This suggests that this fresher AW layer (37.2 – 37.7) is resident at the surface to the north of the MC and so forms part of the outflows.

Summary: In January 2011 three important features are observed in the IC, a strong NC exporting 0.8 to 1.0 Sv from the Balearic sub-basin, a rapid and significant strengthening of this current in response to the arrival of WIW to the channel, and strong inflows from the south associated with a fresher AW. The increase in transports associated with the appearance of WIW in the channel is of 0.82 Sv over 3 transects (T3 to T6). This is equivalent to the change associated with the previously defined seasonal signal of 0.9 Sv (Pinot et al. 2002), occurring over 6 to 7 days. In fig. 11b it can be clearly seen that inflows of the same fresher water mass occur contemporaneously in the IC and MC, with a slightly fresher range of salinities seen in the inflows through the MC, however this fresher AW does not always reach the threshold salinity for AWr. This fresher AW appears likely to lie to the north of the MC at the surface as it also forms part of the outflows through this channel.

canalesFeb2011

IC: In February a strong NC is present in the west of the channel, although not as strong as at the end of January 2011. In T3 (16/02) the NC extends from the shelf break to 0.6°E and to 300 m depth, with core geostrophic velocities of ~20 cm s^{-1}, transporting -0.68 Sv southwards and with a downward tilt of the isopycnals of order 5.3 x 10^{-3} ($\Delta z/\Delta x$) to the western channel edge (fig. 12a). Cold WIW (θ 12.6 °C, S 38.0) is present in the surface core of the current. In the east of the channel fresher AW inflows remain strong, with the freshest AW (S < 37.7) in the surface 0 to 50 m and a total transport northward of +0.58 Sv. A small, ~10 km diameter, anticyclonic vortex structure is visible in geostrophic velocity (fig. 12a) between 0.6 and 0.8°E, which appears to have developed in the surface 100 m between the inflows and outflows. By T4 (19/02) this has deepened and moved west, perhaps interfering with the flow of the NC and reducing its width. In T5 (21/02) the vortex structure may have temporarily blocked the path of the NC and transports southwards have fallen from a steady -0.68/0.69 Sv in T3/T4 to -0.22 Sv, the isopycnals have also flattened (see fig. 12a).

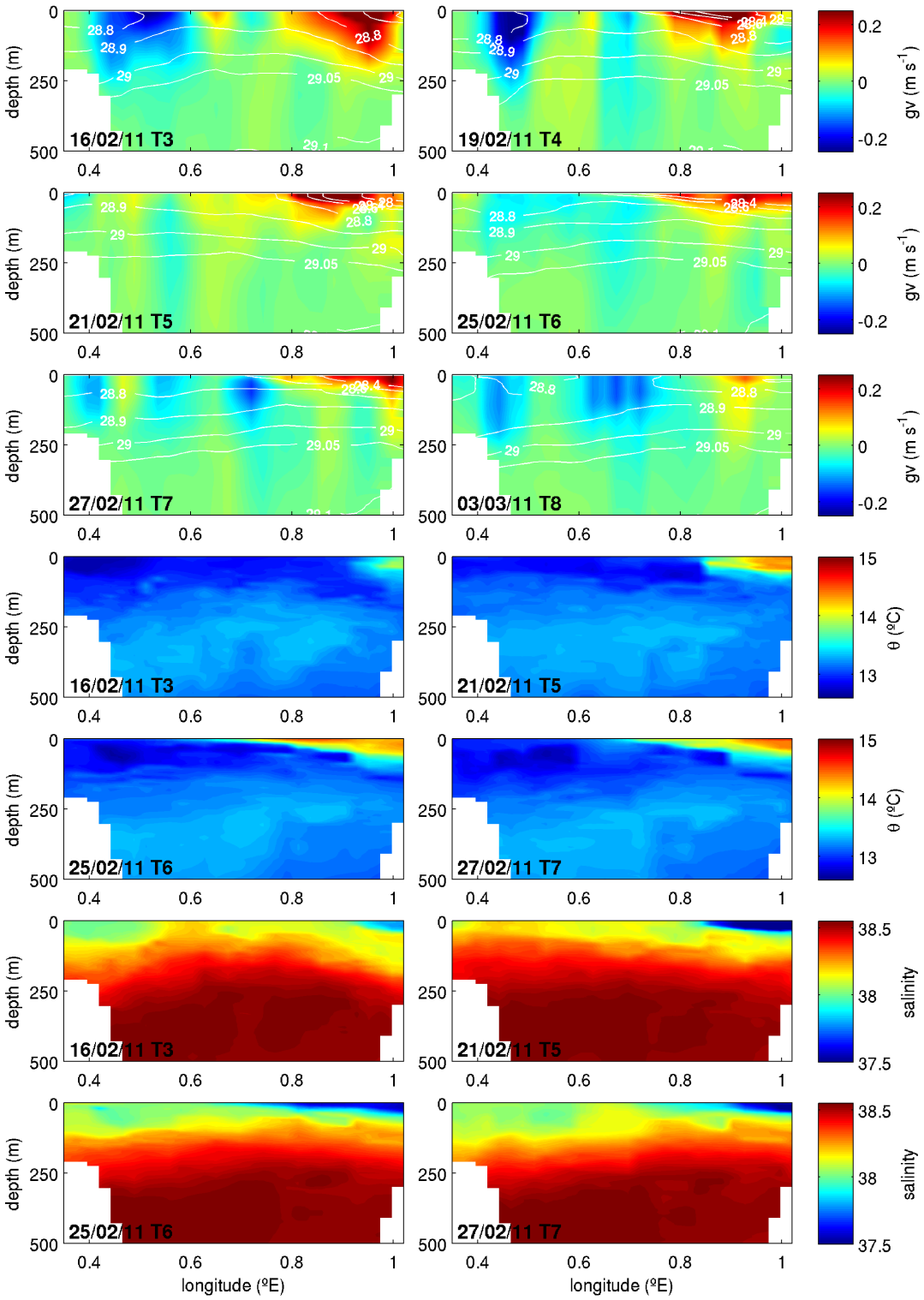

Figure 12a. Geostrophic velocity (gv), potential temperature (θ) and salinity sections for canalesFeb2011. The transect numbers and mean date are marked in the bottom left of each panel, geostrophic velocities northward are positive and southward are negative, and selected isopycnals are marked in white.

The structure is no longer visible in T6 (25/02) and transport is again of order -0.5 Sv southward. Cold WIW is visible in patches in the surface 100 m, associated with flows of the NC extend across the channel to 0.8°E and have a stream-like appearance in geostrophic velocity, from T6 to the end of the mission in the IC, T8 (03/03). This stream like appearance is perhaps an indicator of flow interference from mesoscale structures and again there could be a small vortex structure, centred at 0.45°E, in T7. In θ/S two distinct WIW minima are visible, with salinities of 38.0 and 38.2, which are associated with the entrance of specific lenses of WIW into the channel (e.g. in T7). At the start of the mission the inflows of fresh AW are of a similar volume to January, of order +0.5 Sv, from T6 these inflows reduce to +0.1 Sv in T8. The θ/S plot (fig. 12b) again indicates that there is an inter sub-basin exchange of water mass, with distinct mixing lines between the colder southward flowing WIW and AWo and LIW and the fresher AW inflows.

MC: As in January, in T1 (11/02) a layer of lower salinity AW (37.2 to 37.8) lies across the surface of the MC, to depths of 50 m. However the isopycnals dome upwards in the surface 100 m and the geostrophic velocity indicates a paired outflow/inflow structure, centred at 2.0°E that penetrates to depths of ~200 m. The transport of water masses in and out of the sub-basin is relatively evenly balanced (+0.38/-0.34 Sv) suggesting, with the other features, that this could be a cyclonic eddy or paired inflow/outflow. However as the outflows are located away from the more usual shelf edge location, an eddy is perhaps the more likely explanation.

Summary: In the February mission there is evidence of mesoscale activity in the channels, a small eddy of order 10 km in the IC, appeared to interrupt the flow of the NC over 2 to 3 days with a decrease in transports of order 0.5 Sv, and there was a cyclonic eddy in the MC. Strong inflows of fresher AW continue in the east of the IC, with the same range of salinities as in January. The MC appears to be partially 'blocked' by this cyclonic eddy and the water masses predominantly re-circulate, as suggested by the even pattern of transport in and out of the Balearic sub-basin. Distinct WIW minima appear in the IC, with different temperature/salinity characteristics, which evolve through successive transects as distinct lenses or bodies of WIW appear in channel, suggesting that we could be observing WIW from distinct formation events as it crosses the IC 'choke' point.

Note: this mission was concurrent with the ships mission RADMED_0211, the ship and glider data concur and a detailed comparison between the contemporaneous ship and the glider transects is available in Appendix D. The difference made by the higher temporal and spatial resolution of the glider sampling is apparent in this comparison.

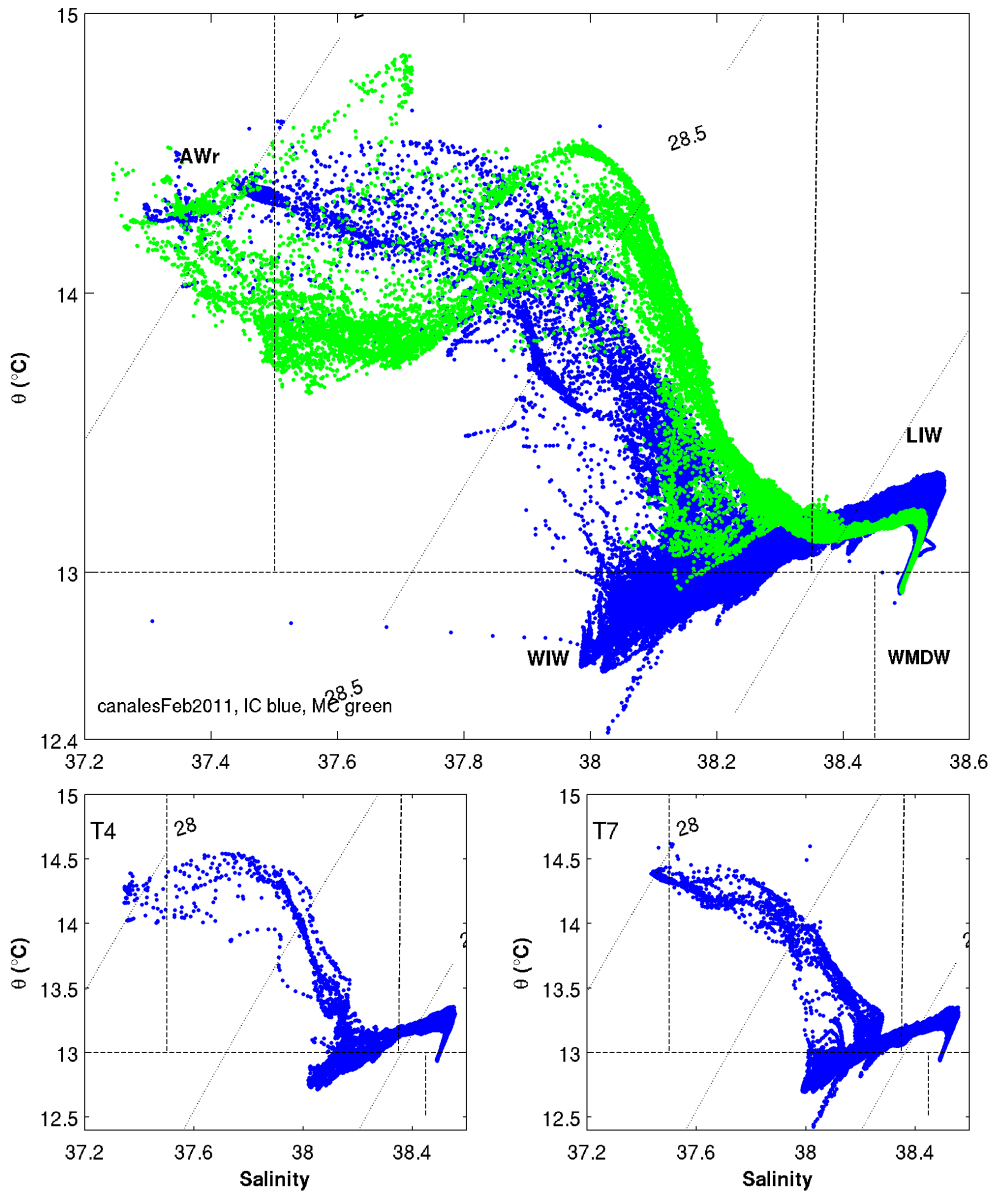

Figure 12b. θ/S plots for canalesFeb2011.

The IC transects are marked in blue and the MC transects in green. The lower panels show details of the fresher AW inflows (T3) and WIW salinity minima (T7).

canalesMar2011

IC: In T3 (26/03) there is an uneven sub surface temperature minimum layer (θ 12.6 to 12.8 °C) at 100 m, associated with small scale perturbations in the isopycnals (fig. 13a). In salinity and density two larger dips can be seen between 0.6 and 0.7°E and 0.9 and 1.0°E (with S 38.05 to 38.1 and σ 28.8 to 28.9 kg m^{-3}). In geostrophic velocity paired velocity structures of diameter ~22 km are visible, suggesting 2 anticyclonic eddies with velocities of order 15 - 20 cm $s^{-1}$and penetrating to depths of ~250 m, with WIW (θ 12.6 to 12.8 °C and S 38.1) lenses at their core. Around these 2 eddies are filaments of negative velocity, suggesting that streams of the NC continue to flow southward, this is reflected in the water transport with a stronger component of southward flow, -0.71 Sv versus +0.44 Sv, northward. The fresher AW Inflows (S ~37.4), as seen in January and February, are reduced but continue on-shelf in the east. In T4 (29/03) and T5 (01/04) the eastern WIW lens (θ 12.6 °C and S 38.05 to 38.1) increases and deepens and the eastern eddy increases in strength and moves west to be centred at 0.8°E. The western eddy is weaker and no longer clearly visible, although the NC still appears to be at least partially blocked, fig. 13a and b. In T6 an eddy structure centred at 0.6°E occupies much of the channel and in T7 (10/04) the larger eastern eddy is again clearly visible with a cold core of WIW (θ 12.6 °C and S 38.05 to 38.1), having now increased in strength and size to a structure of diameter 38 km, with velocities 20 to 30 cm s^{-1}, and with associated dips in the σ 28.9 kg m^{-3} isopycnal of order 100 m (fig. 13a). In SST from 01/04/2011 an eddy like structure is clearly visible in the east of the channel, see fig. 13c. In the west of the channel in T7 there are strong southward velocities associated with cold WIW (fig. 13a); this could be a remnant of the western eddy, the southward side augmented by the NC and with the inflows on shelf, or alternatively, the NC flow with a weaker on-shelf counter current. The water volume transports in the channel indicate NC flows, with a stronger southward transport of -1.2 Sv compared to +0.6 Sv flowing northward, e.g. -0.6 Sv of net southward (NC) flow. In support of this pattern, in SST southward flows of colder water are visible from the Gulf of Lion to the IC (fig. 13c), with some evidence of inflows on shelf. The inflows of fresher AW are either low, as in T3 and T7, or not present, as in T4 to T6, blocked by the eastern eddy, see fig. 13b.

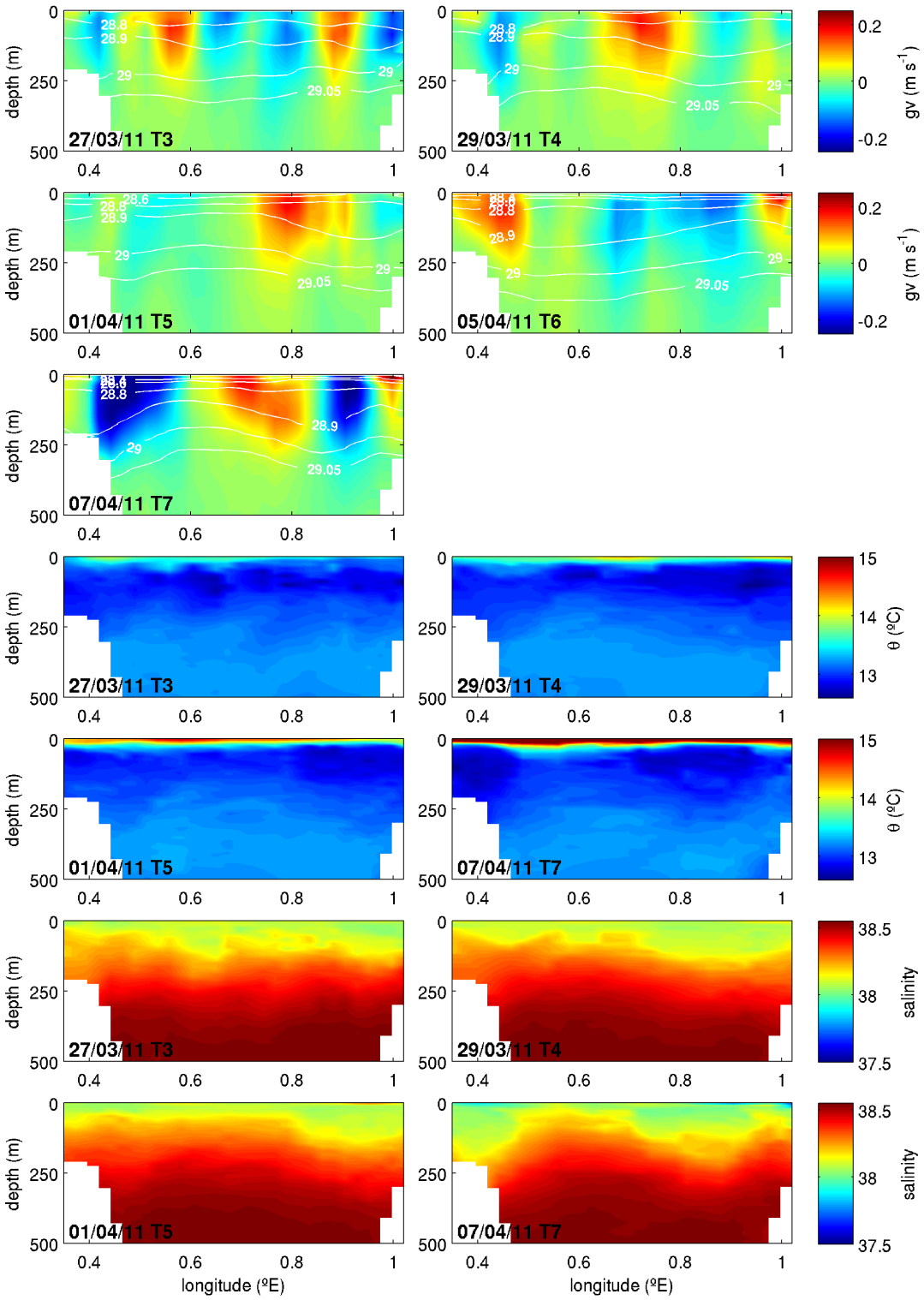

Figure 13a. Geostrophic velocity (gv), potential temperature (θ) and salinity sections for canalesMar2011. The transect numbers and mean date are marked in the bottom left of each panel, geostrophic velocities northward are positive and southward are negative, and selected isopycnals are marked in white.

MC: In T1 (20/03) inflows of a low salinity water mass (S ~37.4) are concentrated in the southwest from on-shelf to mid channel (1.9°E) and, as previously, a low salinity surface layer is visible across the channel. The inflows are of order 20 cm s^{-1} with transport northward of +0.47 Sv, the outflows weaker -0.23 Sv and on-shelf in the northeast (see Appendix G).

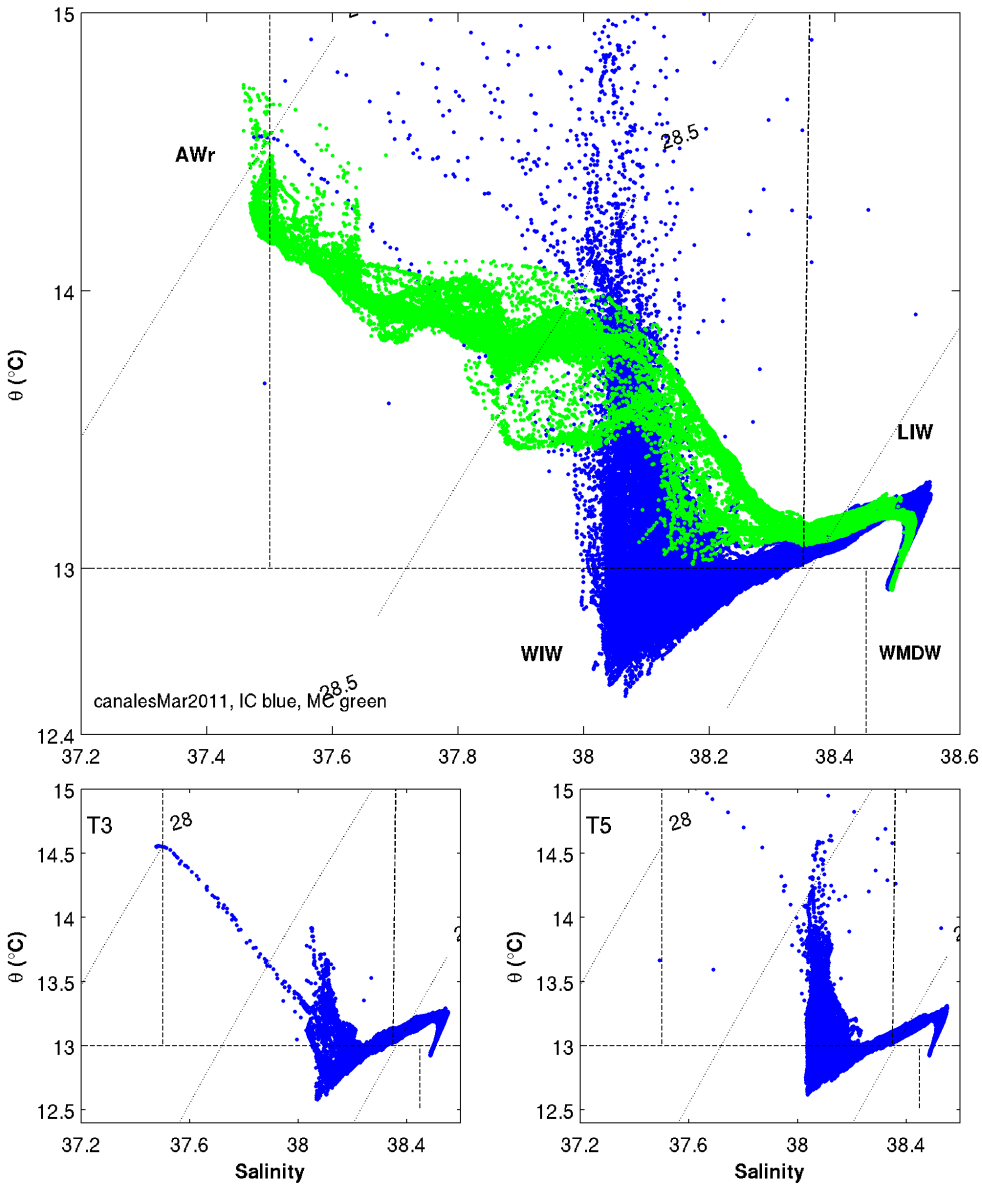

Figure 13b. θ/S plots for canalesMar2011.

The IC transects are marked in blue and the MC transects in green. The lower panels show fresher AW inflows (T3) and the WIW minima associated with the temperature minim layer and lower salinity lenses of the anticyclonic eddies, and, no fresher inflows (T5) with a slightly more fresh WIW minima. The fresher inflows that do occur in T3 are a close match to those inflowing through the MC (green in upper panel).

Summary: In March and April 2011 the IC is dominated by mesoscale activity associated with sub surface lenses of WIW, that impede both the AW inflows northward and the flow of the NC southward. The IC is partially blocked by two anticyclonic cold-core WIW eddies, that change position and strength during the mission; the eastern eddy increases in size from 22 to 38 km width and moves west to be centred at 0.8°E, while the western eddy perhaps leaves the channel or moves on-shelf between T4 and T5. In T6 the NC is reinstated, transporting -0.6 Sv of water south, while in the east an anticyclonic eddy re-circulates water mass volumes of order 0.6 Sv. In the MC fresher surface waters continue to inflow. There are some fresh AW inflows in the IC however they are for the most part blocked, see θ/S plot in fig. 13b, although there is some evidence of continued inflows on-shelf.

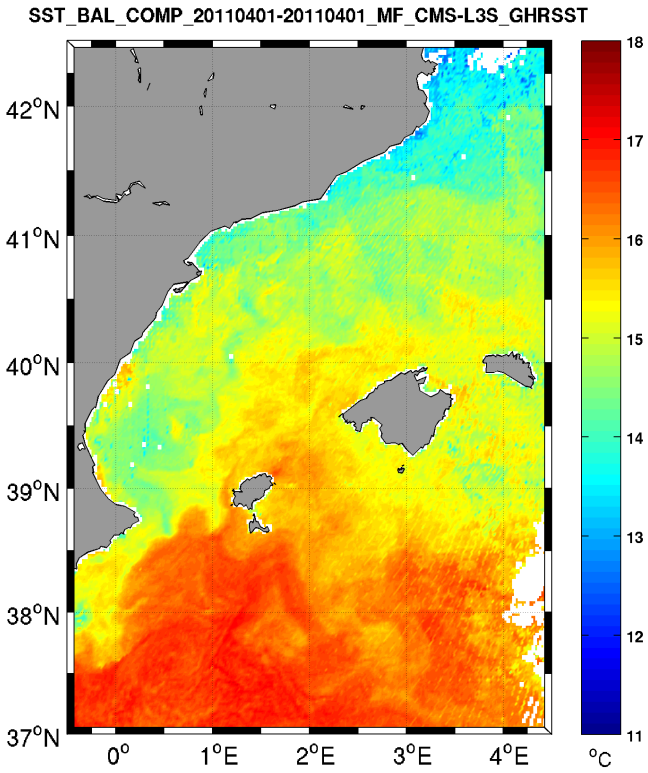

Figure 13c. SST for 01/04/2011, from GHRSST.

canalesMay2011

IC: In T3 (10/05) there is again a strong NC, with southward transport of -1.2 Sv and a gradient of 7.3 x 10^{-3} (Δz/Δx 190 m/25 km) as the isopycnals tilt down to the western channel edge. In the east there is a dip in the isopycnals centred at 0.8°E and between 50 to 200 m (σ 28.8 – 28.9 kg m^{-3}), then from ~1.0°E the isopycnals slope to the eastern channel

edge (fig. 14a). An anticyclonic structure is visible in geostrophic velocity associated with the dip (0.65 to 0.95°E), reaching depths of 200 m and with a diameter of ~35 km and associated geostrophic velocities of order 10 to 15 cm s^{-1}. This structure has a cold temperature minimum core (θ 12.8 °C at 150 to 200 m) and could be a remnant of the eastern anticyclonic eddy seen in March (there is some similarity in the characteristics of this water mass, θ 12.8 °C S ~38.1). There is a shallow, surface to 20 m depth, inflow current at ~1.0°E. Due to problems with the salinity in T4 (13/05) the data for the central section of the channel is not usable[7]. However based on the data that is available it appears likely that the anticyclonic eddy has left the channel and there is now a central doming of the isopycnals centred at 0.7°E. In T5 (16/05) this central doming structure is clearer and stronger (the $\Delta z/\Delta x$ gradient of the isopycnals in the west changing from 4.5 x 10^{-3} T4 to 5.5 x 10^{-3} T5), uplifting the AW/LIW interface in the centre of the channel and penetrating to 400 m depth (fig, 14a). The geostrophic velocity and transport values suggest a strong channel wide paired velocity structure, centred at 0.7°E, with geostrophic velocities of order 30 cm s^{-1}, which transports +0.84 Sv and -0.81 Sv in and out of the sub-basin. This is perhaps a cyclonic eddy or a type of balanced inflow/outflow exchange, occurring perhaps as temporary adjustment to the departing of the eastern eddy present in T3 to T4, as in T6 (19/05) this structure has passed out of the channel (fig. 14a). In T6 the NC is reinstated, transport southward is again -1.2 Sv, and, although the transect is short in the east[8] it appears that the isopycnals flatten after 0.62°E. Interestingly filaments of cold, low salinity water appear to be coming from the western shelf area, perhaps accounting for a second WIW minima (θ 12.9, S 38.0) that that appears in θ/S in T6 (fig. 14b). A shallow inflow current of order 20 m depth is a persistent feature at ~1.0°E across T3, T4 and T5, and in T5 there are fresher salinities (S 37.2 to 37.7) present above the thermocline (0 to 20 m) associated with this inflow (fig. 14b). There are also similar inflows on shelf in the west of the channel and some evidence that these fresh inflows are present in T4.

[7] Between 0.65 and 0.95°E in T4 there is considerable spiking in the salinity data at the thermocline which renders this section of transect un-usable. The spiking is reminiscent of the thermal lag/capacity induced mismatch between temperature and salinity measurements as described in Chapter 2. One possible explanation is that the glider CTD had a temporary blockage, for example small piece of debris that impeded the flow and caused a mismatch between the waters sampled by the temperature and salinity sensors, before being flushed out. The length of the section affected, in comparison to the features studied, means that infilling with nearby profiles would be unrealistic. It is coincident with the eddy observed in the T3. The data to the west, east and below 200 m in the centre section, that are usable and from this it is possible to infer the pattern of features in θ, S, σ and geostrophic velocity. This section was not however suitable for use in the transport of water mass analysis.

[8] Transect T6 extends to 0.9°E

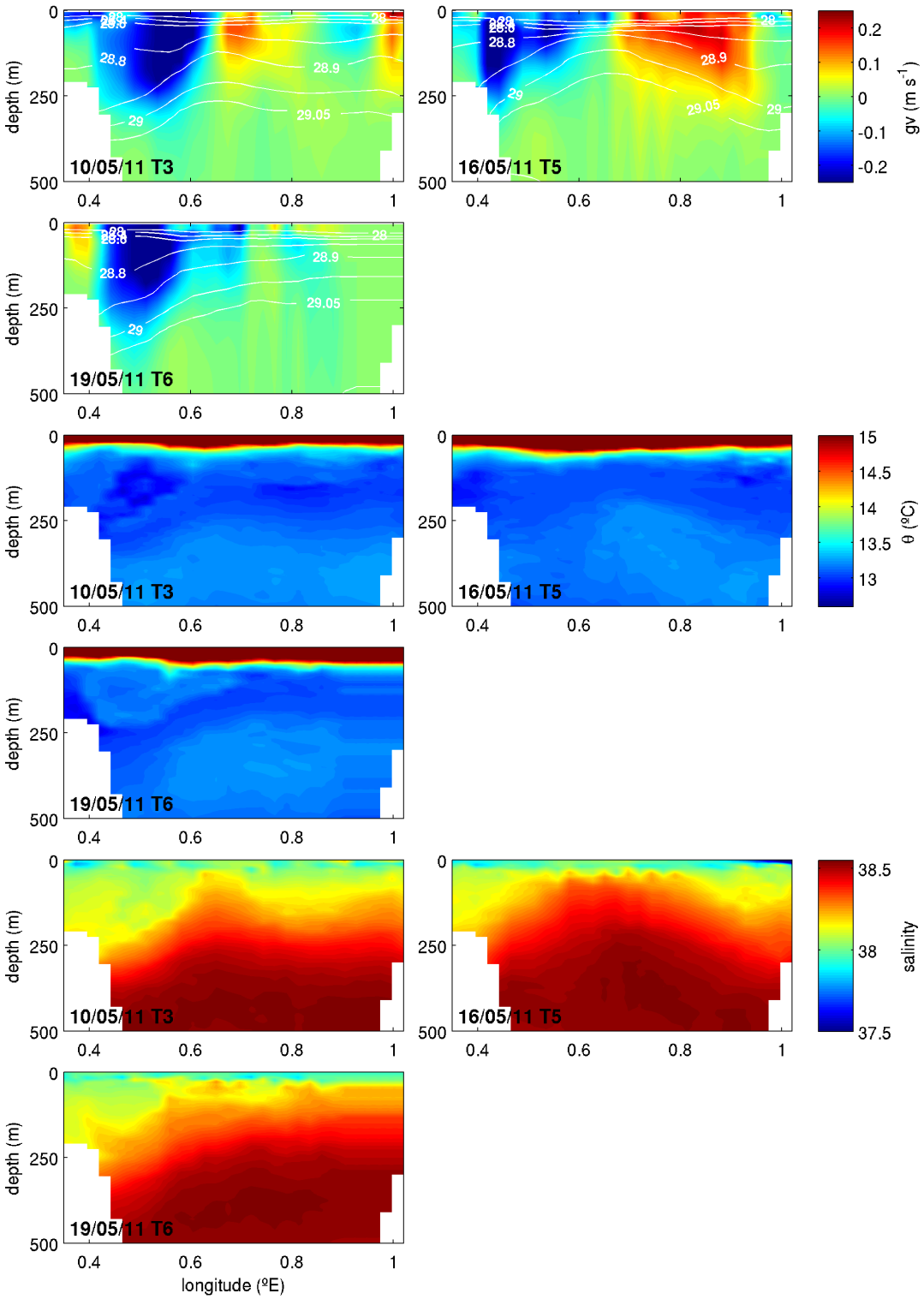

Figure 14a. Geostrophic velocity (gv), potential temperature (θ) and salinity sections for canalesMay2011. The transect numbers and mean date are marked in the bottom left of each panel, geostrophic velocities northward are positive and southward are negative, and selected isopycnals are marked in white.

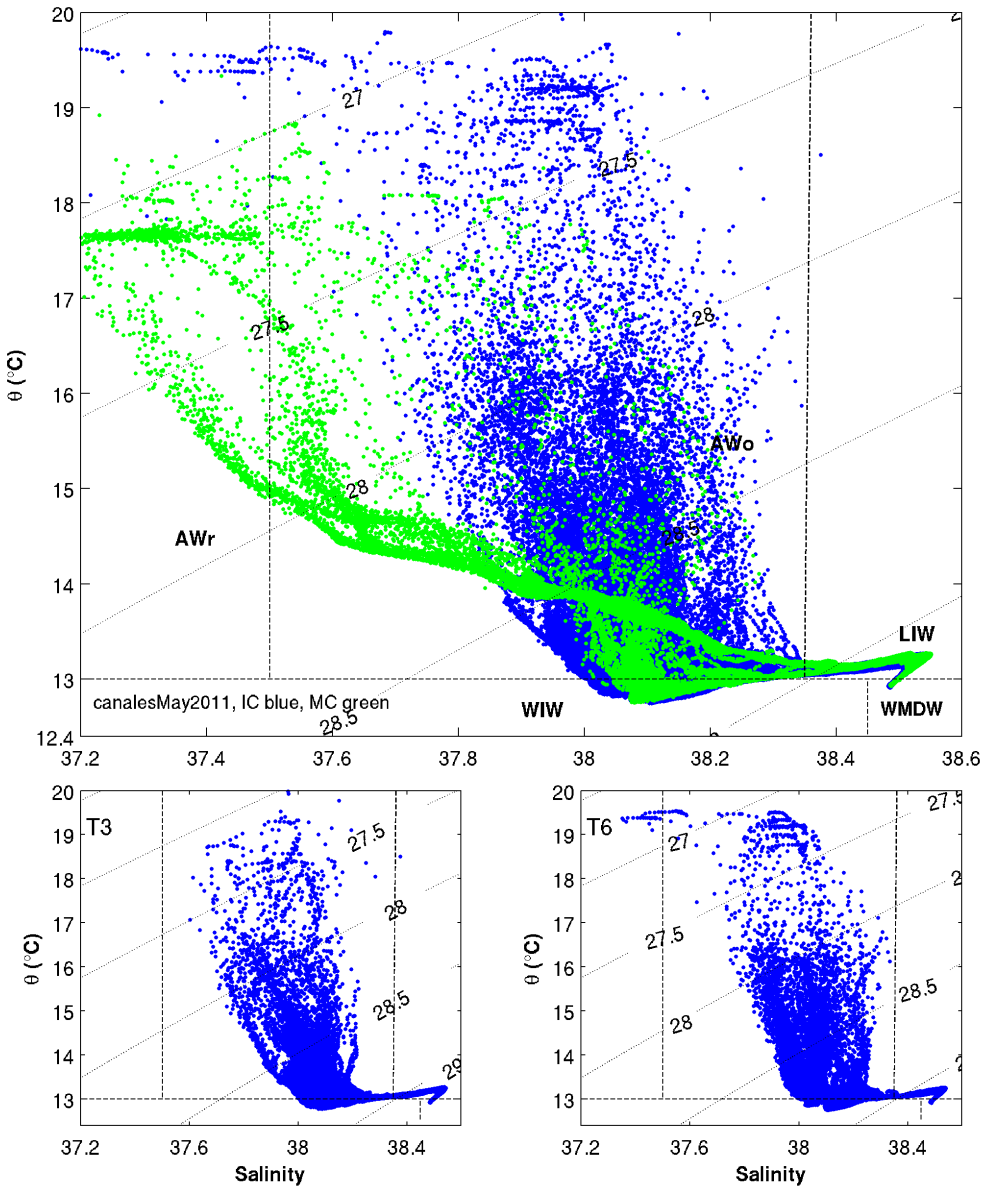

Figure 14b. θ/S plots for canalesMay2011.

The IC transects are marked in blue and the MC transects in green. The lower panels show the single WIW temperature minima (T3) and the double minima (T6). Visible in the MC data are 'crossed' mixing lines indicating that a north-south exchange is occurring through the channel, there is one mixing line from WIW to AWo, representing the mixing of waters of northern origin, which is crossed by mixing line from LIW to AWr, representing the mixing of waters of southern origin. WIW does not often outflow through the MC.

MC: In T1 (05/05)**,** as previously, there is a lower salinity fresher AW layer across most of the channel, with salinities of 37.2 to 37.7. This layer is deeper in the in the northeast, penetrating to depths of ~60 m, shallowing 10 to 20 m depth in the southwest (1.7°E). At ~200 m depth a thin and patchy temperature minimum later is visible in the southwest of

the channel from 1.8°E to the channel edge. Geostrophic velocity inflows of order 20 cm s^{-1} occur in the northeast, from mid-channel (~1.9°E) to the channel edge, and penetrating to 120 m depth. Weaker outflows, of order 10 cm s^{-1}, are associated with the patchy WIW on-shelf in the southwest. The transport values reflect this pattern, with inflows of +0.35 Sv and outflows of -0.22 Sv. Two strong mixing lines are visible in θ/S, one from WIW to cooler surface waters and the other from LIW to fresher, warmer surface waters, which clearly demonstrate that a north/south exchange of water mass is occurring through the MC (fig. 14b, upper panel in green).

Summary: In the IC the patterns visible in θ, S and geostrophic velocity suggest a complex interplay between mesoscale and basin-scale processes. It seems possible that the eastern eddy, as seen in March, has endured in the channel over a timescale of 1.5 to 2 months (its time of arrival is unknown). The NC is present with transports of order -1.2 Sv, possibly interrupted for 3 to 6 days as the anticyclonic eddy passes from the channel and a strong cyclonic circulation briefly replaces it. The inflows of fresher AW, seen in the earlier missions continue through the MC, but are blocked through the IC at the start of the mission (T3). Later in T4 and T5, some very superficial (0 to 20 m) fresher AW inflows occur in the east and west of the IC.

canalesJun2011

IC: In T3 (08/06) the NC is visible in the sections of geostrophic velocity as a negative (southward flowing) current, extending from 0.35 to 0.5°E, partially on-shelf in the west and penetrating to 200 m depth. In T4 (11/06) an upward doming in the isohalines and isopycnals, from 70 to 200 m, suggests a small cyclonic structure with diameter of order 10 km has formed, perhaps associated with the weak NC at the channel edge (fig. 15a). In T5 (14/06) this feature shifts west to occupy the channel edge and the weak NC moves into the channel, centred at 0.6°E and carrying low temperature (subsurface temperature minimum) waters southwards (fig. 15a). In T6 (17/06), although the isohalines show an upwards doming at the western channel edge the isopycnals no longer show this structure and generally slope down towards the eastern channel edge from 0.5°E (fig. 15a).

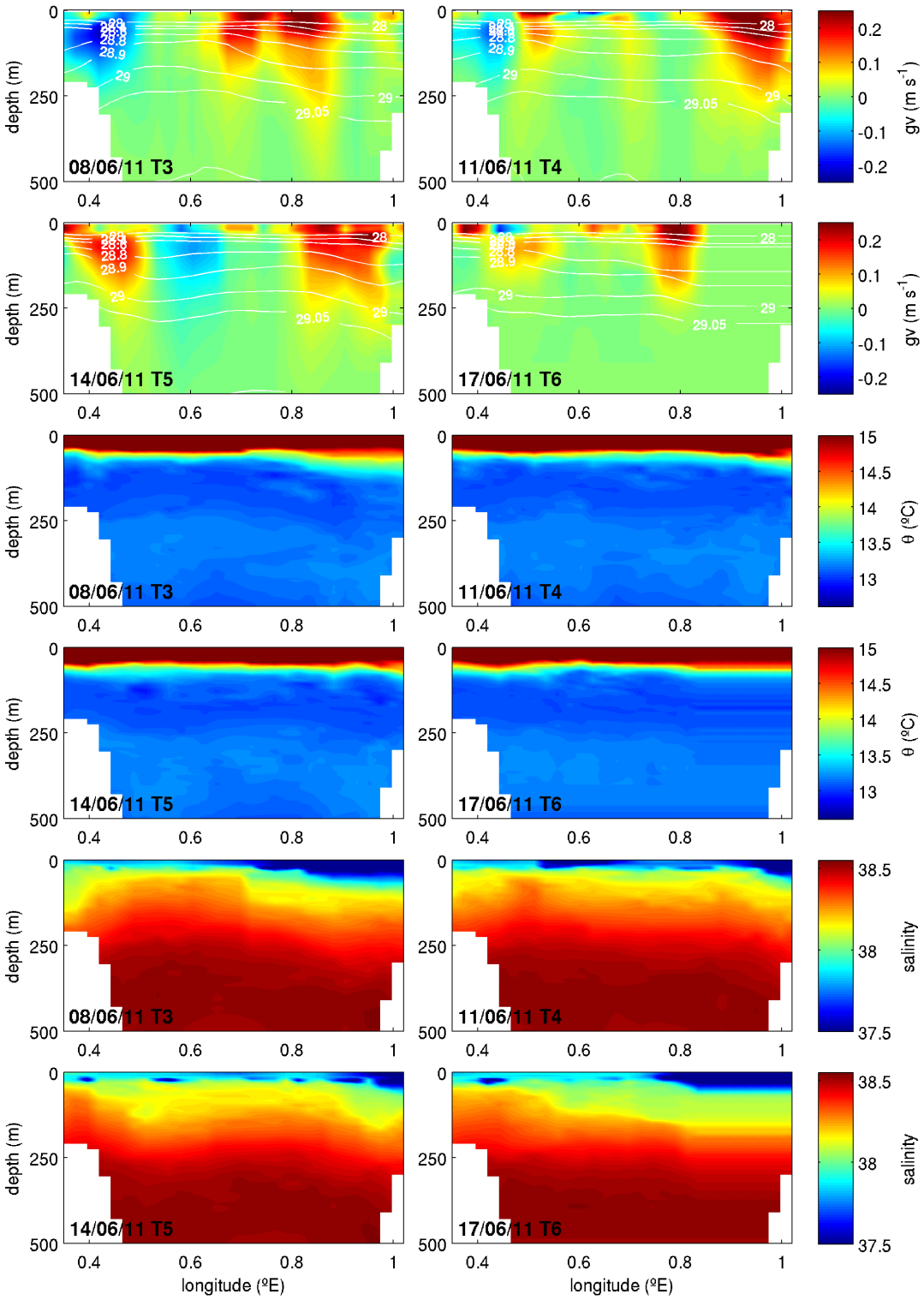

Figure 15a. Geostrophic velocity (gv), potential temperature (θ) and salinity sections for canalesJun2011. The transect numbers and mean date are marked in the bottom left of each panel, geostrophic velocities northward are positive and southward are negative, and selected isopycnals are marked in white.

The AW inflows appear to be strong and to have moved west to occupy the central and eastern part of the channel[9]. In θ/S there are strong and distinct mixing lines from WIW (θ 12.8 °C, S 38.1) to the surface and from LIW to fresher AW surface waters (S ~37.6), indicating a distinct inter sub-basin exchange of water masses. There is now very little WIW (θ < 13.0 °C) present in the IC (fig. 15b). Across the mission there is a consistent inflow of order +0.8 Sv, the inflow current is initially located in the centre of the channel, in T3 0.7 to 0.9°E, and then in T4 to T6 the current is in the east, extending from 0.8°E to the eastern channel edge and penetrating to depths of 300 m (deeper than in previous months). There are fresher AW inflows in the surface 0 to 70 m of this current, with salinity in the range 37.2 to 37.7 (fig. 15b). A weak and shallow NC is present in the west of the channel consistently across the mission, visible in the shallow westward tilt of the isopycnals, with gradient of order of 7.0 x 10^{-3} ($\Delta z/\Delta x$), from 0.5°E to the western channel edge. In T3 (08/06) and T4 (11/06) the inflow current has maximum geostrophic velocity of order 40 cm s^{-1}, the outflows are half this velocity and more shallow.

MC: In T1 (03/06) there is a temperature minimum layer across the channel between 100 and 300 m, thickest in the southwest. Again fresher AW (S 37.2 – 37.7) lies across the surface from 0 to 50 m depth. The channel is split between stronger deeper outflows in the southwest (two streams, one on shelf and one at the southwest channel edge to 300 m depth and with geostrophic velocities of order 20 cm s^{-1}) and shallower inflows in the northeast (to 100 m, again in two streams or filaments, off-shelf and on-shelf reaching geostrophic velocities of 25 cm s^{-1} on-shelf), and the associated transport values are -0.72 and +0.19 Sv respectively (see Appendix G for sections). There does not appear to be the same strong signature of an inter sub-basin exchange in the MC. The mixing line now extends from WIW to fresher AW inflows, suggesting that the fresher waters are to the north of the MC and form part of the outflow through this channel (fig. 15b).

Summary: In June there is a shift from an outflow to an inflow dominated pattern of transport/exchange in the IC, the isopycnals slope down the eastern edge of the channel from 0.7°E with a shallow tilt in the isopycnals, with gradient of ~3.6 x 10^{-3} ($\Delta z/\Delta x$), for NC at the western shelf edge (fig. 15a). Across the mission the exchange/transport of water masses north and south is consistent, with strong inflows transporting +0.8 to +0.9

[9] Transect T6 is short (0.8°E) and the glider only sampled to 400m depth. Although not suitable for the calculation of transport we can use the 0 to 400 m sections of θ, S, σ to infer the structure present in the channel.

Sv northward and weak NC outflows transporting -0.2 to -0.3 Sv southward. An upward doming of isohalines and isopycnals, between 50 and 150 m at the edge of the western edge of the channel in T3, relates to small cyclonic feature that appears to influence the location of the weak NC flows.

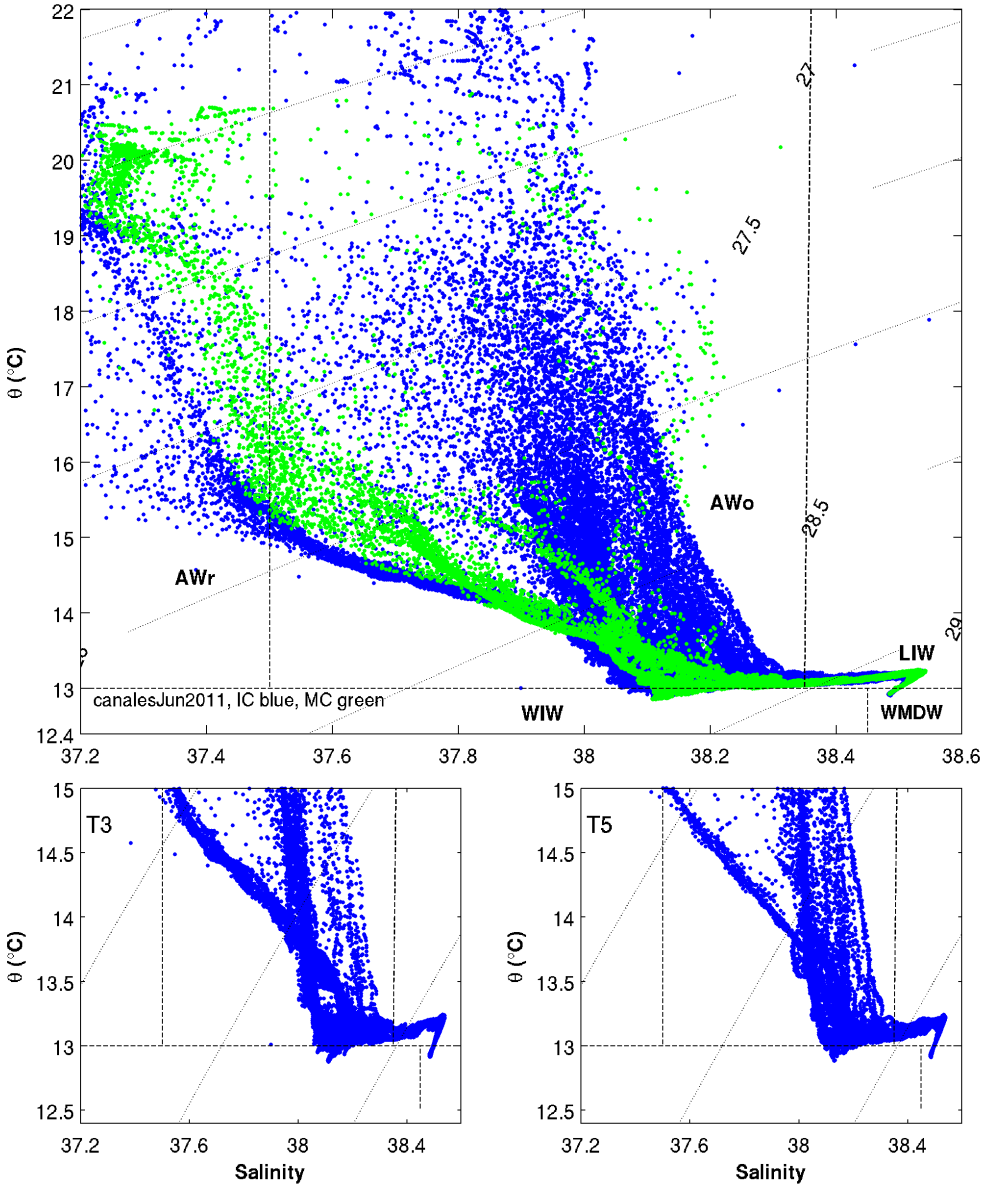

Figure 15b. θ/S plots for canalesJun2011.

The IC transects are marked in blue and the MC transects in green. The lower panels show the strong crossed mixing lines (T3) and (T5), between inflows (LIW to fresher AW) and outflows (WIW to more saline AWo), the IC and MC are closely matched in the water mass characteristics of the inflows (upper panel).

The AW inflows appear to have been active for the entire period of the glider observations, January to June 2011. In the IC these fresher AW inflows occur in the surface from 0 to 70 m and were substantially interrupted by eddies in March and early May, however inflows continued through the MC. The water mass characteristics of the outflows in the MC and contemporaneous satellite imagery (see fig. 13c and discussion in Chapter 5) suggest that this fresher AW lies to the north of the MC throughout this period. Although the IC and MC are clearly connected in terms inflows of water masses, the MC does not reflect the same water mass in outflow and in 2011 little WIW appeared to pass out of the Balearic Basin through this channel. In addition, the fresher AW does not always reach the threshold salinity for AWr ($S \leq 37.5$), particularly in the IC.

After a successful initial 6 months of glider operations SOCIB encountered a period of repeated mission failures, resulting in a 8 month gap in the glider mission record (see Table 2 and discussion in Chapter 6 for more details).

3.2 Glider missions 2012

canalesMar2012

To date this is the only 'canales' mission undertaken with a Seaglider. These gliders travel more slowly in the horizontal than Slocum gliders and although the mission commenced at the end of March 2012, the glider reached the IC in mid April. It should also be noted that the time taken to transect the IC is longer.

IC: In April a large (diameter ~70 km), deep (to the full depth of the channel) and strong (velocities of order 40 cm s^{-1}) anticyclonic eddy occupied the width of the deep central section of the IC: this eddy is clearly visible in the sections of geostrophic velocity for T3 (11/04) and T4 (16/04), fig. 16a. At the core of the eddy there is a large temperature minimum lens (θ ~13 °C) with salinity ranging from 38.2 to 38.4, and the eddy has core velocities of order 40 cm s^{-1} with 5 cm s^{-1} at depths of 400 m. The isopycnals bow down to the full depth of the channel and the LIW maxima are pushed down by ~250 m in the centre. The core of this eddy is more homogeneous and warmer than the colder, patchier WIW seen in 2011 and the salinities associated with core are 0.2 PSU more saline than the low temperature water masses observed in 2011 (compare figs. 12b and 16b). Filaments of colder WIW (θ 12.6 to 12.8 °C) are visible on the east and west sides of the base of the core (fig. 16a) and in θ/S as colder WIW that mixes up to a θ ~13 °C rather than to the

surface (fig. 16b, T4). This strong anticyclonic eddy recirculates +1.30 and -1.48 Sv of water mass north and south respectively and has a strong surface expression (θ ~14.5°C, at least 1° colder than the surrounding surface water) that one would expect to be able to pick up in SST. In T3 (11/04) in the east there are some shallow, 0 to 40 m, on-shelf inflows of less saline waters (S 37.6 - 37.8), these are not observed in T4 (16/04) and the difference between the transects can be seen in θ/S, see fig. 16b. In both transects there are surface waters, from 0 to 40 m and between 0.4°E to 0.5°E, with slightly fresher salinities of 38.0, as compared to salinities of 38.2 associated with the eddy. These could represent lower salinity waters from the south of the IC that are brought into the channel with the north flowing side of the eddy, fig. 16a and b.

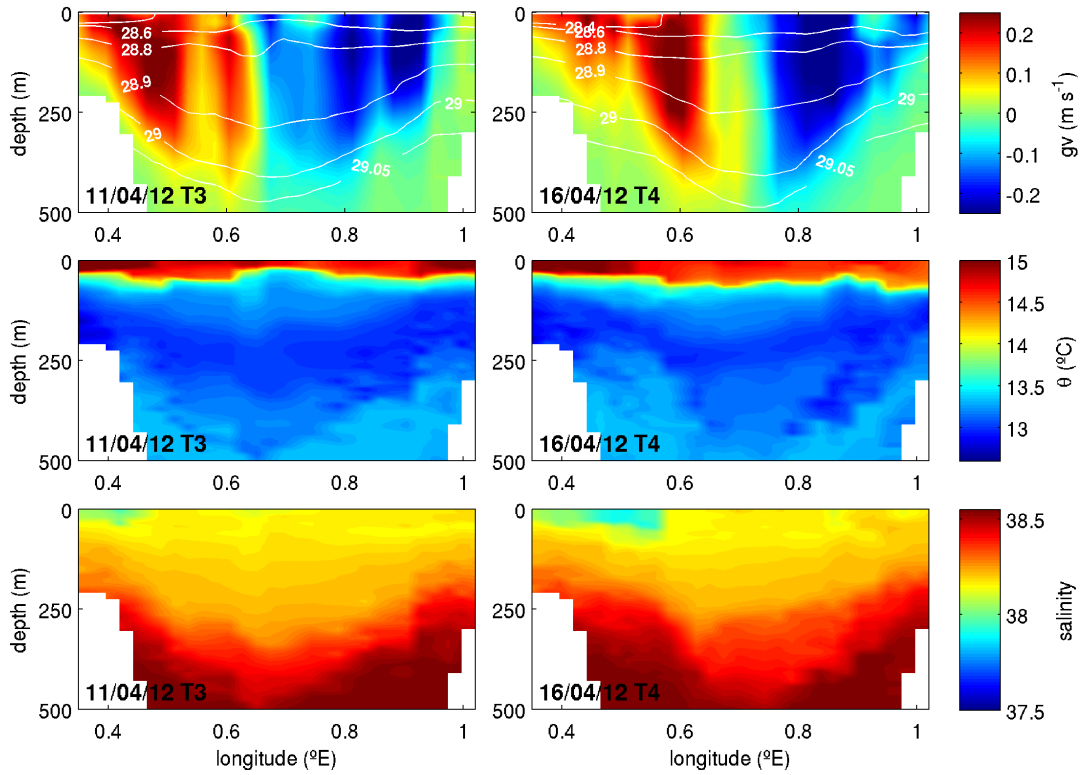

Figure 16a. Geostrophic velocity (gv), potential temperature (θ) and salinity sections for canalesMar2012. The transect numbers and mean date are marked in the bottom left of each panel, geostrophic velocities northward are positive and southward are negative, and selected isopycnals are marked in white.

MC: In T1 (29/03) there is a small temperature minimum WIW lens (θ < 12.8 °C and S ~38.25) at ~200 m and located mid-channel, between 1.8 and 1.9°E. This is associated with a dip in the isohalines that does not however translate to a signature in the isopycnals, which remain relatively horizontal across the channel. Fresher waters are visible in the

surface 0 to 40 m in the northeast, with salinities of 37.7 (fig. 16b) and which are associated with shallow inflows of order 10 to 15 cm s^{-1} (see Appendix G for sections).

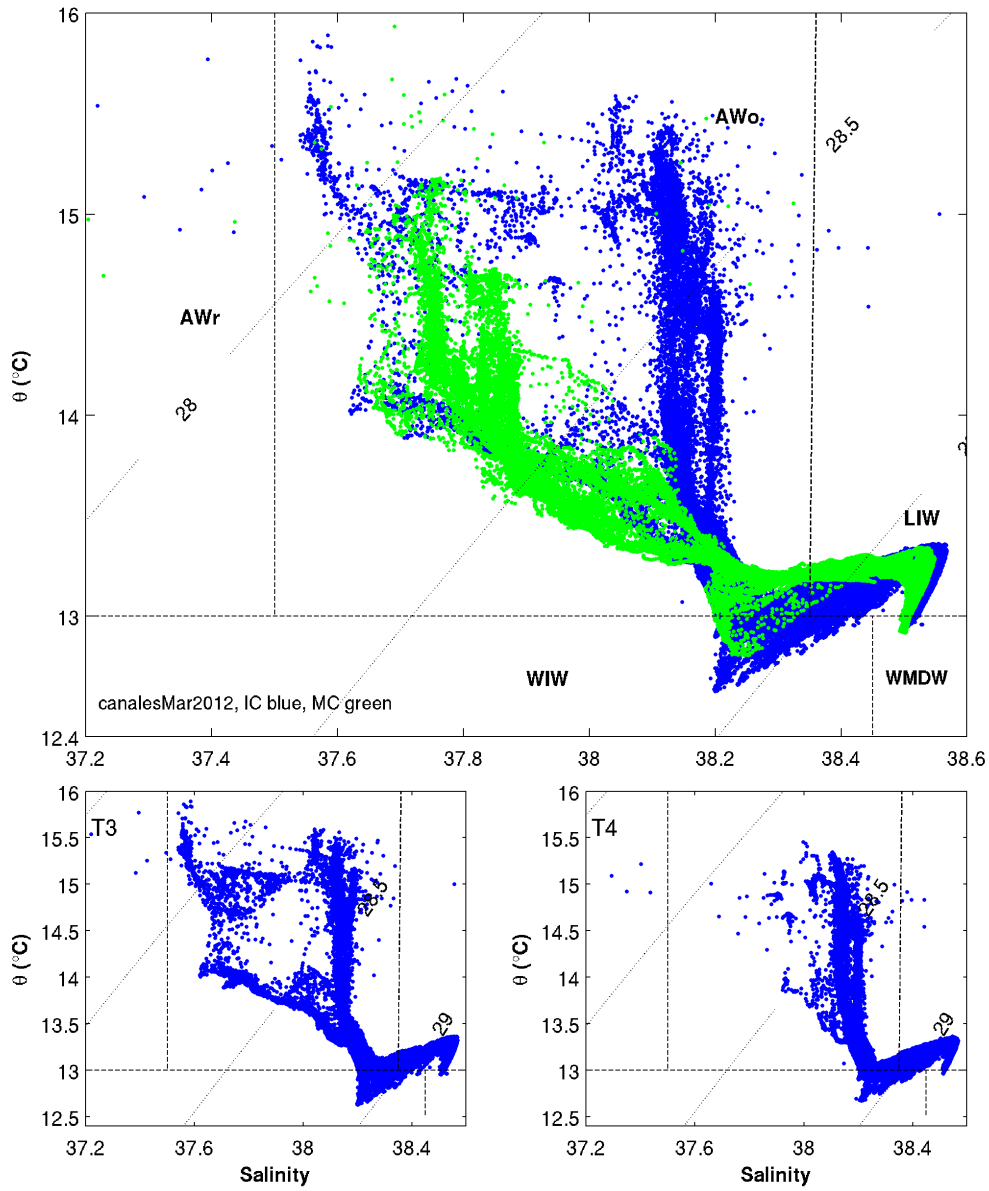

Figure 16b. θ/S plots for canalesMar2012.

The IC transects are marked in blue and the MC transects in green. The lower panels show T3 and T4, in the surface the 38.0 salinity waters from the west of the channel can be seen, as can the 37.6 lower salinity inflows in the east in T3, which have the same characteristics as inflows through the MC (upper panel, green).

Summary: A large cold core temperature minimum anticyclonic eddy occupied the IC in April 2012, blocking the path of the NC and probably also of weak and only slightly fresher inflows. These inflows are not as strong or as fresh as those observed in 2011,

lowest salinities are 37.6 to 37.7 as compared to 37.2 to 37.4 in 2011. However as previously, the same water mass is visible inflowing through the MC and the IC, fig. 16b. This clearly represents a distinct water mass, indicating that there is some sub-basin exchange, the salinities however not reaching the fresher levels associated with AW of 'more recent Atlantic origin'.

It should be noted that both the surface AW and intermediate WIW flowing south are 0.2 PSU more saline than in 2011 (compare figs. 12b and 16b), therefore it is possible that these inflows represent AWr mixed with saltier outflows, but more likely that they represent waters that are more local in origin inflowing from the south, that are not of 'more recent Atlantic origin'.

canalesMay2012

IC: In T3 (15/05) there is a temperature minimum layer below the thermocline, between 100 and 200 m, and at the base of this, at 200 to 300 m, the interface to the LIW layer is uneven leading to perturbations of order 50 m in the isopycnals (fig. 17a). In the west there is a small downwards tilt of the isopycnals from 0.5°E to the western channel edge, between depths of 100 to 400 m with a gradient of order ~4.0 x 10^{-3} ($\Delta z/\Delta x$). This signals a weak sub-thermocline NC, centred just off the western shelf edge at 0.45°E and with geostrophic velocity of order 10 cm s^{-1}. The perturbations give rise to some weak 2 to 3 cm s^{-1} banding in geostrophic velocity across the centre of the deep channel, possibly representing weak eddies centred at 0.65°E and 0.95°E. There are also some 0 to 40 m surface inflows in the east of the channel at ~1.0°E. The pattern is similar in T4 (19/05), however the perturbations are stronger and reach greater depths. The weak NC, transporting -0.4 Sv southward, is still visible at the western channel edge and in the centre a weak anticyclonic paired velocity structure is more strongly visible in geostrophic velocity between 0.6 and 0.8°E, penetrating to 200 m depth and with velocities of order 5 to 10 cm s^{-} (fig. 17a). In the θ/S plot there are two distinct, near vertical, mixing lines from WIW to the surface with salinities of 38.2 and 38.3 (fig. 17b), but there is no distinct mixing line for inflows as in the previous mission. In T5 (22/05) there is a fairly homogeneous central water mass (θ 13 °C, S 38.3 to 38.4) lying in a layer between depths of 100 to 300 m and the LIW maxima below this are depressed by ~100 m. However the isopycnals remain horizontal and the pattern of flow is similar to that in T4, with a weak sub-surface NC

visible in the west. In θ/S two distinct WIW minima emerge, at 38.25 and 38.35 (fig. 17b, lower panels T3 and T5).

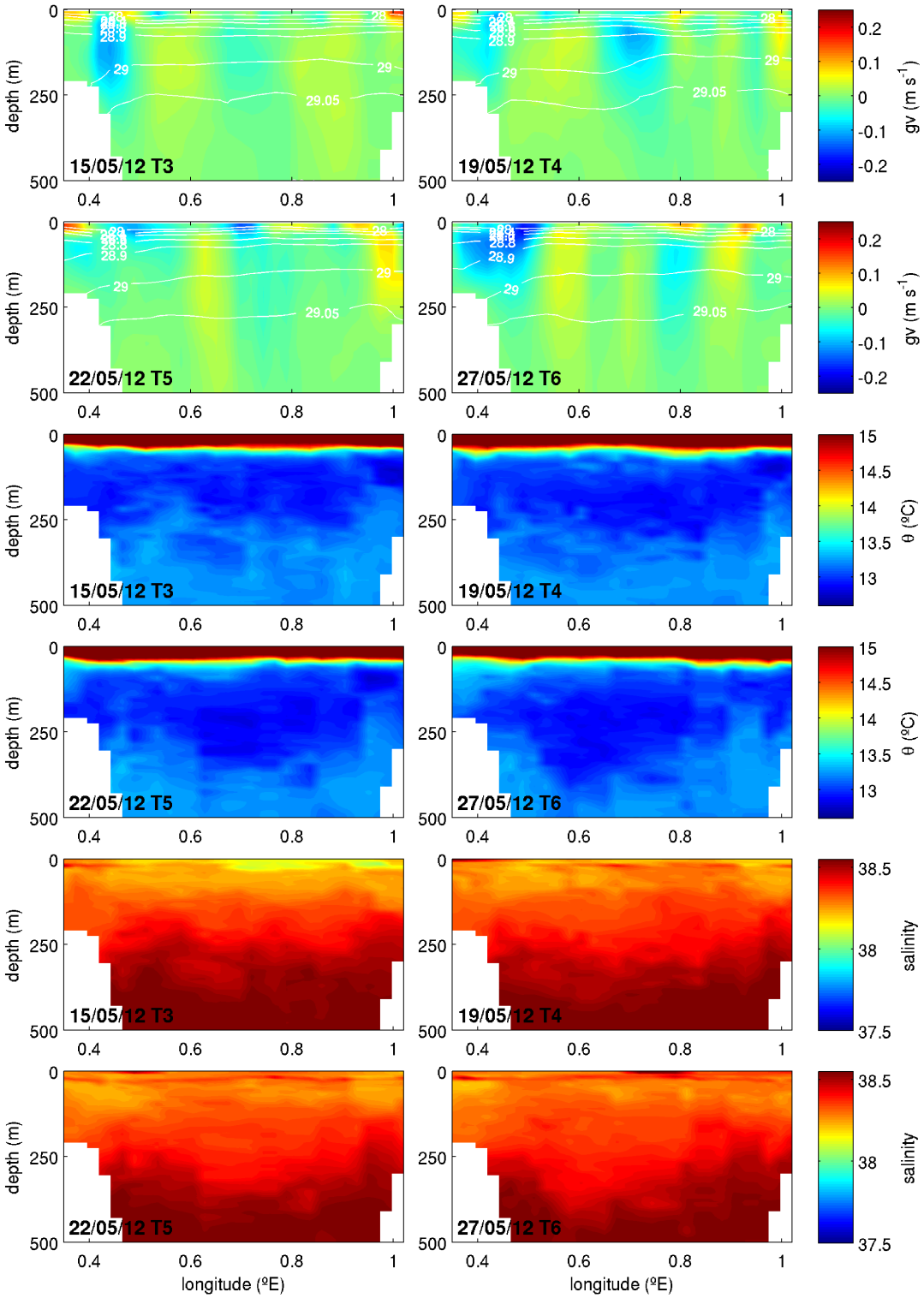

Figure 17a. Geostrophic velocity (gv), potential temperature (θ) and salinity sections for canalesMay2012. The transect numbers and mean date are marked in the bottom left of each panel, geostrophic velocities northward are positive and southward are negative, and selected isopycnals are marked in white.

The picture is similar in T6 (27/05) with a central layer of homogeneous water mass, however in the west of the channel there is a stronger NC, signalled by the steeper tilt of the isopycnals to the western channel edge and transport southward of -0.49 Sv, there is again also some weak velocity banding across the centre of the channel.

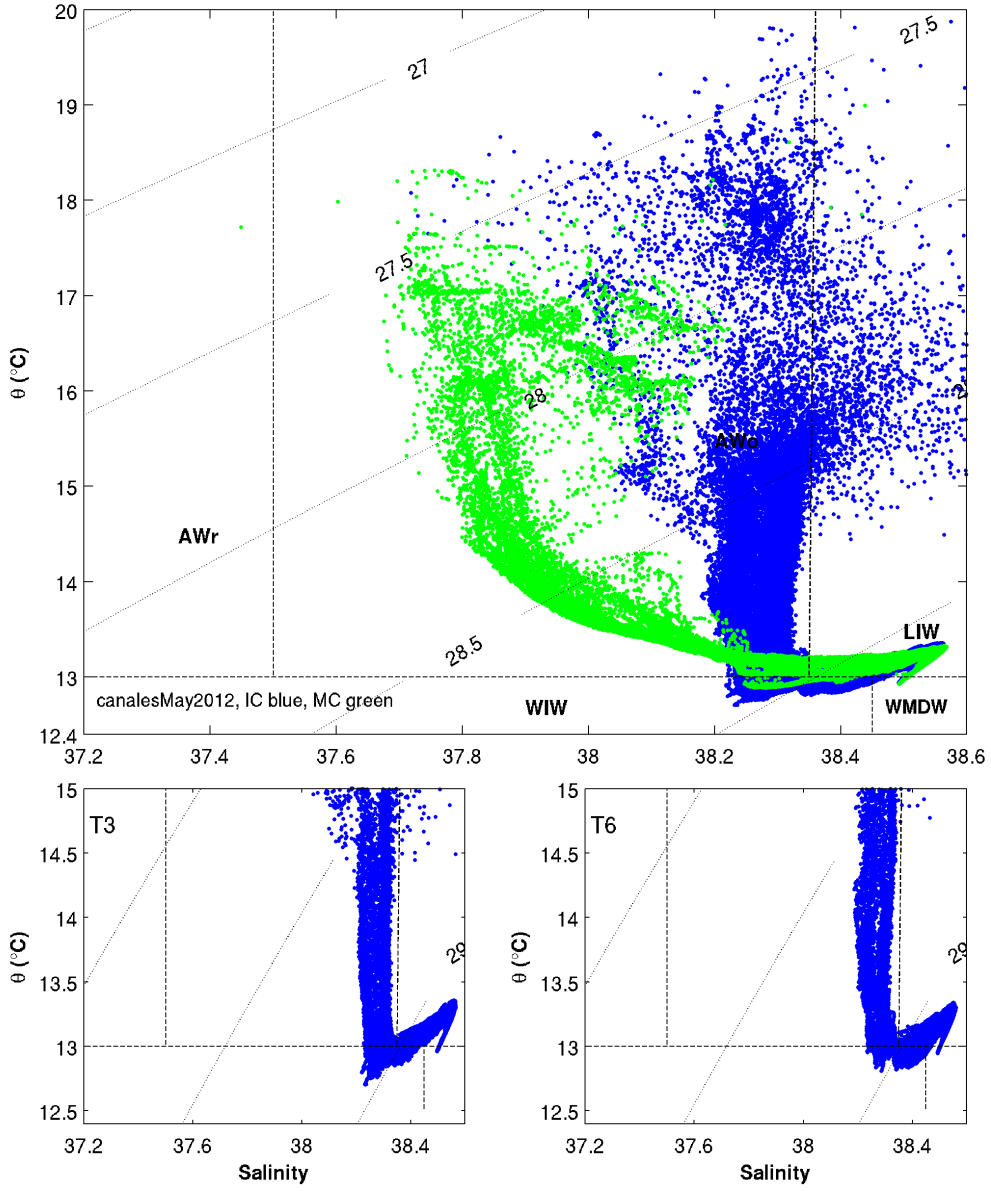

Figure 17b. θ/S plots for canalesMay2012.

The IC transects are marked in blue and the MC transects in green. The lower panels show the distinct vertical mixing lines at 38.25 and 38.35 in T3 and T5. Inflows through the MC (upper panel, green) are distinct and fresher than the southward flow through the IC. The difference in salinity of the southward flow between May 2012 (38.2 to 38.35) and May 2011 (38.1 to 38.2) should be noted (compare with fig. 14b).

MC: In T1 (10/05), at the start of the mission, there is a temperature minimum lens located at ~200 m in the centre of the channel (1.8 to 2.0°E) and the LIW layer is pushed down by 100 m (see Appendix G for sections). The LIW layer is also banked up against the south western channel edge to 250 m and the isopycnals tilt towards the east from 1.7 to 1.8°E. This is associated with a relatively strong inflow current, between 1.75 to 1.9°E and transporting +0.66 Sv northward, which is paired with a weak on-shelf counter current to the southwest. The main mixing curve is from LIW to surface waters of salinity 37.8 and although this is not as fresh as the AW of 'more recent Atlantic origin' seen in 2011, it is however distinct from the more saline AW now flowing south in the IC with salinities in the range 38.2 to 38.35 (see fig. 17b). In this mission the IC and the MC show the same pattern of salinities, inflows however are occurring through the MC only.

Summary: It is possible that the central homogeneous water mass could be the remnants of the large anticyclonic eddy seen in March, that instead of passing through the IC has remained, lost energy and became stratified, and could be partially blocking the channel and causing the mesoscale perturbations. A weak NC outflows in the west, below the thermocline and with transports of order -0.3 to -0.4 Sv, with some weak re-circulated flow. The MC has inflows of a fresher water mass, however these waters do not have the same fresh range of salinities seen in 2011.

canalesJul2012

IC: In T3 (16/07) the isopycnals tilt down to the east channel edge denoting an inflow current and in geostrophic velocity a broad inflow is visible at the eastern edge of the deep channel, to depths of 200 m and with strong surface velocities of 40 cm s^{-1} (fig. 18a). In the west of the channel there is some indication of a weak NC. In θ/S there is one vertical mixing line to the surface with salinities of 38.2 and another mixing line to 14.5 °C with a lower range of salinities (fig. 18b, upper panel in blue and lower panel T3). The pattern is similar in T4 (20/07) although both NC and inflows weaken. In T5 (23/07) the inflow current strengthens and shallows then in T6 (27/07) deepens again to 300 m with possibly 2 streams (located at 0.75°E and at 0.9°E) and the isopycnals tilt from 0.75°E to the eastern channel edge with a shallow gradient of approximately 3.6 x 10^{-3} ($\Delta z/\Delta x$). The NC is weak and shallow, with flattened gradients in the west, however a low 5 cm s^{-1} flow consistently shows along the shelf break across the four transects, resulting in a transport southward of between -0.15 to -0.2 Sv. The inflows are also relatively consistent ranging

from +0.45 to +0.60 Sv, they are not however associated with AW of the fresher salinity ranges associated with waters of more recent Atlantic origin (see fig. 18b).

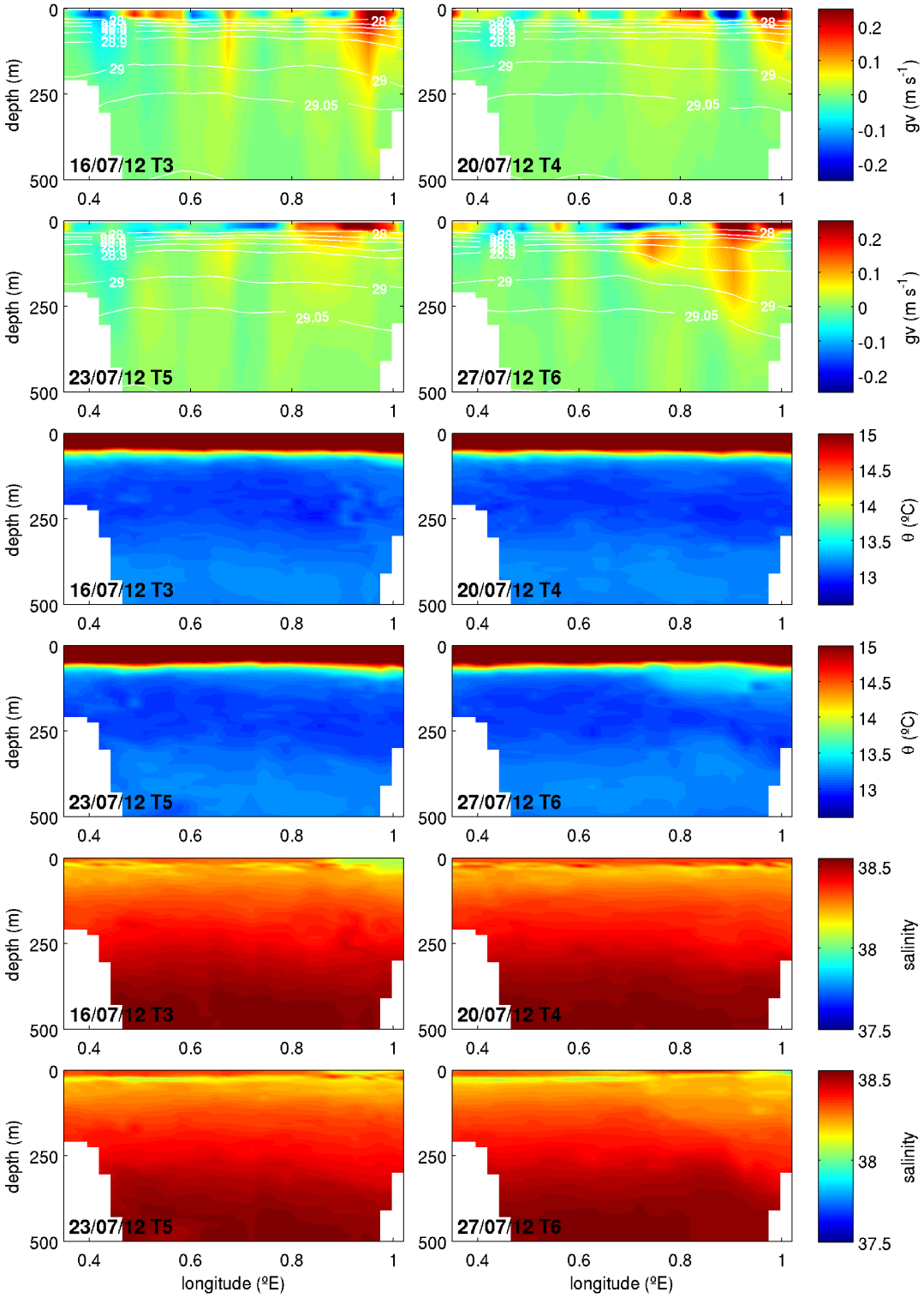

Figure 18a. Geostrophic velocity (gv), potential temperature (θ) and salinity sections for canalesJul2012. The transect numbers and mean date are marked in the bottom left of each panel, geostrophic velocities northward are positive and southward are negative, and selected isopycnals are marked in white.

There is evidence in θ/S however of a lower temperature water mass, with salinities of 38.0 to 38.1 (fig. 18b, lower panels), that could be associated with a patchy subsurface temperature minimum layer between 150 and 300 m.

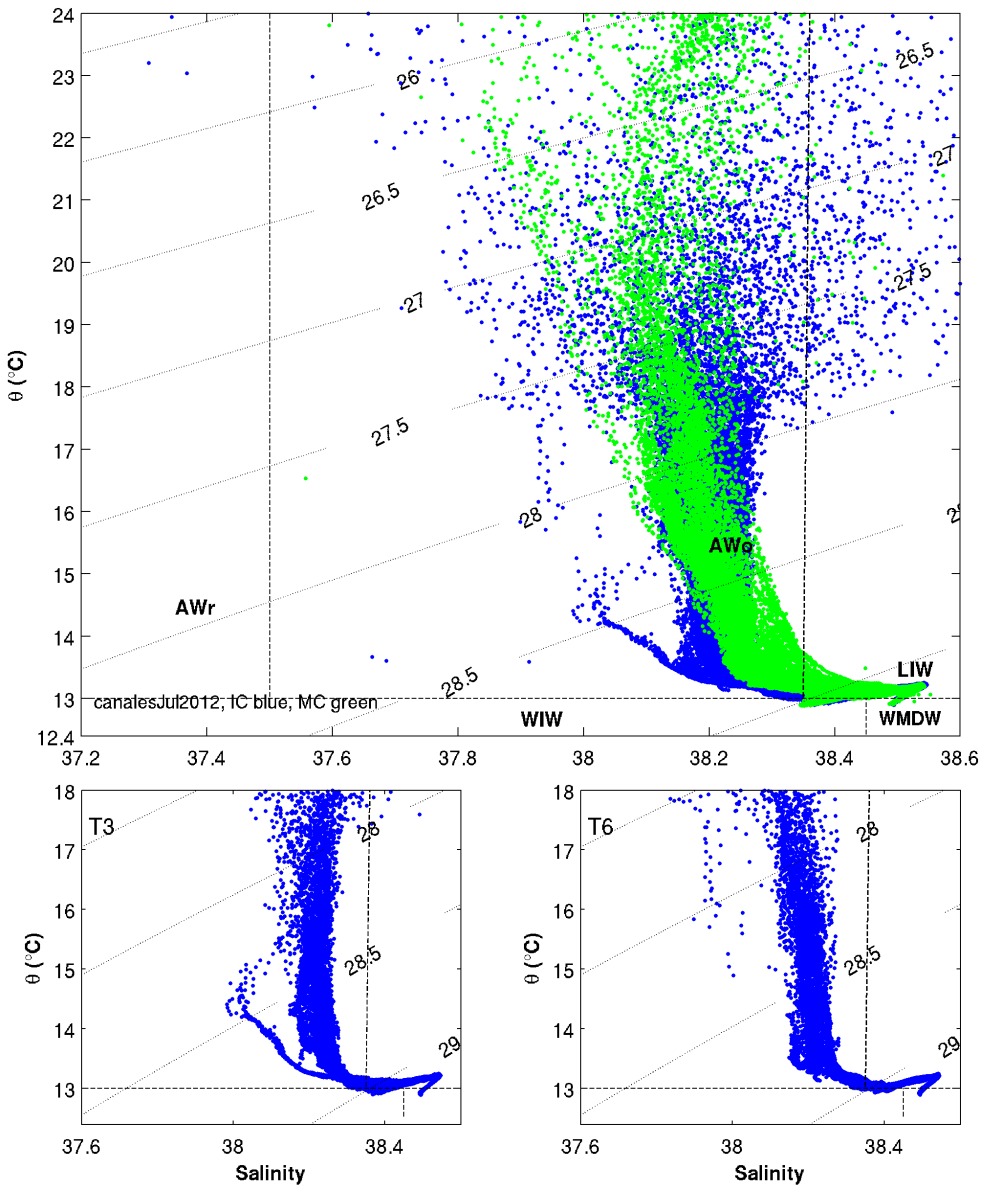

Figure 18b. θ/S plots for canalesJul2012.

The IC transects are marked in blue and the MC transects in green. The strong inflows through the IC (upper panel, blue) are not associated with a fresher AW. A slightly fresher water mass (S 38.0 to 38.1) is associated with θ of 13 to 14.5 °C and visible in T3.

MC: In T1 (10/07) the isopycnals dip to the southwest below the thermocline indicating outflows, however there is also an upward doming in isohalines and isopycnals, centred at 1.9°E, which suggests that there could also be a cyclonic structure present in the MC. In geostrophic velocity flows of order 10 to 20 cm s^{-1} appear paired, centred at 1.9°E and penetrating to depths of 200 m, however the outflow is greater with transport of -0.42 Sv vs. +0.22 Sv for the inflow, indicating perhaps an outflow current of order -0.2 Sv and 0.2 Sv of eddy re-circulation. There is an uneven temperature minimum layer at around 250 m depth below the outflows. In T8 (30/07), 20 days later, the structure seen in T1 remains, but is reduced, as are the associated geostrophic velocities and transports (see sections in Appendix G).

Summary: In July there are the strong inflows that are not associated with a fresher AW of 'more recent Atlantic' origin. There is a thick temperature minimum layer and the IC and the MC are generally consistent in terms of the water masses present. The inflows have been fairly consistent since March, although blocked in May in the IC.

Note: As discussed in Chapter 2, the point of inflexion for Slocum gliders is programmed to be 20 m with the glider programmed to surface every 6 hours for a position fix. This means that in the deep channel the glider generally completes 2 or 3 dives before re-surfacing and thus full 'surfacing' profiles are of order 6 km apart, and thus the surface 0 to 20 m has a lower sampling resolution than the remaining depths. With strong seasonal thermocline, such as in July 2012, located at around 20 m this can lead to banding in geostrophic velocities between surfacing profiles and some disconnect between the surface 20 m and below. It should however be noted that there is also a genuine disconnect above and below the strong summer/autumn thermocline, which makes this surface 0 to 20 m difficult to interpret, as it is a mix of sampling and a genuine disconnection between features above and below the strong seasonal thermocline.

canalesAug2012

IC: In T4 (30/08), late August, a complex sub-surface eddy structure is visible, in a bowing down of the isohalines and isopycnals in the centre of the channel, between 0.6 to 0.7°E, from below the thermocline to 500 m and the LIW maxima are depressed by some 200 m in the centre (fig. 19a). In geostrophic velocity this appears as a paired anticyclonic

structure with velocities of order 10 to 20 cm s^{-1} centred at 0.6°E. The core of this structure is stratified, with salinities ranging from 38.2 to 38.4.

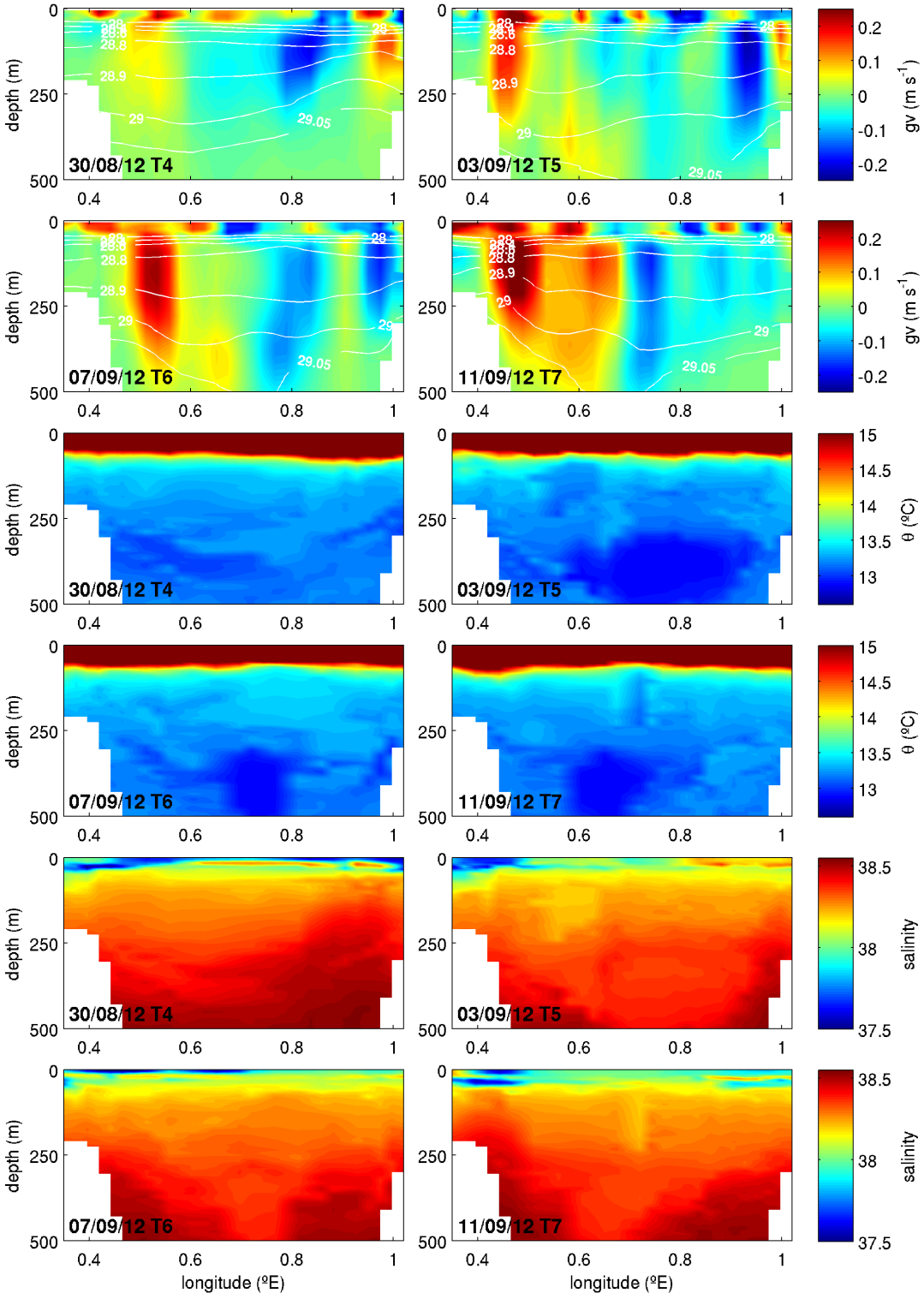

Figure 19a. Geostrophic velocity (gv), potential temperature (θ) and salinity sections for canalesAug2012. The transect numbers and mean date are marked in the bottom left of each panel, geostrophic velocities northward are positive and southward are negative, and selected isopycnals are marked in white.

To the east of the channel, ~0.9°E, there is an uplifting of isohalines and isopycnals towards the surface and an associated uplifting of the LIW maxima. In the west of the channel, from 0.2 to 0.5°E (on-shelf to the channel edge), and in the east, from 1.0 to 1.1°E, lower salinity waters (with S 37.2 to 37.8) are visible below the thermocline to 70 m depth and from 0 to 70 m depth respectively (fig. 19a). In θ/S two mixing lines are visible; one vertical to the surface with salinities of order 38.25 and another from LIW to a sub surface θ 18 °C and S 37.4 water mass, signifying distinct patterns of mixing for the inflows of less saline AWr (see fig. 19b, lower panel T4). In the west the inflows are associated with the north flowing side of the eddy, in the east with an eastward tilt to the channel edge in the isopycnals and isohalines from a peak centred at 0.9°E (fig. 19a). In T5 (02/09) at the start of September, the westerly low salinity (S 37.4) waters are still present, associated with the north flowing side of the eddy. The dip in isohalines and isopycnals has moved east and become more complex, with two dips visible the isopycnals between depths of 100 to 400 m and centred at 0.6 and 0.9°E. The westerly dip is associated a cohesive lens of water mass with salinity 38.4 lying between 100 and 250 m. Below this, from 300 to 500 m, lies a broad low temperature (θ ~13 °C, S 38.35) lens of water mass, associated with a broad dip in the isopycnals centred at 0.7°E. In geostrophic velocity the eddy appears to have moved eastwards to be located more centrally, with some vertical shear in the velocities around 0.6°E and at 200 m depth. In T6 (07/09), 9 days after the start of the IC transects, a cold WIW core to this eddy structure appears in the centre of IC between 0.6 to 0.7°E and at a depth of 300 to 550 m (fig. 19a). This core is associated with salinities of 38.35 to 38.4 (see fig. 15b, lower panel T6) and velocities strengthen to 20 to 30 cm s^{-1}. The eddy now penetrates to depths of 500 m and in the centre of the channel the LIW maxima are pushed down by 300 m. There is still some evidence of the two dip structures in the isohalines at between 100 and 200m. In T7 (11/09), the last transect, the eddy fully occupies the channel to 600 m depth and the northward velocities reach 50 cm s^{-1} (fig. 19a), the velocities southward are less, ~25 cm s^{-1}, and the LIW salinity maxima is pushed to the base of the channel. In T6 and T7 there are fresher waters (S 37.4 to 37.6) in the surface 0 to 50 m, with a lower salinity core in the west of the channel situated above the north flowing side of the eddy (fig. 19a) and another in the east, as seen in the earlier transects. In the sections of geostrophic velocity the northward and southward flows of this eddy can be seen to change over the course of the mission, stronger southward in T4 and T5 and for T6 and T7 stronger northward, this difference is reflected in the transport values, which change from +0.43/-0.76 (T4) to +1.41/-0.92 (T7).

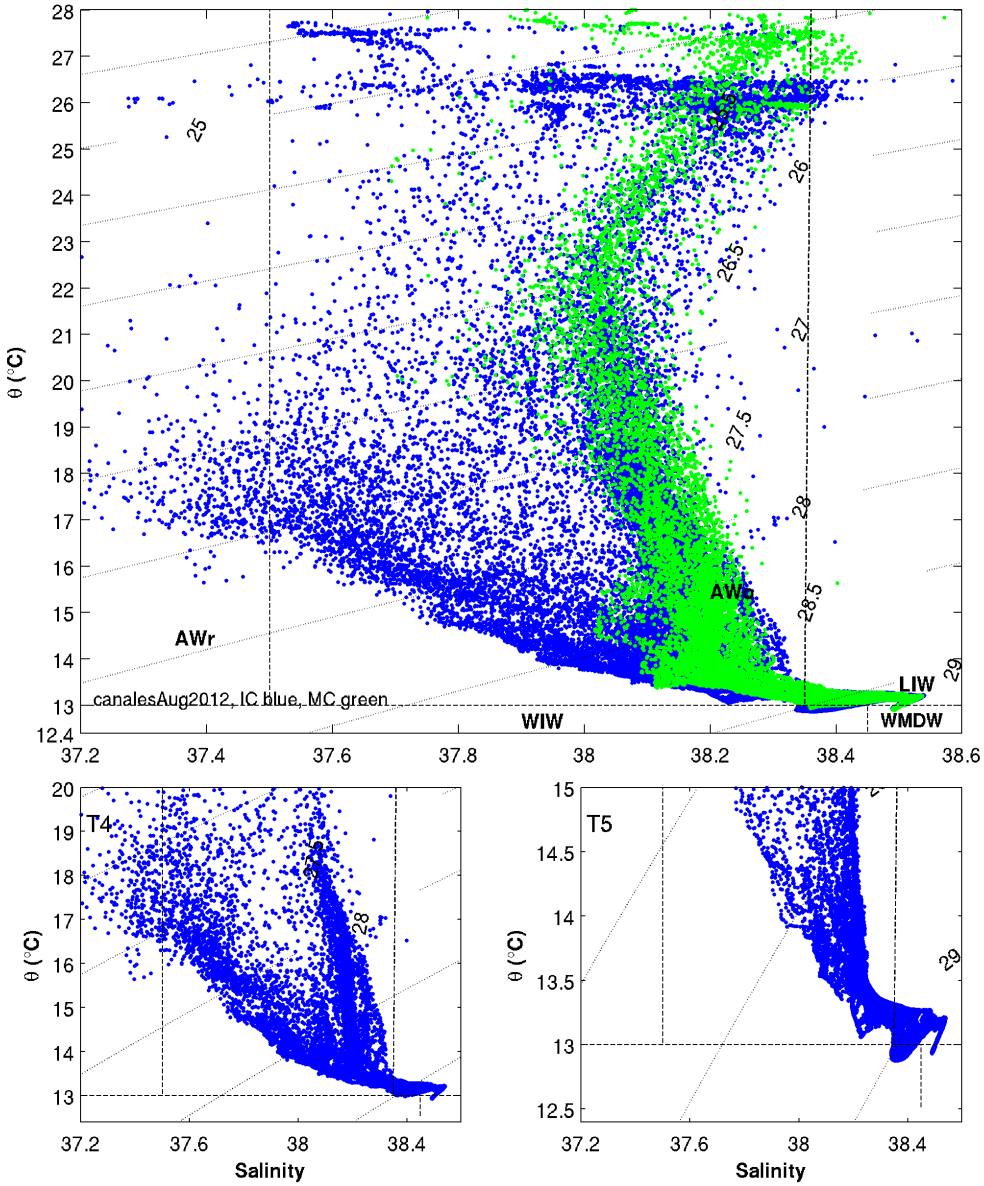

Figure 19b. θ/S plots for canalesAug2012.

The IC transects are marked in blue and the MC transects in green. The lower panels show the lower salinity AW inflows in T4, with salinities as low as 37.4, and in T5 the appearance of the WIW eddy core.

MC: In T2 (22/08) at the end of August the isopycnals dip from 2.0°E to the southwest channel edge and the LIW maxima are depressed by 100 m, in geostrophic velocity an outflow current is visible, associated with transports of -0.65 Sv, and an on-shelf counter current with transports of +0.20 northwards. In September, the transect T9 (15/09) is too

short for transport calculations[10], however it is possible to suggest that there is a shallow outflow current to 1.8°E with some inflows to the east.

Summary: In August the IC is dominated by a major anticyclonic eddy that appears at the start of the mission and then strengthens and deepens as it moves southward, the central WIW core to this eddy enters the IC in T5 and towards the end of the mission the eddy occupies the whole channel. The repeat glider transects of the IC show the evolution of this large and complex structure as it enters the channel, and the high resolution shows other smaller coherent structures in the surface 100 to 300 m, visible in salinity and density, within the lager eddy structure. The eddy lies below the seasonal thermocline. There are inflows of fresher AW in the west of the IC, being drawn in or taking advantage of the north flowing side of the eddy structure. No inflows are seen in the MC, however the later MC transect is short so we are not able to determine what occurs in the northeast of the channel at this time.

canalesOct2012

IC: The glider fought a strong current north of Ibiza and later aborted in the IC due to a leak (water entering the vacuum sealed glider hull) at approximately 0.6°E. Although T4 (29/10) is too short to be used in the transport analysis, the half transect acquired suggests that the anticyclonic eddy from September 2012 could still be present in the channel, as the isohalines and isopycnals are dipped to 500 m and in the geostrophic velocity there is a suggestion of a paired counter current to the east, centred at 0.7°E. There are fresher surface (0 to 50 m) inflows in the east, just on the shelf, with geostrophic velocities of 10 cm s^{-1} and salinities in the range 37.4 to 37.7 (fig. 20), there is however no signature of a WIW core for the eddy structure in θ/S.

MC: In T2 (25/10) the channel is occupied by a cyclonic eddy, the isohalines uplifted by 100 m in the centre, most apparent in the upper 50 to 150 m, and the LIW maxima are gently domed upwards with evidence of an outflow current close to the channel edge in the far southwest of the MC (see Appendix G for sections). In geostrophic velocity a paired velocity structure, centred 1.9°E and penetrating to depths of 300 m, is visible with velocities of order 25 to 30 cms^{-1}. The transport values are +0.66 and -0.36 Sv.

[10] T9 ends at 1.9°E

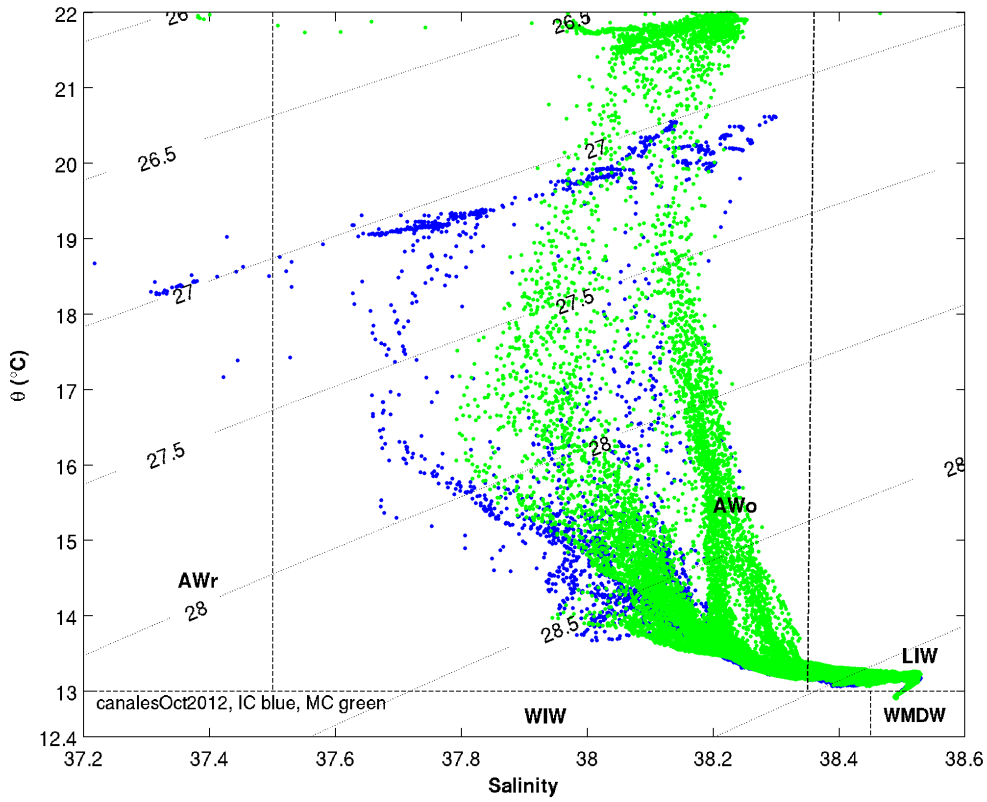

Figure 20. θ/S plots for canalesOct2012.

The IC transects are marked in blue and the MC transects in green. Lower salinity AW inflows are visible in the IC (blue).

Summary: It seems likely that the large anticyclonic eddy seen the IC in August is still present, as are the fresher AW inflows with salinities of 37.4 to 37.6. The MC appears blocked by a cyclonic eddy.

canalesNov2012

IC: In November the seasonal thermocline remains strong, however at the start of the mission, in T4 (03/12), there is evidence in the different depth range of the thermocline across the channel and that a 'winter' thermocline has been exported south with the NC. In the west of the channel the thermocline is deeper and broader, spanning 80 to 150 m, while in the east there is a shallower and more narrow ranged 'summer' thermocline, spanning 50 to 60 m, with warmer inflows above (fig. 21a). This is also evidenced in θ/S, where two close but distinct mixing lines are visible, one from LIW to the surface, truncated at 14 °C and characterised by salinities of 38.2, representing colder southward flows, and the other

mixing up to 16 °C with salinities of 38.3 (fig. 21b, lower panel T4). In the west of the channel the isopycnals tilt down from 0.75°E to 0.45°E at the western channel edge, with a gradient of ~4.6 x 10^{-3} ($\Delta z/\Delta x$), signifying a strong NC that is associated with a colder cohesive water mass of salinity 38.2 to 38.3. In geostrophic velocity the flows are of order 35 cm s^{-1} and penetrate to depths of 250 m (fig. 21a). The water volume transports associated with this strong NC are -1.39 Sv.

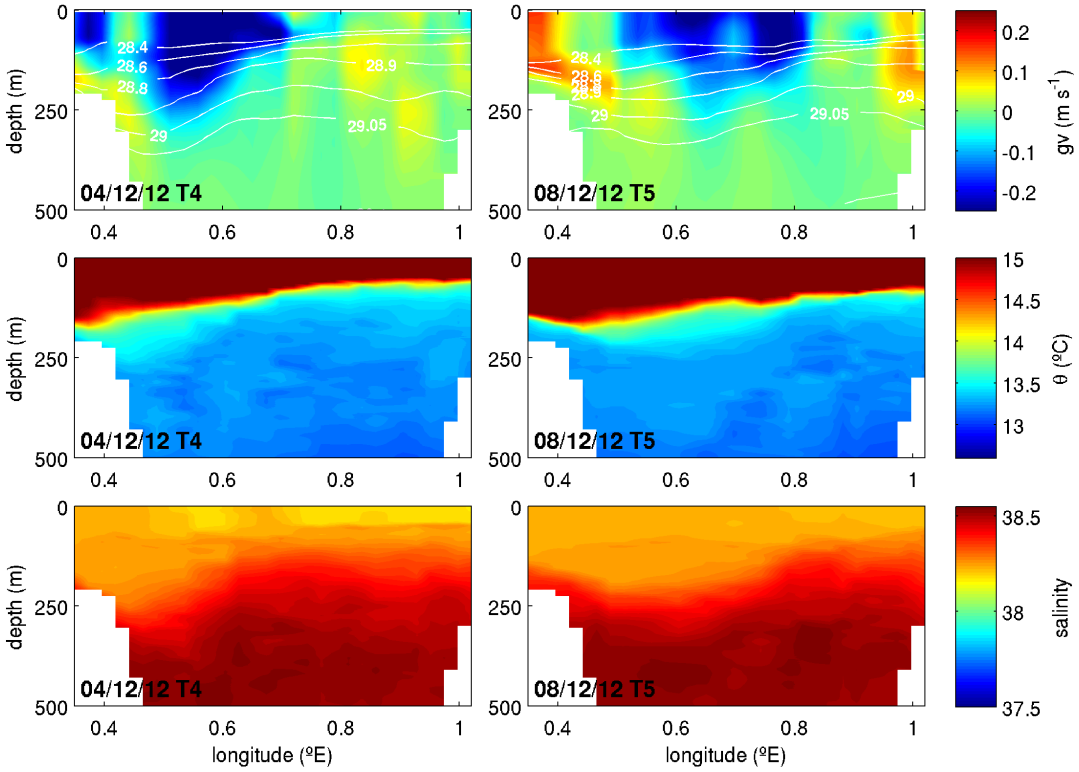

Figure 21a. Geostrophic velocity (gv), potential temperature (θ) and salinity sections for canalesNov2012. The transect numbers and mean date are marked in the bottom left of each panel, geostrophic velocities northward are positive and southward are negative, and selected isopycnals are marked in white.

In T5 (08/12) there is a similar pattern in the thermocline depth ranges, with a broader depth range in the west of the channel associated with a coherent fresher colder water mass. Above this, warmer waters seem to have invaded from the shelf and the NC has moved a little to the east. The isopycnals now tilt from 0.9°E to 0.5°E with a gradient of ~2.9 x 10^{-3} ($\Delta z/\Delta x$). In geostrophic velocity the NC is now visible centred at ~0.7°E with strong core velocities of 30 cm s^{-1} and penetrating to depths of 200 m. The water volume transports associated with this NC are -1.04 Sv. In the east and west of the channel, mainly on-shelf, there are inflows and the water volume transport associated with these increases from +0.20 in T4 to +0.41 in T5. However although the inflows are warmer, salinities are

in the range 38.0 to 38.3 and so there is no evidence of fresher AW of 'more recent Atlantic origin' as seen in August and September 2012 (figs. 21b, 20b and 19b).

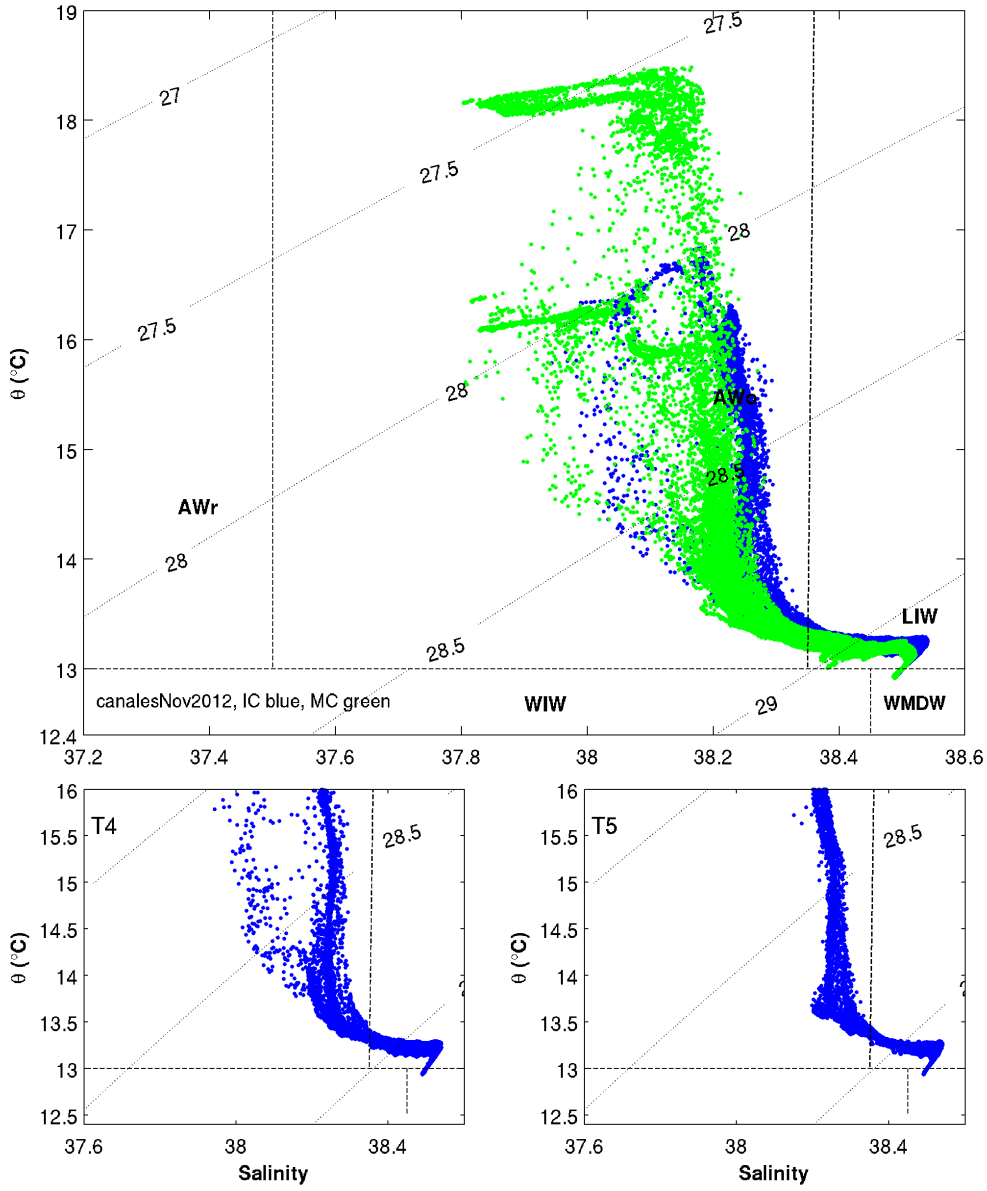

Figure 21b. θ/S plots for canalesNov2012.

The IC transects are marked in blue and the MC transects in green. The lower panels show two mixing lines in T4 and one in T5. During the mission the surface water was cooled by ~2 °C, this is seen in the upper panel where the fresher surface inflows in the MC (green) have a temperature of ~18 °C at the start and ~16 °C by the end of the mission.

MC: T2 (29/11) at the end of November the thermocline remains strong, although deeper than in October, at depths of 50 to 70 m, and there is a marked disconnect between the

38.4 salinity water mass below the strong thermocline and the 37.8 to 38.2 salinity water mass above. The isopycnals have a slight dip to the southwest and in geostrophic velocity there is a small outflow current on-shelf in the southwest of the channel (see sections in Appendix G). Shallow inflows, between 0 and 50 m, of lower salinity water mass, occur on-shelf in the northeast of the channel. In T7 (11/12), there is evidence in temperature of an deeper and broader outflow current in the southwest, from the channel edge to the centre of the MC and to 200 m depth. The inflow of fresher (S 37.8) water mass above the thermocline has extended to mid channel and two mixing lines to the surface are visible in θ/S (fig. 21b).

Summary: A strong 'winter' NC is reinstated with southward transports values of order -1.0 to -1.2 Sv, and a broader and deeper 'winter' thermocline has been exported south with these flows. The inflows are not of a significantly fresher water mass and are superficial (upper 0 to 50 m), they are however fresher and distinct from those flowing south and occur in both channels, with a fresher range in the MC.

3.3 Glider missions 2013

canalesJan2013

IC: In February 2013, T3 (05/02), a cold surface mixed layer lies across the IC and there is a sharp interface, at ~200 m, between the cooler AW (θ 13.0 to 13.1 °C) and the warmer LIW lying below (fig. 22a). This relatively homogeneous surface mixed layer has salinities in the range 38.2 to 38.3. A strong front (the Continental Front) exists in the west of the channel, just off-shelf at 0.4°E, between the warmer shelf waters and the colder surface layer (fig. 22a). Within these cold surface waters is a distinct water mass with salinity 38.2 associated with the NC flowing south and the isopycnals dip westward, from 0.75°E to the western channel edge at 0.55°E, with a relatively steep gradient of order 5.9 x 10^{-3} ($\Delta z/\Delta x$). In geostrophic velocity a strong NC is visible, lying just off the western shelf edge and centred at 0.6°E, with core velocities of order 25 cm s^{-1}, penetrating to ~300 m depth, and transporting -0.9 Sv southward. There is also a weak on-shelf counter current, with velocities of order 5 to 10 cm s^{-1}. The LIW maxima dip down in the west, rise mid channel, and dip again to the east where there are warmer inflows, with the warmest component on-shelf and to approximately 100 m depth. In T4 (08/02) the cold water layer deepens by 75 m in the west and the Continental Front is pushed back on-shelf. The isopycnals steepen slightly to a gradient of 6.0 x 10^{-3} ($\Delta z/\Delta x$) and the σ 28.9 kg m^{-3} isopycnal outcrops at the

surface, as the NC broadens and moves west, see fig. 22a. In the east there are some weak inflows, although warmer, they do not however have a distinctive signature in salinity.

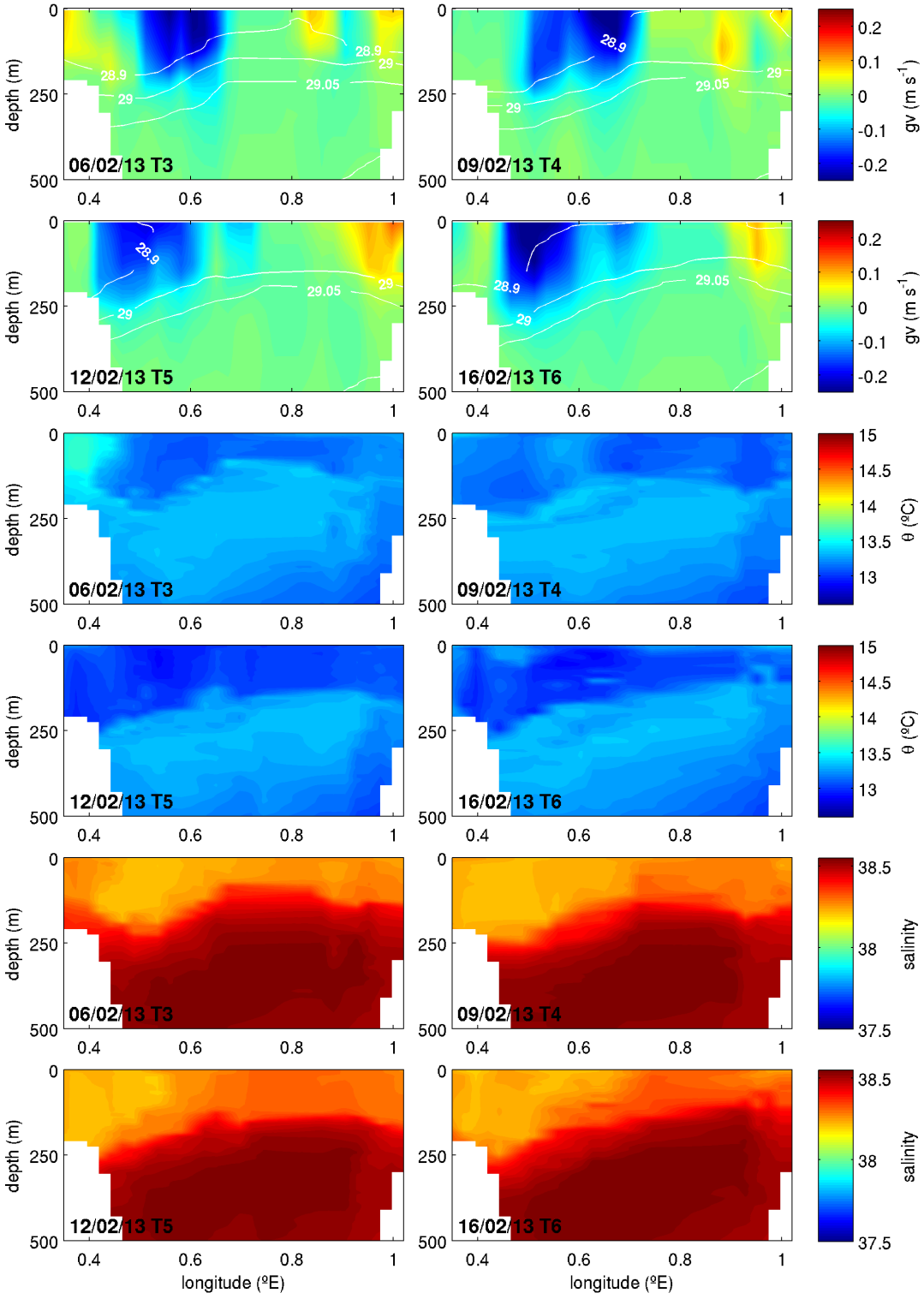

Figure 22a. Geostrophic velocity (gv), potential temperature (θ) and salinity sections for canalesJan2013. The transect numbers and mean date are marked in the bottom left of each panel, geostrophic velocities northward are positive and southward are negative, and selected isopycnals are marked in white.

In T5 (11/02) WIW arrives in the IC for the first time in 2013, with θ 12.8 °C and salinity ~38.2, see fig. 22a and b. The surface mixed layer becomes colder, more homogeneous and extends to near 300 m at the western channel edge, 150 m in the channel centre and 200 m in the east channel margin. As in 2011, with the arrival of WIW the isopycnals tilt more steeply, the NC strengthens and the transport increases. Inflow currents occur at the edge of the channel in the east to ~180 m, however as in the previous transect, although warmer they are not associated with fresher salinities, see fig. 22b. In T6 the isopycnals tilt down to the west across much of the IC and the LIW temperature maximum is pushed down by 100 m in the west and uplifted by 100 m in the east. The transport southward increases to -1.20 Sv, of which ~0.4 Sv is WIW and core geostrophic velocities in the NC are of order 30 cm s^{-1}. The isopycnals steepen particularly sharply in the surface 250m (gradient of 8.6 x 10^{-3} ($\Delta z/\Delta x$) from 0.7°E to the western channel edge). A weak on-shelf counter current in the west and a weak inflow current in the east remain. Once again however there is no fresher AW associated with these inflows and the transports are low, of order +0.1 to +0.15 Sv throughout the mission.

MC: At the end of January, T1 (31/01), the MC has warmer surface waters than the IC (θ 13.5 to 14.5°C), see fig.22b, and there is an uneven seasonal thermocline at ~100 m below which the isopycnals are fairly horizontal. Above the seasonal thermocline, in the surface 0 to 100 m, there are alternating small inflow and outflow currents, marked by temperature contrasts, and a small on-shelf outflow in the southwest with associated transports of -0.5 Sv and 0.23 Sv, see Appendix G for sections.

Summary: A deep mixed layer of cold AW (~13.0 °C) lies above LIW across the IC. The interface of this cold water to the LIW is abrupt and varies in depth across the channel. The LIW layer is pushed down in the west by the cold surface water flowing south in the NC and banked up in the east. Again a large increase in the transports of -0.7 Sv is seen with the arrival of WIW in the channel (T4 to T6). The WIW is not as cold or as fresh as in 2011 (compare figs. 11b and 22b). Inflows of warmer surface waters are consistent and low, of the order of 0.1 Sv, with no fresh signature in salinity denoting AW of 'more recent Atlantic origin'. The MC does not have the same cold surface mixed layer and the thermocline is located at depth 100 m. This observation along with others regarding the fresh inflows in 2011 and lack of WIW outflows, suggests that although the IC and the MC

are generally connected and synchronous with regard to inflows, they are not connected with regard to outflows. In reality perhaps little of the NC flows out through the MC.

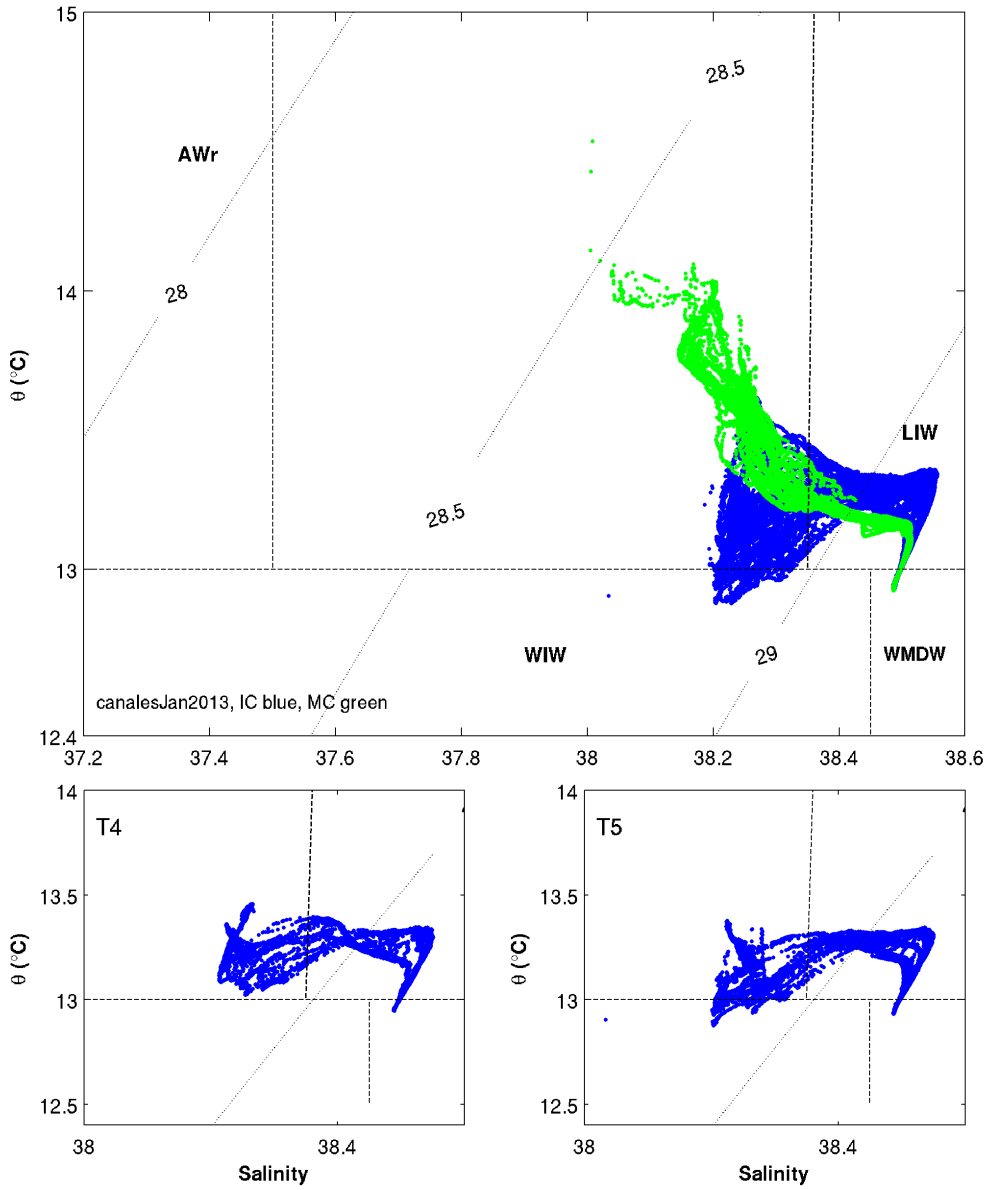

Figure 22b. θ/S plots for canalesJan2013.

The IC transects are marked in blue and the MC transects in green. The lower panels show the arrival of WIW (classic definition θ < 13 °C) in the IC in T5, although a temperature minimum (θ 13 – 13.1 °C) exists in T4, also the absence of lower salinity waters, although weak inflow currents occur.

canalesMar2013

IC: By April 2013, T4 (01/04), the waters in the IC are more stratified and a seasonal thermocline lies at ~40 to 50 m. Cool waters (θ 12.8 °C) flow south with the NC, visible

from 100 to 250 m depth at the western channel edge and the isopycnals tilt downwards to the west with a gradient of 4.3 x 10^{-3} ($\Delta z/\Delta x$), fig. 23a.

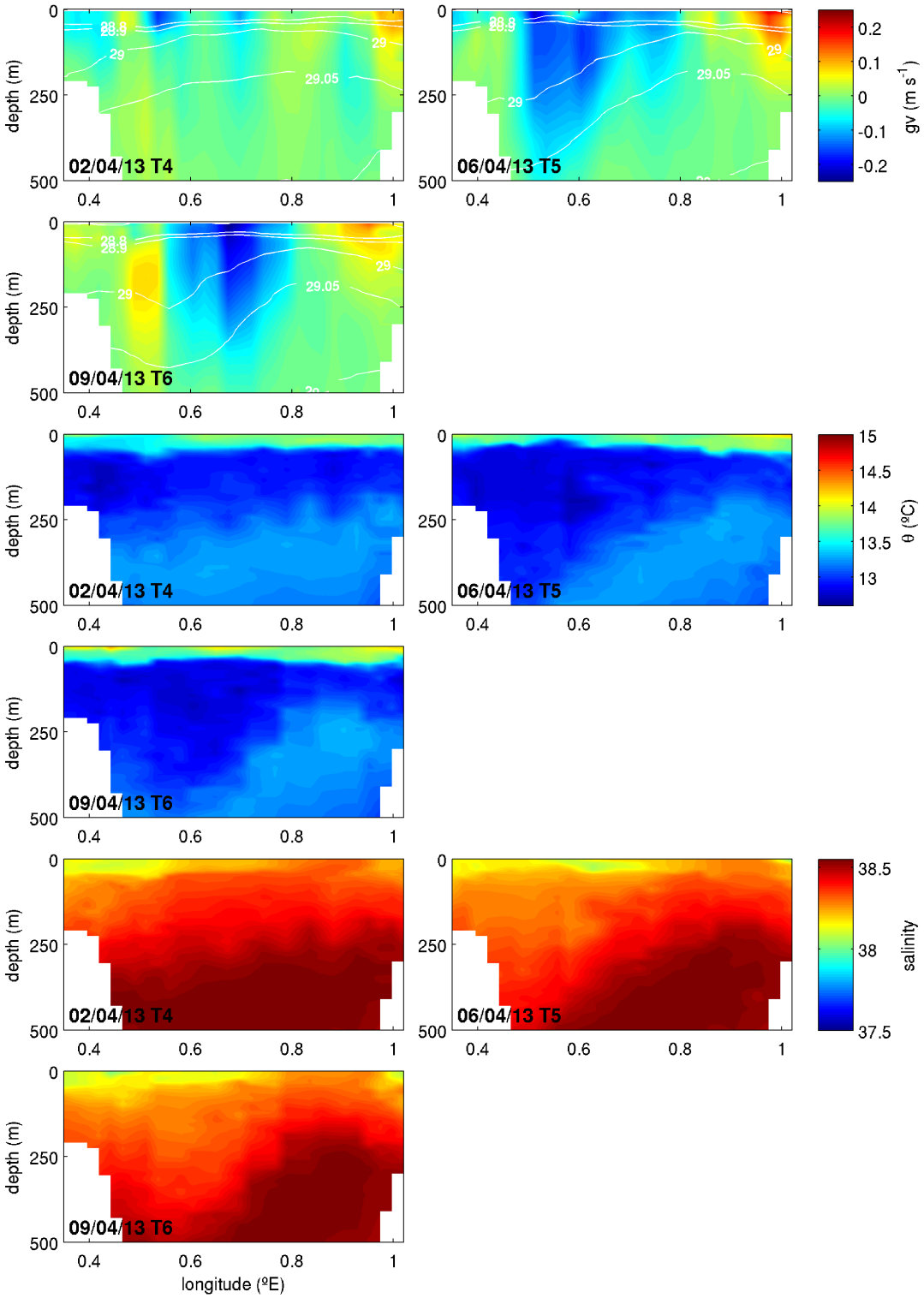

Figure 23a. Geostrophic velocity (gv), potential temperature (θ) and salinity sections for canalesMar2013. The transect numbers and mean date are marked in the bottom left of each panel, geostrophic velocities northward are positive and southward are negative, and selected isopycnals are marked in white.

In geostrophic velocity the NC is visible as 2 streams, at 0.4 and 0.7°E, with associated transport of -0.5 Sv of water mass southwards. The NC is perhaps affected by a small shallow mesoscale feature, seen as a paired velocity structure centred at 0.5°E. In θ/S (fig. 23b), multiple WIW minima are visible, the coldest and freshest (θ 12.5 °C and S 38.1) is associated with a cold water mass visible on-shelf in the west at ~0.2°E and 50 m depth (sea floor). The other relatively warmer and saltier WIW minima (θ 12.8 °C and S 38.2, as in canalesJan2013, and θ 12.7 °C and S 38.3) are associated with the NC flowing south. In addition, in the east there are weak 10 cm s^{-1} inflows in the surface 100 m. In T5 (05/04) the depth of the colder AW associated with the NC increases dramatically, reaching depths of 500 m at the western channel edge and pushing the LIW temperature maxima down in the west to ~ 700 m. The isopycnals associated with the NC now tilt more steeply to the western channel edge with a gradient of ~7.7 x 10^{-3} ($\Delta z/\Delta x$). The geostrophic velocities in the NC strengthen and deepen to 500 m, with an increase in the transport of water mass southward of 0.78 Sv over 4 days, from -0.49 to -1.27 Sv. The colder and fresher WIW (12.5/12.6 °C and S 38.1) now extends further down the western shelf and there are shallow warmer inflows on the eastern shelf, slightly fresher than previous transects with salinity 37.9. In T6 the pattern of transports is similar, with a wedge of cold water to 500 m depth in the west of the channel associated with the NC. Interestingly there appears to be a 'cold core' in the NC, between 0.4 and 0.8°E and at 50 and 200 m depth. In geostrophic velocity the NC has moved offshore and is centred on this cold core, while at the western channel edge there is an inflowing counter current, of order 10 cm s^{-1}, and at the same depth as the cold core, giving the appearance of a paired velocity structure (fig. 23a). Shallow inflows in the east transport slightly fresher waters into the Balearic sub-basin, with salinities of 37.9, and the total transport northward increases with this western counter current to +0.33 Sv. The colder and fresher WIW (12.5/12.6 °C, S 38.1) is still visible on the western shelf. Unfortunately T7 (12/04) is missing data from the central transect (0.5 to 0.8°E), due to a memory buffer overflow problem associated with a software upgrade. Thus there is however data at the start and the end of T7 and from the relative depths of the isopycnals and LIW maxima it seems likely from that there is a similar pattern to T6 in T7, with continued strong NC flows and warmer, fresher (S 37.8) inflows occurring in the east of the channel. Interestingly there is an indication that the colder and fresher WIW, seen on-shelf at 0.2°E in T4 and subsequently extending down the shelf in T5 and T6, is now in T7 cascading into the channel and augmenting the NC flows. This distinctive

colder and fresher WIW (12.5/12.6 °C and S 38.1) could possibly represent a local WIW formation event.

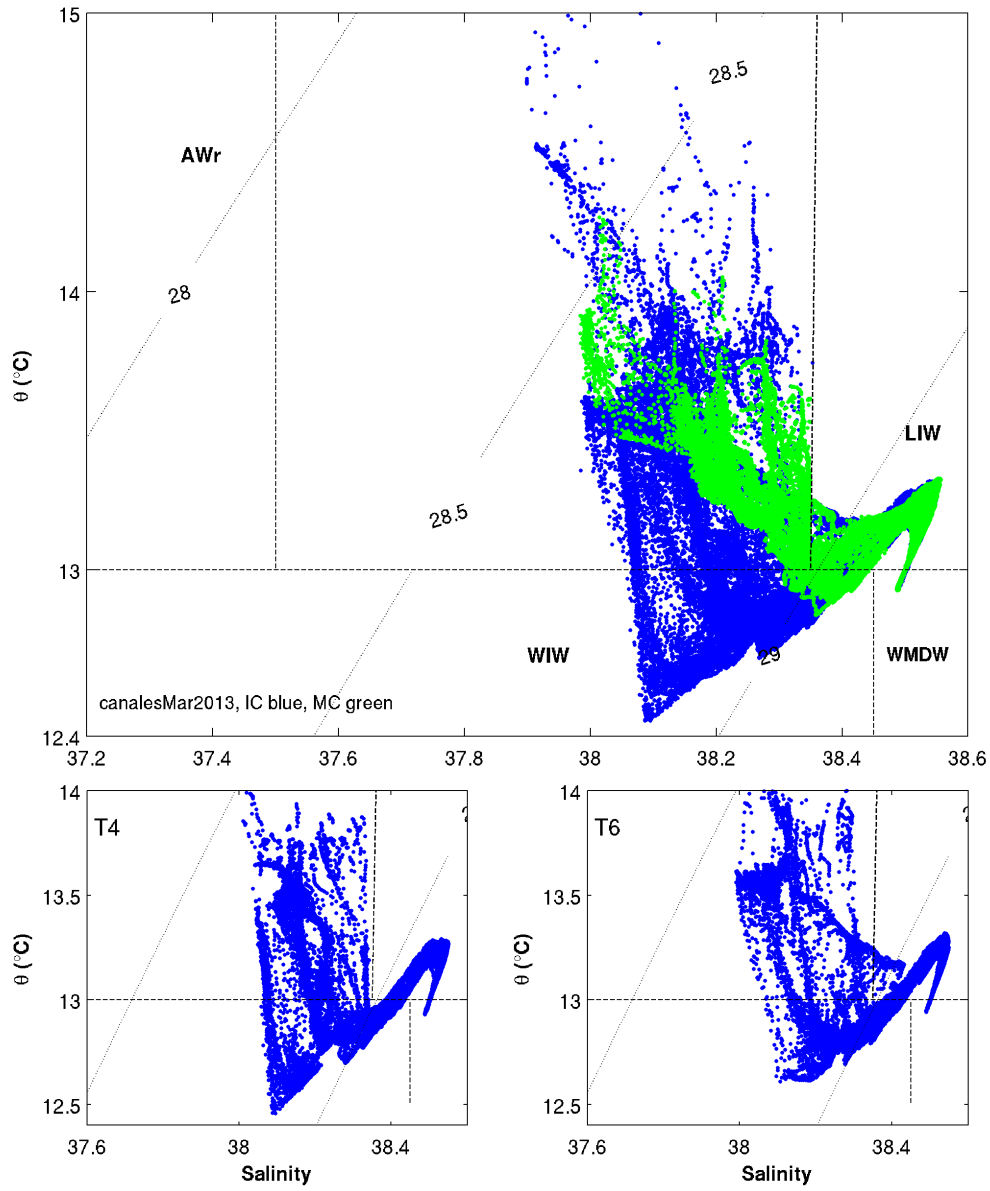

Figure 23b. θ/S plots for canalesMar2013.

The IC transects are marked in blue and the MC transects in green. The lower panels clearly show the 3 distinct WIW minima (θ 12.5/12.6 °C and S 38.1, θ 12.8 °C and S 38.2, θ 12.7 °C and S 38.3) in T4 and T6.

MC: The glider sampled to only 300 m for the initial part of the mission (a test flight) and so this transect is not used for the transport analysis, however in T1 (23/03) it is possible to see an uneven WIW lying between 100 and 300 m across most of the channel with θ

12.8 °C and salinities of 38.35. As in the IC surface inflows occur in the east of the channel with salinity of 37.8.

Summary: The NC varies in strength as pulses of colder water cause the isopycnals to tilt more steeply to the western channel edge, with changes of order 0.8 Sv occurring over 4 days. The eastern inflows are persistent, low in volume, superficial, slightly fresher and occur in both the IC and the MC. The MC has only one of the several variations of WIW observed in the IC. With the increased resolution afforded by the glider 'burst' sampling of the IC a cold body of WIW is observed, gradually cascading down the western channel shelf (Valencia shelf) into the IC. By the final transect (T7) this cold WIW appears to have reached the shelf edge and be cascading into the channel, having taken 10 days to travel from 0.2°E to the shelf edge. This colder and fresher WIW (θ 12.5/12.6 °C and S 38.1) could possibly the product of a local and recent WIW formation event.

canalesMay2013

IC: In late May, T4 (27/05), a sub-surface temperature minimum layer (θ < 13.0 °C) lies across the IC, deeper in the west, to depth 300 m, and shallower in the east, to depth 100 m (fig. 24a). The isopycnals and isohalines tilt gently westward across most of the channel and the NC is represented by a broad flow, appearing as 3 streams (similar to April 2013), with geostrophic velocities of order 10 to 15 cm s^{-1} and transport of -0.69 Sv. At the start of June, in T5 (01/06), the isopycnals tilt more steeply westward and the NC narrows, although it still penetrates to depths of 250 m and the southward transport remains the same. In T6 (03/06) the NC weakens and moves partially on-shelf, now penetrating to 150 m and indicated with a small channel edge tilt in the isopycnals, from 0.6°E downwards to the western channel edge (fig. 24a). The isopycnals are now horizontal across the remainder of the IC. In T7 (07/06) the pattern in isopycnals and velocities are similar and the transport southward declines over the mission from -0.69 Sv in T5 to -0.36 Sv in T7.

MC: In T1 (22/05) the MC has a patchy WIW temperature minimum layer (θ 12.7 °C, S 38.3) lying between 150 - 250 m, this patchy layer is associated with a paired structure in geostrophic velocity (see Appendix G), suggesting a weak anticyclonic eddy centred at 1.85°E and penetrating to depths of 200m. The transport values inflow and outflow are similar, both around 0.27 Sv. In θ/S however the pattern indicates an inter sub-basin

exchange of water masses rather than recirculation (fig. 24b, upper panel green), with distinct mixing lines for the inflows and outflows.

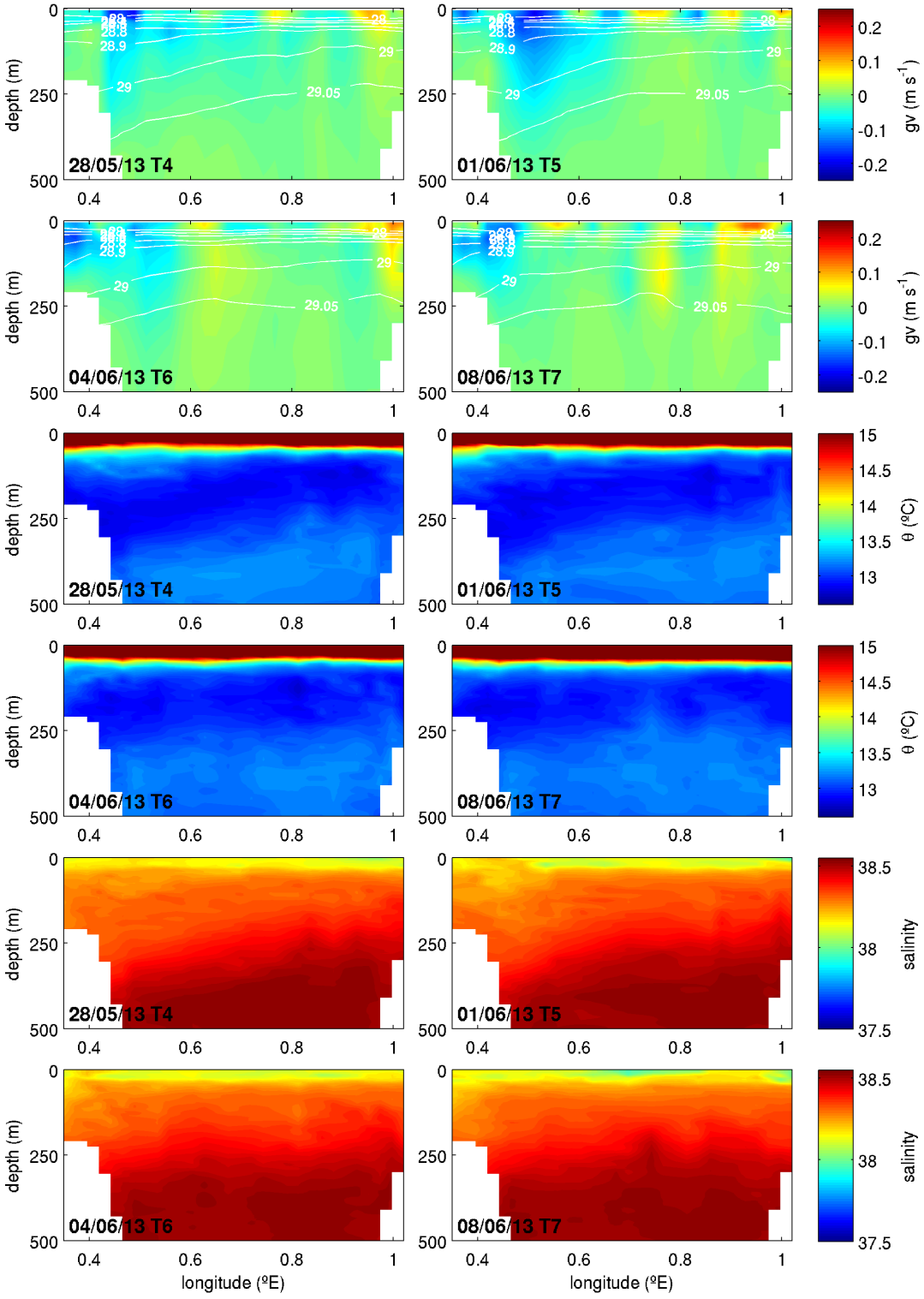

Figure 24a. Geostrophic velocity (gv), potential temperature (θ) and salinity sections for canalesMay2013. The transect numbers and mean date are marked in the bottom left of each panel, geostrophic velocities northward are positive and southward are negative, and selected isopycnals are marked in white.

Summary: Although WIW was produced in 2013 we have not observed the strong spring anticyclonic blocking eddies in the IC that were part of the pattern observed in 2011 and 2012. Perhaps the late production of WIW has delayed eddy formation? It is also however possible that the gliders did not observe 'blocking' events in 2013 due to the timing of the missions.

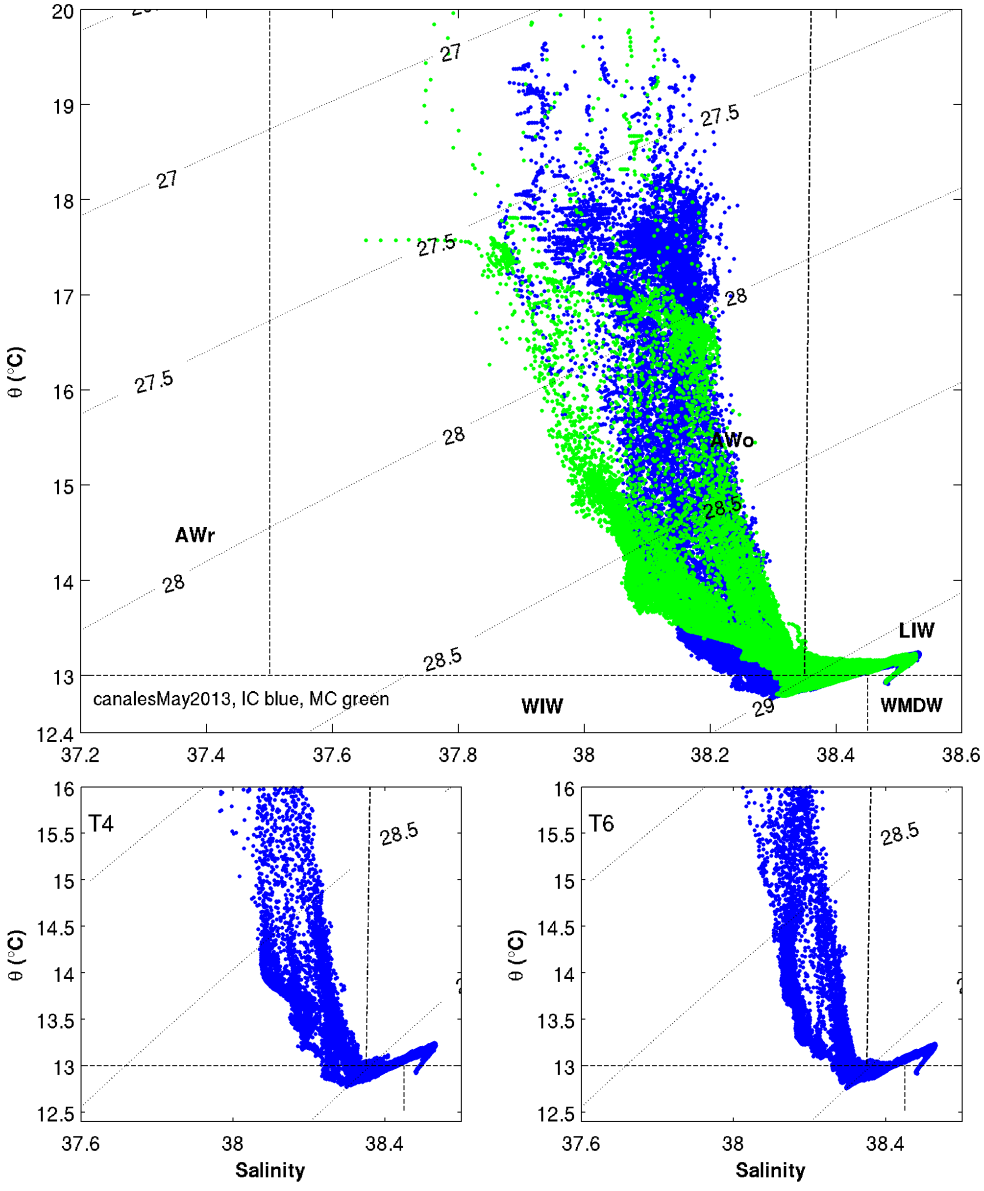

Figure 24b. θ/S plots for canalesMay2013.

The IC transects are marked in blue and the MC transects in green. The lower panels show two mixing lines to the surface in the IC for T4 and T6. In MC (upper panel, green) crossed mixing lines are indicative of an inter sub-basin exchange of water masses, although not of the fresher AW of 'more recent Atlantic origin', as seen in 2011.

During this mission the NC declines to a weaker flow more typical of summer conditions. In the MC there is a weak anticyclonic eddy, which does not however occupy the whole channel.

canalesJul2013

IC: At the start of the mission, T4 (22/07), there is a small sub-surface downwards tilt to isopycnals at the western channel edge (200 to 350 m), signifying weak NC. There is also a shallow central dip in the isopycnals between 0.6 and 1.0°E. In geostrophic velocity a weak subsurface NC is visible at 50 to 200 m depth, with velocities of the order of 5 cm s^{-1}. Above the NC, and above the seasonal thermocline, are stronger inflows (fig. 25a). In the salinity section, above the seasonal thermocline (0 to 50 m), lower salinity waters (S 37.7 to 37.9) are visible, and in the area of the western shelf-break the haloclines are uplifted towards the surface, similar to the pattern observed in summer/autumn 2011. Weak sub-thermocline inflows occur across the mid-channel and a small paired (anticyclonic) velocity structure is centred at 0.9°E visible in the east of the channel (fig, 25a). In T5 (26/07) two lenses of lower salinity (S 37.7) water mass are visible centred at 0.6°E and 0.95°E, above the seasonal thermocline (between 20 and 60 m), see fig. 25a. In the plots of θ/S a specific branch of water mass appears at 15 °C (S 37.7) likely representing these lenses (25b, lower panel T5). Below the lenses the thermocline is perturbed and the isopycnals dip, this perturbation extends to ~150 m depth. Below this the isopycnals have a single central dip, centred at ~ 0.65°E, and a small tilt downwards at the western channel edge, signalling NC flows. In geostrophic velocity a central anticyclonic eddy is visible, associated with the central dip in the isopycnals and a body of water, centred at 0.65°E with θ 13.4 °C and S 38.4. There is also a weak subsurface NC at the western channel edge, between 50 to 350 m. Again, as in the previous transect, above the NC and seasonal thermocline there are inflows, extending from on-shelf to 0.6°E, not as far as the eddy centre, but forming part of the northward flowing component of the eddy. The core eddy velocities are of order 30 cm s^{-1}, however the eddy penetrates with weaker velocities to 400 m. The transport of water in and out of the IC is relatively even in T4 and T5, with slightly more inflow, +0.59 Sv, than outflow, -0.52 Sv. In T6 (29/07) the sub thermocline lens has moved slightly west, as has the deep central dip in the isopycnals and the anticyclonic eddy, now centred at 0.6°E. In consequence the sub-surface southward flows of the NC are almost completely blocked.

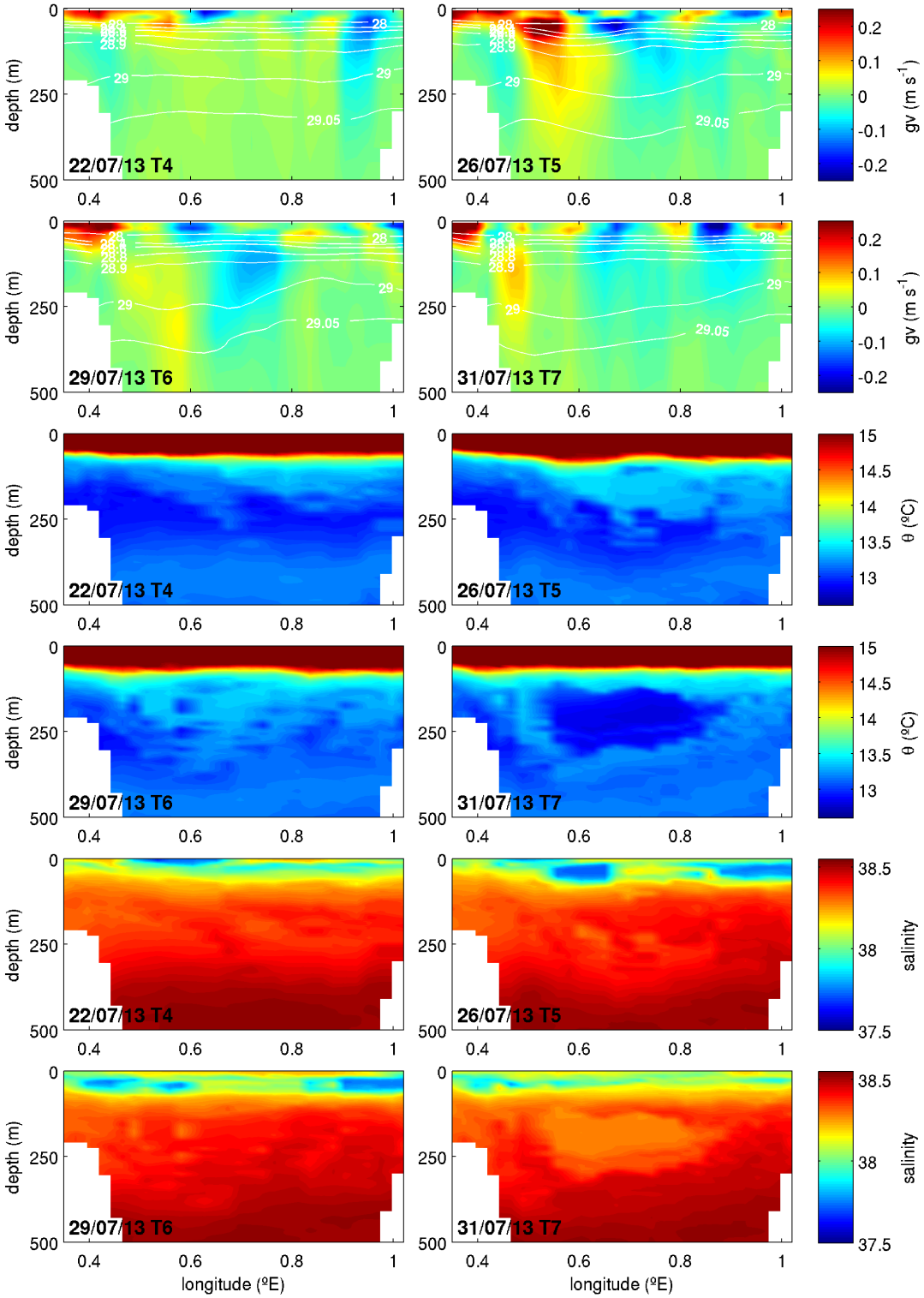

Figure 25a. Geostrophic velocity (gv), potential temperature (θ) and salinity sections for canalesJul2013. The transect numbers and mean date are marked in the bottom left of each panel, geostrophic velocities northward are positive and southward are negative, and selected isopycnals are marked in white.

In T7 (31/07) a cold core to the eddy of WIW (θ ~12.8 °C and S ~38.3) enters the channel, visible as a lens at ~200 m depth (fig. 25a). This large and relatively weak eddy centred at 0.6°E now occupies the central deep channel, with the northward flows against the western channel edge and the southward flows broadly across the east of the channel (fig. 25a). The transport southwards has strengthened to -0.55 Sv and the weak NC is either blocked or contributes to the southward flows in the east of the channel. In the west of the channel, on-shelf and above the thermocline, the inflows remain active.

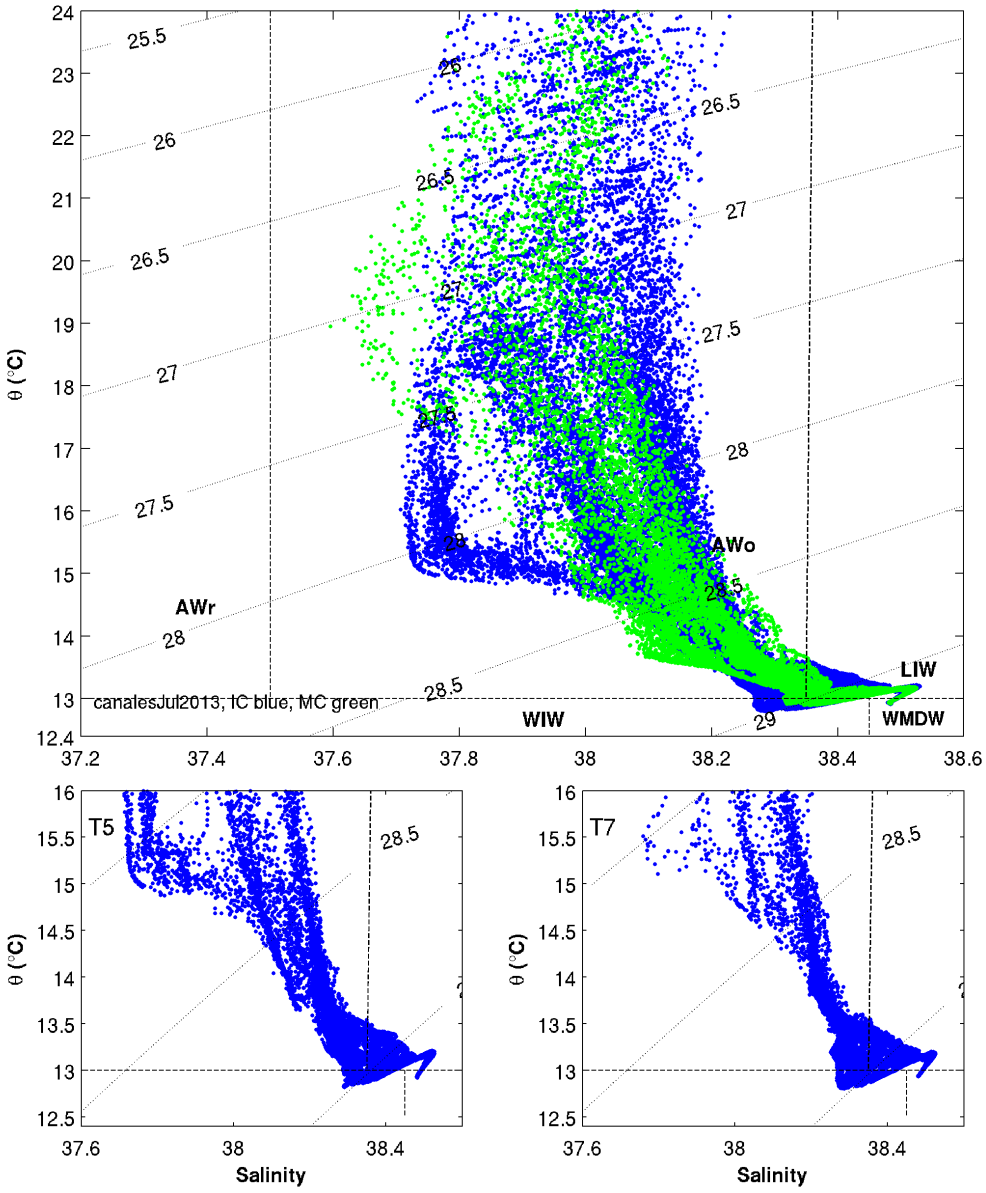

Figure 25b. θ/S plots for canalesJul2013.

The IC transects are marked in blue and the MC transects in green. The lower panels show the branch of lower salinity water in T5 (~15°C) is visible and in T7 an increase in the WIW present in the channel.

MC: By contrast, although the MC has an uneven sub-surface temperature minimum (WIW) layer in T2 (17/07), lying across the channel between depths of 150 and 300 m, there is no mesoscale activity associated with this layer (see Appendix G for sections). As in the IC there are lower salinity surface waters (S 37.7 and θ 18 to 20 °C), fig. 25b. In the northeast of the channel there are some weak inflows, of order +0.21 Sv, associated with the lowest salinity waters and even weaker outflows of -0.12 Sv.

Summary: Mesoscale activity appears in the IC. At the start of the mission the NC is weak, which is as expected in summer but could also be the result of blocking of the NC to the north. A similar pattern occurred across transects in 2011, where a central dip in the isopycnals signalled the entrance of an anticyclonic eddy in the IC before the full structure was evident. During this mission large eddy structure appears in the bowing down of the deeper isopycnals (from T5) before the WIW core of the eddy enters the channel (in T7). As in 2011, a complicated pattern of structures evolves and develops through the repeat glider transects. The surface lower salinity lenses seen in T5 are odd, possibly they represent lower salinity inflows (entering for example on the western shelf) that have become caught in the eddy structure, and then locally modulate the near surface structure of the eddy and associated velocities.

canalesSep2013

IC: In mid September, T3 (18/09), a large lens of lower temperature water is visible in the centre of the channel (from 0.5 and 0.9°E), generally between depths of 200 to 300 m and with a lower salinity (S 38.35) core at 200 m (fig. 26a), below which the LIW maxima are pushed down. The isopycnals indicate a small downwards tilt to the channel edge in the west, signalling a weak NC, and two shallow dips around 0.7 and 0.85°E again around 200 to 300 m depth. In geostrophic velocity two bands of weak outflows are visible with paired weak inflows, representing two anticyclonic velocity structures, the more westerly structure more clearly expressed (fig. 26a). In the west a weak NC is visible close to the channel edge. In T4 (20/09) the anticyclonic eddy structure at 0.7°E emerges more strongly, associated with a dip in the in isopycnals that now reaches to 400 m depth. The structure in the east of the channel is weaker. Overall the transports are weak and relatively balanced north and south (+0.36/-0.30 Sv). In T5 (22/09) on-shelf in the west of the channel there

is a strong, shallow inflow current of order 30 cm s^{-1}, associated with low salinity waters (S 37.5 to 37.7).

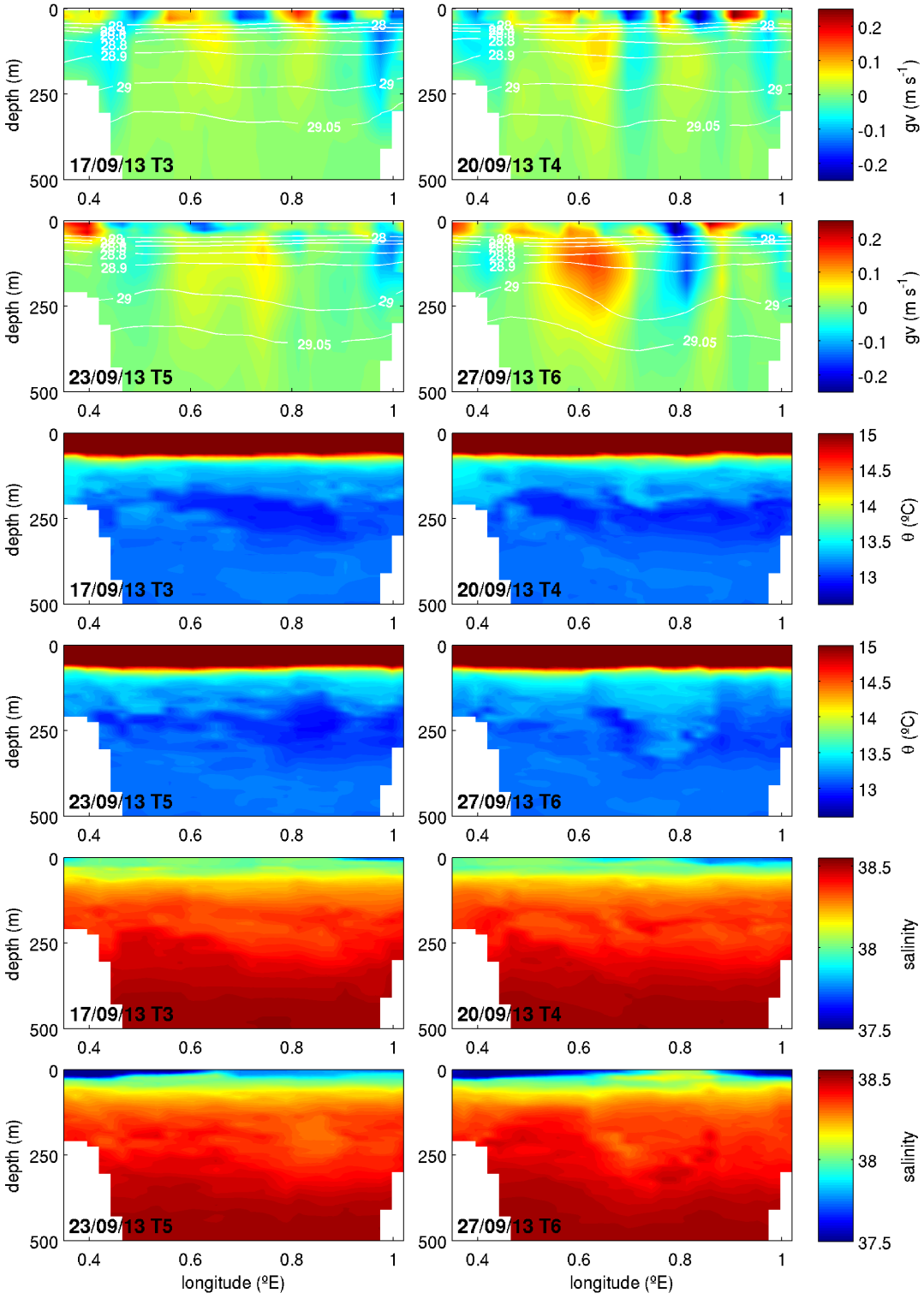

Figure 26a. Geostrophic velocity (gv), potential temperature (θ) and salinity sections for canalesSep2013: The transect numbers and mean date are marked in the bottom left of each panel, geostrophic velocities northward are positive and southward are negative, and selected isopycnals are marked in white.

In the next transect, T6 (26/09), the central (0.7°E) anticyclonic eddy strengthens and occupies most of the channel to depths of 400 m, with associated velocities of order 20 cm s^{-1}. The easterly eddy is weakly expressed, reduced in width and now centred at 0.9°E. A new low salinity lens of water mass (S 38.2) appears at 200 m depth associated with the larger eddy and a separate WIW minima (θ 12.9°C and salinity 38.35) appears in the in the θ/S plot for T6, see fig. 26b. The pattern in salinity above the thermocline suggests that low salinity AW is inflowing on both sides of the channel, associated with the northward flows of these eddies. One inflow is visible as an on-shelf current in the west, with velocities to 50 cm s^{-1} and linked to the northward component of the larger and more central anticyclonic eddy. The other is visible in the east as a strengthened surface current of the northward flowing component of the eastern eddy. One could suggest that these waters are re-circulated, and indeed there is likely some recirculation, however the strength of the surface flows and the pattern of transports suggest that there is a net inflow of fresher AW at the surface of order 0.25 Sv (+0.64/-0.38 Sv).

MC: In T1 (09/09) fresher AW inflows, with salinities of 37.5 to 37.7, occur on-shelf in the northeast of the channel. In addition a more saline temperature minimum layer (θ 13.0 °C and salinity ~38.4) is visible in the northeast and southwest of the MC at 200m, while in the centre (~1.9°E) it is interrupted by an upward doming of the isohalines. As in the last mission this represents a cyclonic eddy with velocities of order 15 to 20 cm s^{-1} and penetrating to depths of 300 m (see Appendix G for sections). As in the IC there is a concentration of inflows on-shelf in the east of the channel, with strong velocities of order 50 cm s^{-1}, transporting fresher AW into the basin. There is a difference in the inflow and outflow transport of water mass, indicating that there is a net inflow of order 0.2 Sv through the MC (+0.56 Sv/-0.37 Sv), probably associated with the strong inflows of fresher AW. In October, at the end of the mission, T8 (02/10), there is little of the temperature minimum layer visible and the central doming of the isopycnals is broader and more subdued. The cyclonic eddy remains visible in geostrophic velocity and now occupies the whole channel, again with geostrophic velocities of order 15 to 20 cm s^{-1} and penetrating to 300 m depth. T8 is slightly short in the east but no inflows are detected in θ/S, and the inflow and outflow transport of water mass is similar, suggesting that the channel is 'blocked' and a recirculation of waters of similar order as before (0.30 Sv) is taking place.

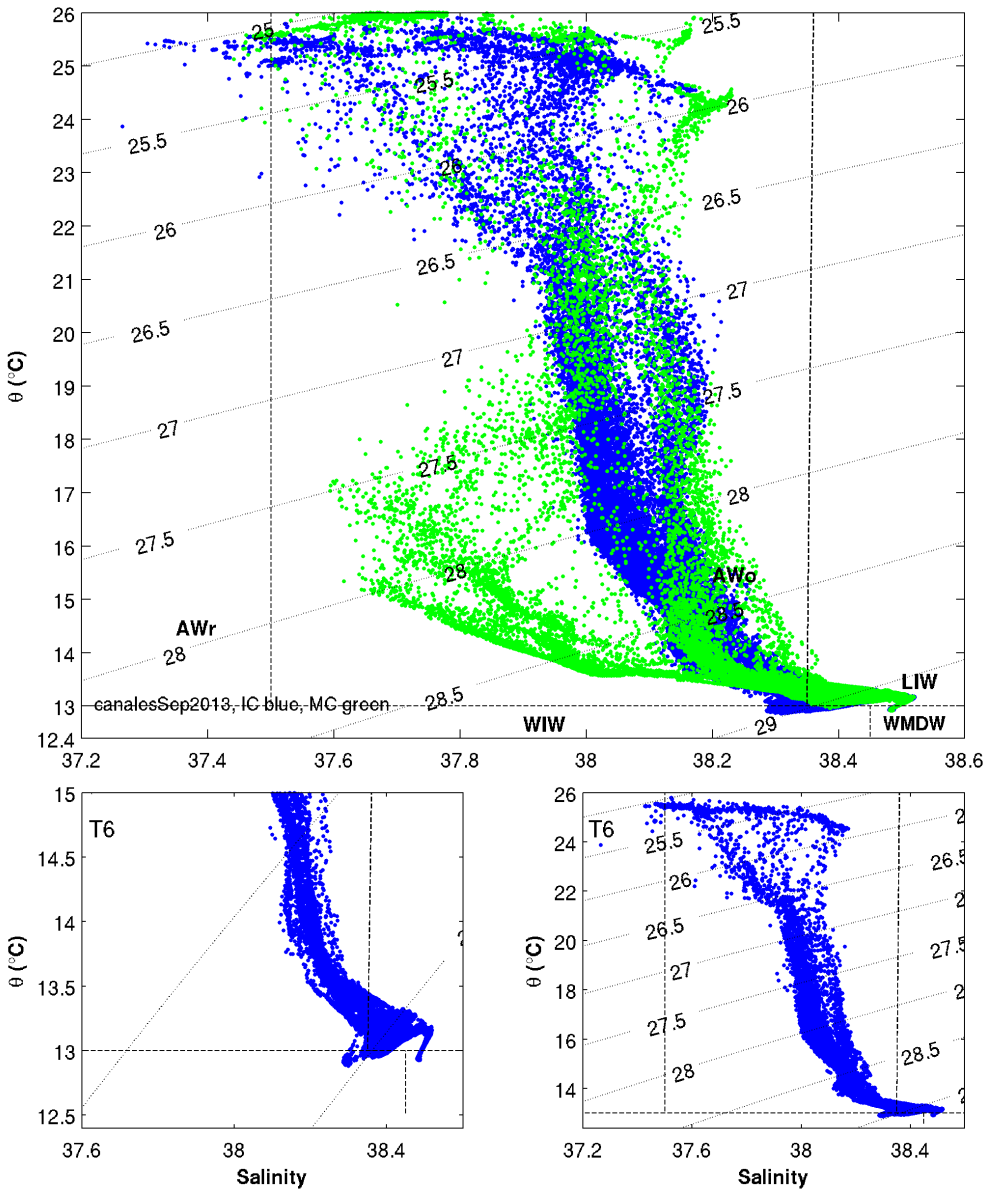

Figure 26b. θ/S plots for canalesSep2013.

The IC transects are marked in blue and the MC transects in green. The lower panels show two θ/S plots for T6 with different temperature and salinity scales. In the left-hand plot the WIW minima is shown and in the right-hand plot the surface inflows of less saline waters. In the MC (upper panel, green) the lower salinity inflows occurring both above (θ 25 to 26 °C) and below the thermocline (θ 15 °C) are seen.

Summary: Over the 9 days of the mission in the IC anticyclonic eddies gradually block the southward flow of the NC. A low salinity subsurface temperature minimum lens (with a WIW core) is present in all transects, and what starts as 2 weak eddies (in T3) evolves through the mission to become by the end of September (in T6), one strong anticyclonic eddy, centred 0.7°E, with velocities of 25 cm s^{-1} and penetrating to depths of 400 m, with a

weaker partner squeezed in the east of the channel at around 1.0°E. The transport of water mass is similar northward and southward, indicating eddy re-circulation, and the values for the transport fairly consistent throughout the mission (0.30 to 0.40 Sv). It is possible the NC is squeezing past the blocking eddies in the west of the channel, as in T3 and in T4 there is a weak net southward flow of ~ 0.1 Sv. At the end of the mission, in T5 and T6, there is a net inflow of ~0.25 Sv likely associated with the appearance of strong surface inflows of fresher AW, that take advantage of the northward flowing components of both eddies to propagate through the channel. This fresher AW enters through both the IC and the MC, with salinities in range 37.4 to 37.7. The inflow currents are strong, with velocities up to 50 cm s^{-1}, and take advantage of the inflow component of eddies in both the IC and the MC, although at the end of the mission the inflows through the MC appear to be blocked. It is interesting to note that the two eddies appear to arrive to the IC at the same time, they are formed around two distinct and different WIW minima

Note: canalesSep2013 was contemporaneous with the ship mission MEDESS0913 and a detailed comparison between synchronous transects of these two missions is available in Appendix D. Also, as discussed more fully for summer/autumn 2012 and in Chapter 2, the combination of the strong seasonal thermocline with a glider inflexion depth of 20 m causes banding in the geostrophic velocity above the thermocline, between the surfacing profiles.

canalesNov2013

IC: This mission is shorter than normal as the glider experienced battery failure and was rescued after completing just one transect of the IC. In T4 (07/11) in the upper 100 m, there is a central bowing of the isotherms with a small dip downwards to the channel edges in both the east and west, which gives the thermocline a wave like appearance. Below 100 m there are two dips in the isotherms associated with two lenses of low temperature WIW at ~300 m depth, at 0.6 and 0.9°E and with salinity of 38.3 and 38.4 respectively (fig. 27a). In θ/S there are correspondingly two WIW minima, just on the border of 13 °C, with salinities of 38.4 and 38.3 (fig. 27b). The central 100 m dip in the isopycnals is associated with a fresh lens of water mass (S 37.8) sitting just below the thermocline at 0.7°E and part of a layer of generally 38.0 salinity water mass that stretches across the channel (fig. 27a). The picture in geostrophic velocity is complicated, there are two subsurface anticyclonic eddies, the stronger in the west at 0.6°E, with velocities of order 20 cm s^{-1} and extending

from 100 to 450 m depth, and a weaker structure in the east, at 0.9°E, with velocities of order 5 cm s^{-1} and extending to 350 m depth. The southward flows of the weaker eddy are narrow and pushed up against the eastern channel edge. These sub-surface eddies have a connection to the surface, however the surface flows (upper 100 m) appear amplified and offset. For example in the in the east of the channel a weak eastern sub-surface southward flow becomes a broad strong 40 cm s^{-1} southward flow, and in the west of the channel, the northward flowing side of the anticyclonic eddy is broader and stronger, 40 cm s^{-1}.

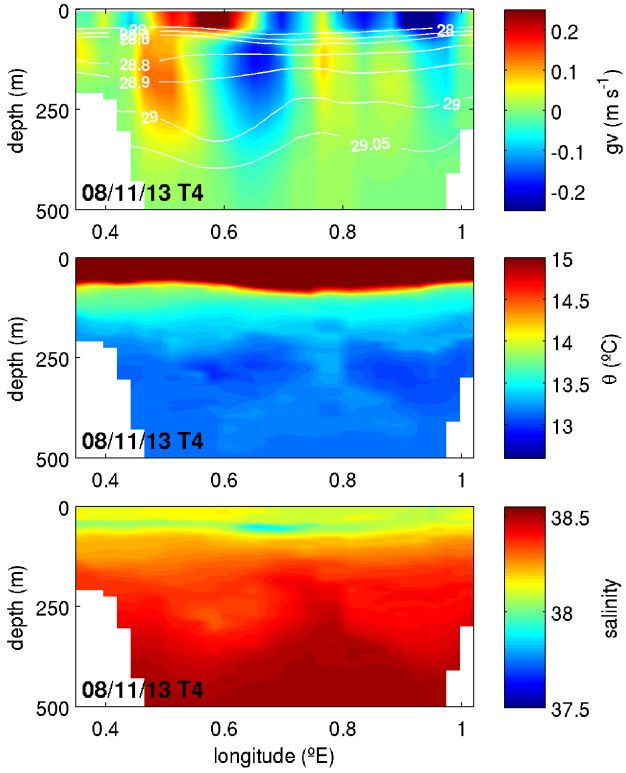

Figure 27a. Geostrophic velocity (gv), potential temperature (θ) and salinity sections for canalesNov2013. The transect numbers and mean date are marked in the bottom left of each panel, geostrophic velocities northward are positive and southward are negative, and selected isopycnals are marked in white.

MC: In T2 (02/11) there is a central bowing down of the isotherms and in the salinity section a homogeneous water mass of salinity 38.4 is visible across the channel at depth 100 to 200 m. There is a disconnect between the dynamics above and below the sharp seasonal thermocline: below an anticyclonic eddy, with velocities of order 15 cm s^{-1} and penetrating to depths of 400 m, but with weaker velocities reaching 600 m, is visible. Above there are strong, 40 cm s^{-1}, inflows of fresh AW (with salinities of 37.2 to 37.6) in the northeast of the channel, and strong outflows, of order 50 cm s^{-1}, in the southwest, associated with slightly lower temperatures than the surface waters in the rest of the

channel and salinities of 38.0 to 38.1. The salinity range of the outflows is indicative of NC AWo flows and suggests these outflows are a branch of the NC that has been deflected by eddies occupying the IC. In θ/S two distinct mixing lines are visible, one fresher to the warmer low salinity water, the other with salinities of 38.0 to slightly cooler surface waters (fig. 27b). There is no WIW (θ < 13.0 °C) present in the MC, but two distinct temperature minimums exist, with salinities of ~38.35 and ~38.4, which could be associated with the core of the anticyclonic eddy (see sections in Appendix G).

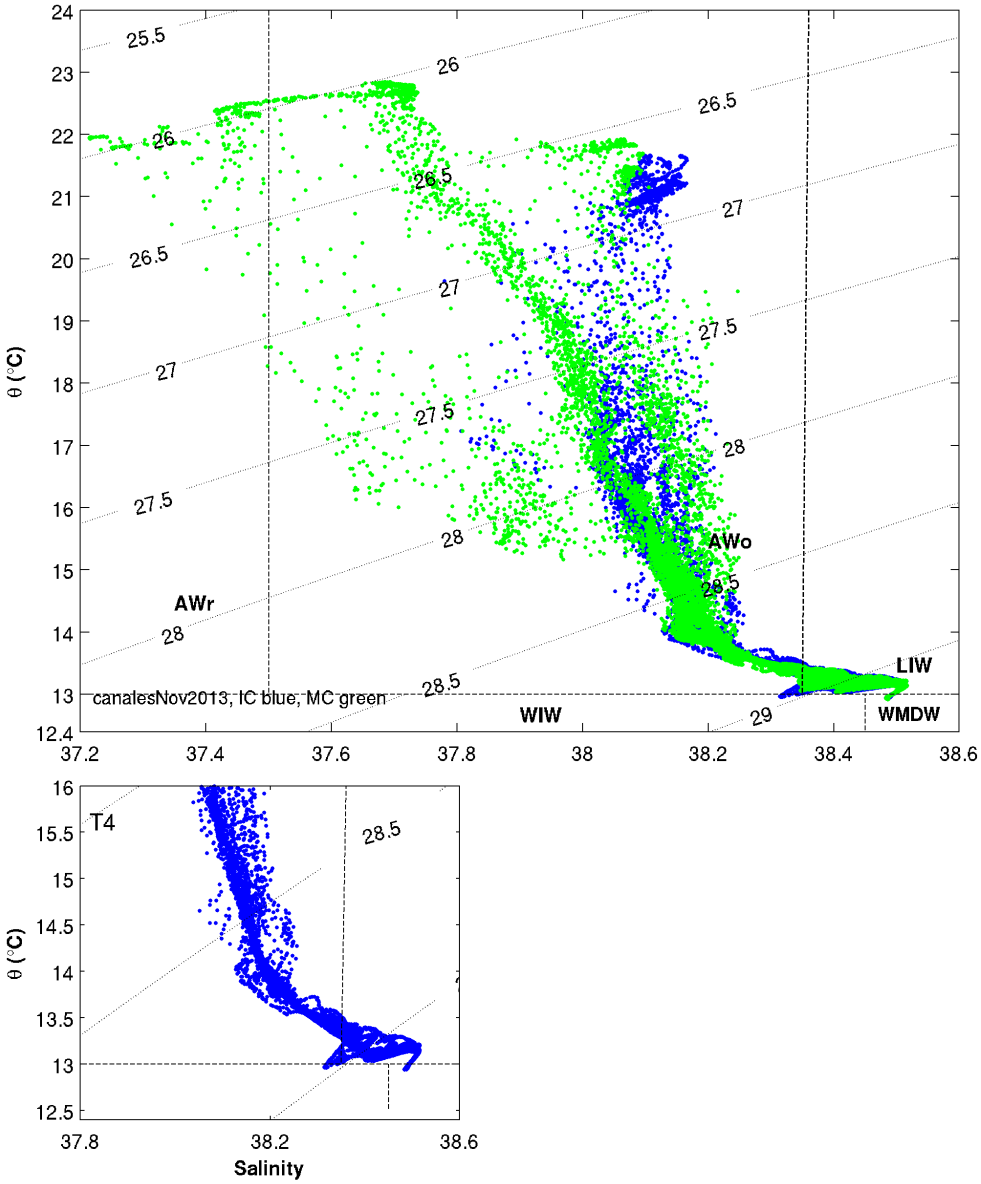

Figure 27b. θ/S plots for canalesNov2013.

The IC transects are marked in blue and the MC transects in green. The lower panel shows the two temperature minima at ~13.0 °C with salinity 38.3 and 38.4.

Summary: It seems likely that the two eddies seen in September are still present in the IC, as the location of two cold WIW lenses is similar. There is an unusually strong thermocline for the time of year (temperatures at the surface are of order 22 °C) and there is disconnect between the dynamics in the surface 0 to 100 m and the deeper layers, creating a complicated pattern of flows. In the MC the cyclonic eddy has passed, replaced by a sub-surface anticyclonic eddy. Inflows of fresher AW occur only through the MC during this mission. In the IC the same eddies likely persisted for 2 or more missions, as noted in the previous mission.

canalesDec2013

IC: At the start of the mission, T2 (05/12) the thermocline slopes generally downwards towards the west, there is however a 3-step pattern to the slope of the thermocline and, as seen in September 2012, a difference in the depth range of the thermocline between the west and the east of the channel (fig. 28a). In the west, the first step of the thermocline tilts down from 0.6°E to the western channel edge and the thermocline is deeper with a broader depth range (80 to 150 m). The slope of the isopycnals and the deeper thermocline both indicate NC flows, transporting water column properties from the north to the IC. Between the 0.6 and 0.7°E the thermocline has a small reverse in the gradient, then in the centre of the channel, from 0.7 - 1.0°E, the isopycnals tilt downwards to the west, more gently this time. Finally in the eastern edge of the channel, there is a third small 'step' (reverse in gradient of the thermocline) from 1.0°E to the channel edge, with warmer waters above (fig. 28a). From the centre to the east of the channel the thermocline is shallower and sharper (60 to 90 m). In the west of the channel and just below the broader range thermocline (at 100 to 150 m) the isotherms, isohalines and isopycnals dip steeply down to the edge of the channel, from 0.6 to 0.4°E. Below (150 m), this gradient becomes steeper and the isopycnal minima moves east, so that at ~200 m there is a pattern familiar from September and November 2013, with 2 dips in the isotherms, isohalines and isopycnals, one located at 0.5°E the other at 1.0°E. The western structure is more broad, visible from the channel edge to 0.7°E and associated with a water mass with the following general properties: θ ~13.5 °C, S 38.2 to 38.4 and σ 28.8 to 28.9 kg m^{-3}. The eastern structure, from 0.9°E to the eastern channel edge, is associated with water mass of θ 13.2 to 13.5 °C. Both structures are visible in salinity and density from below the thermocline to depths of 400 m, the eastern structure is however less visible in temperature. This appears likely to represent the two sub-surface anticyclonic eddies seen in September and

November. The western eddy with broad strong 40 cm s^{-1} southward velocities, that have a surface expression between 0.5 and 0.7°E. While in the east, the paired anticyclonic velocity structure is weaker. However strong 30 cm s^{-1} northward velocities are visible at the surface at 0.9°E associated with the sub-surface structure, with weak southward flows. The pattern is complex, possibly representing a situation where the two sub-surface eddies interact and dominate flow at depth, while above the thermocline they influence the path of the fresher AW inflows and the NC through the channel. So that in the west the southward eddy flow is augmented by the NC flow, taking this route through the 'blocked' channel, as suggested by the stronger southward velocities at the surface in the west, the broader 'winter' thermocline and by the change in the slope of the isopycnals from just below the thermocline where they tilt to the channel edge (as frequently seen with an NC flow) to deeper depths where the westerly tilt has moved offshore and 'merged' with the deep eddy structure. In the east of the channel, the fresh surface inflow takes advantage of the northward flow direction of the more easterly eddy. This picture has an additional element of complexity, although 2 eddies are clearly visible in density, some cyclonic pairing between the inflows in the eastern structure and the outflows of the western structure, also suggest a central doming centred around ~7.8°E. The transport of water mass north and south, indicate a dominance of southward flows above the recirculation (+0.71/-1.40 Sv), again indicating a NC, transporting of order 0.7 Sv, is flowing through the channel. Although the eddy cores are not WIW, given the similarity in the location and extent of the structures, it seems possible that they are the same eddies as seen previously in the September and November missions. Which, as to be expected of mesoscale features of long duration, have evolved and interacted with each other and with the strengthening winter NC and the fresh AW inflows. There are also two similar but distinct mixing lines to the surface, which likely signify the distinct water masses associated with the two eddies as well as fresher inflows of salinity 37.6 to 37.8 (fig. 28a and b) at the surface in the east of the channel. These patterns are not however static, but evolving. Two days later in T3 (09/12) the two eddies appear to be passing out of the channel, after a long residence. The thermocline still has a 3-step appearance but the thermocline range has now broadened across the channel and in the west there is also evidence of a front located at 0.5°E above the thermocline. Below the thermocline there are remnants of the eddy structures in salinity, however the isopycnals appear stratified below 200 m, with only small-scale perturbations in the 100 to 200 m depth range. In geostrophic velocity two southward

flows are visible at 0.5°E (to 200 m depth) and at 0.85°E (to 100 m depth), both apparently paired with northward flows, making smaller cyclonic surface eddies.

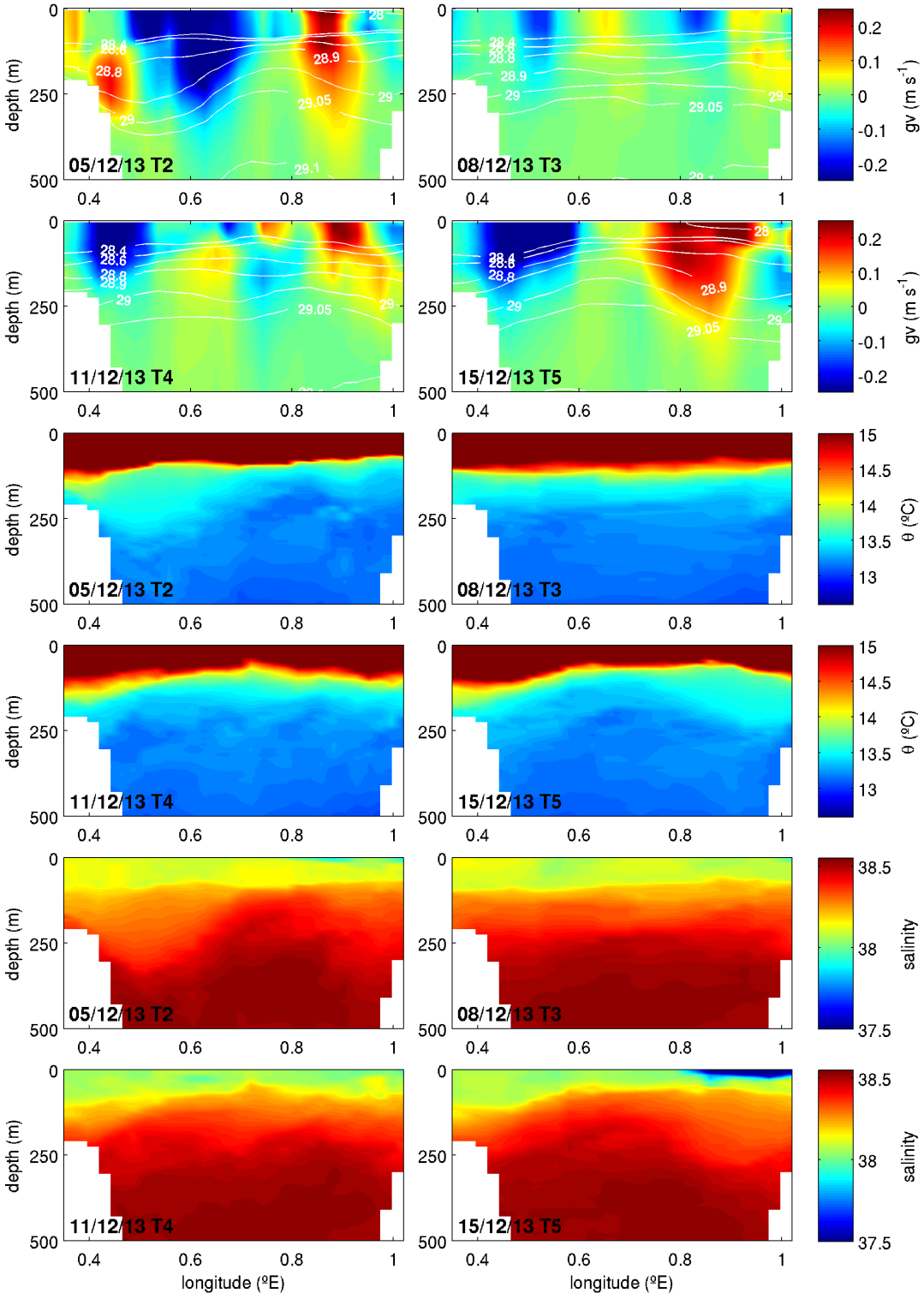

Figure 28a. Geostrophic velocity (gv), potential temperature (θ) and salinity sections for canalesDec2013. The transect numbers and mean date are marked in the bottom left of each panel, geostrophic velocities northward are positive and southward are negative, and selected isopycnals are marked in white.

The transport of water mass both north and south is low, +0.20 and -0.54 Sv. The dynamics of the IC are perhaps in a transition phase in T3, with smaller mesoscale disturbances after the passing of the long lasting sub-surface eddies. In T4 (09/12) the pattern is evolving, the thermocline still has a 3-step appearance, however the western step, with a broader depth range thermocline, now stretches from the western channel edge to 0.8°E, and the isopycnals tilt downwards to the channel edge indicating the NC flows at the western channel edge. In the centre of the channel, from 0.8 to 0.95°E, the thermocline tilts down to the east, and in the east of the channel from 0.95°E the thermocline rises and then dips to the channel edge. The pattern in geostrophic velocities indicate a sub-thermocline (sub 100 m) anticyclonic paired velocity structure in the centre of the channel (from 0.6 to 0.8°E) with velocities of order 10 cm s^{-1} and to depth of 250 m, with a surface cyclonic velocity pair above. To either side of this central pairing are, in the west the NC with velocities of 40 cm s^{-1} extending to 200 m depth, and in the east fresh inflows, with velocities of 25 cm s^{-1} extending from 0 to 100 m depth. The transport values are -0.84 Sv and +0.48. Five days later, in T5 (15/12), the pattern appears more stable with strengthened inflows and outflows. The thermocline still has a 3-step pattern, with a steepening of the westward slope of the isopycnals in the westerly step, a shallower central step. In the east the isopycnals still dip down to the eastern channel edge. The NC flows are associated with a more homogeneous 38.05 salinity water mass above the thermocline and in the east fresher AW inflows, with salinities in the range 37.4 to 37.7, are visible in the surface 30 m. Below the thermocline there is still a central doming of isotherms, isohalines and isopycnals (between the thermocline at 100 m and 500 m depth) and the geostrophic transports are relatively equal north and south +0.94 and -1.08 Sv. This suggests a balanced inflow and outflow dynamic, as the water masses do not seem to be re-circulated and as there is a difference in the pattern of stratification between the east and west sides of the channel. The pattern in geostrophic velocities, as before, suggests a sub-surface cyclonic structure, however the salinity, temperature and density indicate an easterly sub surface anticyclonic eddy, perhaps a remnant of the two eddies that originally occupied the channel. The dynamics in the IC appear particularly complex during canalesDec2013 and a rapid evolution occurs over the 4 transects and 15 days of the glider mission in the IC.

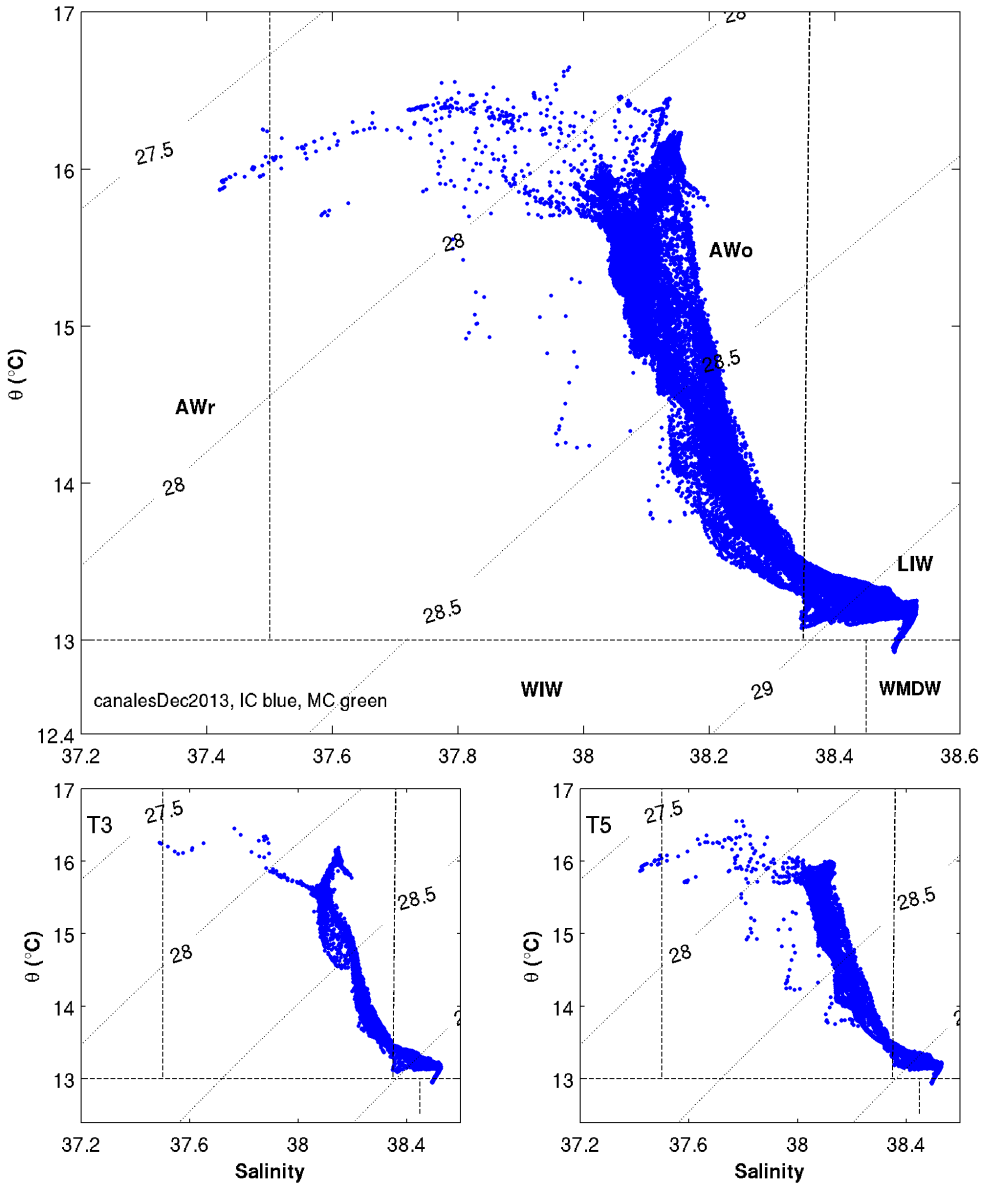

Figure 28b. θ/S plots for canalesDec2013.

The IC transects are marked in blue (note there were no transects of the MC this mission). The lower panels show showing the increase in inflows of fresher AW from T3 to T5, with salinities in the range 37.4 to 37.8.

Summary: It seems likely that the remnants of the September and November eddy pattern persist into December, but by T4 the eddies are passing out of the channel. In all transects we see some indication of fresher AW inflows occurring in the east of the channel, with salinities ranging from 37.4 to 37.7 in the surface 0 to 30 m, these strengthen from T2 to T5 (fig. 28b). In T2 to T4 there is evidence of more inflows on-shelf and by T6 they extend across the channel to 0.8°E. There is a consistency in the patterns of water volume

transports and in the pattern seen in the depth range of the thermocline, that indicate both the presence of the NC and that the inflows are consistent and take advantage of the velocity fields created by the sub-thermocline mesoscale activity to propagate through the channel. The pattern of sub-thermocline mesoscale activity is complex and interesting, the presence of the two dips in the isopycnals suggests that paired anticyclonic eddies lie at the base of the mesoscale structures, however there is also the suggestion of a paired cyclonic pattern in T3 and in T5. In T5 the NC and the inflows are both strong and a sub-surface anticyclonic structure remains in the east of the channel, perhaps influencing the inflows occurring above the thermocline. The signature of inflows is not fully captured by the glider transect and appears to extend further on shelf.

Note that this mission was synchronous with the ships mission SOCIB_Dic13 and a detailed comparison between the ship (CTD and ADCP) and the glider transects of these missions is available in Appendix D. Also note that due to the synchronous sampling of the IC that no transects of the MC were obtained this mission.

3.4 New observations across the glider missions

The scientific focus for the glider monitoring is the characterisation of sub-seasonal to seasonal variability in the exchange of water mass and associated dynamics in the IC. Thus the sampling strategy for the glider 'canales' missions has been to sample the IC as frequently as practical, across the same transect, given platform and mission constraints. The result is different to other time series, with intense multiple transect 'burst' sampling of the IC taking place over periods of 20 days, separated by weeks, and with samples across all months of the year. The transect-to-transect view generated with this quasi-continuous sampling is a key advantage of the glider monitoring in this dynamic location and, as seen in this chapter, has provided unique insight into the high degree of variability, the drivers of this variability and the evolution of dynamic features in the IC.

The seasonal arrival of WIW to the IC is captured, the isopycnals steepen in response to the influx of this cold fresh water mass, the NC deepens and strengthens, and there is a significant increase in transport of water mass southward. Thus far the glider data indicates that this strengthening could be an annual occurrence. Previously only a study by García Lafuente et al. (1995) mentions a change associated with WIW in the channel, however this observation was not expanded upon. Pinpointing the arrival of WIW in the IC also provides insight into the potential source of these waters. Heslop et al. (2012) suggested the

Ebro Delta region as the likely source of the January 2011 WIW, based on the average speed of the NC at the time and the indication in atmospheric data from the sea surface (buoy data) of a particularly cold event some days previously. This is in line with finding of Vargas et al. (2012) who recently identified WIW formation for winter 2009/2010 occurring along much of the Spanish mainland shelf to the north and south of the IC during this particularly cold winter.

The majority of eddies observed in the IC during 2011 to 2013 period were anticyclonic and had cold cores ($\theta \leq 13$ °C or ~ 13 °C). Additionally they can also be categorised into 3 general types: smaller eddies of 10 km diameter, that interrupt or modulate the flow for a few days e.g. February 2011; medium eddies of 20 to 30 km diameter that in pairs, centred at 0.6°E and 0.9°E, become wedged in the IC and bloc or modulate the flows for months e.g. March 2011 and September 2013; large 70 km diameter eddies, centred at 0.7°E, that occupy the full width of the channel and block or modulate the flows for months (e.g. March 2012 and August 2012), and can penetrate to depths of 500 m or more. The 10 km smaller eddies have not been noted in the IC previously, but have been noted in other glider datasets in the Mediterranean (Bosse et al. 2013). Although the general dimensions of the large and medium eddies have been previously noted (e.g. Pinot et al. 2002), the blocking of the channel by paired medium eddies, that interact, shift and block for several months, has not previously been noted as a re-occurring pattern.

Eddies occur both in spring and autumn, however the view from gliders suggests that the autumn eddies are somewhat different to those observed in spring. The autumn eddies are at least partially disconnected from the surface, lying below a strong seasonal thermocline. In addition they appear to modulate the surface pathways of the flows through the IC, rather than completely block the flows. The cold cores of the autumn eddies are also generally more stratified, in contrast to the more homogeneous lenses of distinct WIW seen in the spring anticyclonic eddies. The dynamic structures associated with these autumn eddies are thus generally more complex. The blocking events, with either a single large anticyclonic eddy or a pattern of two anticyclonic eddies 'wedged' in the channel, can persist for 1 – 3 months. By contrast, the MC was generally blocked by one eddy, cyclonic or anticyclonic, centred at ~1.9°E and occupying the whole channel. Interestingly a recent study of EKE from altimetry data in the Balearic Basin (Mason et al. 2012), found that the EKE is highest in autumn and weakest in spring, suggesting some difference is detected

between the spring and autumn eddy field. The combined mission-to-mission and transect-to-transect view from gliders is of particular benefit in observing how eddies enter and evolve in the IC and in correctly identifying the type of event.

The glider observations of inflows of fresher AWr are also important to our understanding of the channel dynamics. The inflows are generally visible as surface flows in the upper 0 to 70 m (100 m maximum), with salinities in the range 37.2 to 37.8, and occur synchronously in the eastern side of both the IC and the MC. The MC can have a slightly fresher range of salinities than those observed in the IC (e.g. 37.2 to 37.7 in the MC vs. 37.4 to 37.7 in the IC, in 2011). In 2011 the AW inflows were present in January/February through both channels and continued through to June, when the glider record ends for 2011. There was a pause in inflow through the IC in spring 2011, when the channel was blocked by eddies (canalesMar2011), however fresher inflows continued to enter through the MC. These observations give some pause for thought in terms of what is generally understood about these fresher inflows. Several authors have mentioned the summer decline of the NC as promoting fresh inflows (Pinot et al. 1995, Pinot and Ganachaud 1999, Pinot et al. 2002), and it has been suggested that Atlantic bluefin tuna follow these spring inflows of fresh water mass into the region (Alemany et al. 2010, Reglero et al. 2012). Spawning when sea surface temperatures reach threshold levels (θ >20.5 °C, preferentially 21.5 to 26.5 °C) in their preferred spawning grounds, which is close to the salinity front between AWr/AWo (Alemany et al. 2010, Balbín et al. 2014).

The presence or absence of inflows through the channels in spring, and hence the location of the AWr/AWo front north or south of the Balearic Channels, has therefore been related to the presence of 'blocking' eddies and WIW in the channels (Balbín et al. 2014). In 2011 however, the AWr inflows occurred strongly before, after and concurrent, through the MC, with 'blocking' eddies in the IC. It therefore seems likely that the AWr/AWo salinity front lay to the north of the Balearic Channels throughout this period of inflows, a view that is supported by satellite observations, which show a front to the north of the MC from February through to June in 2011in SST (fig. 29).

The inflows in 2011 illustrate three clear points regarding fresher AW inflows, firstly these inflows do not appear to be seasonal, secondly they are of several months duration, and thirdly they occur concurrently through both channels and their progress is not necessarily

halted by the presence of anticyclonic WIW 'blocking' eddies in the IC. It may be that the timing of the blocking of the IC is important, for example to the migration route of Atlantic bluefin tuna on their way to the AWr/AWo front influenced spawning sites, however if it is simply the location of the AWr/AWo front that these fish seek, then it would seem likely they would have spawned north of the channels in 2011, despite the presence of WIW 'blocking' eddies.

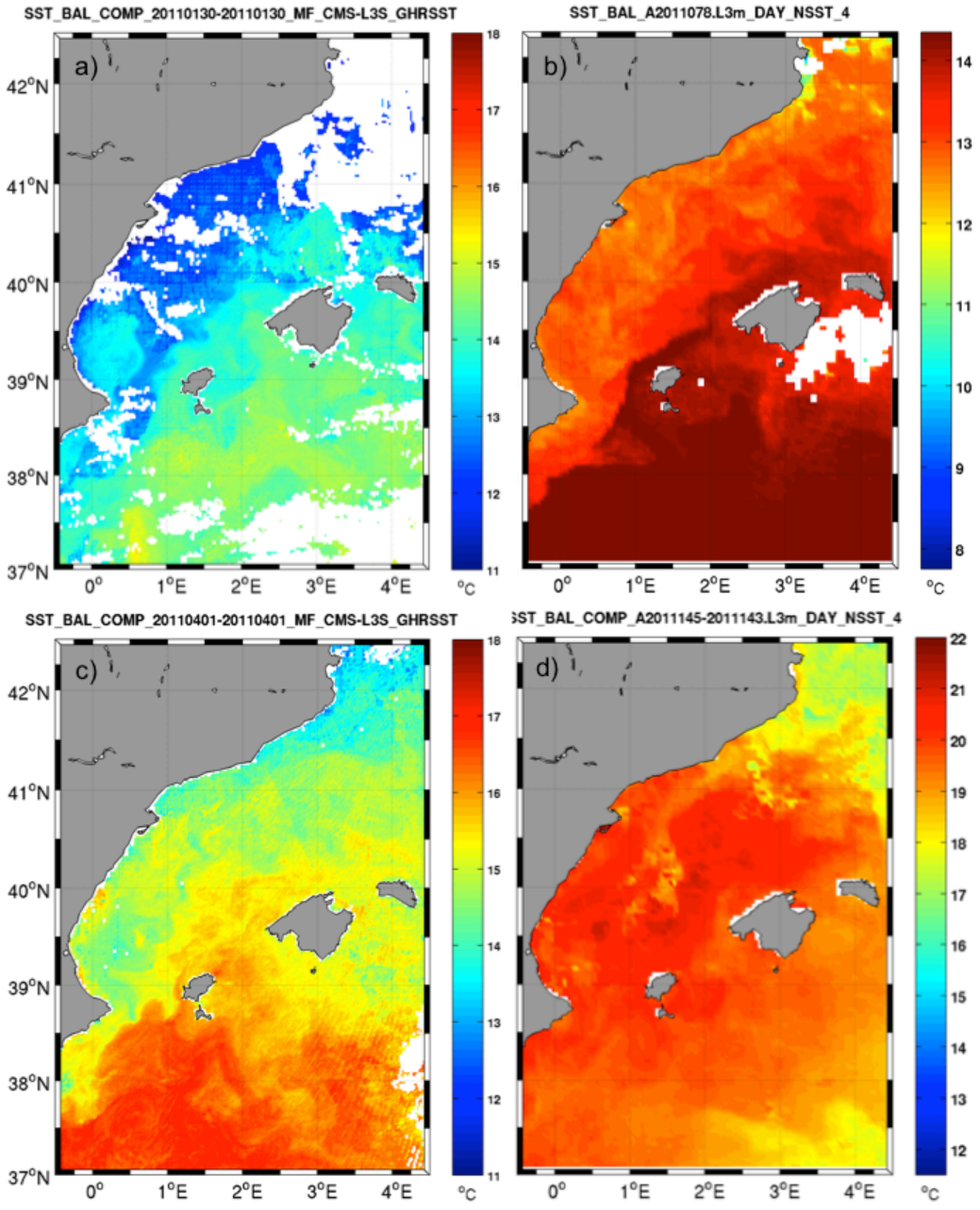

Figure 29. SST from January to May 2011.

a) 30/01/2011, b) 19/03/2011 (Day 78), c) 01/04/2011 and d) 22/05/2011 (day 142). A front is visible in SST north of the channels from end January to May 2011. Note: the temperature scales are different as SST changes considerably from January through May.

Finally, the higher spatial resolution afforded by the glider's profiles make visible new smaller-scale, sub 10 km, features and dynamics. For example, in April 2013 a low temperature body of WIW ($\theta < 12.5$ °C), initially observed high on the western shelf area of the IC is seen to gradually migrate down shelf along the sea floor over a period of 10 days, reaching the channel at the end of the mission, where it appears to strengthen the NC flow. Again in September 2013 strong shelf to channel exchange processes are captured, when filaments of higher salinity water are observed from shelf floor extending into the deep channel, perhaps associated with the movement on/off shelf of the NC in response to eddy activity in the centre of the channel. This level of detail is not visible in the traditional ship CTD data. See Appendix D for a comparison between ship and glider transects, including this example. Although beyond the scope of this thesis, a follow-up study could investigate the shelf to open ocean interactions in the IC, for example, by looking at turbidity and oxygen, as well as temperature and salinity.

The quasi-continuous (monthly and 'burst' sampling) of the glider monitoring allows us to observe the evolution of the dynamics from transect-to-transect. The detail from glider 'burst' sampling of the IC provides a new view of variability, the dynamic evolution of features and of reoccurring features, which was not previously possible with single seasonal transects or sparse moorings. The evolution observed is complex, with the temporary mesoscale structures providing a good indication of just how dynamic the mesoscale field is in this region of the Mediterranean. Notwithstanding this complexity, consistent patterns in T, S, ρ and geostrophic velocity are also detected and these provide the basis for the 'modes' or patterns proposed for the dynamic elements of the IC, as outlined below.

3.5 Proposed 'modes' for the Ibiza Channel exchange

With observations across all seasons, 4 seasonal 'modes' are proposed for the dynamic IC exchange (fig. 30, first 4 panels). An additional episodic 'mode', the 'AW inflow' mode, is also proposed (fig. 30, lower panel), which represents the vigorous AWr inflows that can occur over several months and can be combined with other modes. These represent the repeated spatial patterns observed by gliders during the 2011 to 2013 period, and expand on the 3 'modes' initially proposed by Heslop et al. (2012).

Seasonal modes	
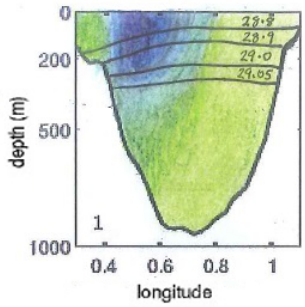	'**winter NC' mode:** The NC is a strong southward flow, generally from the western shelf edge to 0.6/0.7°E and to depths of 300 - 400 m, with typical velocities of 20-40 cm s-1 and transport of 1.0-1.2 Sv, e.g. canalesJan2011 T1 and T4. The density gradients tilt from 0.65/0.7°E to the western channel edge and the LIW maxima are pushed down by 100-150 m in the west of the channel. This mode initiates with the autumn increase in NC strength and is in place from November to February.
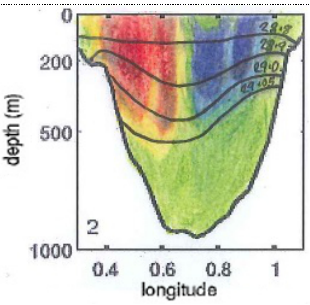	**'spring eddy' mode**: There are 2 spatial variations of this mode. 1) a large energetic anticyclonic eddy (as depicted), of order 70 km diameter, penetrating to 400-600 m depth and centred at 0.7°E, with velocities of 30-40 cm s^{-1}, that 'blocks' the IC e.g. canalesMar2012 and canalesMar2013, or 2) two medium anticyclonic eddies, of 25-30 km diameter, centred at 0.6 and 0.9°E, that become wedged in the channel, interact and combine to 'block' the IC, e.g. canalesMar2011.
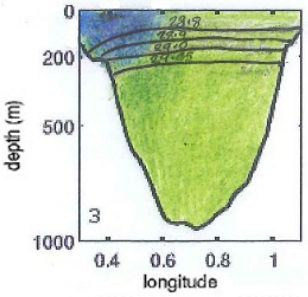	**'summer NC' mode:** The isopychnals in a 'summer' pattern are generally horizontal across the centre of the IC with a small downwards tilt at the west channel edge, denoting a weak and shallow NC, with transport of order 0.2 to 0.4 Sv. For examples odf this mode see canalesJun2011 and canalesJul2012.
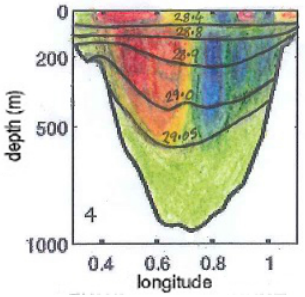	**'autumn eddy' mode**: In autumn there is another active eddy period, with same spatial variations, a single large eddy (as depicted to the left), centred at approx. 0.7°E, or two medium eddies centred at 0.6 and 0.9°E, for examples see canalesSep2012 and canalesDec2013. Autumn eddies however lie below the thermocline and are disconected from the surface. They do not fully 'block' the IC, instead modulating the surface pathway of the flows.
Episodic mode	
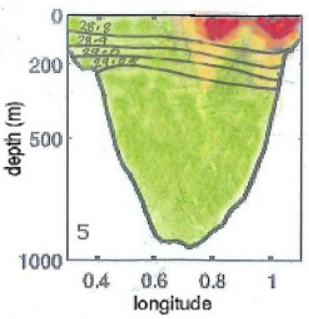	**'AW inflows'**: This episodic mode can be combined with any of the other modes. It is typified by a shallower tilt in the isopycnals at the eastern edge of the channel or a more general easterly slope fro the centre of the channel (as depicted). For examples see canalesJan2011 ('AW inflows' and 'winter NC') and canalesJun2011 ('AW inflows' and 'summer NC'). 

Figure 30. Summary of 'modes' proposed for the Ibiza Channel exchange.

The four proposed seasonal modes and single episodic mode are shown as sections in geostrophic velocity, with key isopycnals marked as black lines, σ 28.8, 28.9, 29.0 and 29.05 (plus 28.4 for 'autumn eddy' mode).

The annual cycle of the 4 seasonal 'modes' could generally be described as follows. The NC appears to strengthen in autumn to ~0.6 Sv, after weak summer flows of the order of 0.1 to 0.4 Sv, with onset around October/November. In late November/early December the observations suggest an additional rapid strengthening of the NC to the strong 'winter NC' mode, associated with transport of the order of 1.0 to 1.2 Sv (fig. 30). With this onset of stronger flows the autumn eddies appear to depart the IC, perhaps being swept from the channel as the current strength increases. A variation of the 'winter NC' mode occurs when WIW appears in significant quantities in the IC following winter storm events in January/February/March. This causes a dramatic steepening of the isopycnals associated with the NC, a deepening of the NC to 500 m depth, with a 300 m deepening of the LIW maxima and with a coincident increase in transport to 1.5 – 1.7 Sv (examples are canalesJan2011 T6 and canalesJan2013 T6). In spring, the IC can become 'blocked' by eddies and transport of watermass northward and southward is more balanced, reflecting the re-circulatory nature of the flows. As described earlier in section 3.4, the spring eddies ('spring eddy' mode) are generally anticyclonic, have WIW cores and a clear dynamic connection to the surface. They also appear to more effectively block the IC than those observed later in the year. In autumn, eddies also appear in the IC, however the eddy cores are more stratified and on the boundary of WIW (~13 °C). Also they lie below the seasonal thermocline, but are connected to the surface and appear to modulate rather than block the surface flows ('autumn eddy' mode). Both spring and autumn eddies show similar spatial patterns, either a single large centrally located eddy of order 70 km diameter, centred at 0.7°E (as shown in fig. 30), or 2 medium eddies, centred around 0.6 and 0.9°E and of order 20 to 30 km in diameter. There appears to be a transition period in autumn, before the onset of the 'winter NC' mode, and in spring, before the onset of the 'summer NC' mode, when transport southward is of order 0.6 Sv, the isopycnals are less steep and the NC more shallow, penetrating to 250 m (for example see canalesMay2013). This could be termed a 'weak winter NC' mode, however as this pattern it is short-lived and not clearly different from a 'summer NC' mode, it is not defined here as a separate mode.

The 4 modes proposed are possibly too simplistic and more patterns may emerge with time, however it should be stressed that the ability to propose the modes at all is a result of the new sampling capability of gliders. The repeated transect-to-transect view of the IC allows a greater sense of the prevailing dynamics to emerge over a 15 to 20 day mission, as well as pinpointing specific events in time and their impact on the exchange. The relatively

fast repeat of the missions enables an interconnection to develop between missions, months and seasons, based on the evolution of these features.

In general, the 4 seasonal 'modes' represent a interplay between basin-scale and mesoscale dominated dynamics, although the timing of the modes will differ from year to year and some modes may even not be present some years. The AWr inflows can occur with the 'winter NC' and 'summer NC' modes, and indeed across more than one season, as seen in 2011. Although inflows may be present with the 'autumn eddy' mode their surface flow is modulated by the sub-thermocline eddy structure.

CHAPTER 4: Variability, sub-seasonal to interannual

More than a decade ago Pinot et al. (2002) used data from 2.5 years of ships missions, combined with data from sparse moorings, to characterise the seasonal cycle of transports of water mass in the IC. They defined a winter (March) maximum of 1.2 Sv in the transport of water mass southward, coincident with a minimum of 0.2 Sv in the transport of water mass northward, and a summer (July) minimum of 0.3 Sv in transport southward, coincident with a maximum of 0.7 Sv in the transport of water mass northward (table 4 below). This definition was in line with earlier climatological estimates (Font, Salat and Tintoré, 1988) and some earlier single mission studies (Pinot et al., 1995). Some other estimates of water mass transport were however different, see table 4.

Reference	Date	Survey	South (Sv)		North (Sv)		Net (Sv)	
Ibiza Channel			**Winter**	**Summer**	**Winter**	**Summer**	**South**	**North**
Font, Salat and Tintoré, (1988)	historical data	Ships CTD	-1.00	-0.50				
Castellon et al., (1990)	May - June 1989	Ships ADCP		-0.24				
Lopéz-Jurado and del Rio, (1994)	Nov 1990 - May 1991	Ships CTD	-0.65	-0.56	+1.08	+0.51		
Pinot et al., (1995)	May - June 1991	Ships CTD		-0.20		+0.50		
Pinot and Ganachaud, (1999)	June 1993	Ships CTD		-0.55		+0.55		
Pinot et al., (2002)	Mar 1996 – Jun 1998	Ships CTD	-1.20	-0.30	+0.20	+0.70	-1.05	+0.35
Mallorca Channel								
Pinot et al., (2002)	Mar 1996 – Jun 1998	Ships CTD					-0.30	+0.05

Table 4. Transport estimates for the Ibiza Channel from historical ship missions.
The transports southwards are denoted as negative and the transports northwards as positive, it is worth noting that most cruises took place during the summer.

No clear pattern of north or south transport in the MC emerged from this study, Pinot et al. (2002) did however suggest that a seasonal cycle existed in the net transport (here net means the sum of the positive and negative transports), with a summer maximum of 0.05 Sv (July) transport northward, and a winter minimum of 0.3 Sv (March) transport southward. Similarly the pattern of net transport in the IC was determined as a winter maximum of 1.05 Sv southward and summer maximum of 0.35 Sv northward, leading to the conclusion that the IC was dominated by outflows while the MC was the preferred route for southern waters to travel north, although the net transport does not back this second statement up.

4.1 High frequency variability

The transport of water mass north and south through the IC for all the glider missions are shown in fig. 31. In this figure the complexity of the Chapter 3 mission descriptions are encapsulated and we are able to visualise the inflows and outflows per water mass for the complete glider time series. This style of figure, first published in Heslop et al. (2012), was developed as an efficient means of conveying the detail of the exchange of water mass through the Balearic Channels. Each bar in the figure represents the total transport of the different water masses for each transect, the transport northward is positive and the transport southward is negative, each mission is represented by a 'cluster' of bars, and the different water mass types are indicated by colour. The total transport northward or southward is the total height of the bar (i.e. the sum of all the water masses above or below the zero line).

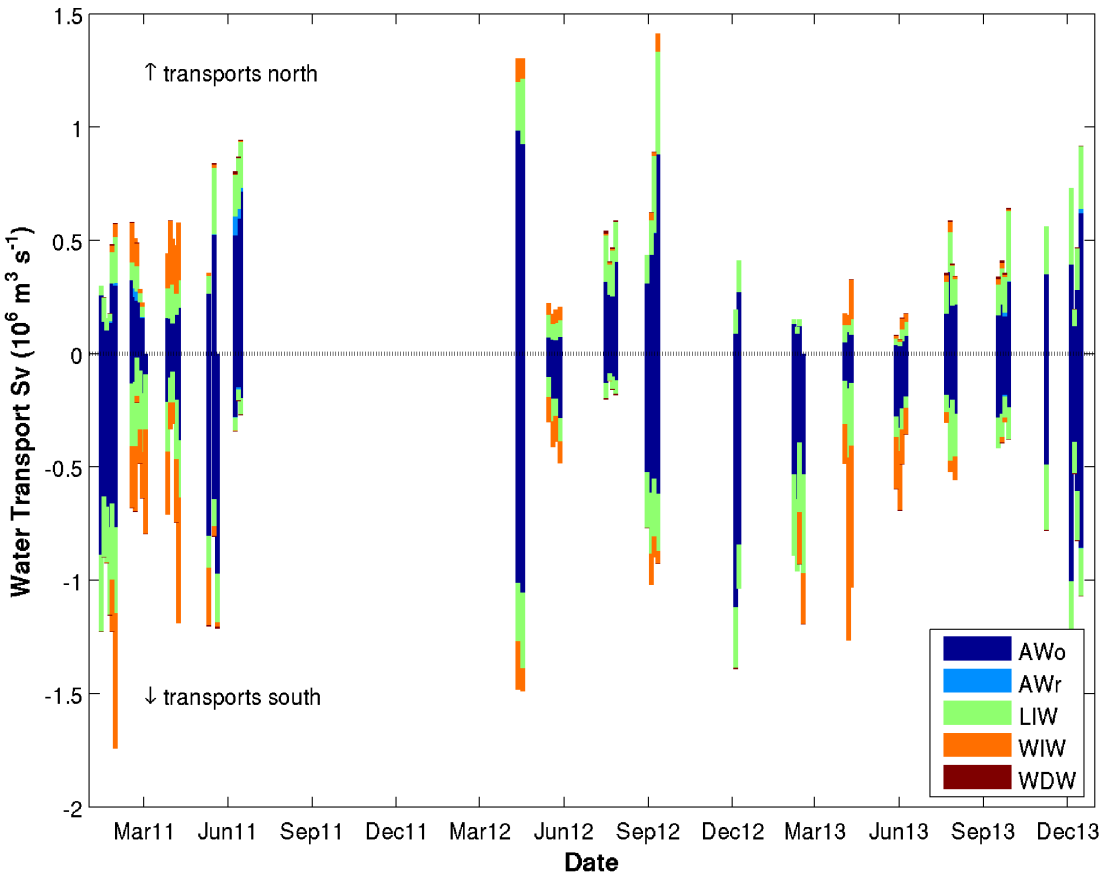

Figure 31. Geostrophic transport in the Ibiza Channel by water mass.
Each bar represents the water mass transport for a single (2-day) glider transect of the deep (central) part of the channel. The total bar height is the total volume of water transported, the transport northward is positive and transport southward is negative, and the different water masses are indicated by colour (see legend, where WDW stands for WMDW).

What is immediately striking in this representation of the watermass exchange is the high frequency variability in transport, occurring between transects. For example in January 2011 there is an increase of 0.82 Sv in the transport southward over 7 days with an increase of 0.51 Sv between transects (3 days). Again in March 2013 there is a similar increase in southward transports, 0.79 Sv in 3 days. Both of which are coincident with the initial winter arrival of WIW to the IC. High frequency changes are also associated with mesoscale perturbations, for example in December 2013 a change of 0.86 Sv is observed in the transport southward through the IC and in March 2011 the transport decreases by 0.7 Sv between transects. Additionally in February 2011 and May 2011 changes of the order of 1 Sv are seen in the water mass exchanges. In the transport of water mass northward changes of order 0.4 to 0.5 Sv occur between transects in January 2011, May 2011, August 2012, associated with mesoscale variability, and in December 2013 associated with AW inflows. All theses examples represent changes in the transport of water mass of the same order as the previously defined seasonal cycle (0.9 Sv southward and 0.4 Sv northward, Pinot et al. 2002), occurring over timescales of days to weeks.

In summary, glider monitoring reveals high variability in the transport of water mass, with changes of the same order as the previously defined seasonal cycle occurring over timescales of days, the changes observed are driven by 3 processes:

- The arrival of WIW
- The arrival/departure of eddies
- Strong AW inflow

Other patterns can be seen in the IC transport figure (fig. 31), the high temporal resolution of the glider data enables us to pinpoint the arrival and departure of WIW (marked in orange) in the IC in 2011 and 2013, e.g. 27/01/2011 and 11/02/2013. Patterns of balanced transport, where similar volumes of water masses flow both north and south, e.g. in March 2011, March 2012 and August to November 2013 are also visible. These occur when the IC is occupied by eddies and a relatively balanced recirculation of water masses is taking place. The instances of particularly high balanced transport (>1 Sv) are related to the activity of single large eddies (e.g. March 2012, September 2012). See fig. 31a for a version of the IC transport figure, fig. 31, with an overlay of the prevailing dynamics related to the 'modes' proposed in Chapter 3, section 3.5, to connect the concept of patterns in the transport with

patterns in the main dynamic features of the IC. There is also the suggestion of a seasonal pattern in the southward transport, visible in the decline in transport volumes from January/March to June 2011 and 2013. This is explored more fully in the next section, when the combined glider and ship dataset is analysed and long-term mean transport values derived.

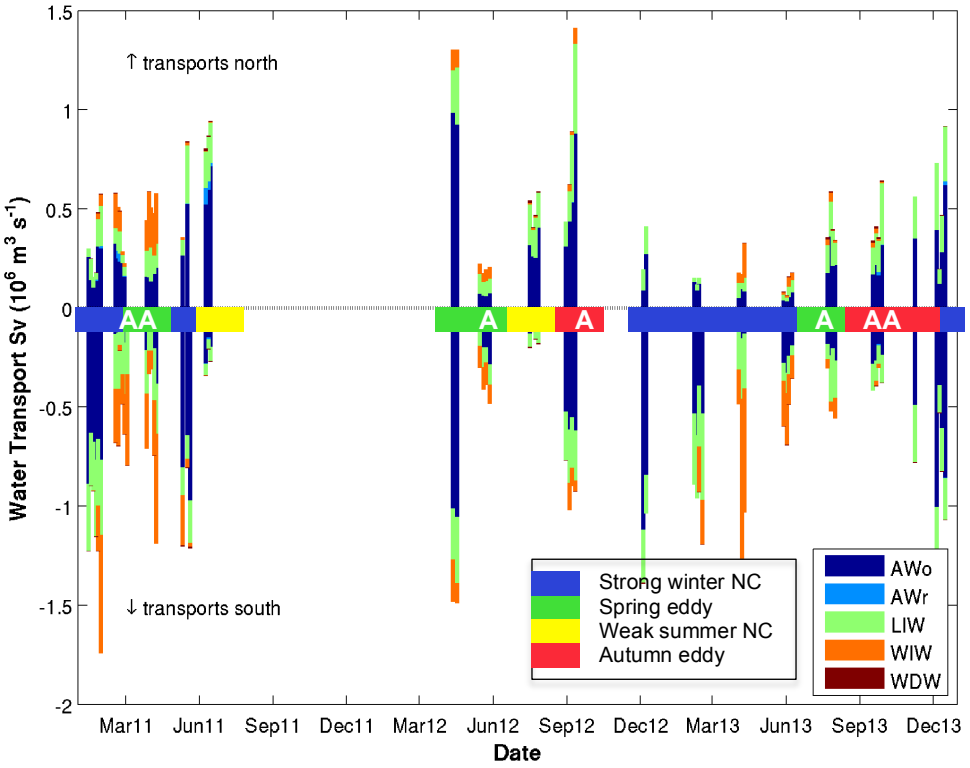

Figure 31a. Geostrophic transport in the Ibiza Channel with 'modes' and eddies.
As for fig. 31, with the addition of colour bars to represent the prevailing 'modes' of circulation associated with the transport during each mission. The coloured bars represent the different 'modes' described in Chapter 3, section 3.5, dark blue signifies the strong 'winter NC' mode, green the 'spring eddy' mode, yellow the weak 'summer NC' mode, and red the 'autumn eddy' mode. The eddy pattern and rotation are also noted, 'A' signifies a single large anticyclonic 'blocking' eddy, typically 70 km in diameter and centred at 0.7°E, and 'AA' two anticyclonic 'blocking' eddies, typically 20-30 km in diameter and centred at 0.6 and 0.9°E.

The transport of water mass per transect for the MC is shown in fig. 32, however with the lower sampling resolution of this channel there is not the same transect-to-transect view of variability. In comparing this figure with that for the IC, the connection between the channels with respect to the fresher AWr inflows is clear. As described in Chapter 3, when AWr inflows occur in the IC they also occur in the MC, e.g. January to June 2011 and Dec 2013. However the assertion that the MC is the preferred route for the fresher inflows (Pinot et al. 2002) does not appear to match the pattern seen in the glider missions, in

which a significant quantity of the AWr inflows occur through the IC, in fact the MC exports AWr out of the Balearic Basin when the AWr/AWo front lies to the north of the channel, see section 4.3 for more details on transport of this fresher water mass.

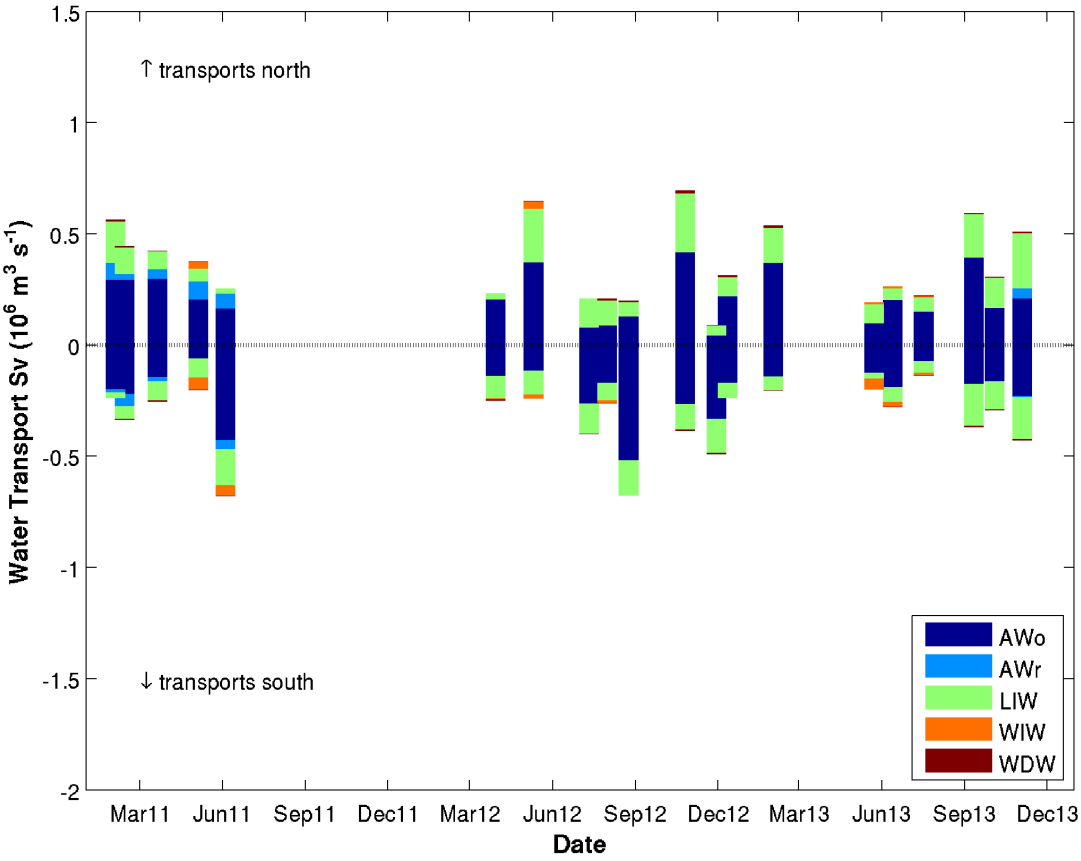

Figure 32. Geostrophic transport in the Mallorca Channel by water mass.
Each bar represents the water mass transport for a single (2-day) glider transect of the deep (central) part of the channel. The total bar height is the total volume of water transported, the transport northward is positive and transport southward is negative, and the different water masses are indicated by colour (see legend, where WDW stands for WMDW).

Similar transport figures were produced for the ship dataset, however the sparse sampling means that they do not provide much insight into either high frequency or seasonal variability and so are not included here.

4.2 Seasonal variability

For the analysis of seasonal variability the 3 years of intensive glider missions were combined with the 18-year record of more sparse CTD data from ship missions, covering the time period from 1996 to 2013. In this combined dataset are 115 complete transects of the IC, 63 from glider and 52 from ship missions, and 68 complete transects of the MC, 20

from glider and 48 from ship missions. See table 5 below for a representation of the distribution of the two datasets by month and year.

IC	Jan	Feb	Mar	Apr	May	Jun	Jul	Aug	Sep	Oct	Nov	Dec
1996			s	s	s	s		s				
1997		s		s	s		s	s				
1998	s					s						
1999					s							
2000									s		s	
2001			s			s					s	
2002			s		s				s			
2003			s			s				s		
2004			s		s					s		
2005			s			s				s		
2006				s		s						
2007							s			s		
2008		s		s			s			s		
2009					s							
2010				s								
2011	gggg gg	s gg gggg	gg	ggg	s ggg	s ggg	s					
2012				gg	gggg		gggg	g	ggg			gg
2013		gggg		s gggg	g	s ggg	gggg		ssss gggg		g	gggg ss

MC	Jan	Feb	Mar	Apr	May	Jun	Jul	Aug	Sep	Oct	Nov	Dec
1996			s	s	s	s		s				
1997	s			s	s		s	s				
1998	s			s		s						
1999					s							
2000											s	
2001				s	s	s					s	
2002			s		s				s			
2003					s					s		
2004			s		s					s		
2005			s			s			s			
2006				s		s				s		
2007							s			s		
2008		s			s		s				s	
2009					s		s					
2010				s								
2011		gg	g		s g	g	s					
2012			s g		g		gg	g		g	g	g
2013	g		s		g	s g	g		g	g	g	s

Table 5. Distribution of sampling of the Balearic Channels from 1996 to 2013.
The tables show the temporal distribution (year/month) of transects sampled in the Ibiza Channel (above) and the Mallorca Channel (below). Transects sampled by gliders are 'g' and ship are 's'. It should be noted that only complete transects, suitable for the transport analysis, are included in the tables.

Plotting this combined dataset by month enables several patterns to emerge, see fig. 33 for IC and fig. 34 for MC. In the IC a seasonal signal is clearly visible in the southward transport of water mass, with weaker transport in summer across June, July and August,

strengthening in autumn to a winter maximum in December and January. In February to March there is perhaps a decline in water mass transport detectable, indicating the months of greater 'blocking' of the IC, followed by a strengthening of geostrophic transport again in April and May, before a decline to the summer minimum. The geostrophic transport northward, by comparison, does not appear to show a clear seasonal signal, the volumes transported are variable across all months.

The arrival and longevity of WIW (orange) is also clearly indicated, generally WIW arrives to the IC in late January/February and leaves by June, and is rarely present from August through December. The inflows of the fresher AWr (light blue) appear throughout the year, there does appear to be a higher incidence of fresh AWr inflows in June, however this could be due to sampling bias, as the ship data are more heavily sampled in late spring to summer (April to July), than at other times of the year, see table 5.

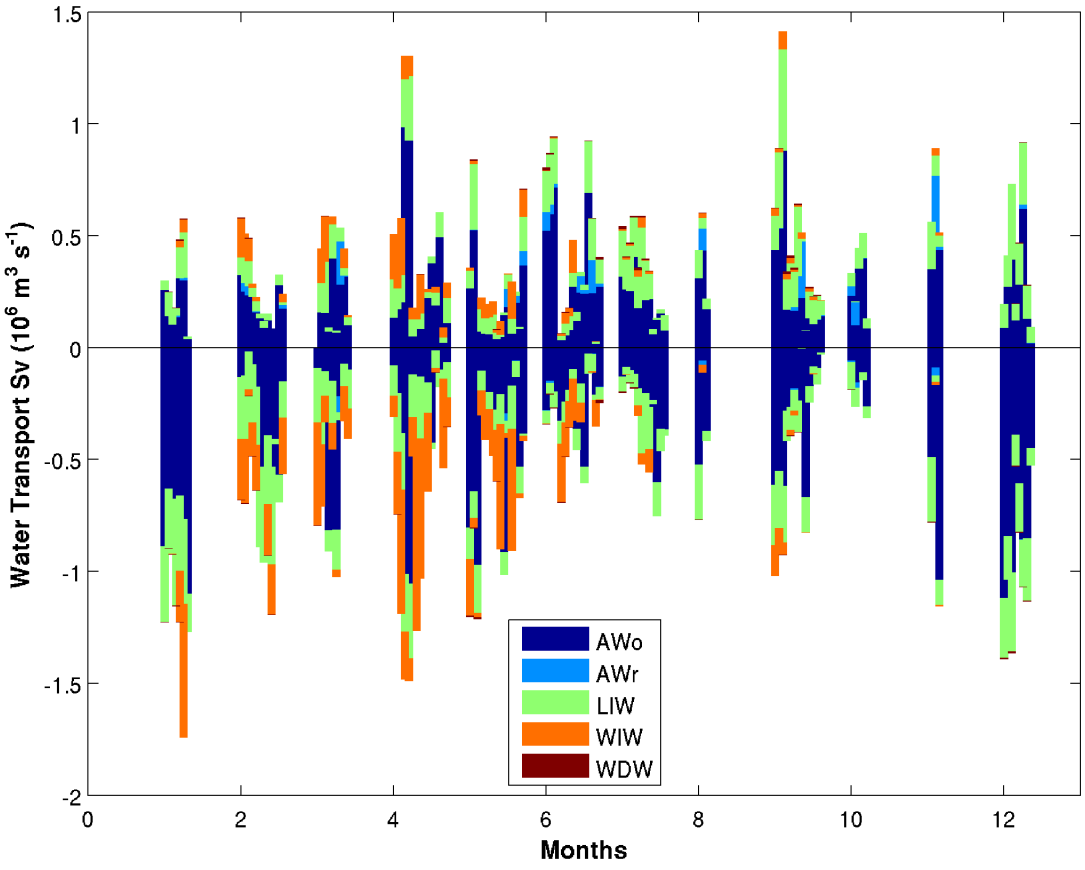

Figure 33. Geostrophic transport of water mass in the Ibiza Channel by month.
Each bar represents the transport for a single transect, glider or ship. The total bar height is the total volume of water transported, the transport northward is positive and transport southward is negative, and the volume

of the different water masses is indicated by colour (see legend, where WDW stands for WMDW). Note: only valid (sufficiently complete) transects are included, see table 5.

Plotting the mean geostrophic water mass transport by month for the MC, does not reveal the same strong seasonal pattern, fig. 34. Again the fresher AWr inflows (light blue) appear to be more concentrated in the summer, in this case in May and June, however again there are also more transects sampled during these months (see table 5) and so more events would naturally be captured. What this figure does show is that AWr, when present, plays a greater role in terms of the percentage of the total volume of water transport northward in the MC. It is also clear that little WIW is exported through this channel, and that which is, passes through the channel later in the year (April and June).

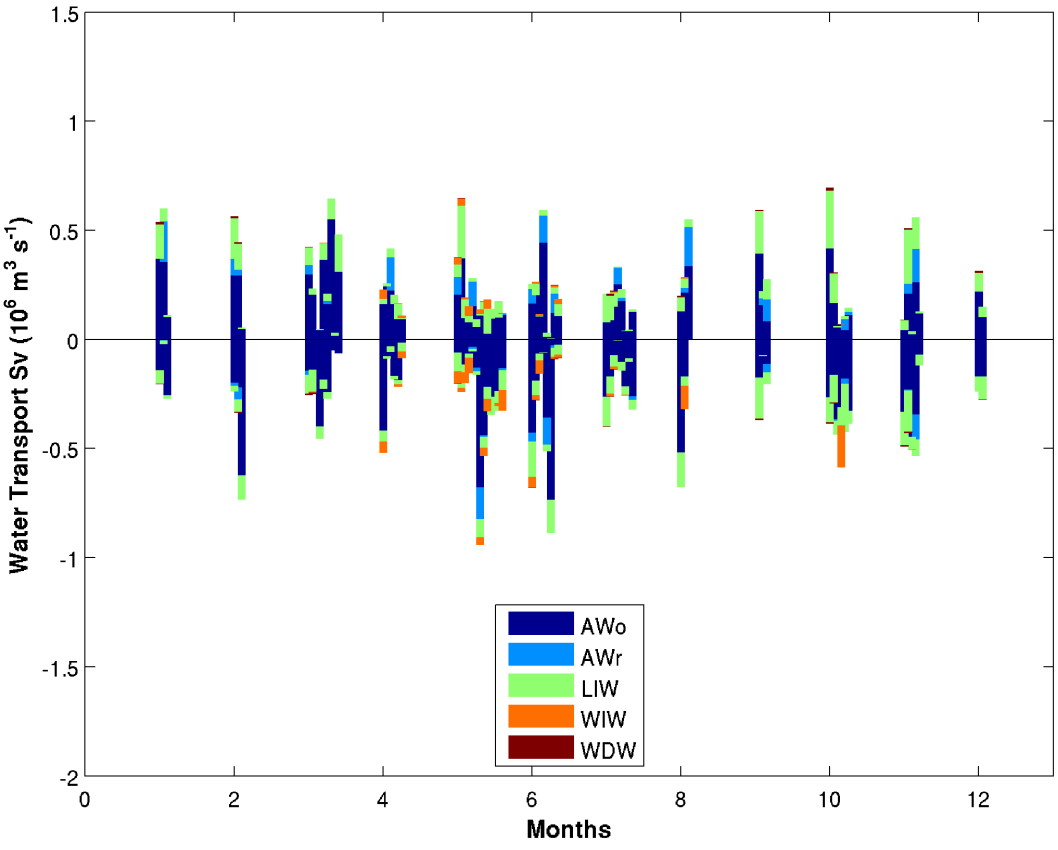

Figure 34. Geostrophic transport of water mass in the Mallorca Channel by month.
Each bar represents the transport for a single transect, glider or ship transect. The total bar height is the total volume of water transported, the transport northward is positive and transport southward is negative, and the volume of the different water masses is indicated by colour (see legend, where WDW stands for WMDW). Note: only valid (sufficiently complete) transects are included, see table 5.

In order to quantify this seasonal cycle in the IC, the mean volume of water transported per month for all transects (glider and ship) was calculated and a 3-month moving average

applied to create a smoothed seasonal cycle for transport north and southward through the IC, fig. 35 black dashed line. Although at first glance this seasonal cycle perhaps does not appear to represent a cycle against the high in-month variability (stars and dots), the results support what was visible in fig. 31 and 33, namely that a seasonal cycle in the southward transport of water mass exists, with an amplitude greater than the variance. However there is no discernable seasonal signal above the high variability, for the northward transport of water mass.

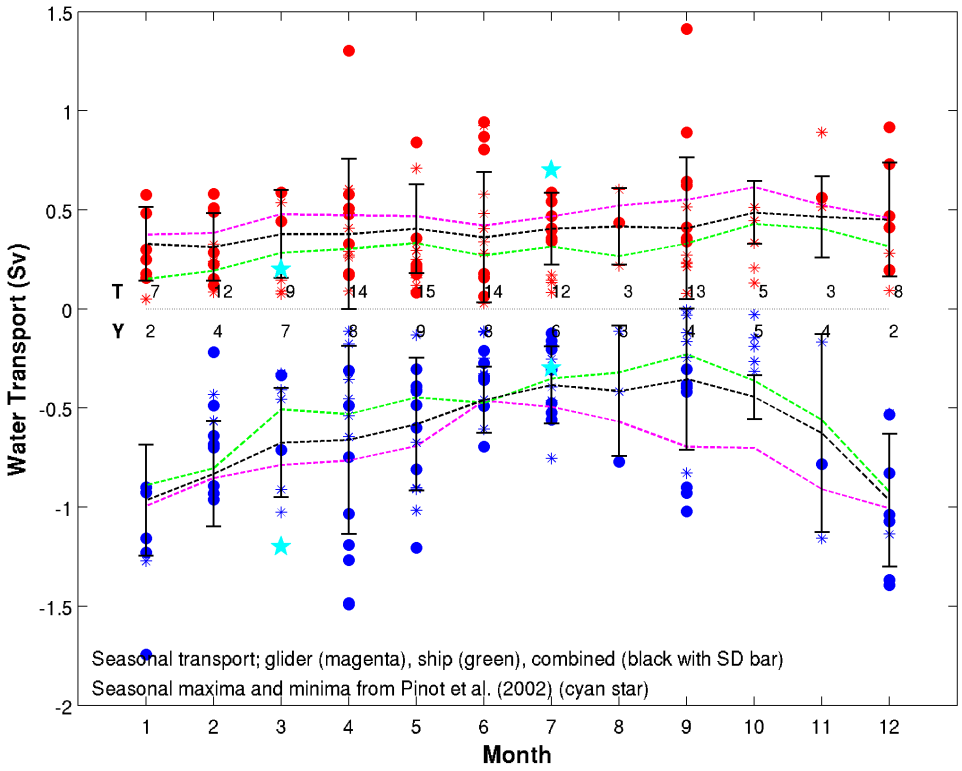

Figure 35. Mean seasonal cycle for geostrophic transport in the Ibiza Channel.
For the combined dataset (black dashed line with bar to represent SD) and glider data only (magenta dashed line), the ship data (green dashed line) calculated from the monthly mean of the per transect transport values, with a 3-month moving average applied. The transport per transect is binned and plotted per month for glider (dots) and ship (stars) data. The Pinot et al. (2002) previously defined transport maxima and minima are also shown (cyan stars). The number of samples in the monthly mean is indicated along the baseline; above the baseline is the number of transects (T) and below the numbers of years (Y) in the monthly sample.

The good agreement between the seasonal cycles developed from the two independent datasets, glider and ship (fig. 35, magenta dashed line and green dashed line respectively), with their different sampling strategies and temporal scales, offers additional and compelling support for this new view of seasonality in the IC exchange. As noted in the glider and ship comparison study (Appendix D) geostrophic transport values for ship CTD

data are likely lower when mesoscale features are present in the channel. This is due to the more coarse sampling resolution that inherently averages small spatial scale variability and can perhaps be seen in the greater divergence between the seasonal curves for the transport southward in spring and autumn. The spread of the individual transect transport values (fig. 35, glider dots and ship stars) highlight the high degree of variability in the transport within any one month.

With this new interannual mean seasonal cycle in southward transport there is a maximum transport in December of order -1 Sv and a broad minimum of order -0.4 Sv, from July through to September. This is in general agreement with that previously defined by Pinot et al., 2002 (fig. 35, cyan stars), however, now, a complete month-by-month picture of the cycle is defined and the timing of the cycle has shifted, with a winter maximum 2 month earlier and the duration of the summer minimum increased to 3 months. The new mean seasonal cycle is however similar in timing and magnitude with early studies of seasonality in the NC from the south of France (Astraldi et al. 1989, Millot 1999). These identified a winter maximum transport of order 1.0 Sv and a summer minimum transport of order 0.3 Sv (June to August). The cycle is also in agreement with previous observations of a strengthening of the NC in October (Astraldi et al. 1989). However although the autumn gradient of the seasonal cycle suggests a fairly rapid increase in transport (current strength) through October, the smoothed data does not show a sudden autumn increase in NC strength in autumn observed by Bethoux (1988) and identified by Birol et al., (2008), and as also suggested by the glider mission analysis in Chapter 3.

In northward transport the monthly mean values remain relatively stable throughout the year, varying between +0.3 Sv and +0.5 Sv, with an interannual mean of +0.38 Sv. If anything there is a minimum in February (+0.3 Sv) and a maximum in October (+0.45 Sv), but a signal of this amplitude is not significant above the high variability (as indicated by the SD, black bars). This lack of a seasonal signal in the northward transport seems reasonable following glider observations as described in Chapter 3. However the finding is at odds with earlier research that describes a summer reverse in the exchange (Pinot et al. 1995, Pinot and Ganachaud 1999, López-Jurado et al. 2008). In general the studies propose that that a seasonal decline in the NC allows southern waters to 'progress' into the Balearic Basin. Given the emphasis that has been placed on the relationship between seasonal fresh inflows and the spawning grounds of regional commercial fish stocks (Alemany et al., 2010;

Reglero et al., 2010; Balbín et al., 2013), it is important to understand if we are missing a seasonal component not visible in the total volume transports, therefore an analysis of the annual cycle by water mass is undertaken in the next section.

With this new definition of a mean seasonal cycle, potential 'anomalous' events were identified and investigated. The particularly strong southward flow events in January 2011 and April 2012 (figs. 31, 33 and 35) are related to strong WIW flows and therefore not likely to be anomalous. Strong flows of WIW also occur in 1996 and 2004 in the ship data (not specifically indicated but visible in fig. 33), which again suggests that strong flows associated with WIW are not anomalous. In September 2013 strong flows, both north and south, are related to large 'blocking' eddies, as two such large eddies have been observed in the 3 years of glider data and also previously (e.g. Pinot et al., 2002), it again seems unlikely that these are 'anomalous' occurrences. The most anomalous event in the 18-year record of IC transects are the particularly large inflows of fresher AWr, of order +0.35 Sv, observed in September and November 2009 (not specifically indicated but again visible in fig. 33). This AWr inflow occurs across at least 2 months and thus is similar in pattern to the recent glider observations, in addition AWr inflows of order 0.2 Sv occurred in 2002, which again suggests that although strong, the 2009 inflows may not be anomalous. Thus the high flow events observed across both glider and ship datasets, excepting the November 2009 inflow about which a question mark remains until more AWr inflow events have can be observed, appear to be part of the high but normal sub-seasonal variability in the IC exchange.

A similar analysis for water transport in the MC was undertaken, with a somewhat puzzling result (fig. 36). Unlike in the IC, the mean seasonal cycle produced by the independent ship and glider datasets appear to be out of phase and no clear picture is visible above the high in-month variability. The sampling of the MC is low from December to February, and in August. In addition the number of glider transects available overall for analysis is lower than for the IC, as the glider sampling of this channel was lower. Therefore the dataset is perhaps not yet sufficient or sampled consistently across the year to define a signal, if one exists above the level of variability.

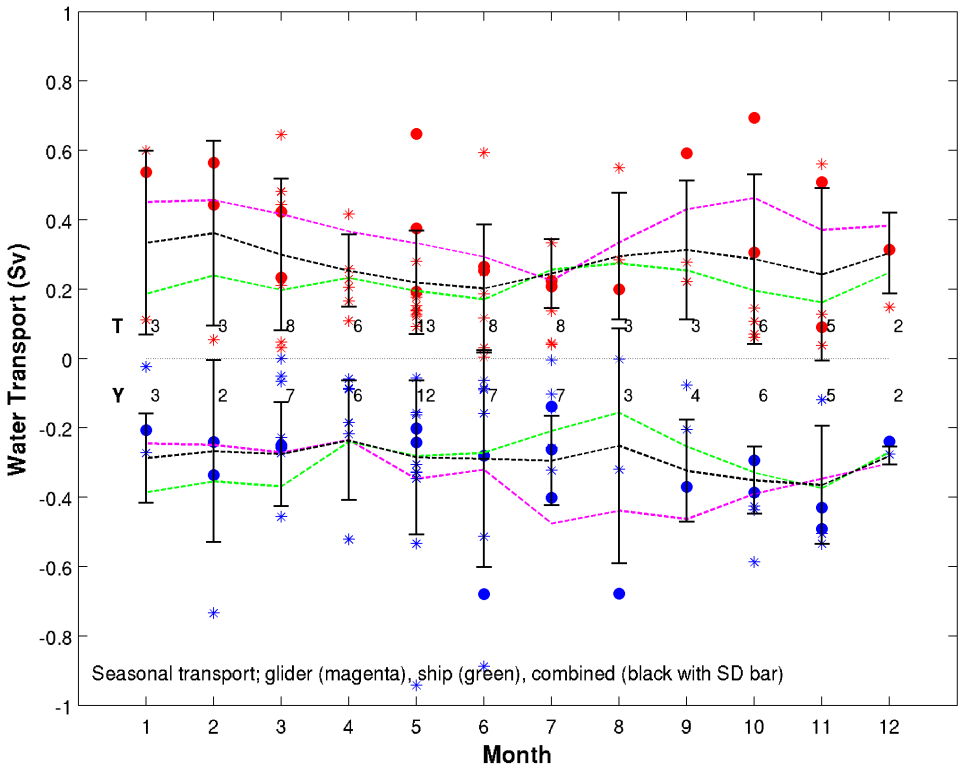

Figure 36. Mean seasonal cycle for geostrophic transport in the Mallorca Channel.
For the combined dataset (black dashed line with bar to represent SD) and glider data only (magenta dashed line), the ship data (green dashed line) calculated from the monthly mean of the per transect transport values, with a 3-month moving average applied. The transport per transect is binned and plotted per month for glider (dots) and ship (stars) data. The number of samples in the monthly mean is indicated along the baseline; above the baseline is the number of transects (T) and below the numbers of years (Y) in the monthly sample.

In terms net transport the IC has a mean seasonal net outflow in winter, of order -0.5 to -0.7 Sv (fig. 37), the mean outflow volume is around twice the inflow volume creating a net winter outflow. In summer the outflow volume is more or less balanced by the inflow volume to give virtually no mean net summer transport into the Balearic Basin. For the MC, the striking difference between the mean seasonal cycle calculated from ship and from glider datasets is clear in the net transport, where the mean net transports for glider and ship are opposing, which raises an intriguing question, has the MC changed its role or is this due to a bias in sampling? More observations are required in order to look at this question. However in terms of the mean interannual transport through the MC the two datasets are in agreement, with transport of order +0.25 Sv for the inflow and of order -0.29 Sv for outflow, suggesting that there is little net exchange through this channel. In this respect the independent glider and ship datasets are in agreement.

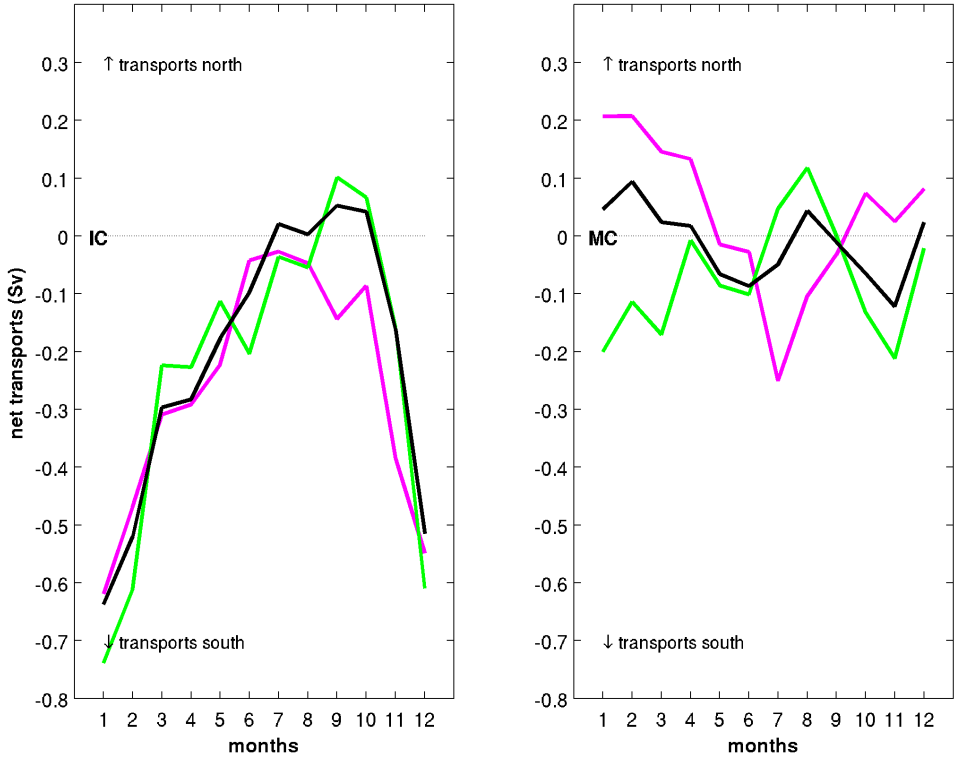

Figure 37. Seasonal cycle of net transport in the Ibiza and Mallorca Channels.
The net transport is derived from the sum of the northward and southward components of the 3-month moving average of the mean monthly transport (seasonal cycles), for the combined glider and ship dataset (black), for glider only (magenta), and for ship only (green).

4.3 Seasonal variability by water mass

Here we will look at the variability of the annual signal by water mass, which provides a new view of the annual cycle in the transport by water mass through the IC and MC, against which numerical models and future observations can be compared. As noted in the previous section the MC is less well sampled and therefore the patterns presented here may evolve with further years of glider sampling.

AWo

The mean annual cycle of transport of AWo is shown in fig. 37. This indicates, as might be expected, an NC influenced seasonal cycle in the transport of surface waters southwards through the IC (varying from -0.7 Sv in winter to -0.3 Sv in summer), and a relatively constant inflow (varying between +0.2 and +0.3 Sv), giving a net outflow in winter and a long summer period, June to October, of no net AWo flow. In the MC it is interesting to note that the inflow into the Balearic sub-Basin is of the same order as the IC, but that the

annual pattern of outflow is much less and does not exhibit the same as the NC led seasonal cycle, if anything there is a hint that the inflow and outflow are in synch, and there is little net exchange of AWo through the MC. This figure also indicates that when the IC is blocked, March/April, that the northern branch of the NC likely strengthens the Balearic Current, as there is little evidence that it strengthens outflows through the MC. The rapid decline of the transport in February/March is due to the entrance of WIW; see fig. 45 at the end of this section.

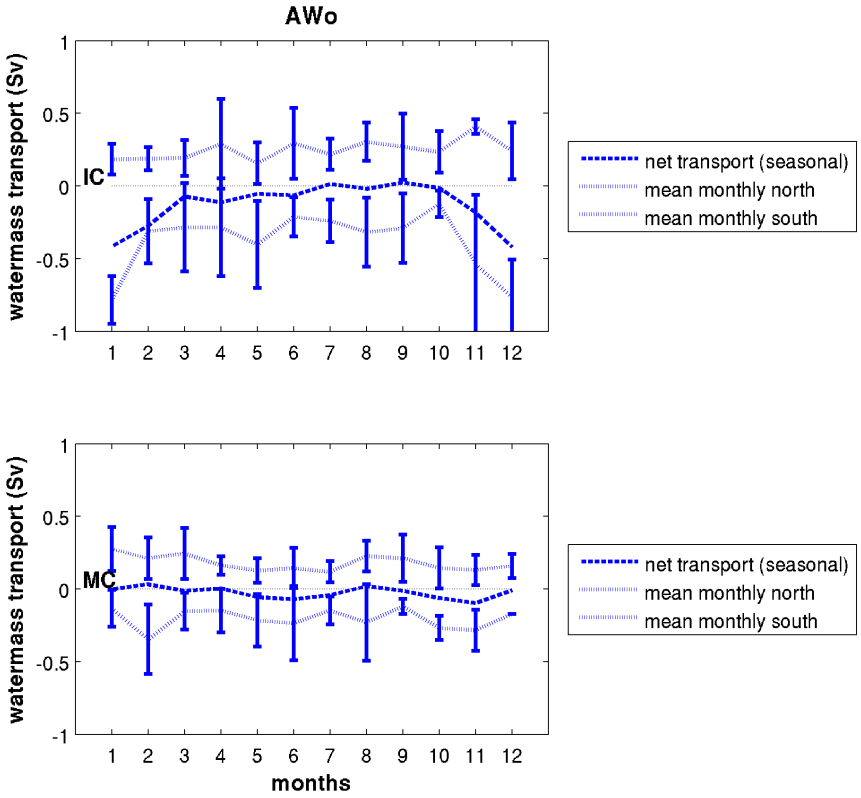

Figure 38. Mean seasonal cycle for the transport of AWo.
The net transport (dashed line) is the sum of positive and negative mean monthly transports with a 3-month moving average applied.

AWr

As noted in Chapter 3 the regional definition for fresh AW (Lopez-Jurado et al. 2008) does not appear to capture the full range of fresher inflows through in the IC and the MC. In addition, θ/S characteristics of the surface waters of the Alboran Sea indicate there are two types of surface layer water mass to the south (for an example see Allen et al. 2008), firstly a fresh water mass with salinities of order 36.7, presumably representing waters recently entered through the Straits of Gibraltar and a second broad envelope of surface waters with salinities in the ranging from 37.2 to 37.8. This second broad envelope of water mass

has a similar range of salinities as those observed flowing through the Balearic Channels, and incidentally is also similar the salinities preferred by Atlantic bluefin tuna, 36.9 to 37.7 (Alemany et al. 2010). A short test was therefore performed to observe the effect of increasing the range of salinities used to define AWr (from S ≤ 37.5 to S ≤ 37.7) on the pattern of water mass transport. The results, fig. 39 and 40, show that with the expanded range of salinities there is little increase in the number of AWr inflow events observed. In the IC there is one new AWr inflow event now detected in September 2012 and additional inflows for the MC in September 2013, however there are already AWr inflows detected for this period through the IC. The main effects are to increase the volume of fresh AW inflows, particularly in the MC, and make the pattern of inflows more consistent between the two channels. For example in 2011, AWr inflows into the Balearic Sea occur from January to June, through both the IC and MC, except when interrupted in the IC in March and April by 'blocking' eddies. The analysis suggests that the fresher AWr inflows are Alboran Sea surface water of the second broad envelope type and that for the Balearic Channels defining AWr as S ≤ 37.7 could better represent these fresher AWr inflows.

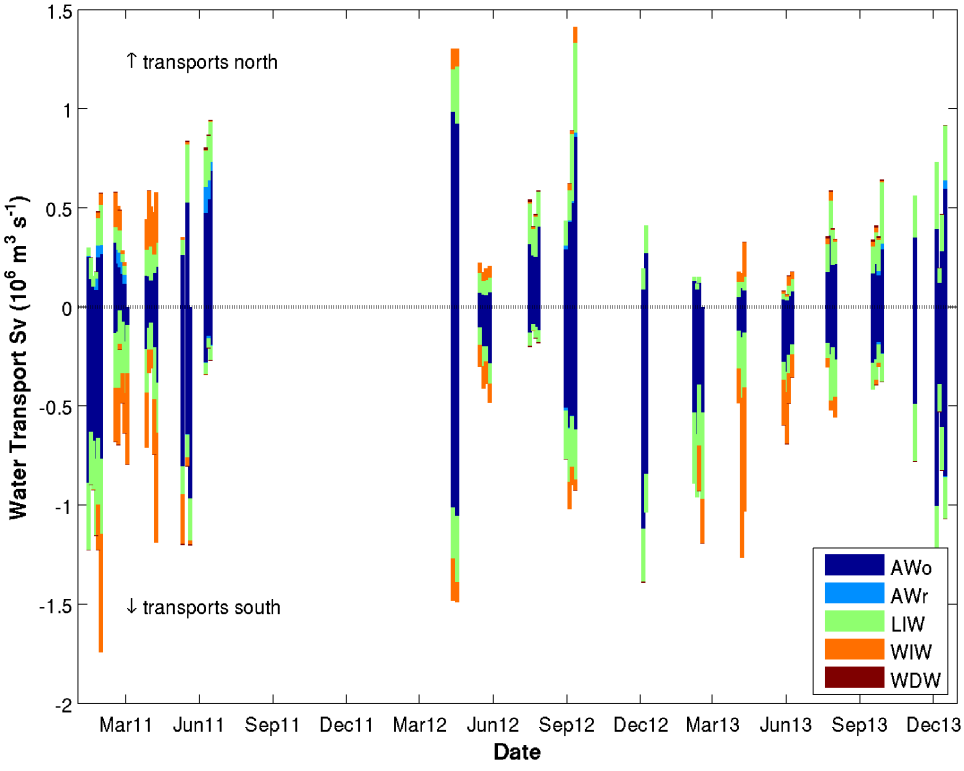

Figure 39. Transport of water mass in the Ibiza Channel, with S ≤ 37. 7.

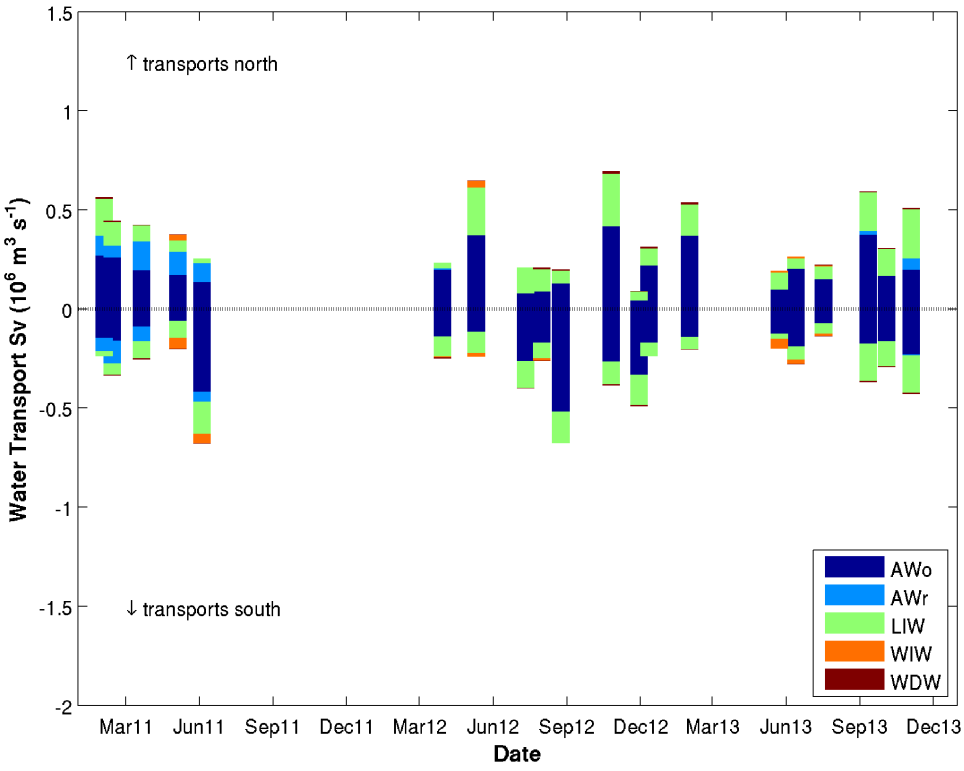

Figure 40. Transport of water mass in the Mallorca Channel, with S ≤ 37. 7.

Comparing the annual cycle of AWr with S ≤ 37.5 and with S ≤ 37.7, a small difference can be seen in pattern of the net transports (fig. 41 and 42). In fig. 41 the interannual mean cycle in transport of AWr (S ≤ 37.5) indicates that small volumes of AWr can inflow throughout the year and they appear to be stronger in autumn in the IC, though this is likely influenced by the strong inflows in November and December 2009. Notwithstanding the results are interesting, as they indicate that in the IC there are inflows throughout the year with little or no AWr outflow, and in the MC inflows and outflows occur throughout the year, with net inflows in summer (June to October) and winter (December to February), although the net flow is always positive. With S ≤ 37.7, fig. 42, there is a change in volume for the AWr inflow through the IC, the seasonal cycle of net inflow now varies between +0.025 and +0.05 Sv throughout the year and the pattern of the net transports is less influenced by the very strong events sampled in 2009.

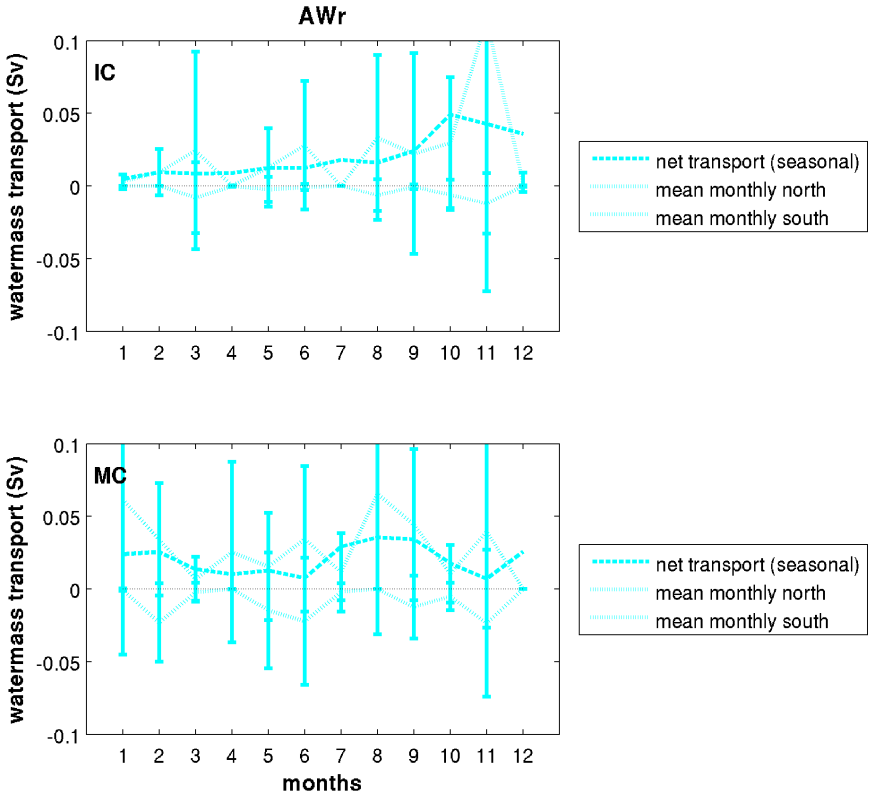

Figure 41. Mean seasonal cycle for the transport of AWr with S ≤ 37.5.
The net transport (dashed line) is the sum of positive and negative mean monthly transports with a 3-month moving average applied.

In the MC there is inflow and outflow throughout the year, the net inflow maxima is similar to that in the IC, with a peak in net inflow in summer from July to October (+0.05 Sv in August). As seen in Chapter 3 the MC exports the fresher AWr, when it is present to the north of the channel, however the net flows are positive in summer and are generally close to zero in winter and spring suggesting that if an AWr inflow event occurs in the summer a net inflow of AWr would likely be observed in the MC. For both channels the results are based on a relatively small number of events and more observations of AWr inflow are needed to complete the picture.

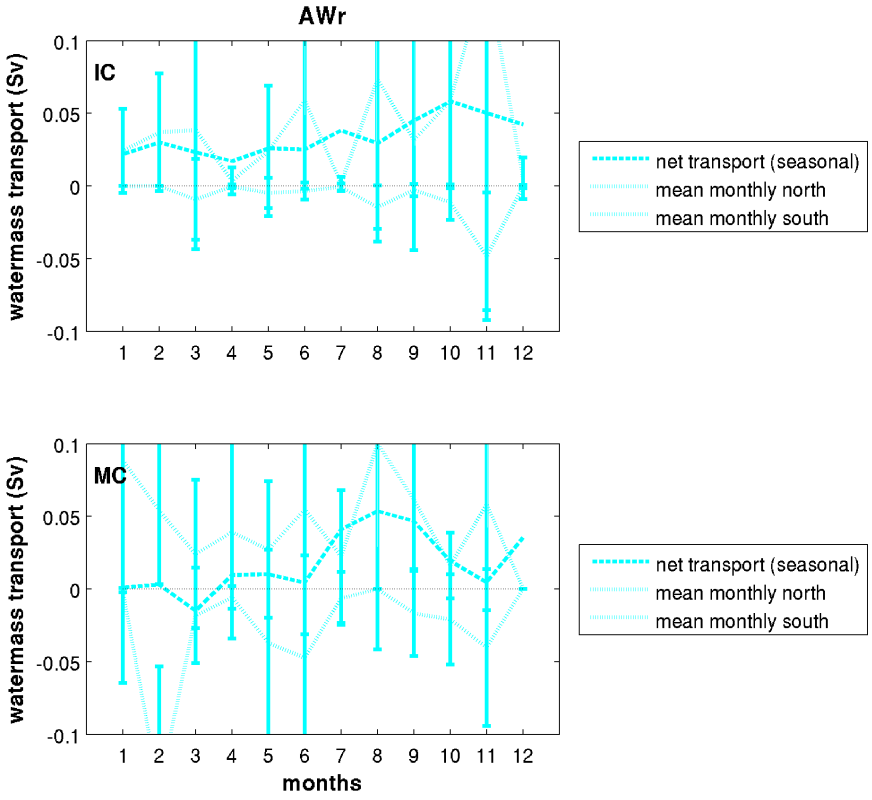

Figure 42. Mean seasonal cycle for the transport of AWr with S ≤ 37.7.
The net transport (dashed line) is the sum of positive and negative mean monthly transports with a 3-month moving average applied.

LIW

The mean annual pattern for the transport of LIW follows that of AWo (fig. 43), influenced in the IC by the seasonal cycle of the NC. The transport of LIW southwards varies from -0.25 Sv in winter to -0.1 Sv in summer, with a relatively constant +0.1 Sv transport northward. This means that there is a net outflow of LIW in winter and a long summer period, June to October, of no net flow. In the MC the inflow of LIW into the Balearic sub-basin is of the same order as the IC (+0.1 Sv), while outflows vary between -0.05 and -0.1 Sv. There is little or no net exchange of LIW indicated through the MC.

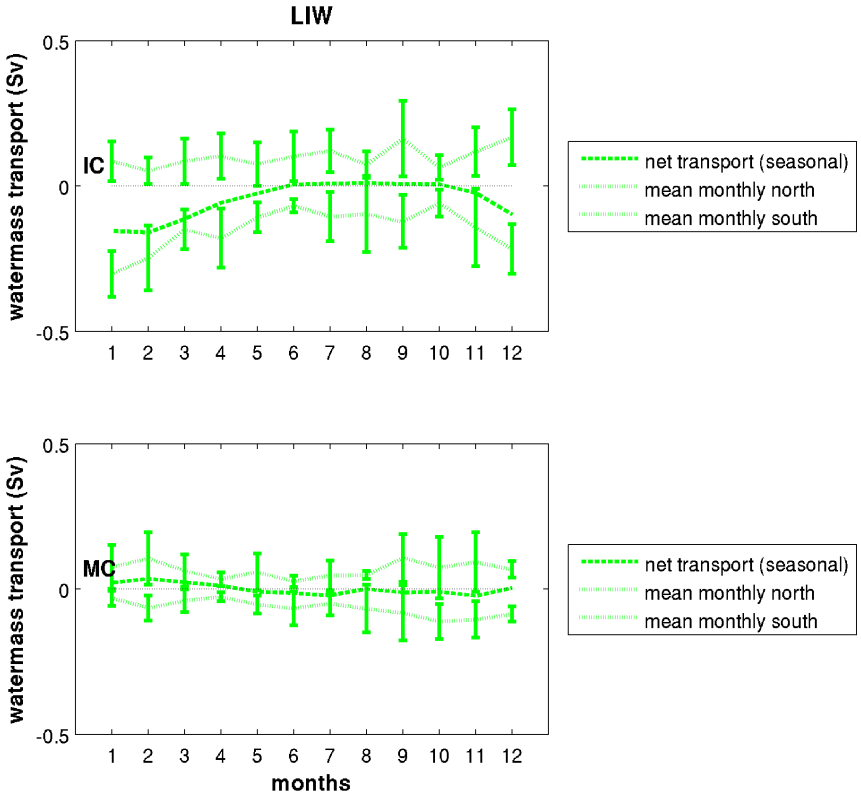

Figure 43. Mean seasonal cycle for the transport of LIW.

The net transport (dashed line) is the sum of positive and negative mean monthly transports with a 3-month moving average applied.

WIW

The mean monthly transport values for WIW are shown in fig. 44. An annual cycle for the transport of WIW is clearly visible in the IC, with southwards transports of the order of 0.1 Sv in January, rising to 0.2 Sv across March and April, before declining to close to zero in July. At the peak some of the flows are re-circulated (by eddies) giving a mean net transport of order 0.1 Sv from January to May. From this net flow the mean annual export of WIW through the IC was estimated as 2.59 x 10^{12} m^3, which interestingly is in close agreement with an earlier estimate by Allen et al. (2008). Although the high variability in the observations mean that this annual cycle on WIW transport is not statistically significant, it is in good agreement with the observations, as described in Chapter 3, and the seasonal pattern identifiable in fig. 33. Very little WIW exits through the MC.

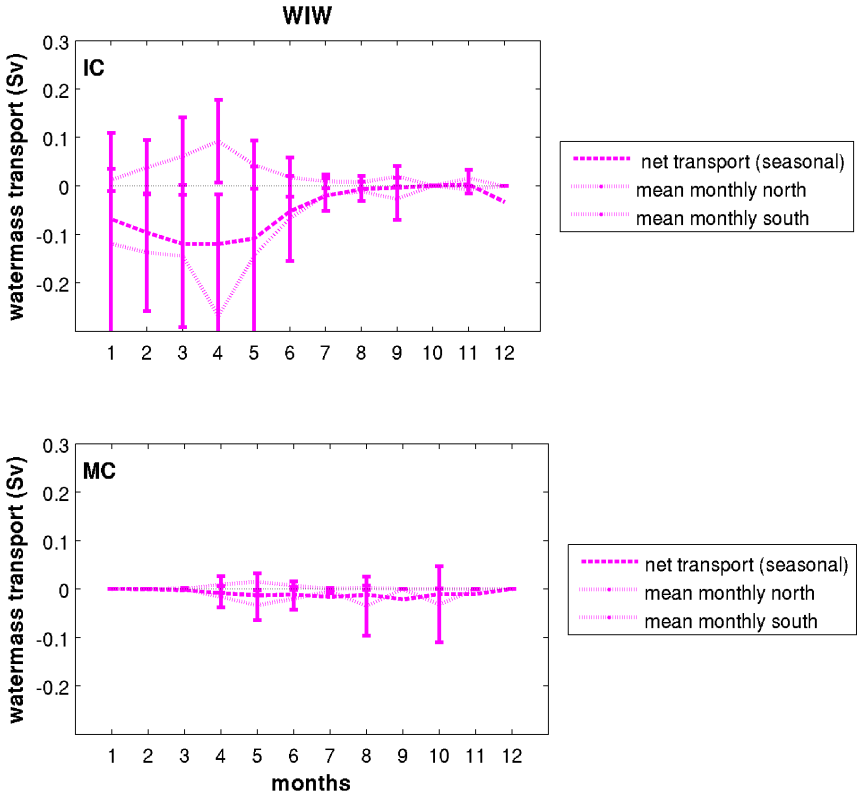

Figure 44. Mean seasonal cycle for the transport of WIW.
The net transport (dashed line) is the sum of positive and negative mean monthly transports with a 3-month moving average applied.

WMDW

The geostrophic assumption and use of a reference level of zero velocity as used in the calculation of geostrophic transport means that the transport of WMDW through the IC is not fully captured. In addition WMDW is mainly encountered below depths of 1000 m, the limit of the glider observations and of the IC sill, therefore an analysis of the transport of this watermass is not included here.

In summary, for the first time annual mean patterns are proposed for each of the water masses that pass through the IC and the MC, which will be particularly useful in analysing interannual variability in WIW production and NC strength. The AWo and LIW flowing south through the IC are clearly imprinted with the seasonal cycle of both the NC and WIW. The transport of AWo and LIW southward decline earlier in spring than the total transport, as WIW enters the channel and takes part of the total transport volume (fig. 45). There is some suggestion of a seasonal difference in the AWr inflows through the MC with

the broader definition of AWr (S ≤ 37.7), where a net inflow in summer occurs during an inflow event.

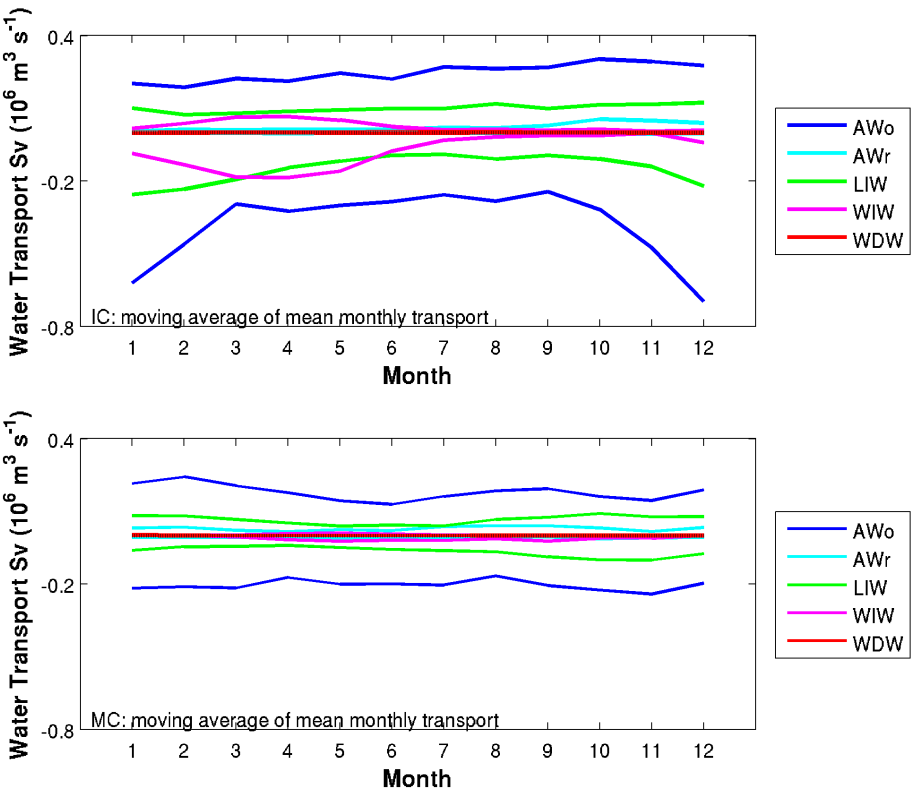

Figure 45. Seasonal cycle of transport for all water masses.
The seasonal cycle is the three-month moving average of the mean monthly transport, the cycle for each watermass is indicated by colour (see legend, WDW is WMDW).

4.4 Spatial patterns

Variability in the spatial pattern of geostrophic velocity was analysed through an EOF study of the 61 complete glider geostrophic velocity sections across the IC, see Chapter 2 for details of methods. The first EOF (EOF1) for geostrophic velocity in the IC accounts for 42% of the variance, the second (EOF2) for 13%, the third (EOF3) for 9%, and the fourth (EOF4) for 5%. The amplitudes of EOF1 show a seasonal shift in sign from negative in winter and early summer, to positive in spring and autumn, see fig. 46a (top left panel). The lower panels of fig. 46a show a representation of a negative (winter) EOF1 from month 1 (January) and a positive spring/autumn EOF1 produced by adding the interannual mean to EOF1 with the relevant monthly mean amplitude applied. The negative amplitude EOF1 (month 1) shows an NC and AW inflows, which is similar in pattern to the 'winter NC' mode combined with 'AW inflow' as proposed in Chapter 3, fig 30. The positive amplitude EOF1 (month 9) has a similar pattern to the 'autumn eddy' or

'spring eddy' mode. EOF1 therefore relates well to the physical features identified in Chapter 3, and depending on whether the amplitude is positive or negative, it represents either a strong NC with AW inflows or a large anticyclonic 'blocking' eddy (fig. 46a).

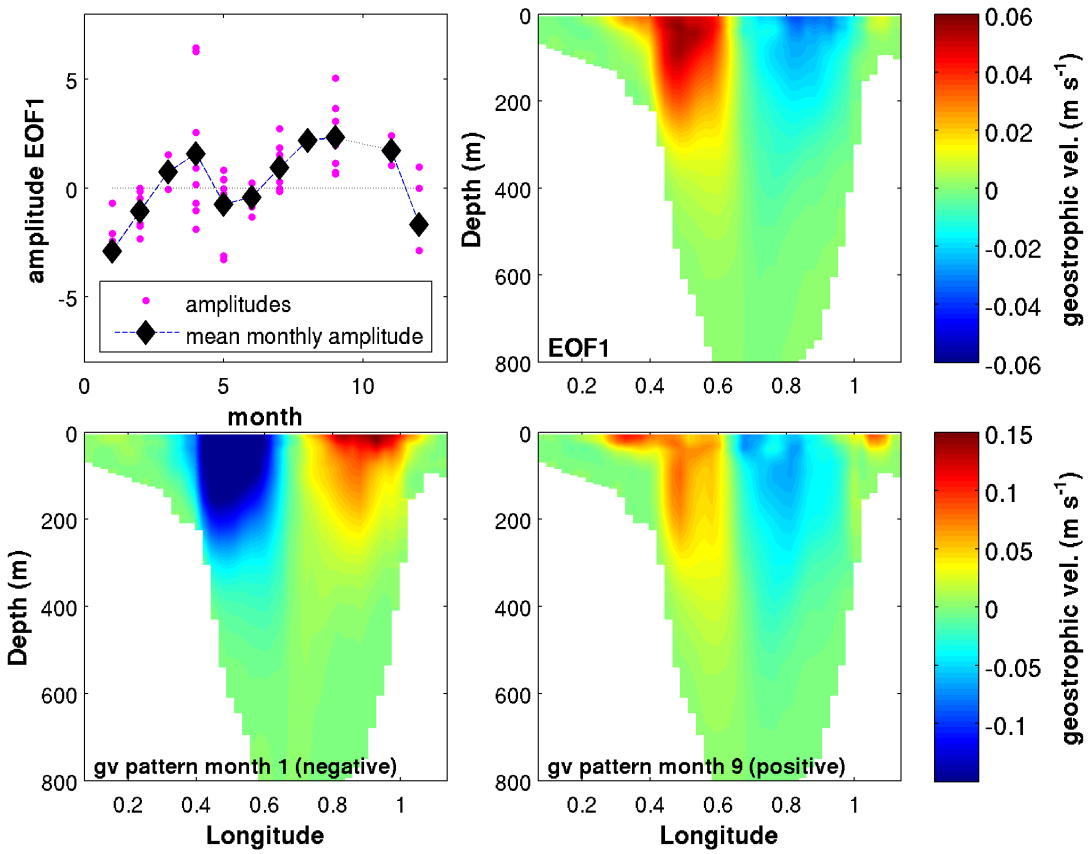

Figure 46a. EOF1 of geostrophic velocity in the Ibiza Channel.

The upper RH panel shows the pattern in geostrophic velocity of EOF1 in the IC, the upper LH panel shows the amplitudes by month for EOF1 (magenta dots) and the mean amplitude (black diamonds/black dotted line). The lower LH panel shows a representation of a 'winter' pattern in geostrophic velocity for the EOF and the lower LH panel a representation of an 'autumn' pattern, both created using the inter annual mean for geostrophic velocity (see Appendix H) and the relevant amplitude.

With the monthly mean amplitude (black dashed line, fig. 46a) providing a representation of a seasonal cycle in amplitudes and therefore patterns in geostrophic velocity in the IC, indicates a seasonal interplay between mesoscale and basin scale dynamics, with a spring (positive amplitude) mesoscale period from March to April and an autumn mesoscale period from August to November.

EOF2, constituting 13% of the spatial variability, can also be related to physical patterns seen in geostrophic velocity in Chapter 3. The amplitudes are generally weakly positive, with some stronger negative values, fig. 46b. When weakly negative the EOF could

represent a reduced NC 'squeezed' to the western edge of the channel by a blocking anticyclonic eddy, some disconnect with the surface suggests a similarity with autumn eddy patterns. The stronger negative amplitudes indicate an NC moved offshore, with some counter current inflows along the western channel edge, a pattern seen for example during canalesDec2013.

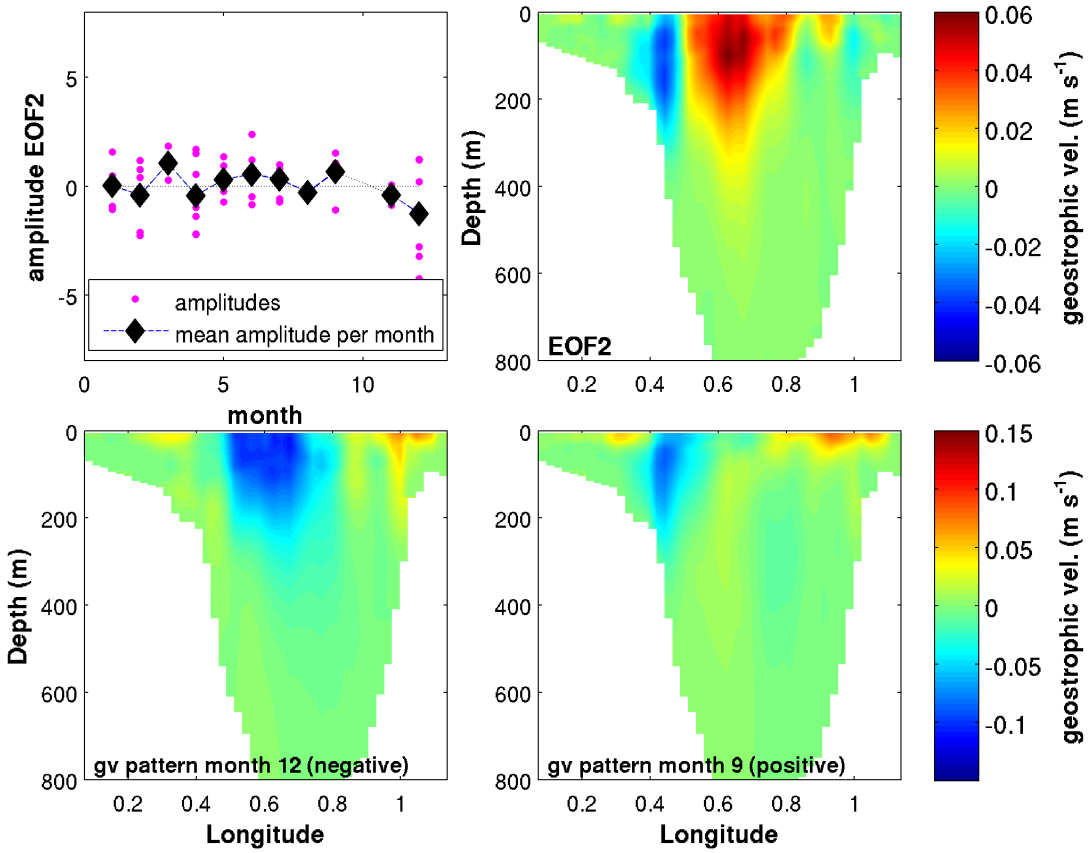

Figure 46b. EOF2 of geostrophic velocity in the Ibiza Channel.

The upper RH panel shows the pattern in geostrophic velocity of EOF2 in the IC, the upper LH panel shows the amplitudes by month for EOF2 (magenta dots) and the mean amplitude (black diamonds/black dotted line). The lower LH panel shows a representation of a 'winter' pattern in geostrophic velocity for the EOF and the lower LH panel a representation of an 'autumn' pattern, both created using the inter annual mean for geostrophic velocity (see Appendix H) and the relevant amplitude.

EOF3, constituting 8% of the spatial variability, can also generally be related to physical patterns seen in Chapter 3, fig. 46c. The amplitudes are again positive and negative. The negative amplitudes, occurring in spring and late summer/autumn, appear again to be related to the mesoscale blocking of the IC, possibly representing an NC not completely blocked by a large eddy. The positive amplitude version of EOF3 appears more related to a pattern of weak summer NC flows with eastern inflows of AW.

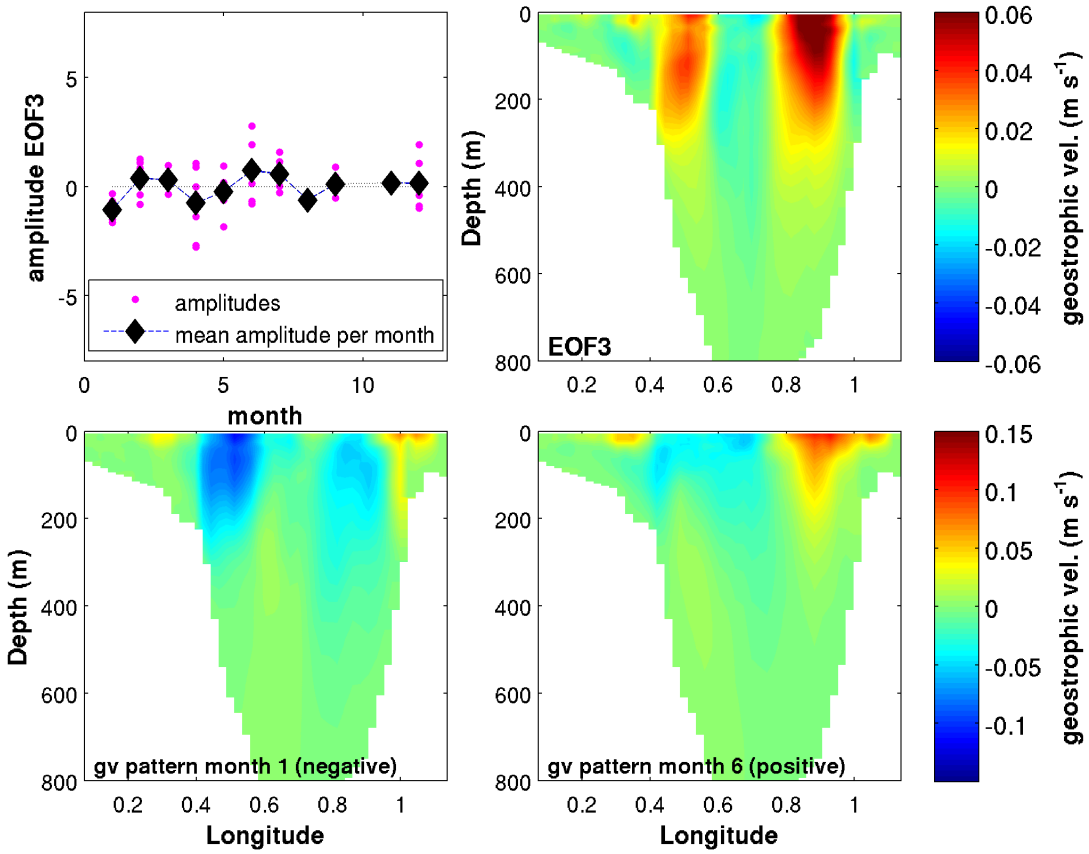

Figure 46c. EOF3 of geostrophic velocity in the Ibiza Channel.

The upper RH panel shows the pattern in geostrophic velocity of EOF3 in the IC, the upper LH panel shows the amplitudes by month for EOF3 (magenta dots) and the mean amplitude (black diamonds/black dotted line). The lower LH panel shows a representation of a 'winter' pattern in geostrophic velocity for the EOF and the lower LH panel a representation of an 'autumn' pattern, both created using the inter annual mean for geostrophic velocity (see Appendix H) and the relevant amplitude.

EOF4 constitutes just 5% of the spatial variability (fig. 46d) and although the EOF suggests that it is related to the double blocking eddy pattern seen in some of the glider missions, when added to the interannual mean it does not produce patterns in geostrophic velocity with a distinct physical meaning.

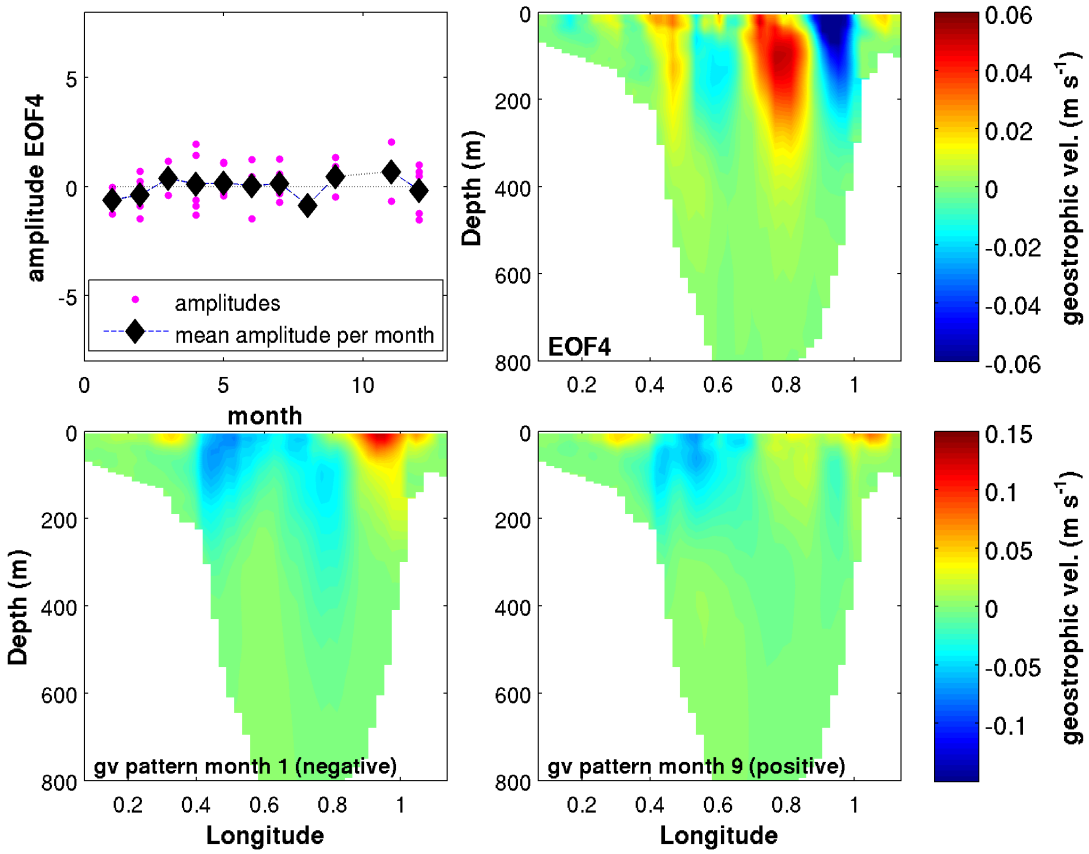

Figure 46d. EOF4 of geostrophic velocity in the Ibiza Channel.

The upper RH panel shows the pattern in geostrophic velocity of EOF4 in the IC, the upper LH panel shows the amplitudes by month for EOF4 (magenta dots) and the mean amplitude (black diamonds/black dotted line). The lower LH panel shows a representation of a 'winter' pattern in geostrophic velocity for the EOF and the lower LH panel a representation of an 'autumn' pattern, both created using the inter annual mean for geostrophic velocity (see Appendix H) and the relevant amplitude.

In summary, the first 3 EOFs appear to be associated with the interplay between basin scale and mesoscale dynamics, which is expressed most strongly in EOF1 where the mean amplitude analysis provides an initial characterisation for the timing of a spring and autumn eddy 'season'. In other EOFs the NC is visible in different patterns: squeezed up against the western channel edge due to a blocking eddy, offshore with a subsurface channel edge counter current, and as a weak 'summer NC'. EOF4 appears to be at the limit of meaningful patterns, but hints at a duel blocking eddy configuration. The patterns from the EOF study match with patterns seen in geostrophic velocity and EOF1 in particular matches well with the 'modes' proposed in Chapter 3, fig. 30, supporting the suggestion that dominant modes exist.

4.5 Limitation of data and methods

During the sampling, processing and analysis of ocean variables a number of assumptions and/or approximations are made. The key assumptions in this study can be summarised as follows:

- The geostrophic velocity derived transports are sufficiently well calculated
- Glider transects can generally be viewed as synoptic
- Ship CTD and glider transects can be sensibly combined for analysis

1. The geostrophic assumption and the assumed reference level of zero velocity

The principal weakness in the geostrophic assumption is the use of an assumed reference depth of zero velocity. Which means that deep flows are not represented and, if velocities at depth are significant, geostrophic velocity is underestimated. In addition, although this study is primarily concerned with the patterns and dynamics of structures driven by the density field, an ageostrophic component of flow will also exist and which should be borne in mind. Some authors consider the geostrophic assumption and thermal wind method for deriving geostrophic velocities out-dated (Wunsch 1978), however this method is still widely used in oceanography where single or repeat transects have been captured and there is no reliable source of bottom current information e.g. Cunningham et al. (2007) and Bryden et al. (2005). The inverse box model methods proposed by Wunsch (1978, 1996) overcome the problem of an assumed reference level of no motion and were used in the CANALES experiment (Pinot et al., 2002). However this method has its own approximations and requires the synchronous capture of a closed box of ocean, which is often not practical or economic. In the IC and MC a sufficiently synoptic sampling of a closed box or 'triangle' with gliders is possible, with multiple gliders (2 or more), however this sampling strategy would significantly impact the cost and complexity of each mission, for potentially minimal gain in terms of precision and no change in terms of the findings.

Other authors have used the glider estimated depth averaged velocity (DAV) to provide an estimate of bottom currents, which are then used instead of a reference level of zero velocity in the geostrophic assumption, e.g. Hatun et al. (2007), Gourdeau et al. (2008), Todd et al. (2009), Martin et al. (2009) and Glenn et al. (2008). Gliders produce estimates of DAV as an integral function of their navigation system; in order to correct their trajectory for currents, gliders compare their actual position, obtained at the surface from

GPS, against their anticipated position estimated by dead reckoning, and the difference between the two positions represents the DAV. However this estimate is made using the gliders internal compass and experiments have shown that there can be large errors in the compass heading measurements. For example Merckelbach et al. (2008) found the difference between true heading and the glider compass heading varied between 3 and 35°, depending on the glider (3 Slocum deep gliders were tested) and the compass heading. In a similar experiment, undertaken at IMEDEA, an error of between 0 and 14° was recorded depending on the compass heading (1 Slocum glider was tested). These compass errors are influenced by the configuration of internal components in the glider hull, such as batteries, weights and sensors, and will vary from mission-to-mission. Therefore in order to avoid the introduction of unknown errors into the geostrophic calculation, due to erroneous estimates of DAV, the glider compass error should be measured for each mission (ideally before and after) and the DAV variable corrected in the post-mission data processing. To assess the use of the DAV variable an analysis was undertaken to look at the differences between the glider DAV and a DAV derived from geostrophic velocities for a mission with an uncorrected DAV variable, see Appendix D. The results from this analysis indicated that the glider DAV and the geostrophic velocity estimated DAV obtained for the deep central channel section showed a mean difference of order 2 to 3 cm s^{-1}, which is similar to the errors inherent in the glider DAV calculation method (Merckelbach et al. 2008). This relatively good agreement, within the level of calculation error, suggested that the geostrophic velocity estimate is capturing much of the velocity signal. To date, a measurement of compass error was completed for only one of the SOCIB glider missions used in this study, canalesSep2013, therefore in the interests of simplicity and to avoid the introduction of unknown and potentially large errors into the geostrophic calculation, the glider DAV were not used.

A sensitivity test was however undertaken to assess the impact of the zero velocity assumption on the estimates of geostrophic transport, using reference level velocities derived from the literature. There was some difficulty in defining an 'appropriate' estimate for the base of profile current as those in the published literature were sparse and the samples of bottom current velocity available close to the level of accuracy of the instruments and/or methods (see Appendix B for details). Notwithstanding the results were interesting and strongly point towards the need for caution in applying a bottom current that does not have a good physical basis. They also provide a general estimate of

the order of magnitude of the sensitivity of the geostrophic transport calculation to the assumption of a level of zero velocity, which is of order of 10%.

A comparison between glider derived geostrophic velocity section and total velocity section from a contemporaneous vessel-mounted Acoustic Doppler Current Profiler (VM-ADCP) was undertaken (see Appendix D). This comparison, shown below in fig. 47, is between glider canalesDec2013 T2, with the glider travelling east to west across the IC, and an overnight VM-ADCP velocity section from the ships campaign SOCIB_Dic13, with the ship travelling west to east. As can be seen there is excellent agreement between the two sections, both in terms of the pattern of velocities but also in terms of the amplitude of the velocities. In both, the NC is visible, penetrating to the same depths, with a similar form and with the same range of velocities, the inflows in the east are also captured and there is an indication in the VM-ADCP of the subsurface counter flow at the western channel edge as visible in the glider geostrophic velocity section.

The glider geostrophic velocities indicate that the inflow current reaches the surface, whereas in the ADCP section this current appears to be partially disconnected from the surface. In addition inflows are visible on the Ibiza shelf area in the VM-ADCP data that are not captured by the shorter glider transect and/or geostrophic velocity calculation. The ADCP section does not provide information on the velocity at depth, however the comparison is a clear indication that, for the upper 300 m, the geostrophic assumption and methods are adequately capturing the pattern and amplitude of the velocity associated with the dynamic processes under study. The very good agreement in velocity amplitude also indicates that the bottom reference velocity is not very different from 0 and that the ageostrophic terms may not be significant in this region, as suggested by Bouffard et al. (2010) in comparing glider with altimetry data.

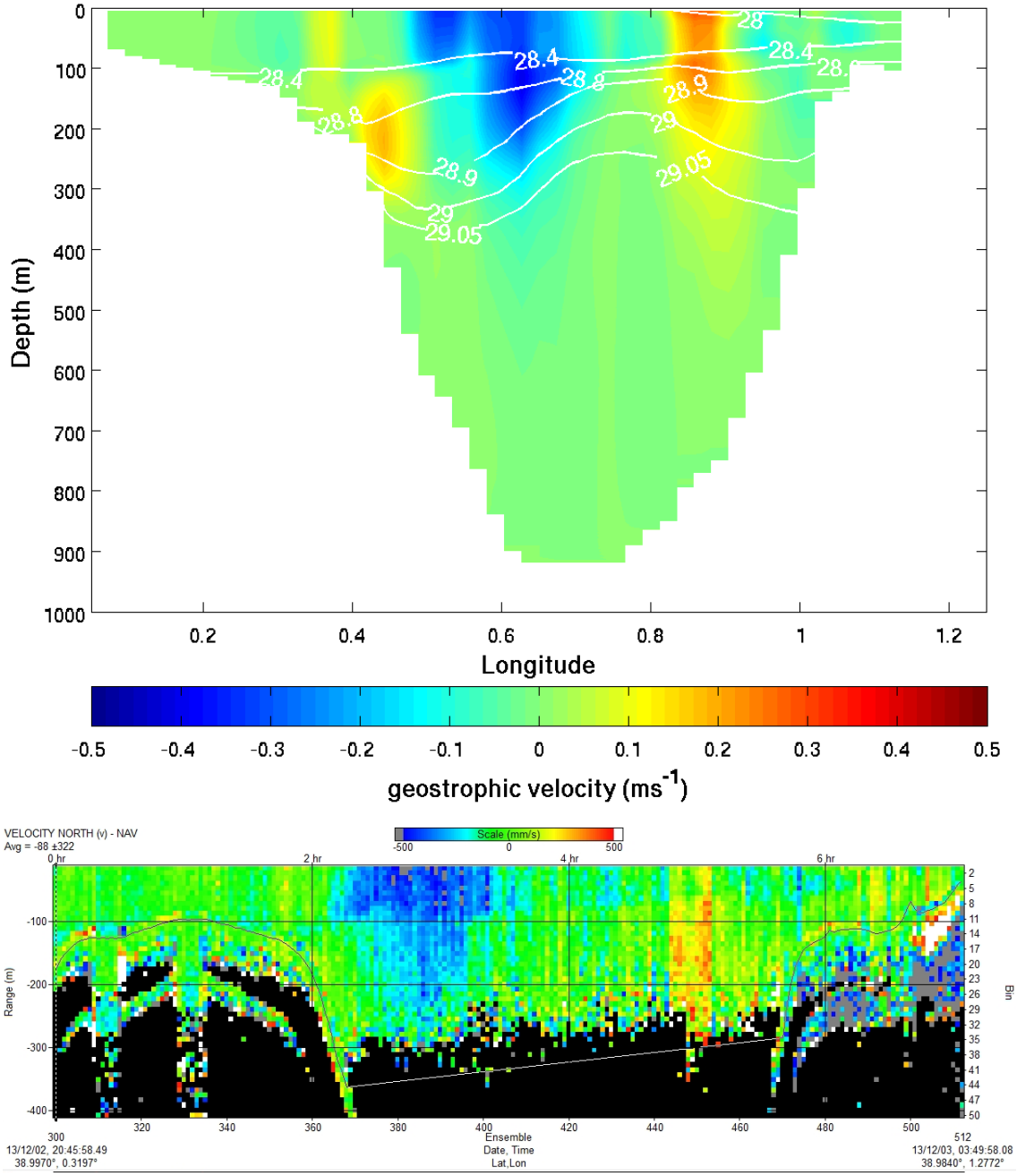

Figure 47. Geostrophic velocity section for glider and contemporaneous VM-ADCP.
The glider section is from canalesDec2013 T2 (03/12/2013 21:26 to 06/12/2013 09:57) and theVM-ADCP velocity section from the overnight transect of ship mission SOCIB_Dic13 (02/12/2013 19:00 to 03/12/2013 03:00). Southward velocities are negative and northward velocities are positive, and both sections have the same velocity scale. The ADCP transect starts at 0.32 °E and ends at 1.3 °E, the edge of the channel can be seen where the black area shallows.

Although the geostrophic calculation appears to be reasonably accurate for the upper part of the water column there will be an underestimation of deep flows, due to the reference level of zero velocity assumption. In the Pinot et al. (2002) study the plots of current data from a mooring on the Spanish continental slope show flows of up to 4 cm s^{-1}, occurring in

pulses of days to a week, at depths of 870 m. In an earlier study the transports of WMDW southwards through the IC were determined by inverse box model methods to be of order 0.02 Sv per annum (Pinot and Ganachaud 1999), therefore variability in these deep flows is not be expected to strongly influence the variability discussed in this chapter, which is dominated by changes in the surface and upper to mid level flows. These pulses of deep flows are however worthy of further study.

2. Synopticity in glider transects

For the analysis of the geostrophic transport of water mass, the glider sampling of the IC is assumed to be synoptic, however some of the observed variability could be induced by a smearing of signals from higher frequency dynamic structures, such as internal waves, due to the relatively slow speed of the glider in the horizontal (25 cm s^{-1}). Recently Rudnick and Cole (2011), in a study of a 400 km glider transect in the Pacific Ocean, suggested for geostrophic velocity and other depth dependant variables that glider data is accurate for wavelengths of greater than 30 km. Within the IC many features are 30 km or less, therefore an analysis was undertaken to determine if a pattern of change in properties related to the temporal component of sampling could be found (Appendix E). For this analysis the patterns in repeat transects of the glider data, on depth and density surfaces, were analysed for the sections of the transects sampled more closely in time vs. those sections sampled more distally in time. The results showed no detectable pattern in the variability between transects related to the temporal proximity of the sampling, implying that transect-to-transect variability is primarily caused by changes in the prevailing dynamics.

Inevitably glider data will contain an element of variability that is a function of both the sampling resolution and the smearing of signals in time, this cannot be identified and therefore cannot be removed, however the analyses suggests that for the transports and features under study that the glider transects of the IC can be considered as representing a sufficiently synoptic view of the channel, a view that is reinforced by the close agreement between ship and glider data (Appendix D).

3. Ship CTD sections can be sensibly combined with glider CTD sections

A detailed comparison between glider data and ship-based sections was undertaken (see Appendix D); a ship transect has a lower spatial resolution but more synoptic (6 to 8 hour)

view of the Ibiza Channel as compared to the higher horizontal resolution but less synoptic (1.8 to 3.5 day) view provided by gliders. This analysis shows that both ships and gliders observe the same structures and that there is a coherent evolution in features observed between glider and ship transects. The analysis also clearly shows that the higher resolution of the glider sampling provides greater visibility of mesoscale to sub-mesoscale features and dynamics, and, when such activity is present, the more coarse resolution of the ship sampling leads to a lower derived geostrophic transport.

The good agreement between glider and ship sections, confirm that the ship and glider sections can sensibly be compared, and indeed when a glider mission is sub-sampled to the resolution of a ship mission it is remarkably similar to the synchronous ships transect. However the analysis suggests that the transport derived from ship sections will generally be lower than that from the glider sections, which is as what is seen in the annual mean cycles of flows north and south (see fig. 35, this chapter) and also provides a possible explanation for the increase in the gap between the glider and ship curves in spring and autumn, when levels of mesoscale activity are higher.

The difference between mean annual cycles of north and south flows from the glider and ships datasets, as seen in this chapter (fig. 35), is relatively consistent and a mean difference in transport can be determined (0.21 Sv for southward flows and 0.18 Sv for northward flows). The ship derived transport values could potentially be uplifted by these mean values, however, this would not dramatically affect the results and would likely mask true variability, so for reasons of clarity such differences are noted but not applied.

The geostrophic transport calculated for the deep (central) part of the IC are taken to be representative of the 'total' geostrophic transport for the channels, however as seen in Chapter 3 shelf transports could also play a role, particularly for the inflows which are frequently seen on-shelf in the east of the IC. To analyse the impact of this assumption a study was conducted comparing the pattern of transports in simulated glider transects sampled from the Balop forecasting system (Tintoré et al. 2012). These show that in the simulated glider transects, the deep channel represents between 96 to 100% of the transports southwards and between 93 to 94% of the transports north. This matches the observations. The dominant feature in southward transport is the NC, which is generally located on the western edge of the IC, in-channel and along the shelf break, while the AW

inflows are generally observed in-channel and on-shelf. This suggests that a margin of error, of 2% and 6%, could be applied to the north and southward transport respectively.

In summary, for the purposes of the geostrophic velocity calculation and transport analysis, the assumption that the glider transects can be assumed 'synoptic' is valid. The methods used to estimate the geostrophic velocity calculation, namely the deep channel and geostrophic assumption, appear to be sufficiently representative of the transport of water mass, excepting the deep flows and the absolute volumes of fresh AW inflows. In the future more accurate determinations may be possible using the glider DAV variable, once regular post mission compass correction procedures are performed, however the comparison with ADCP velocity sections from the December 2013 R/V SOCIB mission (see above) indicate that the methods selected perform well, within a general margin of error of order 10%, which may not be detectable by visual comparison.

CHAPTER 5: Discussion

Three years of intensive glider monitoring has delivered new insight into seasonal to sub-seasonal variability in the inter-basin exchange of water masses at an important 'choke' point in the Mediterranean basin scale circulation. In combination with data from an 18-year record of ship based campaigns, concrete definitions of seasonal cycles of transport of watermass can now be determined, where they exist, above the sub-seasonal variability. The quasi-continuous glider monitoring enables models for the seasonal pattern of flow through the IC to be proposed, and the relative roles of the IC and MC in the north/south exchange to be clarified.

In the IC, gliders observed high frequency variability in both the northward and southward inter-basin exchange of water mass. In southward flows changes of 0.8 to 0.9 Sv occurred over timescales of days to weeks, caused by the arrival of WIW to the channel and by the arrival, departure and shifting of spring and autumn eddies. In northward flows, changes of order 0.4 to 0.7 Sv occur over days and are related to AW inflows and to the spring and autumn mesoscale activity. Although previous surveys had noted high cruise-to-cruise variability, they were insufficient to show that in fact the volumes of water exchanged through this narrow 'choke' point fluctuate on 'weather' timescales. For the first time the high frequency glider sampling has shown that variations in the transport of water, as large as those previously only identifiable as seasonal or eddy driven, occur over timescales of days to weeks.

The high frequency changes were caused by 3 factors: the arrival of WIW to the channel, the arrival, departure or shifting of eddies in the channel, and by strong AW inflows. Cold and relatively fresh WIW floods south with the NC after winter storm events, altering the density structure of the current and rapidly increasing the transport southward, for example by 0.5 Sv in 2 days (canalesJan2011). This is confirmation that such winter events can have a direct and important impact on circulation variability. The high temporal resolution of the glider data also pinpoints the winter arrival of WIW to the IC, which could be used to develop a picture of potential up-stream production regions and associated episodic storm events for this important winter mode water, as in the example by Heslop et al. (2012) for winter 2010/2011.

An analysis of the combined glider and ship dataset provides a full seasonal cycle for the southward transport in the IC based on the mean monthly transport (Chapter 4, section 4.1), where previously only a seasonal maxima and minima were defined (Pinot at al. 2002). For the transport of water mass southward, this new cycle is in general agreement with the previous definition in terms of magnitude. However, the winter maximum is 2 months earlier, December/January, and the summer minimum is broad, 3 months duration. A new seasonal range of 0.6 Sv is also implicit in this, which further highlights the scale of the high frequency sub-seasonal variability. This new month-by-month cycle for the southward transport through the IC can be taken as a proxy for the NC, and corresponds well, in both timing and magnitude, with the seasonal variation in the NC as observed off the south coast of France (Bethoux 1982, Bethoux 1988, Astraldi et al. 1989, Millot 1999).

New seasonal cycles for the individual water masses are also analysed. Although these cycles are less robust due to the high variability, they provide insight into the roles of the different water masses and channels in the north/south exchange. In particular, the new seasonal cycle for WIW provides a benchmark, against which the interannual variability in the timing and production volume of WIW can be assessed, and an estimate of the mean production volume of WIW can be made (Chapter 4, section 4.3). It also suggests that little WIW passes through the MC and provides a clear indication that this channel is not a significant southward pathway for the NC.

For the northward transport of water mass through the IC this study finds no seasonal cycle determinable above the high frequency variability. If a seasonal cycle does exist, it is of order 0.1 to 0.15 Sv and thus would not be determinable even with significantly more data. In fact the interannual mean level of transport appears to remain relatively consistent throughout the year, at ~0.4 Sv. Furthermore, inflows of fresher AWr seem to be episodic events of several months duration and unrelated to the season. During these fresher AW inflow events, the IC and MC are closely connected, with inflows of the same water mass occurring through both channels. The previously held assumption, that inflows had a seasonal component related to the decline of the NC (Pinot at al. 2002, amongst others), is not supported by the glider and ship data. In addition to the seasonal inflows, Pinot et al. (2002) also described 'energetic inflows', and it would seem probable that these are the episodic AW inflow events observed by the gliders. With this analysis however these vigorous and fresher AW inflows can be more fully characterised, as events of several

months duration, occurring concurrently through both the IC and MC, and with the freshest component of the inflow occurring at the surface (0 – 100 m).

Previous authors had identified the IC as the dominant channel in the inter sub-basin exchange and the MC as the preferred route for inflows (Pinot et al. 2002). In this study the IC is confirmed as the dominant channel in the southward exchange with a clear net flow southward in winter, of the order of 0.5 - 0.7 Sv, and with little or no net exchange in summer. Although the sampling of the MC was lower, some insight into the role of this channel in the exchange can still be gained. The long-term mean transport suggests that this channel is neutral, with little or no net exchange, and although the MC plays a limited role in the transport of waters of northern origin south (with the NC), it is of equal importance during fresher AW inflow events, when similar volumes inflow through both channels.

Although no seasonal cycle is detected for the inflows, a seasonal cycle is however apparent in the pattern of the IC 'blocking' eddies. This pattern is visible in the glider observations (Chapter 3) and forms an integral component of the modes, as proposed in Chapter 3, section 3.5, 'spring eddy' and 'autumn eddy' modes. This seasonality is also apparent in the EOF analysis (Chapter 4, section 4.4), which suggests a seasonal interplay between basin scale and mesoscale dynamics in the IC. The monthly pattern of amplitude of the first EOF provides an initial quantification of when 'blocking' eddies are active in the channel, in spring from March to April, and in autumn from September to November. The observations in Chapter 3 also indicate a difference in the structure of these eddies: spring eddies have a surface expression and are more likely to 'block' the channel, whilst autumn eddies are predominantly sub-thermocline and interact with and modulate the surface flows.

Vigorous mesoscale activity has long been observed in the Balearic Basin (Astraldi et al. 1999), including spring/summer 'blocking' eddies in the IC (Pinot and Ganachaud 1999, Pinot et al. 2002). However for the first time the glider data provides a seasonal cycle for the 'blocking' eddy activity and rich detail regarding the different types of eddies, with a seasonal difference between the eddies and two spatial patterns for the 'blocking' events identified. One pattern with a single large 'blocking' eddy, of diameter 70 km, and another with two interacting medium eddies, of diameters 20 – 30 km. All eddies were associated

with cold cores of WIW (or near WIW). The 'canales' glider missions have not yet observed a year without WIW production, however a temperature minimum layer has been detected in the Mediterranean MEDAtlas database for most years (Allen et al. 2008) and so it is anticipated that the seasonal blocking of the IC would also occur most years.

A surprising result of this analysis is that the variability in the northward and southward components of the IC exchange are not inter-connected and therefore likely have different drivers. For the NC variability is generally attributed to air-sea fluxes and DWF in the Gulf of Lion (Madec et al. 1991, Millot 1999, Malanotte-Rizzoli et al. 2013), however to date no study has directly linked the two (Malanotte-Rizzoli et al. 2013). It has also been suggested that wind activity could cause the winter strengthening of the NC (Pinot et al. 2002), however other authors found that the mechanical transfer of energy from wind is not a major driver of circulation strength in the Balearic Sea (Font 1990, Garcia et al. 1994). The new seasonal cycle for southward transport through the IC provides a means to investigate the drivers of NC variability and thus the basin scale circulation. As DWF generally occurs from late January through to early March, which is somewhat later than the observed autumn strengthening of the NC, the strength of the winter DWF is not indicated as a direct influence on the seasonal cycle in this research.

Some thought is therefore required as to the mechanism for the autumn increase in strength. One mechanism could be through the autumn 'preconditioning' for DWF in the Gulf of Lion, which is characterised by both the cooling of surface waters and the wind driven spin-up of the Gulf of Lion gyre. In order to assess this, the new seasonal cycle of transport through the IC could be compared against the timing and strength of similar cycles of heat loss, from moorings or atmospheric models (e.g. from NCEP/NCAR latent heat), and wind activity to assess if the seasonal cycles coincide. Additional glider observations of the NC 'up stream' of the IC could also help clarify the timing. There is, both in the new glider observations and other studies (Bethoux 1982, 1988, Pinot et al. 2002, Birol et al. 2010), the suggestion of a sudden autumn increase in the strength of the NC. Again the drivers of this sudden increase are not known, however the timing of this onset, as observed by gliders, could be compared to wind and heat loss data in the Gulf of Lion and Balearic Basin, to see if a link could be determined.

It seems most likely that elements in the IC exchange with a determinable seasonal signal are driven by atmosphere/ocean interactions to the north, which implies that the eddy occupation of the channel is also a product of these northern drivers. How could this work? One mechanism is that the increased strength in the NC, associated with WIW formation, engenders baroclinic instability and spawns eddies, focused around key topographic features in the Balearic Basin, that are then swept south (Crépon et al. 1982, Wang et al. 1988, Tintoré et al. 1990, Masó and Tintoré 1991, Font et al. 1998b, Pinot et al. 2002). Although this explanation could account for the eddy occupation of the IC in spring and for the link with WIW, it does not account for the predominance of anticyclonic eddies. It could also be hypothesised that autumn eddies represent older eddies, that have remained semi-static in periods of light summer flows and become covered by the seasonal thermocline, which then migrate south as the NC strengthens in autumn, and are perhaps swept from the IC when the NC reaches full 'winter' flow strength. Alternatively they could form as the NC strengthens in autumn. However this seems less plausible given the timing and nature of their appearance, which is sub-thermocline and can be earlier in autumn than the increase in NC flow. A detailed comparison with regional models could provide a means of investigating the lifecycle of these IC eddies.

It is anticipated that the fresher AW inflows are driven by intermittent gyre patterns to the south, in the Alboran Sea, as suggested by García-Lafuente et al. (1995) and Pinot et al. (2002). A hypothesis supported by the nature of these events: vigorous, consistent in terms of water mass and simultaneous through the IC and MC, which could easily be caused by a common and intermittent southerly driver. To confirm this hypothesis satellite altimetry and SST could be studied for the period of the fresher AW inflow events observed by gliders, to ascertain if there are any similarities in the southerly gyre or frontal patterns during these events. If a connection can be established this would provide predictive capability for the fresh AW Inflow events and by extension the location of the AWr/AWo salinity front, north or south of the Balearic Channels.

This study therefore finds that the patterns of northward and southward transport through the IC are not inter-dependant, which changes the previously held view of the regional circulation. Additionally, the influence of fresh AW inflows on the regional ecosystems is not dependant on seasonality or the eddy driven 'blocking' of the IC, but likely on a southerly, episodic and predictable variability in the basin scale circulation.

The modelling of such a complex area as the Balearic Basin is challenging, as the processes implicated in the circulation are numerous, complex, and exhibit a wide range of spatial and temporal variability. Some regional models (e.g. MFS) appear to have a stronger component of northward flow. A detailed comparison between glider observations and model simulations has the potential to uncover the underlying reasons for such a bias and so improve model representation at a regional and ultimately basin scale (already in progress). Studies to compare the newly defined seasonal signals with wind and atmospheric data, and the incidences of fresher AW inflows with the continuous record of satellite altimetry to the south are also recommended (already in progress).

The repeated sections of temperature, salinity, density and geostrophic velocity obtained with gliders indicate a pattern of an underlying basin scale circulation that re-emerges or re-instates as the mesoscale interference wanes and shifts, and specific spatial patterns in the mesoscale events. These observations provide the basis for the seasonal 'modes' proposed for the dynamic features of the IC exchange (Chapter 3, section 3.5) and provide a model against which other regional studies can be compared. Although qualitative these modes are supported by the numerical analysis. The patterns of spatial variability in geostrophic velocity across the IC produced from the EOF analysis are clearly very similar to the 'modes' proposed in Chapter 3, section 3.5. In the first EOF (EOF1), the pattern in geostrophic velocity oscillates between a negative amplitude giving a 'winter NC' or 'summer NC' mode and a positive amplitude giving a 'blocking' eddy pattern, similar to the 'spring eddy' and 'autumn eddy' modes. The seasonal shift in the EOF amplitude between positive and negative, that produces this effect, also provides an estimate of the mean timing for these modes. The mean seasonal cycle for southward transport (Chapter 4, fig. 35) is confirmation of the seasonal pattern of the NC flow depicted in the modes and provides values for the levels of transport associated with the 'winter NC' and 'summer NC' modes. The link between these modes and the pattern of geostrophic transport through the IC is shown in Chapter 4, Fig. 31a. An additional spatial pattern for the fresher AW inflow events, which can be combined with any of the seasonal modes, is provided in order to capture this important but non-seasonal component of the exchange.

This style of quasi-continuous glider monitoring at critical circulation points could easily be applied elsewhere in the Mediterranean, and recent studies suggest that the location of such

transects could be optimised for physical, biological and operational modelling applications. Rossi et al. (2014) used tools from Network Theory to analyse larval dispersal over 30 to 60 day periods and identified 'hydrodynamic' provinces defined by known physical oceanographic features. The location of which are similar to the boundaries for 'bio-regions', as identified by D'Ortenzio and Ribera D'Alcalá (2009) from satellite ocean colour chlorophyll concentration. Perhaps such studies could be used to identify a network of key glider monitoring transects, which would improve the characterisation of surface and intermediate flow variability, provide insight into biogeochemical fluxes at important ecosystem boundaries, and so benefit the modelling of physical and eco-systems.

Combined the results of this research deliver a step change in our understanding of circulation variability, at a key 'choke' point in the Mediterranean, with implications for regional and basin scale oceanography. The north and the south of the western Mediterranean are connected via the exchange through the narrow IC 'choke' point and so among the questions that this work poses are:

- How do regional models currently represent the IC exchange?
- What happens to the strong seasonal signal of the NC further south?
- Do the 'blocking' eddy events affect the Alboran Sea circulation?

The observations of high frequency variability, point towards the likely ubiquitous nature of high frequency variability in major Mediterranean and global ocean currents, and to the need for sustained ocean observations to unravel sub-seasonal, seasonal and interannual signals. Interannual signals cannot be fully understood with only 3 years of glider data, however to date no events visible in the glider or ship data seem unduly anomalous and these issues will be an on going focus for the glider mission data analysis.

The relative newness of the glider as a platform for sustained ocean observations required a robust exploration of the data quality and reliability, which has formed a key component of this PhD. This has resulted in a greater understanding of glider data and its uses, methods of processing, correction and calibration, and a measure of the sensitivity of the results to the processing methods. This will be useful to others working with glider datasets. Despite the challenges of the data processing, the value added through using gliders is also clear. With the fast repeat glider sampling a fresh, almost real-time, view of the IC is provided.

Within missions and seasons, in response to hydrographic and mesoscale changes, the NC is observed to broaden and deepen, to move further offshore or on-shelf, and to develop multiple streams of flow. Eddies are observed to evolve in almost real-time and their signature is captured across missions and months. The episodic nature of the fresh AW inflows is also captured. This level of insight is unique to the glider dataset and has been instrumental in determining patterns in the exchange dynamics that underlie the high levels of variability. Transects from the earlier ship campaigns, with a seasonal sampling focus, appear as 'snapshots' in time and did not manage to capture such a coherent picture of the circulation. In the benchmark CANALES experiment (Pinot et al. 2002) a seasonal maximum and minimum were defined. However the glider observations, combined with the historical ship data, have enabled components of the circulation to be robustly characterised at sub-seasonal to seasonal timescales and have brought fresh insight into the governing forces of this important inter sub-basin exchange, which leads to the prospect of predictive capability for fisheries management.

CHAPTER 6: Perspectives on glider monitoring

In a 1989 article H. Stommel foresaw the potential of the emerging glider technology, envisioning in 2021 that a fleet of some 1000 gliders would be operational across the globe, 50% monitoring for climate change and pollution and 50% for scientific studies. We are not there yet but the power of this platform for oceanographic observations is clear. This study establishes the benefits that glider monitoring can deliver. However gliders are complex platforms to operate and in this section some perspectives from the 3 years of glider endurance line operations at the SOCIB Glider Facility are provided. The SOCIB Glider Facility is one of the first groups in Europe to operate a long-term glider monitoring section, called an 'endurance' line and signifying regular-to-continuous glider missions operated over years. The 'canales' glider missions, with not greater than one month between missions, are termed quasi-continuous monitoring.

SOCIB commenced monitoring the Ibiza Channel 'endurance' line in January 2011, however after a successful initial 6 months of glider operations SOCIB encountered a period of repeated mission failures, coincident with the delivery and commissioning of 4 new gliders. Undoubtedly one of the problems was an overstretching of resources, and consequently the glider team was reinforced with additional technical support. However the SOCIB Glider Facility also learnt from these failures and developed several strategies for repeatable, successful glider operations. The IC endurance line monitoring strategy reflects a balance between the scientific focus, the constraints imposed by the glider platform and study area, and the lessons learnt regarding the successful operation of glider 'endurance' lines. Below are noted some of the key elements of the SOCIB 'endurance' line operations, these comments are orientated towards regular-to-continuous glider missions, however it should be noted that other types of glider operations exist, such as single mission process studies. Other types of mission may have additional operational considerations or a different sampling emphasis depending on scientific priorities.

6.1 Key elements of glider 'endurance' line success

Team work: A glider team is important. This team encompasses glider operators who are involved with the gliders on a day-to-day basis, and others, scientists, data management and field operations personnel, whose expertise and support is required to capture and deliver high-quality ocean data. As a rule of thumb, to operate one or more 'endurance' lines for the long-term, a team of three glider operators is desirable, two possible, and one, simply

not realistic. Several glider teams in Europe have developed and operated successfully with one primary and dedicated scientist/glider operator, however for long term 'endurance' line operations I do not believe that this is practical, and that a team is required to operate, use, make available and exploit the data. Gliders are complicated instruments, routinely deployed. Glider operators need to be high-level technicians with knowledge of several fields, including communications, programming and engineering, they also require good planning and coordinating capability. The preparation of a glider for a mission is not trivial and is vital to the gliders survival in the water (e.g. ballasting, batteries), marine authorities need to be notified of mission plans, and field teams need to be coordinated for launch and recovery. Gliders are semi-autonomous; the glider operator monitors their progress (e.g. for SOCIB Slocum glider missions the gliders surface every 6 hours during a 22 day mission) and the require piloting should a problem arise. With regular operations this generally means some extra out-of-hours work and recognition needs to be given for this. Finally, gliders are complex instruments and therefore some mission failures are inevitable, disappointing though this might be solution finding, rather than attributing blame, is essential for the team.

A realistic timetable for glider preparation and launch: The preparation of gliders for a mission takes several days, allowing sufficient time for this is important. Our goal of 'not more than one month between missions' means that the launch date is not rigid, there is time to prepare the glider, to take advantage of weather windows and fit with other SOCIB operations, we frequently re-launch in under a month, but we rarely exceed this time. Too much pressure leads to mistakes.

Documented procedures: Gliders are complex technical platforms and so detailed glider pre-mission and post-mission procedures, with checklists and templates for laboratory intervention reporting, have been developed. This has helped reduce glider preparation time, failure and delays.

Easy launch: Deploying locally, in places that can be easily reached with a fast RIB and using field technicians for deployment/recovery has meant that SOCIB can take advantage of short weather windows and personnel availability (glider pilots can work from the labs or home) to ensure that missions are not delayed. Subsequently our launch and recovery timing is more flexible and responsive.

Investment in infrastructure and technology: SOCIB has invested in a pressure chamber, which enables the lab testing of gliders to their dive depth before deployment, saving time and resources associated with leak failures. Lithium batteries are more

expensive and require special storage facilities and spare science bays in case of failure, however they increase mission length, which in the case of the Ibiza Channel monitoring means that they can be used for 2 or 3 Slocum glider missions and which can reduce mission preparation time significantly.

Automated data management: Gliders generally sample the ocean at higher resolution than traditional ship based sampling and this is a key advantage of the platform. However this also produces a large quantity of data (profiles of the ocean) and so requires the development of automated procedures for glider data management. SOCIB has within its mission a commitment to ocean observations for science and society, including free, easy and timely access to data. Therefore a key element of the SOCIB glider endurance line strategy was the data management strategy, encompassing real time and delayed mode quality control, calibration and data visualisation. Although SOCIB has a particularly strong focus in this area, I believe that a data strategy is vital for all glider endurance line monitoring. To implement a data management strategy requires cooperation across the glider team, from glider operators, to scientists and data centre personnel. The SOCIB data processing system, established in the last 3 years, works for both Slocum and Seaglider data, for real-time and delayed mode, and encompasses basic quality control, salinity correction, calibration, production of netCDF files for data download and tools for data visualisation, search and discovery. These glider data processing tools are freely available from SOCIB's website.

Flexible mission objectives: The objective of 'not more than one month between missions…. and multiple transects of the IC', enables flexibility in terms of launch sites, timing, vessel use and exploitation of opportunities (e.g. synchronising glider/ship missions or vessel operations for launch) whist maintaining the 'endurance' line.

In summary the key issues that have enable effective, efficient, economic and regular glider missions at SOCIB are; a multi skilled team, including glider operators, field technicians, scientists and data management, who have gained experience and confidence in working together, using flexible deployment procedures, plus investment in equipment for time and cost savings in glider preparation/deployment, and, the vital integrated data management process.

6.2 Costs of data acquisition

There is justified reluctance to look at costs, because different scientific objectives will require very different types of missions. However as a guide for planning and budgeting,

and for other operators interested in implementing similar types of missions the cost of operations for the SOCIB missions are provided below. The costs (and key elements for success) are different if, for example, the mission is a single multi-glider experiment or if the glider monitoring is distant to the glider lab location and requires the transport of gliders by ship or air. Therefore it should be emphasised that these costs are meant as guide for similar, regional, glider endurance line monitoring.

The annual operating costs of the SOCIB Glider Facility have remained relatively consistent over the 3 years of operations. For 2013 the total cost of glider operations was 305,570 €, which includes personal, fixed and variable operations and an overhead of 20%. Personnel account for 67% of the total costs, 24% for variable and 9% for fixed and other costs (see Appendix I for details). For SOCIB the largest components of the operational costs are batteries, iridium communications and calibration, which account for 83% of the variable operations. Insurance is a rising mission cost and vessel costs for different types of glider missions can be significantly more important, for example if the gliders require transport to a distal ocean basin site for operation.

SOCIB glider operations 2013 - endurance line and external sceintific users	
Total number of missions	10
Number of missions - Endurance Line	7
Number of missions - External scientific users	3
Total Number of days on mission	242
Number of days (on mission) - Endurance Line	148
Number of days (on mission) - External scientific users	94
Total Number of km on mission	5225
Number of km (on mission) - Endurance Line	3355
Number of km (on mission) - External scientific users	1870
Total Number of profiles on mission	4578
Number of profiles (on mission) - Endurance Line	3705
Number of profiles (on mission) - External scientific users	873
Cost of data aquisition for various metrics 2013:	
Mean per mission	€ 30,557
Mean per day in the water	€ 1,263
Mean per week of glider operations	€ 8,839
Mean per km of glider operations	€ 58
Mean per profile sampled	€ 67

Table 6. Cost of data acquisition, per mission, days, km's and profiles.

The cost of glider data acquisition across the different measures is calculated from the total annual cost of SOCIB glider operations in 2013 divided by the relevant measure (missions, days, km's and profiles), this total annual cost includes personal, operational costs (variable and fixed) and an overhead of 20% (to cover in-kind and contingency), the details are available in Appendix I.

The SOCIB 2013 glider operations are summarised above by number of missions, days on mission, kilometres travelled and the number of profiles collected, see table 6. These are then used to provide a mean cost of glider operations per mission, day, km and profile. For the missions in 2013 this gives a mean cost per day of 1,263€, a mean cost per km of 58€, a mean cost profile of 67€ and a mean cost per mission of 30,557€ (table 6). As the 'canales' endurance line missions and those completed for external scientific users are of different duration, the mission cost is possibly not the most useful metric. The other metrics however are more useful, but should be clearly understood before being used for planning or budgeting. The days of operations count all days on mission, which includes time transiting to the sampling site, for example in the case of 'canales' missions around the island of Ibiza. The km's travelled on mission, similar to the days on mission, includes distance transiting to the sampling sites. The cost per profile is the mean cost for all profiles sampled, some profiles are shorter than others depending on the bathymetry and not all are used in any one study, for example this study uses just those in the IC and MC. However as different profiles may be used for different studies, and thus all profiles are deemed valuable. Finally it is worth emphasising that these costs are provided as a guide for the planning, budgeting or comparison for similar types of operations to SOCIB, namely long term quasi-continuous monitoring of local (relatively) transects, with a standard sensor package and CTD sampling at full resolution.

6.3 Future outlook for gliders

The future, as envisioned by H. Stommel is not yet a reality, there are now some 700 gliders available and 15 'endurance' lines in operation in the global ocean. However the obvious benefits that gliders bring means that their usage is likely to increase and there are many opportunities for the expanded application of gliders. Below are some of the opportunities and areas that require addressing for the expanded use of gliders:

Opening access to external scientific users: Operating gliders requires expertise and infrastructure, providing a method of opening access to external scientific users to these platforms is important, in order to broaden the scientific questions addressed and expend skills glider data use. This can be done through adding additional 'external' sensors to existing glider monitoring operations or through providing funded open access glider mission days, examples include the JERICO TNA open access program, the SOCIB glider

open access program and RUTGERS University 'piggy backing' of acoustic sensors on existing 'endurance' line glider operations for the detection of tagged fish.

Quick technological advancement: New sensors and new gliders will quickly expand the capability of this platform. New deep gliders will expand water column coverage from 1000 m to 2500/3000 m (Slocum) and possibly up to 6000 m (Seagliders). New semi-powered gliders may have the capability to monitor in faster current flows[11]. New sensors (optical and acoustic) are rapidly expanding the range of observations that gliders can address, although some thought will need to be given to the methods of data calibration for these new glider mounted sensors. Finally, although not relevant in the Mediterranean, under ice operation is also actively being addressed and delivering important new observations.

Co-location of biological and physical sampling: To date glider operations have been predominantly of physical parameters. However the ability to co-locate physical observations over the long term and at high resolution with biological observations, from marine mammal noise, to electronic tag recorders, to a range of new biogeochemical sensors, will require the development of new multidisciplinary working groups to provide a step change into research and understanding of ecosystem function and response.

Blue growth: Gliders are likely to play an increasing role in supporting the commercial use of the oceans e.g. in aquaculture, through the monitoring of variability in physical processes and biogeochemical variables and through assimilation into models providing the information to support the sustainable use of our oceans.

Increasing use for environmental monitoring and support for emergency response: Gliders are being taken up by the private sector as well as governments for environmental monitoring and will be important for monitoring of oil spills, pollutants, dredging activities or issues such as harmful algal blooms.

Design improvements for launch and recovery: The launch and recovery of gliders from ocean vessels requires improvement, the current methods are awkward at best and at times risk damaging the instruments.

[11] The current velocity maximum that gliders can reasonable navigate is of order 40 cm s^{-1}

Glider support services: The investment in personnel to operate gliders, to process the data and to assimilate the data into models is perhaps lagging behind the technological development curve of the glider platform itself. There is a skills shortage and more extensive training packages should also emerge to support the current offer. For example glider manufacturers could offer a supported start-up package to help expand glider platform use, as setting up a glider facility takes time and expertise. Regional data hubs, developed for the processing and quality control of a range of glider sensor observations, may also need to emerge, especially for 'endurance' line monitoring. Regional piloting support services or automated piloting for out-of-hours operations, will also be increasingly be used. Some of these needs could be met by the private sector in terms of new companies providing glider skills and glider support services.

Although not applicable to all ocean science questions, gliders are a rapidly developing ocean-observing platform, poised to make a significant contribution in unlocking knowledge of ocean variability, across a range of scales from sub-mesoscale and sub-seasonal to basin and interannual. As a scientific community we should therefore seek to address how to equip and manage more glider operations, overcoming the shortage of glider skills, addressing the issue of long-term 24/7 piloting, and the automated processing and quality control of large glider datasets.

CHAPTER 7: Conclusions

This PhD has used the data from a recently initiated glider monitoring program, to characterise variability in key components of the Mediterranean circulation that act through the Ibiza Channel. The Ibiza Channel is a key 'choke' point in the basin scale circulation of the Mediterranean Sea and governs an important north/south exchange of different water masses, which is known to impact regional ecosystems, in a zone of high biodiversity. The quasi-continuous glider sampling at this location has enabled important sub-seasonal to seasonal variability to be captured and the development of a model to characterise complex patterns of transport. The main results and the influence this has on our understanding of the regional and basin scale circulation are summarised below.

Gliders captured high frequency variability in the exchange through the Ibiza Channel, with changes in transport of the same order of magnitude as the seasonal signal, occurring over just days to a week. Although previous seasonal ship surveys had noted a high cruise-to-cruise variability in transport, they were insufficient to show that the water volumes exchanged through the Ibiza Channel 'choke' point fluctuate on 'weather' timescales. The drivers of this variability were also captured. This is an important finding and clearly demonstrates the need to resolve circulation processes at sub-seasonal timescales, in order to understand ecosystem response and the impact of future climatic change.

At seasonal timescales the traditional view of the north/south exchange through the Ibiza and Mallorca Channels has been overturned. Southward flows of the Northern Current through the Ibiza Channel are characterised as having a seasonal cycle, in line with the previous view, however now a full annual cycle is defined with strong winter flows in December/January (1.0 Sv) declining to a broad summer minimum flow between June and August (0.4 Sv). The northward component of the exchange is characterised as variable around an interannual mean flow of order 0.4 Sv, contrary to the generally held assumption that seasonal inflows from the south spread northward through the Balearic Channels in summer, in response to the decline of the Northern Current. In fact, through the summer, the net flow through the Ibiza Channel is shown to be broadly neutral.

Other complex components of circulation interact with this simple seasonal pattern; vigorous inflows of fresher AW that are known to influence the summer spawning grounds

of Atlantic bluefin tuna occur, and anticyclonic eddies become wedged in the narrow Ibiza Channel and block or modulate the flow. The inflows of AW of 'more recent Atlantic origin' are clearly identified as sporadic events of several months duration that occur simultaneously through both the Ibiza and Mallorca Channels. It is hypothesised that the driver for these inflow events lies to the south, in specific but intermittent gyre patterns in the Alboran Sea. The eddies, although long identified as playing an important role in 'blocking' the Ibiza Channel in spring/early summer, are now better characterised, through observations and EOF analysis, as having a clear seasonality associated with characteristic structures. In spring, these eddies are most likely to occupy the Ibiza Channel between March and April, as either one large (70 km diameter eddy) or two medium (25 - 30 km diameter) eddies, that effectively block the flow. In autumn, eddies most likely occur between September and November, again as either one large (70 km diameter eddy) or two medium (25 - 30 km diameter) eddies, and are sub-thermocline structures that modulate or influence the pathways of the surface through channel flows.

For the first time, this analysis shows that the northward and southward components of the exchange are only physically linked when they meet in the channels. Those elements that exhibit seasonality are influenced by drivers to the north (atmospheric patterns), namely the Northern Current and mesoscale activity, those that do not are driven by episodic gyre configurations to the south (wind and inflows from the Atlantic) and local mesoscale variability (complex multiple sources). The Balearic Sea thus represents a true north/south transition zone and the Ibiza Channel, the last 'choke' point in the upper open thermohaline circulation cell of the Mediterranean, governs the transmission of this seasonality southward.

The contribution that the glider monitoring has made to characterising variability in the regional flow patterns at seasonal to sub seasonal scales is clear; furthermore a sense of characteristic flow structures or patterns has also emerged. These patterns are the basis of the 'modes' described at the end of Chapter 3, which reflect an annual interplay between basin scale and mesoscale dynamics. Although observation based they are substantially supported by the dominant modes of variability identified in the EOF analysis, and provide a new descriptive framework in which to place past and future observations.

This research, and the glider monitoring that underpins it, has enabled a step change in our knowledge of circulation variability at an important and complex area in the Mediterranean circulation. The glider observations are part of the regional observing system, operated by SOCIB, so how does this PhD work integrate with the objectives of an ocean observing system? Initial studies such as this, are a vital first step for long-term monitoring initiatives, serving to characterise and codify data quality control procedures, deliver quality controlled data streams ready for model assimilation and to identify relevant monitoring metrics that can be integrated into data products of regional relevance. For example, products from this study might include indicators of the seasonal anomalies in strength of the NC (above the interannual mean), estimated production sites of WIW, and the prediction of fresh AW inflow or WIW formation events. A key next step is also to use this new knowledge to improve the regional numerical models and to develop, from the combination of models and monitoring, forecast capability around issues of relevance, a clear example being the spawning sites for Atlantic bluefin tuna.

The research also provides insight into the role of gliders as a component of multi-platform, integrated ocean observing systems. As gliders are poised to make a significant contribution to this effort, the oceanographic community should address how to manage more glider operations, including the shortage of glider skills, the 24/7 piloting, increasing access and the automated management and quality control of glider data. The insight gained from 3-years quasi-continuous monitoring with this still relatively new technology, is significant and will be of relevance to other current and future glider operators.

In response to climate change, the globalisation of society, and increasing human pressure along our coastlines, our relationship with our global ocean resource is undergoing a period of rapid change, with implications for ocean science and scientists. The future, in economic and lifestyle terms, will rely on a shift in our relationship with this marine asset to one of informed management. This shift will rely on an increased knowledge and understanding of the oceans; although there are many components to this, ensuring the physics of our ocean circulation is well characterised, from sub-seasonal to decadal scales, is an important baseline building block in this process. Characterising, unravelling and understanding variability has been a major component of this work and is an important inter-disciplinary theme in science today, as important in oceanography as it is in medical research (see TED talk by Malcolm Gladwell, 2006).

This study forms a part of the 'quiet revolution' that multi-platform ocean monitoring is making to our knowledge of ocean variability. The results provide a critical contribution to the characterisation of ocean variability for the long-term, with application to resource management, ecosystem interaction and future climate prediction, through better constraining ocean models and improving marine forecasting.

APPENDICES:

Appendix A: Ship missions

No.	Source	Survey Name	start date	end date	Days	Channels	Calibration	ADCP	Notes	IBAMAR ID
1	IEO-COB	CANALES_0396	05/03/1996	08/03/1996	3	IC/MC	Bottle			98
2	IEO-COB	CANALES_0496	05/04/1996	08/04/1996	3	IC/MC	Bottle			99
3	IEO-COB	CANALES_0596	14/05/1996	17/05/1996	3	IC/MC	Bottle			305
4	IEO-COB	CANALES_0696	10/06/1996	13/06/1996	3	IC/MC	Bottle			102
5	IEO-COB	CANALES_0796	31/07/1996	03/08/1996	3	IC/MC	Bottle			109
6	IEO-COB	CANALES_0297	30/01/1997	05/02/1997	6	IC/MC	Bottle		sparse profiles IC (5/11) missing last profiles E & W	114
7	IEO-COB	CANALES_0497	02/04/1997	05/04/1997	3	IC/MC	Bottle			117
8	IEO-COB	CANALES_0597	26/05/1997	29/05/1997	3	IC/MC	Bottle			121
9	IEO-COB	CANALES_0697	30/06/1997	03/07/1997	3	IC/MC	Bottle		sparse profiles IC (5/11) missing last profile E & W, & MC (5/10) missing last profile W	122
10	IEO-COB	CANALES_0897	01/08/1997	04/08/1997	3	IC/MC	Bottle			125
11	IEO-COB	CANALES_0198	26/01/1998	31/01/1998	5	IC/MC	Bottle			128
12	IEO-COB	CANALES_0498	01/04/1998	04/04/1998	3	MC	Bottle			130
13	IEO-COB	CANALES_0698	16/06/1998	23/06/1998	7	IC/MC	Bottle			137
14	IEO-COB	CIRBAL_0599	25/05/1999	30/05/1999	5	IC/MC	Bottle			135
15	IEO-COB	CIRBAL_0900	19/09/2000	26/09/2000	7	IC	Bottle		MC too short	146
16	IEO-COB	CIRBAL_1100	14/11/2000	20/11/2000	6	IC/MC	Bottle			147
17	IEO-COB	CIRBAL_0301	24/03/2001	04/04/2001	11	IC/MC	Bottle			151
18	IEO-COB	CIRBAL_0501	04/05/2001	10/05/2001	6	MC	Bottle		IC too short	152
19	IEO-COB	CIRBAL_0601	02/06/2001	13/06/2001	11	IC/MC	Bottle			153
20	IEO-COB	CIRBAL_1101	13/11/2001	24/11/2001	11	IC/MC	Bottle			155
21	IEO-COB	CIRBAL_0302	21/03/2002	01/04/2002	11	IC/MC	Bottle			317
22	IEO-COB	CIRBAL_0502	20/05/2002	02/06/2002	13	IC/MC	Bottle			165
23	IEO-COB	CIRBAL_0902	24/09/2002	05/10/2002	11	IC/MC	Bottle			169
24	IEO-COB	CIRBAL_0303	21/03/2003	24/03/2003	3	IC	Bottle		MC shallow in E	172
25	IEO-COB	CIRBAL_0503	28/05/2003	10/06/2003	13	IC/MC	Bottle			173
26	IEO-COB	CIRBAL_1003	04/10/2003	13/10/2003	9	IC/MC	Bottle			178
27	IEO-COB	CIRBAL_0304	12/03/2004	25/03/2004	13	IC/MC	Bottle			181
28	IEO-COB	CIRBAL_0504	12/05/2004	25/05/2004	13	IC/MC	Bottle			183
29	IEO-COB	CIRBAL_1004	16/10/2004	25/10/2004	9	IC/MC	Bottle			186
30	IEO-COB	CIRBAL_0205	27/02/2005	10/03/2005	11	IC/MC	Bottle			231
31	IEO-COB	CIRBAL_0605	12/06/2005	23/06/2005	11	IC/MC	Bottle			232
32	IEO-COB	CIRBAL_0905	22/09/2005	28/09/2005	6	IC/MC	Bottle			198
33	IEO-COB	CIRBAL_0406	14/04/2006	07/05/2006	23	IC/MC	Bottle			199
34	IEO-COB	CIRBAL_0606	16/06/2006	15/07/2006	29	IC/MC	Bottle			201
35	IEO-COB	CIRBAL_1006	10/10/2006	25/10/2006	15	MC	Bottle			202
36	IEO-COB	RADMED_0707	07/07/2007	21/07/2007	14	IC/MC	Bottle		MC is short 1 profile in W (9/10)	244
37	IEO-COB	RADMED_1007	01/10/2007	18/10/2009	17	IC/MC	Bottle			203
38	IEO-COB	RADMED_0208	09/02/2008	02/03/2008	22	IC/MC	Bottle			204
39	IEO-COB	RADMED_0408	20/04/2008	05/05/2008	15	IC/MC	Bottle		MC missing in S, but keep in transports	206
40	IEO-COB	RADMED_0708	01/07/2008	06/08/2008	5	IC/MC	Bottle			212
41	IEO-COB	RADMED_1008	15/10/2008	19/11/2008	4	IC/MC	Bottle		IC some profiles missing in E (9/11) MC missing profile in SW (9/10)	218
42	IEO-COB	RADMED_0309	15/03/2009	10/04/2009	26	IC/MC	Bottle		problem with T1 profile (0.8E) remove data	220
43	IEO-COB	RADMED_0509	25/05/2009	12/06/2009	18	IC/MC	Bottle			289
44	IEO-COB	RADMED_0709	04/07/2009	30/07/2009	26	MC	Bottle		IC reduced (7/11) and in E only to 100 m not used for transports, MC profile in SW missing (9/10)	329
45	IEO-COB	RADMED_0410	10/04/2010	16/10/2010	7	IC/MC	Bottle			346
46	IEO-COB	RADMED_0211	14/02/2011	13/03/2011	27	IC	Bottle			505
47	IEO-COB	RADMED_0511	02/05/2011	30/05/2011	28	IC/MC	Bottle			512
48	University of Valencia	DERIVA_0611	05/06/2011	23/06/2011	18	IC	Bottle		Water samples from RADMED_0511used for calibration. Transect short in E, data appears more spiky	
49	IEO-COB	RADMED_0711	25/06/2011	27/07/2011	1	IC/MC	Bottle		IC more sparse (9/11) and only to 300 m for W half, use IC transports with caution	503
50	IEO-COB	RADMED_0312	24/03/2012	13/04/2012	20	MC	Bottle		MC v sparse	509
51	IEO-COB	RADMED_0313	15/03/2013	05/04/2013	21	IC/MC	Bottle		Also called PERSEUS_0313	
52	IEO-COB	RADMED_0613	11/06/2013	19/06/2013	8	IC/MC	Bottle		Also called PERSEUS_0613	
53	SOCIB	MEDESS092013	16/09/2013	19/09/2013	4	IC	Bottle	Y	ADCP with Furano navigation data - needs to be post processed to use Ashtech 3D navigation data. 6 trsnsects of the IC	
54	SOCIB	SOCIB_Dic13	02/12/2013	04/12/2013	3	IC/MC	Bottle	Y	2 transects of the IC	

Table A1. Summary of ship missions used in analysis, 1996 to 2013.

Appendix B: Sensitivity test for the reference level of zero velocity assumption

Within this PhD study a base of profile reference level of zero velocity is assumed in the calculation of geostrophic velocity. Although the use of a reference level of zero velocity is still frequently used in studies of geostrophic flow (Cunningham et al. 2007, Bryden et al. 2005 and Ruiz et al. 2014), however due to the depth of the IC and the relative newness of the glider as a platform for sustained observations this assumption has been tested.

A comparison study between glider and ship ADCP data (see Appendix D) strongly indicates that the geostrophic velocity field calculated under this variable level zero velocity reference assumption bears a very close resemblance to that observed with the vessel mounted ADCP, both in terms of spatial pattern and also absolute velocity values. Within the margins of error of the ADCP (accurately measure currents ≥ 5 cm s^{-1}) they are very close and this indicates that the estimates of geostrophic velocity derived here from glider data are an accurate representation of the total flow, to depths of order 400 m. However, although a good indication this does not numerically address the issue. Therefore a sensitivity test was undertaken, through the application of a simulated base of profile reference level of velocity, using published information as a source of base of profile velocity estimates. A review of data on deep flows in the IC identified the following:

1) From Pinot and Ganachaud (1999): Figure 8 provides the absolute geostrophic flow at the bottom of station pairs calculated using inverse methods for one transect of the IC in June 1993. This indicates that the base of profile velocities at the western shelf edge (0.4°E) of the IC are at 0.65°E of order 3 cm s^{-1}, at 1.05°E of order 2 cm s^{-1} and of order 1 cm s^{-1} in between. In addition, the inverse box model methods estimated that the transport from 0 to 600 m depth represents 85% total flow and from 0 to 230 m depth 65% of the total flow in the IC.

2) From Pinot et al. (2002): Figure 11a shows data from current meters located at a mooring A1. The data from current meters at 500 m and 870 m are shown as vector arrows and indicate for the 2 month period shown (July to August 1996) southward flows occurring of days duration, that are generally the same time at 500 m and 870 m and are of similar orders of magnitude. The flows at 500 m are 0 to 4 cm s^{-1} and at 870 m are 0 to 3

cm s^{-1}, with the flows at 500 m orientated south-southeast and at 870 m orientated southeast, perhaps due to the slope of the channel edge. Pinot et al. (2002) stated that flows at depth are frequently equal to, or greater than, those at 500 m and occur synchronously at the two depths. Although the synchronicity of flows at the two depths is confirmed in fig. 11a, it also suggests the velocities are generally lower (of order of 1 cm s^{-1} lower) at 870 m and that they do not exceed those at 500 m.

From theses two sources both static and variable base of profile velocities were created for the sensitivity test, as follows:

1. Static base of profile velocities: Using Pinot and Ganachaud (1999) a base of profile velocity section was created, mimicking the velocities shown in fig. 8 (Pinot and Ganachaud 1999). Deep profiles with bottom velocities of < 1 cm s^{-1} are not considered meaningful by the authors and so these were set to zero. The strength of this estimate is that fig. 8 provides currents at the base of the profiles, what is required. The weaknesses are:

- The current estimates are from a single mission (a single transect) and so give no indication as to variability
- The course resolution (3 data points across the channel)
- They are an estimate of geostrophic velocity and so do not represent total flow
- The inverse method itself is based on assumptions, for example the assumption of a steady state for the 8 day period of the cruise (1 – 8th June 1993)
- Base of profile velocities are of order 1 – 2 cm s^{-1}, which is at the limit of what can be determined accurately accurately by the inverse methods (Pinot and Ganachaul 1999)

2. Variable base of profile velocities: Following Pinot et al. (2002) velocities at depth were derived from geostrophic velocities at 500 m, with a reduction applied. For the few profiles with a base of profile depth of < 500 m, velocity from the nearest neighbour profile was used. The strength of this method lies in the clear link between the currents at 500 m and those at depth, as seen in the mooring data (Pinot et al. 2002, fig. 11a), and in the ability to create base of profile velocities per transect, which would appear to be important given the variability in flow observed in the mooring data. The weaknesses are:

- The mooring in fig. 11a (A1) is located ~20 km to the north of the glider transect

- The estimates are based on the glider estimate of geostrophic velocity at 500 m and so again do not represent total flow. However the comparison with VM-ADCP data (noted above and detailed in Appendix D) suggests that this is a reasonable assumption
- The channel edge profiles, with depth < 500 m, use nearest neighbour velocities which could underestimate the close to shelf edge flow
- The limits of accuracy of the current meters used in the experiment, 1 - 2 cm s^{-1} in the range 0 – 20 cm s^{-1}, are on a par with some of the flows observed (Pinot et al. 2002)

To perform the sensitivity test, the glider missions canalesJan2011 and canalsDec2011 were processed using the zero velocity assumption (hereafter GV zero), and then re-processed using the Pinot and Ganachaud (1999) derived profile velocities (hereafter 'GV P&G 1999') and the Pinot et al. (2002) inspired base of profile velocities derived using the glider geostrophic velocity at 500 m, reducing to 75% and to 50% (hereafter 'GV 500 75%' and 'GV 500 50%', respectively). The base of profile velocities were added to each of the zero velocity assumption derived velocities in the profile and the geostrophic transport calculated as normal for each solution: GV zero, GV P&G 1999, GV 500 75% and GV 500 50%. The glider missions chosen for analysis have NC flows and AW inflows, which is also true of the Pinot and Ganachaud (1999) transect. The results of the tests are shown in table B1 below.

For the GV P&G 1999 solution for base of profile velocity, the percentage difference in the transport northward (positive) is generally less than that in the transport southward (negative), see table X1. For canalesJan2011and for canalesDec2013 the mean percentage difference in transports north were +2% and -6%. Inflows were strong in December 2013 and so the choice of bottom velocity may have influenced this negative result. For the transport north, the result is consistent between the two missions of order +16%, possibly influenced by the strong shelf velocities, as estimated using inverse methods for June 1993.

For the GV 500m 75% and GV 500m 50% solutions to the base of profile velocity, the difference in northward transport is similar to that in southward transport and consistently positive, this seems more realistic as we might expect the zero velocity assumption to provide lower values of transport than those calculated with a base of profile velocity. For canalesJan2011and for canalesDec2013 the mean percentage difference in transports north were of order 6 to 12% and for northward flow 8 to 16%.

		Flows Sv		% diff. GV zero					Flows Sv		% diff. GV zero	
canalesJan2011		**N**	**S**	**N**	**S**		**canalesDec2013**		**N**	**S**	**N**	**S**
GV zero	T1	0.30	-1.23				GV zero	T2	0.73	-1.37		
GV P&G 1999		0.31	-1.42	102%	115%		GV P&G 1999		0.67	-1.48	92%	108%
GV 500 75%		0.28	-1.42	94%	116%		GV 500 75%		0.83	-1.53	114%	112%
GV 500 50%		0.29	-1.36	96%	110%		GV 500 50%		0.80	-1.48	109%	108%
GV zero	T2	0.25	-0.90				GV zero	T3	0.20	-0.53		
GV P&G 1999		0.27	-1.09	108%	122%		GV P&G 1999		0.19	-0.70	97%	132%
GV 500 75%		0.30	-1.01	121%	113%		GV 500 75%		0.21	-0.63	107%	119%
GV 500 50%		0.29	-0.97	114%	108%		GV 500 50%		0.21	-0.60	105%	113%
GV zero	T3	0.16	-0.93				GV zero	T4	0.47	-0.83		
GV P&G 1999		0.14	-1.09	91%	117%		GV P&G 1999		0.43	-0.96	91%	116%
GV 500 75%		0.17	-1.06	111%	115%		GV 500 75%		0.52	-0.93	111%	112%
GV 500 50%		0.17	-1.02	107%	110%		GV 500 50%		0.50	-0.89	107%	108%
GV zero	T4	0.18	-1.16				GV zero	T5	0.92	-1.07		
GV P&G 1999		0.19	-1.35	109%	116%		GV P&G 1999		0.90	-1.23	98%	114%
GV 500 75%		0.19	-1.41	110%	122%		GV 500 75%		0.98	-1.13	107%	105%
GV 500 50%		0.19	-1.32	106%	114%		GV 500 50%		0.96	-1.11	105%	104%
GV zero	T5	0.48	-1.23									
GV P&G 1999		0.48	-1.40	100%	114%							
GV 500 75%		0.58	-1.44	120%	117%							
GV 500 50%		0.55	-1.37	114%	111%							
GV zero	T6	0.58	-1.74									
GV P&G 1999		0.60	-1.93	104%	111%							
GV 500 75%		0.66	-1.94	115%	111%							
GV 500 50%		0.63	-1.87	110%	107%							
mean GV P&G 1999				102%	116%		mean GV P&G 1999				94%	117%
Mean 500 75%				112%	116%		Mean 500 75%				110%	112%
Mean 500 50%				108%	110%		Mean 500 50%				106%	108%

Table B1. Results from geostrophic transport sensitivity to reference velocity test.

The results add to what we know about the potential errors associated with the calculation of geostrophic transport. The GV 500m base of profile velocity solution suggests that an uplift of order 10% could be applied to the geostrophic transport calculated with a base of profile reference level of zero velocity. They also point to higher and less stable levels of sensitivity for higher bottom current values, for example the percentage uplift in transport for both north and south flows is more consistent with the GV 500m 50% solution than with the GV 500m 75% solution which can vary from between +22 to +11%. The use of a 'standard' base of profile velocity (GV P&G 1999) was not as realistic an estimate, given the variability of transport in the IC and the sporadic nature of the deep flows. Nevertheless there is some general agreement in the scale of sensitivity to the GV 500m 50% velocity solution. As noted above, the two methods for creating a representative base of profile velocity for the IC both have weaknesses and strengths.

These results provide insight into the question. However in terms of providing a solution they should be treated with caution, as the creation of the base of the profile velocities is subjective, based on small amounts data and the values are frequently on a par with the measurement or calculation error. Notwithstanding, they do suggest a general level of sensitivity of order 10% could be used as an estimate for the scale of error associated with the zero velocity at base of profile assumption used in the calculation of geostrophic transport.

To provide a more definitive answer to the effect of calculating transport using a reference level of zero velocity, a study using glider DAV, from missions that have had a glider compass correction performed (see Appendix C), is recommended. Performing at least one such mission in conjunction with the VM-ADCP capability of the B/O SOCIB would provide another measure of velocity and add insight into both the zero velocity assumption and the glider DAV variable as a source of relevant bottom current information.

Appendix C: Analysis of glider Depth Averaged Velocity (DAV) variable

When at the surface, gliders calculate the difference between their actual and 'dead reckoned' position in order to adjust their subsequent flight path in order to take account of the effect of ambient currents. This calculation effectively estimates the absolute depth averaged velocity (DAV) between the last and current surfacing event. This glider DAV is however dependent on the accuracy of the on-board compass, used to navigate between waypoints and to determine the 'dead reckoned' position, which due to its proximity to battery packs and other internal components requires a mission specific error calibration procedure (Merckelbach et al. 2008). Without this correction procedure the error in the heading measurements from Slocum gliders can be significant, Merckelbach et al. (2008) found the difference between true heading and the Slocum glider compass heading to be between 3 and 35 degrees, dependant on the heading and glider unit tested. A similar experiment undertaken at IMEDEA in 2010 found the difference between glider compass heading and 'true' heading for a Slocum Coastal glider (Unit 30) to have a maximum error of 14° for headings of 220°, see fig. C1 below.

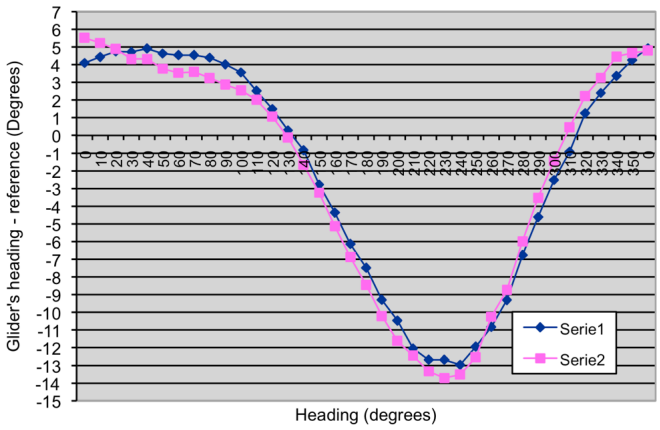

Figure C1. Glider compass correction curve for Slocum Coastal glider (Unit 30).
The plot shows the difference between glider compass heading and the 'true' heading for a series 1 and series 2, 360° circle of the glider around a fixed point, note the good coincidence between curves and the sinusoidal form of the compass correction curve (as found for the deviation or 'swinging' of yacht compass).

For most of the 'canales' glider missions no such compass experiment has been performed (excepting canalesSep2013), and therefore the DAV estimates produced by the glider contain an unknown and potentially large error. Notwithstanding an analysis was

performed to test the agreement between the glider DAV and a DAV produced from the estimated geostrophic velocities to assess if such errors are visible and if they are potentially large. For this test a mission with a pair of 'steady' transects, i.e. similar patterns of geostrophic currents and not too large deviation from the standard transect line, was selected so that the DAV for transects with not too much change and headings at 180° to each other could be assessed. With the hypothesis that if there is an error in the compass, depending on the specific deviation, it could be visible in a difference in the DAVs between transects with headings at 180° to each other. The mission selected was canalesJan2011. A quick test on the average glider heading for all transects was found to be close to 270° or 90°, thus at a first pass the glider internal compass appears to be accurate. The pattern of 'new' GPS fixes is not evenly distributed along transect, which means that the segment of transect for which a DAV value is representative is relatively coarse (as compared to the glider estimated geostrophic velocity values) and of variable length, see fig. C2. Some experimentation was required in order to find the appropriate level of smoothing to apply to the glider DAVs and the geostrophic velocity estimated DAVs (DAGVs) in the horizontal, in order to facilitate inter-comparison. A 27 km smoothing was found to work well and the glider DAVs and the geostrophic velocity estimated DAVs (DAGVs) were then compared for each transect.

As can be seen (fig. C2) the match in T2 is very good between the two estimates of DAV, particularly for the smoothed data. The fit is less good in T4 in the west of the channel, with an underestimation in the geostrophic DAV (DAGV) of order 7 cm s^{-1}, although in the east of the channel the match is good, and in terms of variability across the transect (features observed) the match is also reasonable.

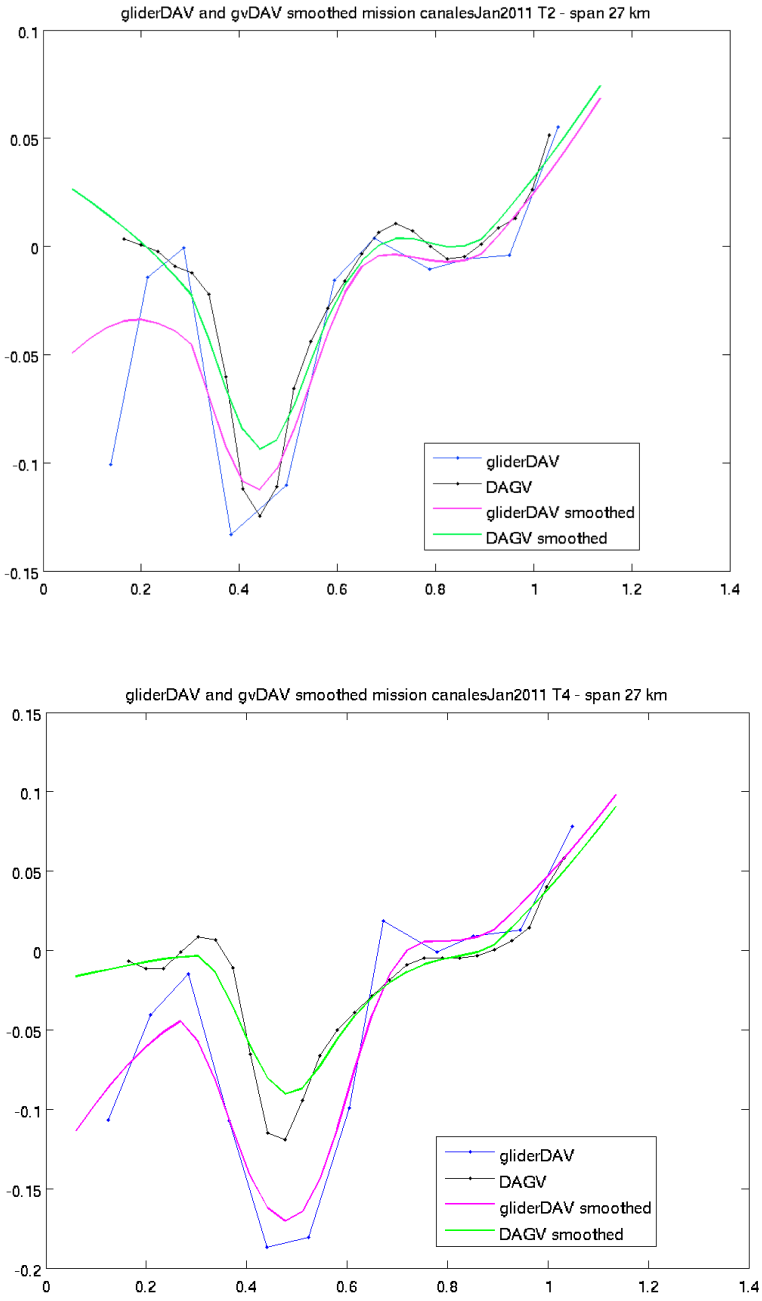

Figure C2. Comparison of glider DAV and geostrophic DAV for canalesJan2011.
Transect T2 (above) and T4 (below), the glider DAV (blue) and geostrophic DAV (black), and smoothed with a 30 km moving average, the glider DAV (magenta) and geostrophic DAV (green).

The same plots for the odd transects reveal a different picture, see fig. C3 below. Here the match between glider DAV and geostrophic DAV although of a similar order of magnitude in the west of the channel, there is the sense of perhaps a displacement of features between the two estimates and a pattern of stronger currents in the glider DAV in the east of the section (from 0.6°E) rather than in the west of the channel as in T4 and T2

(fig. C2). It is impossible to say whether this is due to compass error, difference in sampling intervals, an underestimation of the currents with geostrophic assumptions, or a combination of all three. Interestingly the glider DAV estimation is generally greater, indicating that geostrophic assumptions underestimate the DAV, however this does not explain the pattern of this difference. It is however slightly suspicious that this occurs consistently in the east of the channel for the odd transects (T1 and T3), which could suggest that a component of compass error is at play.

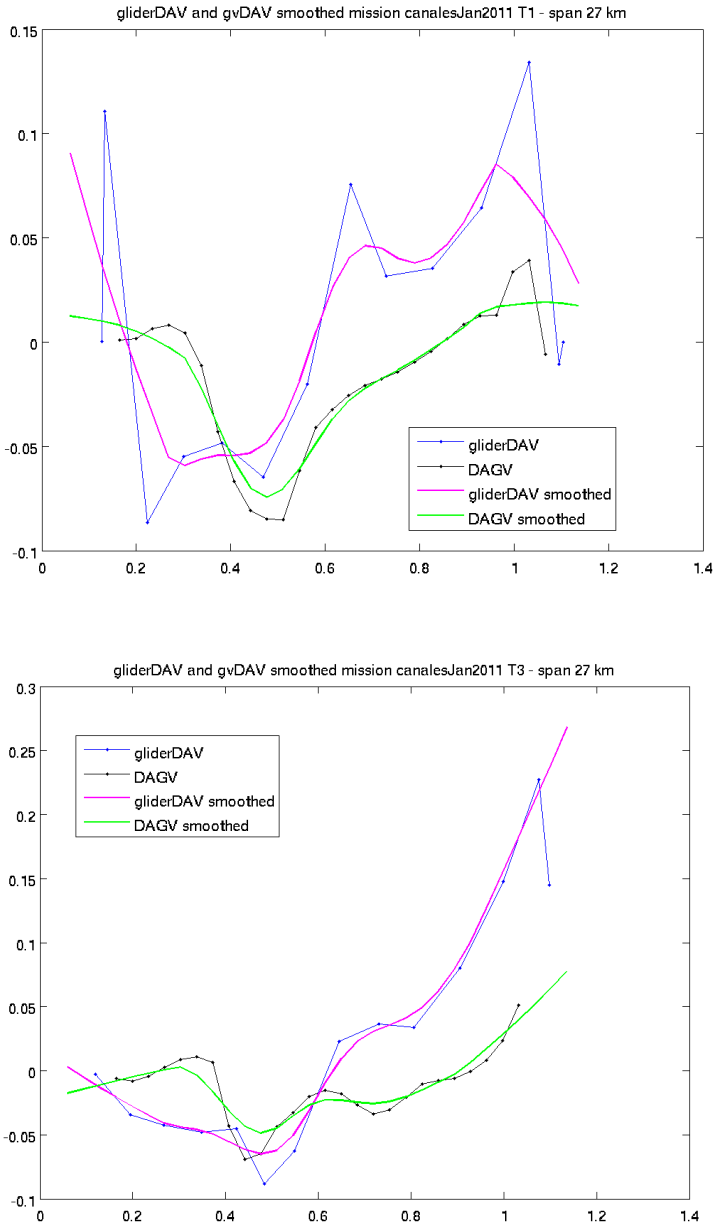

Figure C3. Comparison of glider DAV and geostrophic DAV for canalesJan2011.
Transect T1 (above) and T3 (below), the glider DAV (blue) and geostrophic DAV (black), and smoothed with a 30 km moving average, the glider DAV (magenta) and geostrophic DAV (green).

Overall the agreement between glider DAV and geostrophic DAV is mixed, in some transects it is very good with the mean difference down to the level of estimated errors due to the Slocum glider DAV calculation method (2 to 3 cm s^{-1}, Merckelbach et al. 2008), fig C2. However in other sections although the patterns of velocities across the sections are broadly similar there are also differences, above the level of calculation error. However the pattern of these means that there is the potential of an unknown component of compass heading error in the glider DAV, as the divergence appears to be worse on the odd transect T1 and T3. For the sake of consistency and simplicity the glider calculated DAV, with no means of correcting for any potential error in compass heading, was not used to provide a reference level velocity for this study.

Appendix D: Comparison of glider and ship data

Ships have long been the benchmark platform for open ocean observations across basins, currents and other features of interest[12]. Therefore in this appendix contemporaneous glider and ship transects are compared in order to provide insight into the effect differences in temporal and spatial sampling between the two platforms have on the data and into the assumptions that a) glider and ship transects can be sensibly combined for analysis and b) that glider transects can generally be viewed as synchronous. The differences in sampling between the two platforms can be summarised as follows:

- Profile density: The profile density of the glider data depends on the depth of the profile, in the IC ranging from ~300 m between profiles on-shelf (depths ≤ 200 m) to 1.3 – 3.1 km off-shelf (200 < depths < 950 m, for IC), as compared to a regular 10 km spacing for ship CTD stations.
- Vertical resolution: The ship CTD units generally sample at 25 Hz and the data is then bin averaged to 1 m bins (IEO) or 0.5 db bins (SOCIB), see Chapter 2 for more details. Glider CTD units sample at 0.5 Hz which, with a descent rate of order 0.18 m s^{-1}, gives a sample interval of ~0.5 m. This lower sampling resolution in the vertical impacts the glider data in the application of a salinity correction (see Chapter 2 for more details), however for the features studied here it is not noticeable beyond the initial data processing.
- Horizontal speed: Each 80 km glider transect of the IC takes approximately 3 days for a glider to complete, with ~2 days for the deep central channel section, as compared to 6 to 7 hours for a ship transect.
- Temporal resolution of transects: for the IEO missions (e.g. RADMED, CANALES and CIRBAL) a single transect of the IC and MC was sampled per mission, for the SOCIB missions multiple transects of the IC, with a 10 km spacing between transects, and a single transect of the MC was sampled per mission (see Chapter 2 for details). For the glider missions, multiple consecutive transects were sampled ('burst' sampling), 4 to 6 transects per mission.

[12] Note: there are a few mooring arrays in the global ocean, such as the RAPID array across the Atlantic at 26°N and the Fram Strait Array, however they have a more coarse spatial resolution and no such arrays currently exist in the Mediterranean Sea, to date ships transects remain the benchmark

- Transect location: The IEO ship mission transects were located 15 km to the south or southeast of the glider IC and MC transects (see Chapter 2, fig. 6), the SOCIB ship transects were performed along the same transects as the glider, and also in multiples of 10 km to the south, depending on the mission (again see Chapter 2, fig. 6)

Here we compare three contemporaneous missions in more detail, canalesFeb2011 and RADMED_0211, canalesSep2013 and MEDESS_0913, and canalesDec2013 and SOCIB_Dic13, see table B1 below, for details of the dates, transects and total transport values and Chapter 2, fig. 6 for a map of the transect and profile station locations.

Ship mission	T	Mean date (channel)	Trsp. South (Sv)	Trsp. North (Sv)	Glider mission	T	Start date (channel)	End date (channel)	Trsp. South (Sv)	Trsp. North (Sv)
RADMED_0211					canalesFeb2011	T3	15/02/2011 08:12	17/02/2011 10:46	-0.68	0.58
						T4	18/02/2011 21:54	20/02/2011 12:56	-0.70	0.51
						T5	20/02/2011 20:16	22/02/2011 17:19	-0.22	0.49
						T6	**24/02/2011 10:06**	**26/02/2011 06:30**	**-0.49**	**0.28**
	T1	**26/02/2011 12:36**	**-0.57**	**0.24**		**T7**	**26/02/2011 15:21**	**28/02/2011 13:38**	**-0.64**	**0.23**
						T8	02/03/2011 03:52	03/03/2011 21:38	-0.80	NA
MEDESS092013	**T1**	**18/09/2013 09:24**	**-0.26**	**0.27**	canalesSep2013	**T3**	**15/09/2013 21:55**	**18/09/2013 01:50**	**-0.42**	**0.34**
	T2	**18/09/2013 16:12**	**-0.12**	**0.23**		**T4**	**19/09/2013 13:07**	**22/09/2013 02:34**	**-0.40**	**0.41**
	T3	19/09/2013 10:17	-0.17	0.23		T5	22/09/2013 15:06	24/09/2013 23:45	-0.30	0.36
	T4	17/09/2013 17:22	-0.03	0.21		T6	26/09/2013 14:02	29/09/2013 08:09	-0.38	0.64
	T5	17/09/2013 09:14	-0.13	0.10						
	T6	16/09/2013 17:23	-0.22	0.02						
SOCIB_Dic13	**T1**	**02/12/2013 17:28**	**-1.14**	**0.28**	canalesDec2013	**T2**	**03/12/2013 21:26**	**06/12/2013 09:57**	**-1.40**	**0.71**
	T3	03/12/2013 18:04	-0.53	0.09		T3	07/12/2013 23:58	09/12/2013 14:36	-0.54	0.20
						T4	09/12/2013 23:41	13/12/2013 00:00	-0.84	0.48
						T5	14/12/2013 21:24	17/12/2013 00:00	-1.08	0.94
					sub-sampled	**T100**	**03/12/2013 21:26**	**06/12/2013 09:57**	**-1.34**	**0.34**

Table D1. Details of the glider and ship missions compared.
The synchronous glider and ship transects are highlighted blue and the transport values (Tran.) of water masses north (N) and south (S) are provided. T100 is a glider transect canalesDec2013 T2, sub-sampled to the same profile density as the contemporaneous ship transect SOCIB_Dic13 T1.

In the subsequent sections the most synoptic glider and ship transects from the contemporaneous missions are compared. It should be noted that in the following sections the potential temperature and salinity sections presented in the figures have undergone only initial data processing (Chapter 2): salinity corrections have been applied, the data interpolated to 1m in the vertical and profiles assumed vertical. This is in order for features to be clearly visible prior to interpolation to a grid for the geostrophic calculations. By contract the plots of geostrophic velocity and density are from the gridded data and so have a 6 km smoothing applied (see Chapter 2). The glider data appears to end at 20 m

depth in the temperature and salinity plots, this is a function of the inflexion point of the Slocum glider combined with the type of plot (colour contour) as the more sparse spacing of the glider data mean that the surfacing profiles were not contoured.

Below the glider and ship missions are compared:

February 2011

Sections of potential temperature (θ) and salinity (S) across the IC for canalesFeb2011 and RADMED_0211 are shown in fig. D1.

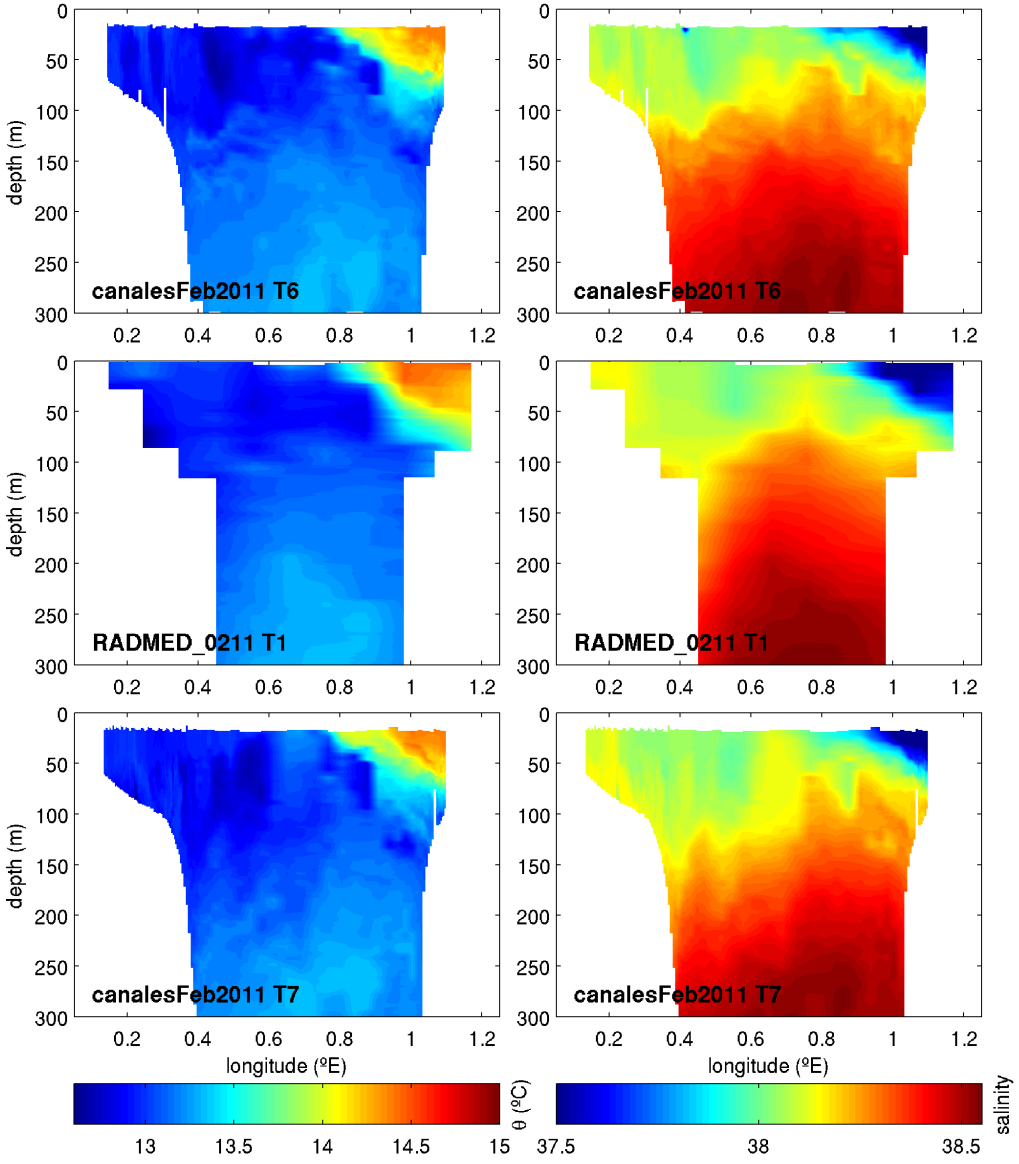

Figure D1. θ and S sections to 300 m for the 3 glider/ship transects in Feb 2011.
The mission/transects are as marked and the data has undergone only initial data processing.

Here it can be seen that there is an excellent agreement in the features seen in glider and ships sections that span 4 days of sampling. For example in the location and extent of the warmer fresher water mass in the east of the channel and in the general slope of isopycnals in the west signifying the south flowing NC, fig. D3. More detail is visible in the glider data, for example in variability in the AW to LIW interface (~38.1 isohaline), some perturbation is visible in the ship section but not as much. In the ship section we see the surface inflows more clearly, as the ship transect extends further to the east and thus captures more of the more of the Ibiza hugging AW inflows.

In θ/S a coherent evolution can be seen between glider and ship transects fig. D2, in T6 (glider) WIW is present with one main minima of salinity 38.0 and two additional small minima at 38.1 and 38.2, in T1 (ship) a day later, the minima at 38.1 has strengthened, and in T7 this 38.1 minima now extends from 12.7 °C/38.1 to 12.4 °C/38.0 and the second minima at 38.2 has also increased.

In geostrophic velocity a broad NC is visible in all sections, there is good agreement between the two glider sections T6 and T7 and in the transport values across the 3 sections, which show a coherent increase from -0.49 Sv (T6) to -0.57 Sv (T1) to -0.64 Sv (T7), as the volume of WIW progressively increases in the channel. The glider sections however indicate that the NC has a stream like structure, not visible in the ship section, which shows a more concentrated current. The pattern in the inflows is similar, a small consistent decrease occurs in the transport from +0.28 Sv (T6) to +0.24 Sv (T1) to +0.23 Sv (T7). On closer inspection the pattern visible in θ for T1 and T7 is in particularly good agreement, with more mesoscale perturbations visible in the glider section.

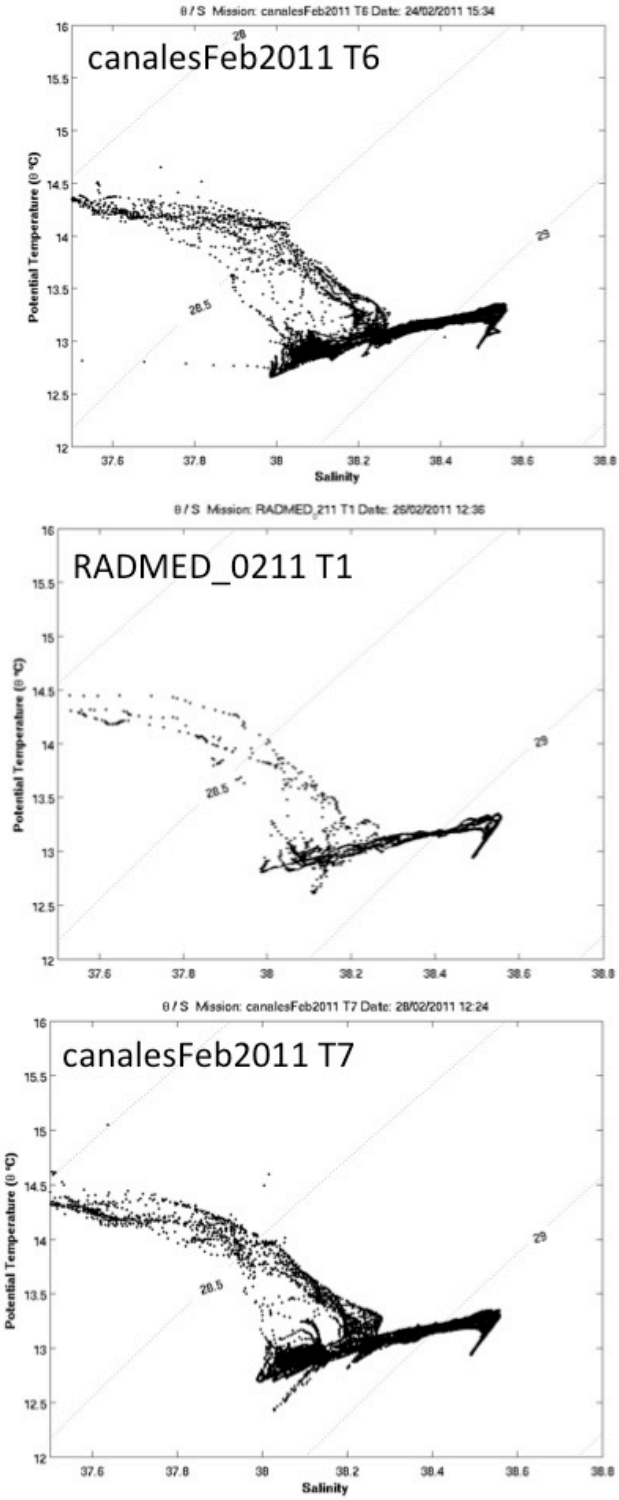

Figure D2. θ/S plots for 3 glider/ship transects in Feb 2011.
The mission/transects are as marked and the data has undergone only initial data processing.

It could be argued some of the additional detail seen in the glider data is due to the slower speed of the glider through the water causing a smearing of signals from dynamic processes and a sampling alias on depth dependent surfaces such as density and geostrophic velocity (Rudnick and Cole 2012). However the good agreement between consecutive glider

sections, T6 and T7, and generally good agreement across all transects and in the water mass volume transport, suggest that variability seen for example in the NC is real.

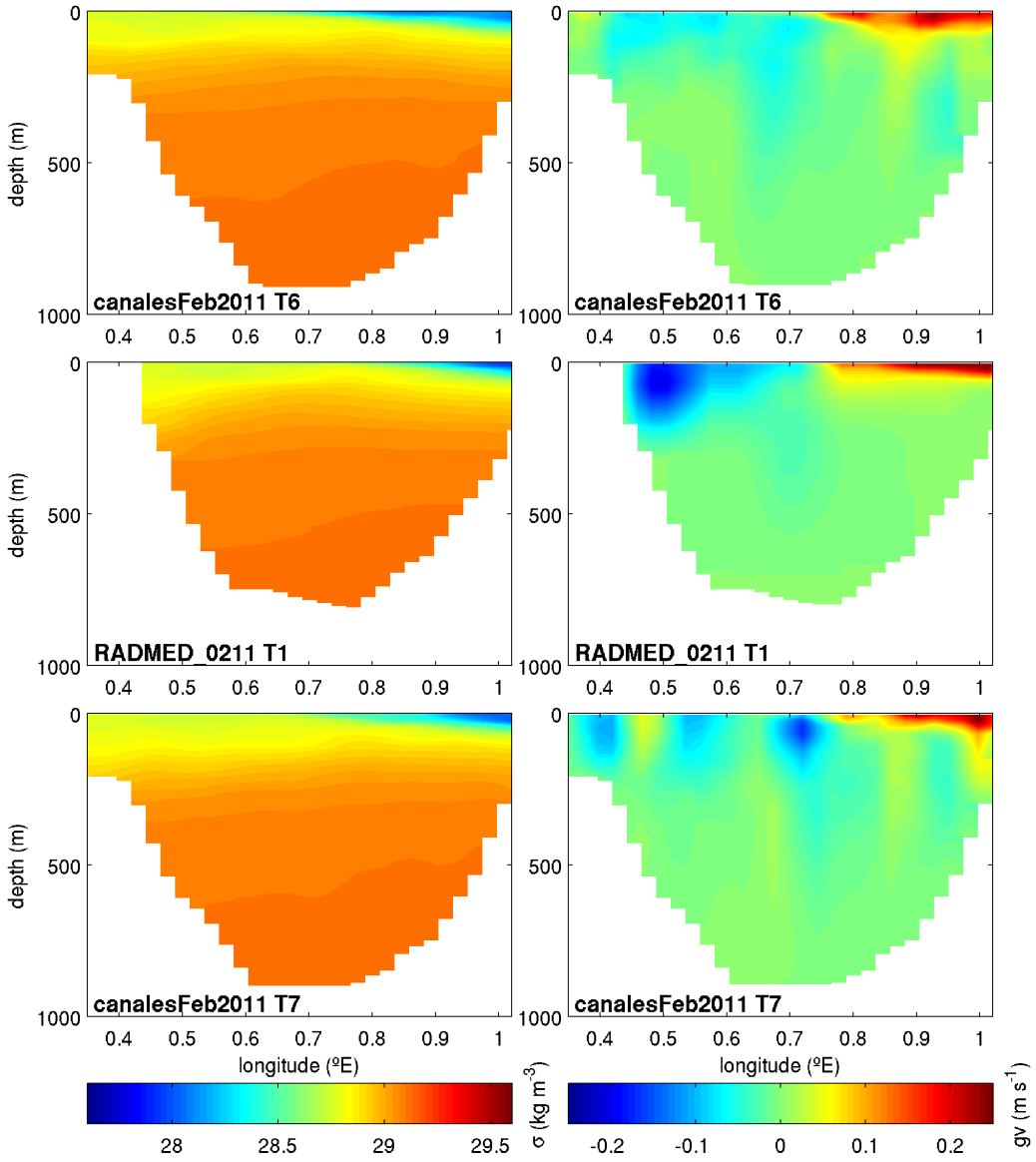

Figure D3. Density and geostrophic velocity for 3 glider/ship transects in Feb 2011.
The missions and transects are as marked, velocities northwards are positive and southwards are negative.

September 2013

In September 2013 the comparison between the potential temperature and salinity sections is again very good, see fig. D4. For example a lower salinity lens is visible in both glider and ships sections at 0.65 °E and 200 m depth. In the west of the channel filaments of higher salinity waters are clearly visible in the glider salinity section T3, fig. D4 a filament is also

visible in ship salinity section T1, at the same location but at a lower resolution and not providing such a strong indication as to the source and structure of the filaments.

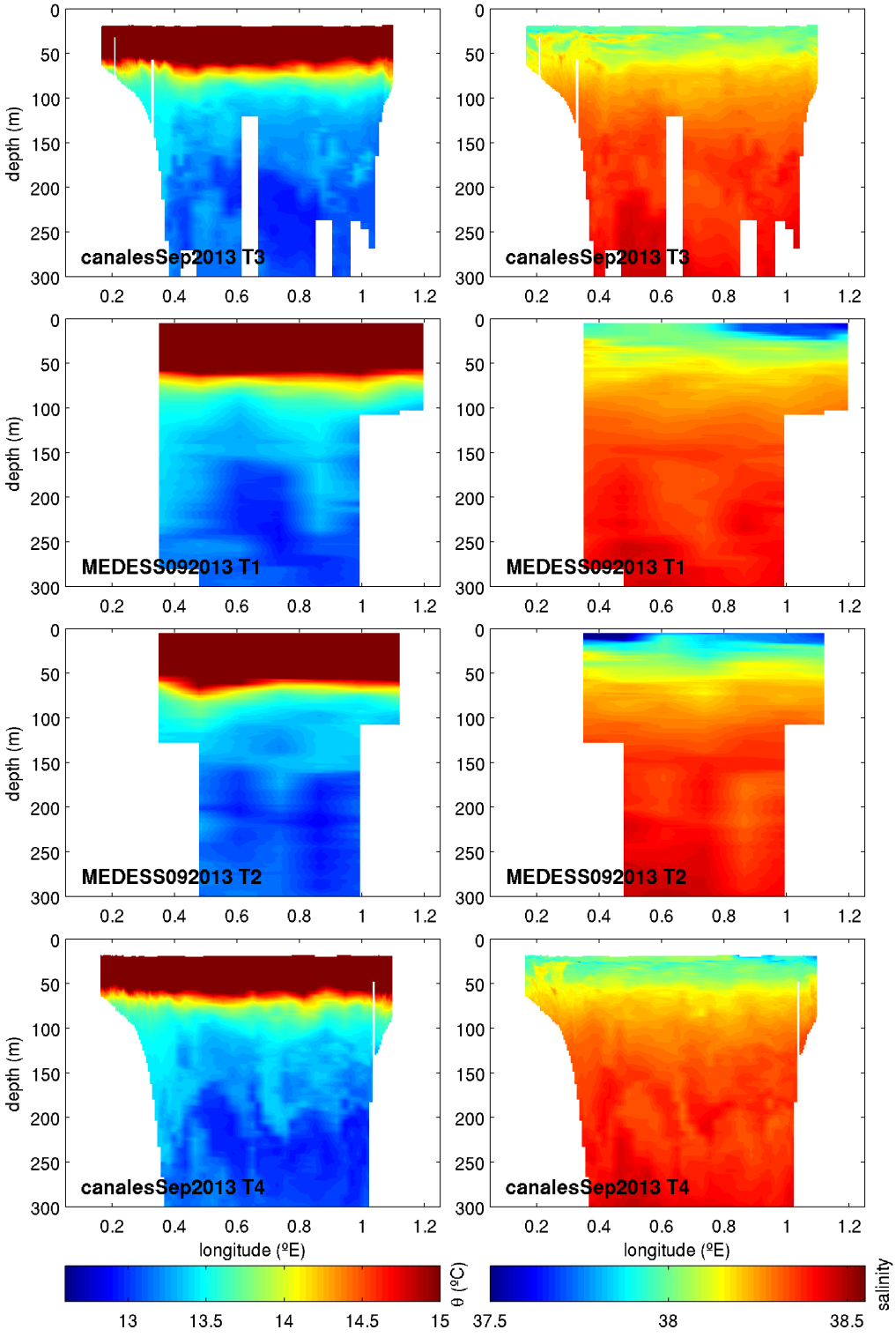

Figure D4. θ and S sections to 300 m for 4 glider/ship transects in Sep 2013.

The mission/transects are as marked and the data has undergone only initial data processing.

The pattern of geostrophic velocity between ship and glider data is again similar, see fig. D5, at the start of the glider mission in geostrophic velocity section T3 (glider) and T1 and T2 (ship), indicate outflows at the far west and east of the IC (0.45 and 0.95°E) with general weak inflows across the centre.

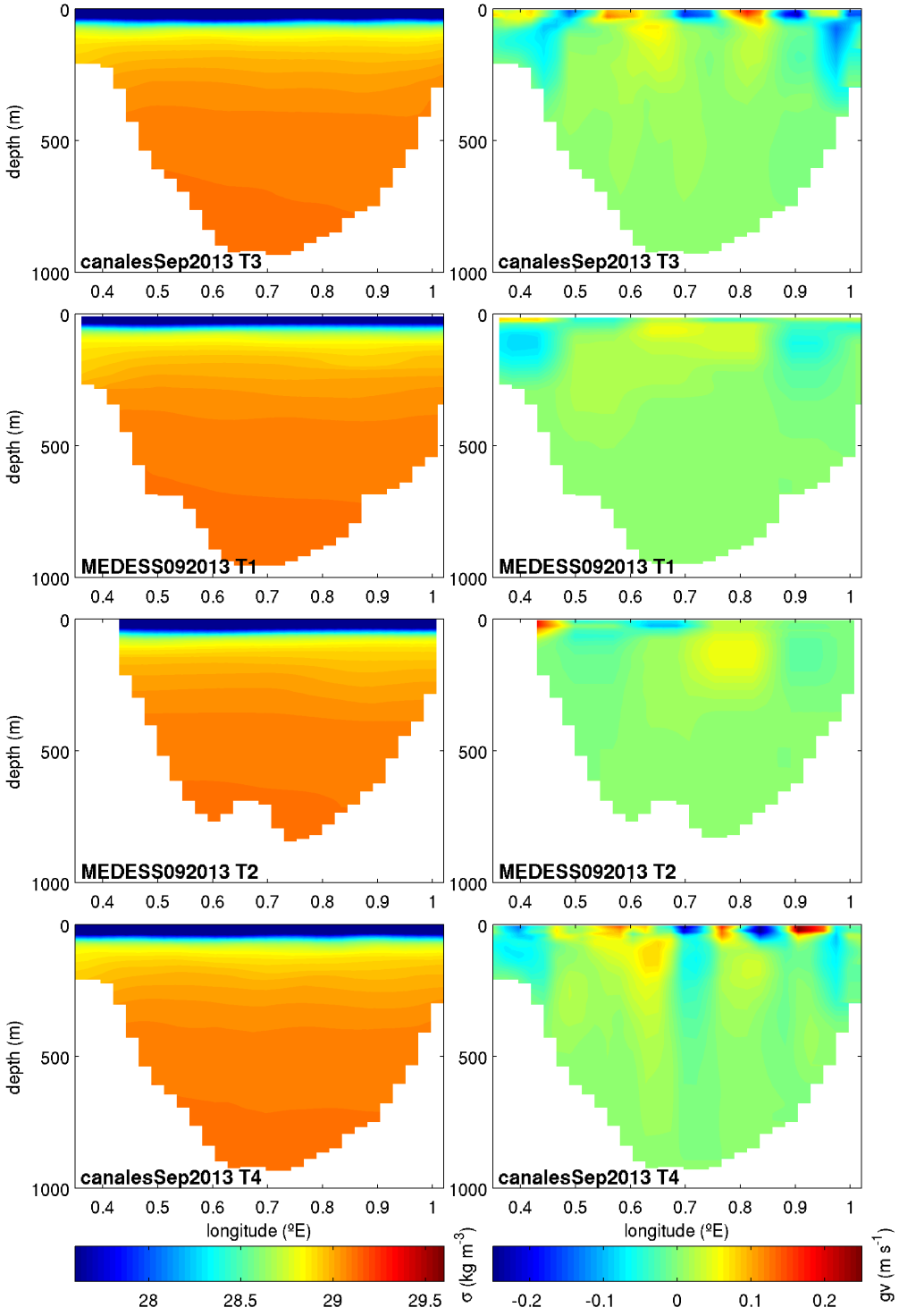

Figure D5. Density and geostrophic velocity for 4 glider/ship transects in Sep 2013.
The missions and transects are as marked, velocities northwards are positive and southwards are negative.

The glider data however shows more mesoscale variability in the pattern across the central section, which in T4 develops into a paired velocity structure, centred at 0.65°E. In T3 (ship) the coarser (10 km) resolution of the sampling does not enable this smaller structure to be seen, although it is possible that the structure was not yet visible, as the transects are a day apart. Later, after the end of the ship mission (24 to 27 September), a cold WIW core eddy appears in the channel, see canalesSep2013 mission description in Chapter 3, in the glider transects T5 and T6.

The resolution in both time and space of the glider sampling allow the dominant features in the IC to be more clearly identified. It also seems likely that the additional detail in the pattern of the mesoscale geostrophic velocities in the glider data leads to a higher estimation of geostrophic transport (see table D1).

December 2013

There is broad agreement in the structure seen in the glider and ship sections of potential temperature (θ), salinity and density (σ) see fig. D6, with a central uplift in the isotherms visible in both transects. Some of the smaller scale structures are also visible in both datasets, for example at 0.4°E a small dip in the halocline between 100 – 200 m. However important detail is evident in the glider data that is not visible in the ship section, for example the isopycnals in the west of the channel uplift at the channel edge and the thermocline is 'stepped' from west to east, a pattern which is related to the structure of the thermocline, see the mission description for canalaesDec2013 in Chapter 3 for more details. An important difference in the depth of the thermocline between east and west is also visible in the glider transect, but not obvious in the ships transect. A glider test section (T100), sub-sampling T2 to the same profile density as the ship CTD station data, i.e. 9 profiles across the IC, with 6 in the deep central channel section, does not well represent this 'stepped' thermocline. Between T2 and T1, 1 day, there appears to be a shift in the central domed structure from 0.8 to 0.7°E, notwithstanding the similarity in detail between the ship and subsampled test T100 glider section is striking, a clear indicator of the additional detail that sampling with gliders provides.

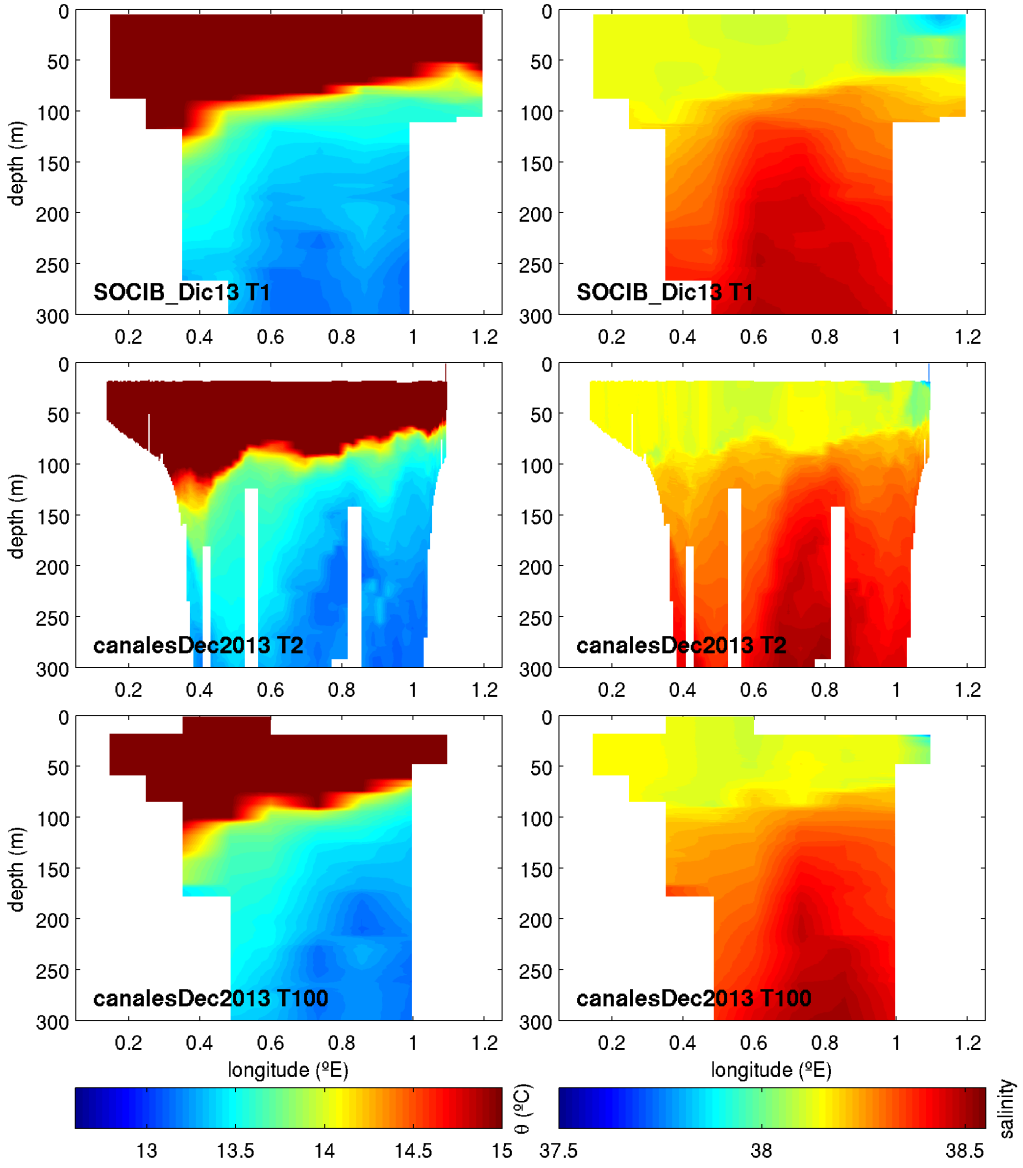

Figure D6. θ and S sections to 300 m for 2 glider/ship transects in Dec 2013.

The mission/transects are as marked and the data has undergone only initial data processing. The section canalesDec2013 T100 is the canalesDec2013 T2 section sub-sampled to the resolution of the SOCIB_Dic13 T1 section.

In the geostrophic velocity section for T2 (glider) we see some pairing of the north and south velocities around the domed isopycnals (fig. D7). The NC is visible as a broad southward current with core geostrophic velocities of order 40 cm s^{-1}. In the east at 0.9°E inflows occur, penetrating to similar depths as the southward flows (~300 m). The central doming centred at 0.8°E and paired velocity, suggest a cyclonic structure. However there is no sense of a weakening of the stratification in salinity, as seen with other such structures, or an impact on other features, such as the depth of thermocline. This more likely

indicates that the southward current is an NC flow, with simultaneous fresher inflows in the east of the channel, these currents likely taking advantage of, or being modulated by, a residual sub-surface structure (see the mission description for canalaesDec2013 in Chapter 3 for more details).

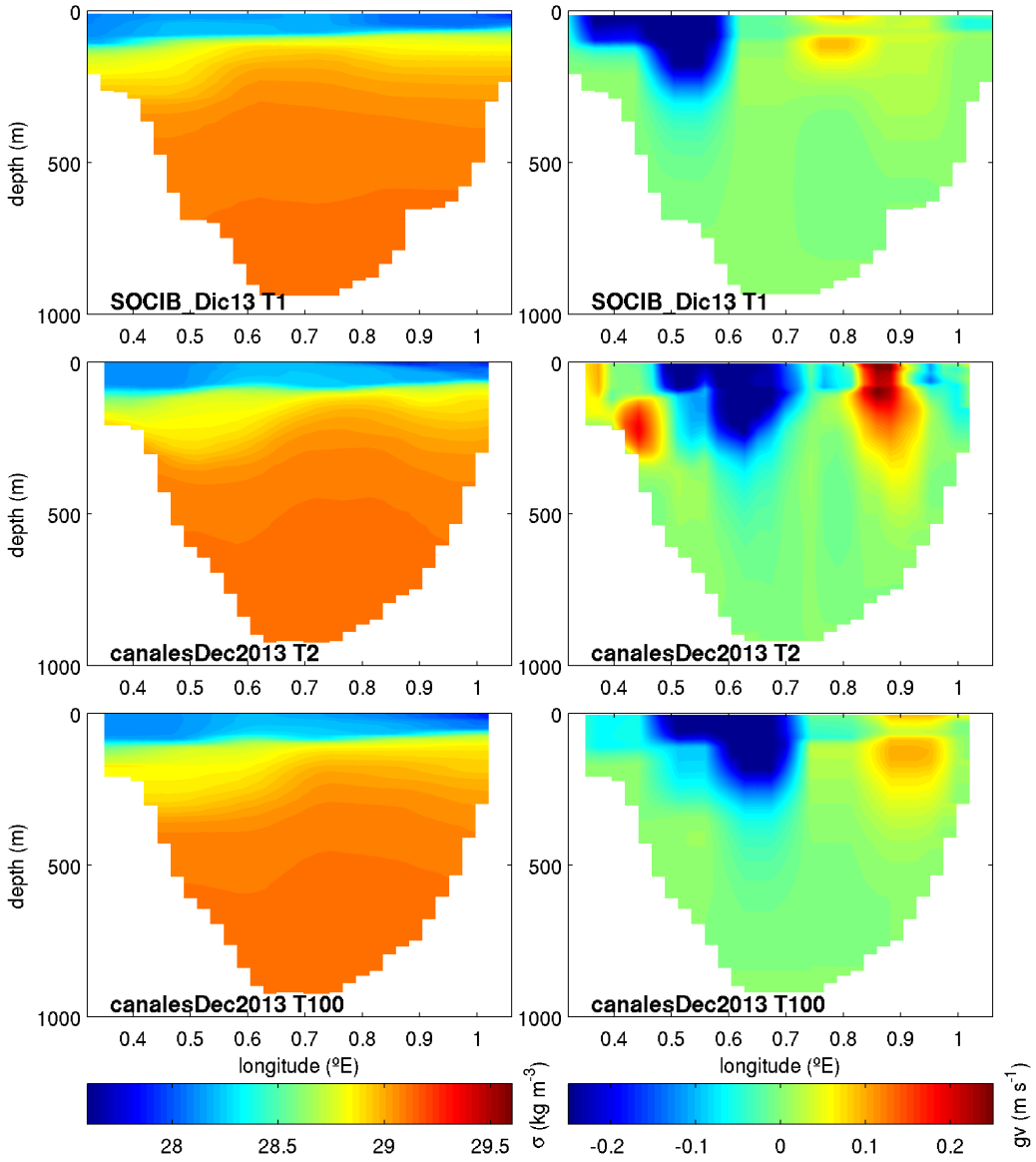

Figure D7. Density geostrophic velocity for 2 glider/ship transects in Dec 2013.
The missions and transects are as marked, velocities northwards are positive and southwards are negative. Note: the section canalesDec2013 T100 is the canalesDec2013 T2 section sub-sampled to the resolution of the SOCIB_Dic13 T1 section.

In the T1 (02/12/2014 15:36 to 21:33) geostrophic velocity section the NC is visible, with a similar shape to the later glider transect T2 (03/12/2013 21:26 to 06/12/2013 09:57),

however there is no representation of the inshore counter current visible as in the glider section. This counter current could have formed as the central doming shifted eastward, however it is also absent in the sub-sampled glider section (T100). In T1 the eastern current appears as a more as a broad inflow of order 5 cm s^{-1} from 0.7°E to the channel edge, with a small subsurface current of 10 cm s^{-1} at ~0.8°E (~100 to 150 m) and similarly in the subsampled section there is a core current with similar velocities located further east at ~0.9°E. In both glider and ship sections there is a clear disconnect between surface velocities and those occurring below the thermocline, e.g. σ ~28.4 kg m-3. As the central upward doming of the isopycnals moves eastward between transects T1 and T2 some of the change in the pattern of flows may be due to this shift, however the striking similarity between the velocity field in T1 and the subsampled T2 section (T100), strongly suggests that the some of the differences are at least in part due to lower resolution sampling. This is also reflected in the transport, where the northward flows are reduced in the subsampled T100 section, as compared to T2 see table D1.

In December 2013 we are also able to compare the glider transects with ADCP data from the B/O SOCIB and fig. D8 shows sections of geostrophic velocity for T2 (03/12/2013 14:00 - 07/12/2013 07:52), with glider travelling east to west, and an overnight VM-ADCP velocity section (02/12/2013 19:00 - 03/12/2013 03:00), with the vessel travelling west to east, are shown. Although the sections are separated by hours to days (the separation time lengthening as glider continues to navigate across the channel after the ADCP section is complete) the match in the pattern and magnitude of velocities is very close.

In both the NC is visible, penetrating to the same depths, with a similar shape and almost exactly the same range of velocities. The VM-ADCP transect also shows a hint of the subsurface counter current at the western channel edge (0.4 to 0.45°E, 150 to 300 m depth) and the on-shelf current, inshore of the NC. In the east of the channel the inflow current is again clearly visible in both sections, penetrating to the same depths and with the same velocities. To either side of this current, in the surface 0 to 80 m above the σ 28.4 kg m^{-3} isopycnal, negative (southward) flow is visible in both sections, possibly stronger in the ADCP section. The main visible difference is that the glider derived inflow current appears to be more strongly linked to the surface, whereas in the ADCP data there is slightly less connection, however the connection is still there. In addition inflows are visible on the

Ibiza shelf area that are not captured by the shorter glider transect and geostrophic velocity calculation.

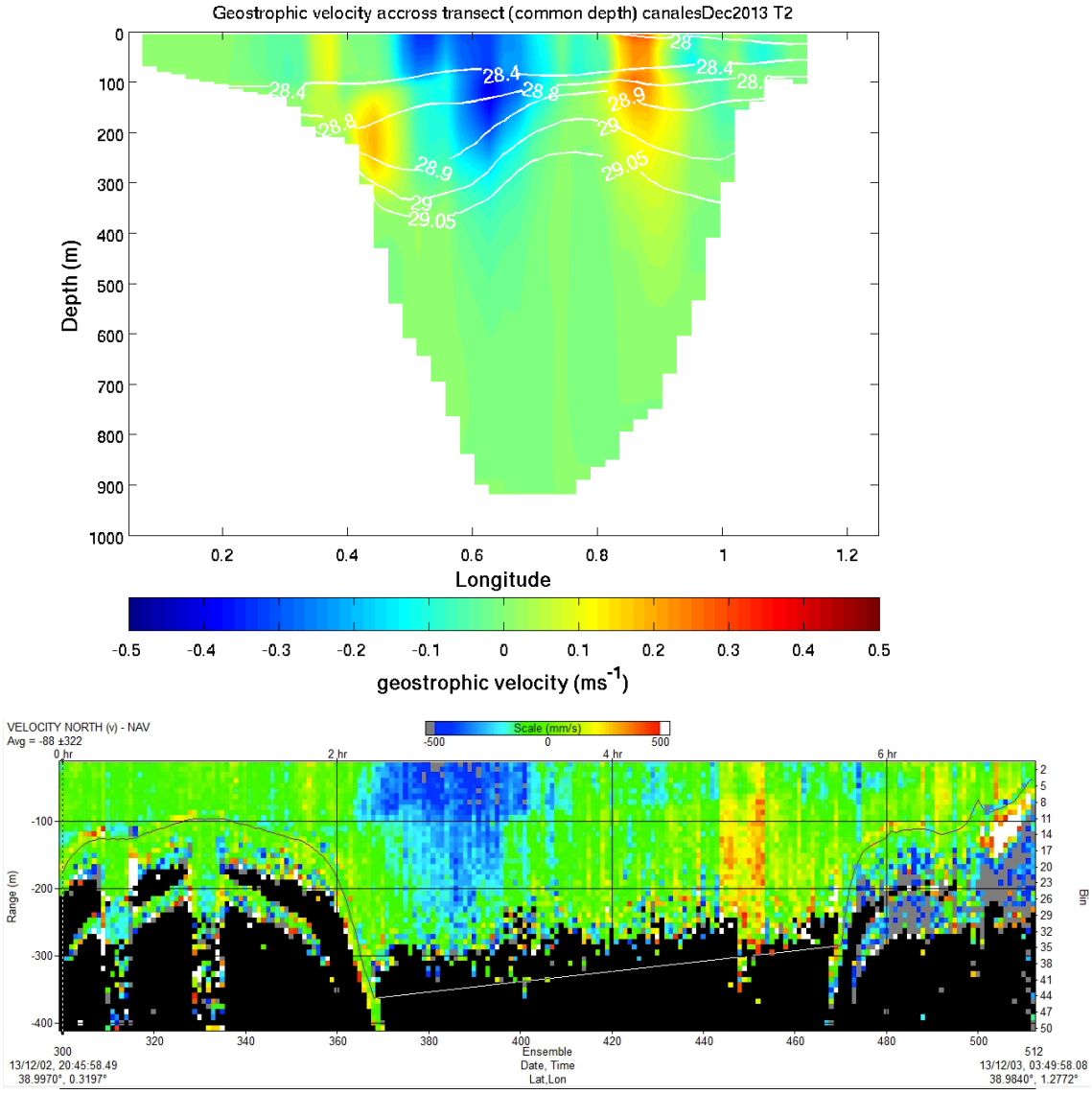

Figure D8. Comparing glider geostrophic velocity to total velocity from VM-ADCP.
Geostrophic velocity from glider transect canalesDec2013 T2 (upper panel) and total velocity from the VM-ADCP overnight section (lower panel), the 2 minute bin ensembles. T2 (03/12/2013 14:00 - 07/12/2013 07:52) and ADCP (02/12/2013 19:00 - 03/12/2013). Note the velocity scales are the same, however the ADCP section is on a time scale and the glider on a latitude scale, velocities southward are negative and northward are positive.

Fig. D9 shows the geostrophic velocity section for the ship transect SOCIB_Dic2013 T1 (02/12/2013 12:34 to 02/12/2013 21:47) and velocity from the VM-ADCP day-time transect (02/12/2013 12:30 to 03/12/2013 19:00) are shown, although the two sections are

similar, the shape of the NC is not captured as accurately in the ship derived geostrophic velocity however the magnitude of the velocities is again a good match.

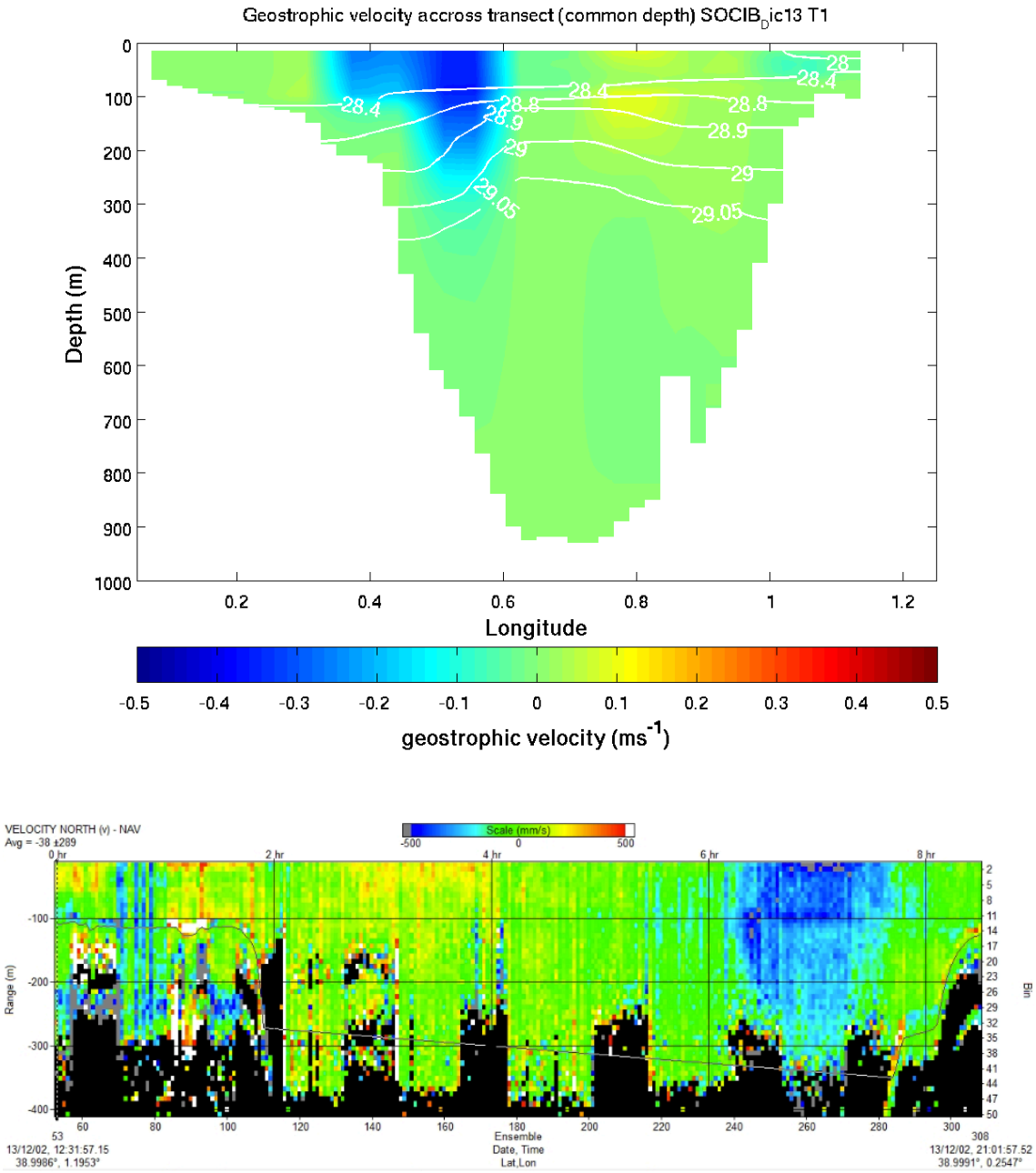

Figure D9. Comparing ship geostrophic velocity to total velocity from VM-ADCP.
Geostrophic velocity from ship transect SOCIB_Dic2013 T1 (upper panel) and total velocity from VM-ADCP day section (lower panel), 2 minute bin ensembles. T1 (02/12/2013 12:34 to 02/12/2013 21:47) and ADCP (02/12/2013 12:34 to 02/12/2013 21:47). Note the velocity scales are the same, however the ADCP section is on a time scale and the glider on a latitude scale, velocities southward are negative and northward are positive.

The subsurface counter current at the western channel edge is visible in the VM_ADCP section (0.4 to 0.45°E, and 150 to 300 m depth) but has little expression in the ships geostrophic velocity. The broad inflow current is of a similar dimensions in the horizontal, however the ADCP data suggests stronger velocities in the surface 0 to 100 m with velocities 15 cm s^{-1}, and the ship section a subsurface maxima with geostrophic velocities 10 cm s^{-1}. Having said that a small flow reversal, on-shelf in the east, seems to be captured in both sections, albeit stronger in the VM-ADCP.

Overall the match is good between the ship CTD geostrophic velocity section and the VM-ADCP section, although not as close as that between the glider and VM-ADCP. The velocities in the main feature, the NC, are similar however other features have weaker velocities in the ships CTD and the representation of the shape of the features is not as closely matched as in the glider section. It is interesting to note that the changes seen in the glider vs. the ships CTD sections are also captured in the VM-ADCP section, e.g. the development of a more intense inflow current at 0.7°E.

Summary of comparison:

Comparing sections of temperature, salinity, density and geostrophic velocity, finds remarkable agreement between the glider and ships transects for the larger scale features and a coherent evolution between transects, separated by days. However the more sparse ship CTD stations do not capture the mesoscale and submesoscale features as well as the gliders, which impacts the interpretation of features and transport values. It could be argued some of the additional detail in the glider sections is due to a combination of sampling alias and the smearing or mixing of variability due to the slower speed of the glider (see Appendix E), however several factors point towards a significant part of this additional detail being real:

- The consistency and good agreement in mesoscale and submesoscale details between consecutive glider transects e.g. T6 and T7 in February 2011
- The very good agreement on location of smaller features observed by both ship and glider but at different resolutions, e.g. filaments of salinity in September 2013
- Sampling on the shelf area is more dense, 300 m between profiles, and yet shows a similar scale of variability in for example isopycnal or isohaline perturbations
- Consecutive ship and glider sections show a coherent evolution

There will always be some element of error that cannot be quantified or removed from the glider data, and this however should always be borne in mind. But for the circulation features under study in the IC and MC the gliders speed through the water and time to complete a transect does not appear to cause a misrepresentation of the circulation features and evolution of those features that is greater than that of the traditional ships survey. In addition the glider sampling adds significant detail to the picture, both in the spatial (horizontal) scale and in the temporal scale with consecutive sampling of transects. The 'burst' sampling of the IC enables the evolution of features to be observed over periods of ~20 day, which aids considerably in identifying the key dynamic features and structures within the IC. The higher spatial resolution provides a higher and likely more accurate estimate of the geostrophic transport in the channels, particularly when there is higher mesoscale activity.

In summary, although the broad picture is similar the detail 'seen' by the higher resolution glider sampling provides insight into mesoscale to sub-mesoscale dynamics and brings the complex dynamics to life. The smoothing effect of the lower sampling can lead to a reduction in the strength of the calculated geostrophic velocities and thus the transports, depending on the scale of the features present.

The exceptionally close match between the glider estimated geostrophic velocity field and the VM-ADCP 2 minute ensemble velocity fields strongly suggests that the assumption that the main flow patterns in the IC can be reasonably described with the geostrophic assumption over timescales of days is valid and for this time period that ageostrophic terms are not significant. It also confirms that the horizontal resolution of the glider data is sufficient to resolve the main features in the channel dynamics, we are not missing features in the surface 300 m with the geostrophic assumption and that even in the surface, above the seasonal thermocline the geostrophic methods are providing valid estimates of the surface mesoscale currents. Therefore the method of calculation of the geostrophic velocity provides a good estimate of the velocity field and by extension the associated transports

This good agreement between glider and ships CTD sections have indicated that the ship and glider sections can safely be compared and combined for analysis, however with the caveat that the transports for the ships CTD sections will, on average, be less than those

from the glider sections, especially for smaller scale features (< 20 km). In addition the transect location 15 km to the south does not appear to make any difference to the transports, a quick check indicated that the difference between mapping the ship transect to the glider standard line is of order 2% in terms of volume of transport and so the ship CTD profiles were mapped and interpolated along the ship transects to avoid any unnecessary distortion.

Appendix E: Synopticity in glider data

Scientific Report – Synchronicity in glider data transects

Reference: ECOST-STSM-ES0904-140312-016227

STSM dates: from 14-03-2012 to 18-04-2012

STSM Applicant: Emma Heslop, IMEDEA (CSIC-UIB), Esporles, Spain.

STSM Host: Dr. John Allen, NOCS, Southampton, UK.

1.0 Background

1.1 Purpose (STMS proposal submitted in Feb 2012)

Glider datasets offer unparalleled resolution (temporal and spatial) however the speed of the glider through the water means that glider transects are frequently collected over a period of days to weeks. An important part of this work will be to assess the impact of synchronicity on the resolution of glider data and the dynamic structures studied. The glider data studied will be a 6 month time series of semi-continuous glider operations along a transect crossing the Ibiza Channel in the Western Mediterranean Sea. This data, collected in 2011 by SOCIB/IMEDEA, has already shown interesting high frequency variability in the geostrophic transports of water masses and the affects of the assumption of synchronicity in the transects (of 2 - 3 days duration) will be analysed using wave spectra analysis, EOF and correlation scale studies. The results can additionally be compared with data from several contemporaneous ships CTD surveys (IEO data). The broad aim of the study is to increase our understanding of the effect of synchronicity in glider data on the observed dynamic structures, and the development of tools and strategies for glider data analysis and experiment design.

1.2 Dataset

Six semi-continuous glider missions were undertaken in the Ibiza and Mallorca Channels, between January and July 2011, using a G1 Slocum Deep Electric Glider (Teledyne Webb Research). Three to six transects of the Ibiza Channel were completed each mission, each transect took on average 3 days to complete, 2 days for the deep section of the channel (off the continental shelf with depths ≥ 200 m). The glider performed a sea-saw pattern through the water column between depths of 20 m and 950 m, whilst navigating a standard transect at 39°N, approximately perpendicular to the main currents and between two surface waypoints at 38.99°N, 0.13°E and 38.98°N, 1.10°E. The glider successfully

performed 23 complete transects of the Ibiza Channel, with an average distance from the transect line of approximately 3 km, occasionally being swept further off track by stronger currents (Table E1). The average distance between the CTD profiles is approximately 2 km in the 'deep' channel (300 m on shelf) and the temporal resolution of the dataset is days-weeks as compared to the seasonal sampling of previous ship-based missions (Pinot et al., 2002; Pinot and Ganachaud, 1999). The CTD data from the glider is used in the following analysis; processed using standard oceanographic techniques adapted to glider data.

Mission	Start	End	Mission length (days)	Ibiza Channel transects	Ibiza Channel CTD profiles
canalesJan2011	01/12/11	02/03/11	22.12	6	212
canalesFeb2011	02/10/11	03/03/11	21.20	6	163
canalesMar2011	03/18/11	04/09/11	22.18	5	149
canalesMay2011	05/03/11	05/20/11	17.26	3	169
canalesJun2011	06/02/11	06/16/11	13.61	3	89
Average			19.27	5	156
Total			96.37	23	782

Table E1. Ibiza Channel 'canales' glider missions in 2011.

1.3 Ibiza Channel Dynamics

The Ibiza Channel governs an important and complex inter-basin exchange of water masses, on the western side of the Ibiza Channel the thermohaline driven Northern Current (NC) flows south carrying volumes of more saline surface waters (0 – 400 m) out of the Balearic Basin, while on the eastern side of the channel inflows of fresher surface water masses of more recent Atlantic origin flow north into the basin to form the Balearic Current (BC). Previous studies have identified seasonal and mesoscale induced variability in theses flows (Pinot et al., 2002).

2.0 Research Design

This work was in part triggered by a recent study (Rudnick et al., 2011) which used glider data, in combination with contemporaneous Seasoar data and wave spectra analysis, to conclude that isobaric structures of wavelengths less than 30 km could not be well resolved in the glider data due to the aliasing and smearing of signals. Structures on isopycnal surfaces were not affected by the smearing of signals from internal waves. This is an interesting result for our dataset, as we analyse geostrophic transports across the glider

transect of the Ibiza Channel based on geostrophic velocity profiles, a depth dependant variable. Plus the dynamic structures we observe, NC, BC inflows and eddies, are of the order of 30 km. The geostrophic transports show high frequency variability, however is an element of this therefore the result of aliasing and smearing of signals in the glider data?

With some ideas in mind a meeting was proposed to gain input from scientists working at NOCS with experience across several areas of oceanography to identify possible techniques to apply to the dataset. The meeting was held at NOCS on 21/03/201, present were Prof. Harry Bryden, Dr John Allen, Dr Adrian Martin, Dr Stephanie Henson and Peter Challenor. The discussion suggested 3 clear areas for investigation:

1. Similarity in rapid repeat ends of transects. The principal being that one might expect greater coherence of structures at the end of the Ibiza Channel transect which is rapidly repeated in time. The glider passes from E to W and then from W to E across the channel and so at one end the data is separated by hours and on the other end 4 - 6 days (the length of time to complete two transects). Patterns of ΔT, ΔS and $\Delta\rho$ were looked at on isobars and ΔT on and isopycnals between consecutive transects.
2. Coherence of structures along density surfaces. An investigation of potential temperature and salinity on density surfaces looked at the coherence of water masses on selected density surfaces.
3. INLA statistical model. Peter Challenor, an expert in environmental statistics, suggested using the INLA statistical model, a new hierarchical spatio-temporal model involving a Gaussian Field affected by a measurement error and a state process characterised by first order auto regressive dynamics and spatially correlated innovations (Håvard Rue et al., 2009, Michela Cameletti et al., submitted). Peter thought that this could work well for the analysis of a continuous series of glider data.

1.0 Analysis to date

3.1 Similarity in rapid repeat ends of transects.

Potential temperature (θ), salinity (S) and density profiles were interpolated (kriging) to 1 km in horizontal 1 m in the vertical and then the difference in T, S and Δ (ΔT, ΔS and $\Delta\rho$) between transects calculated. The results, ΔT, ΔS and $\Delta\rho$ per transect pair, were analysed

for patterns of similarity between the transect ends (E and W) that were rapidly repeated, see Table E2 isobar columns. The totals for 'yes' and 'no' show a similar number of instances, indicating that for approximately 50% of the time a smaller change in ΔT, ΔS and Δρ is discernable at the end of the transect that was sampled closer in time, however that otherwise a comparable amount of change occurred on both sides of the Ibiza Channel transect or occasionally the reverse pattern was apparent. The pattern at a finer scale of change was also investigated ($\Delta T < 0.2$ and $\Delta S < 0.05$), which produced the same results.

This suggests that, for the Ibiza Channel, the amount of change between transects is not consistently biased by the glider sampling, with changes perhaps dependant on the dynamics occurring at the time of sampling of consecutive transects.

Rapid repeat side indicates less change in properties?		**Isobars**			**Isopychnals**		
Mission	**Transect pair**	**ΔT**	**ΔS**	**Δρ**	**ΔT**	**Rapid repeat side**	**Notes**
canalesJan2011	T1_2	marginal	marginal	yes	no	W	
	T2_3	yes	yes	yes	yes	E	
	T3_4	no	marginal	marginal	no	W	
	T4_5	yes	yes	yes	no	E	
	T5_6	no	no	no	no	W	short transect less information in E
canalesFeb2011	T3_4	yes	yes	yes	no	W	
	T4_5	marginal	no	yes	yes	E	
	T5_6	marginal	no	no	yes	W	
	T6_7	no	yes	no	no	E	
	T7_8	yes	yes	yes	yes	W	short transect less information in E
canalesMar2011	T3_4	marginal	yes	yes	yes	W	
	T4_5	no	no	no	no	E	
	T5_6	no	no	no	no	W	
	T6_7	yes	yes	marginal	no	E	
canalesMay2011	T6_7	marginal	no	no	no	W	short transect less information in E
canalesJun2011	T4_5	yes	yes	yes	yes	W	
	T5_6	no	marginal	no	no	E	
Total							
yes		**6**	**8**	**8**	**5**		
marginal		**5**	**3**	**2**			
no		**6**	**6**	**7**	**12**		

Table E2. Change in properties between consecutive glider transects.

The results of looking at ΔT (difference in potential temperature) on isopycnals, representing conservative surfaces not affected by internal waves, are interesting. The plots indicate in January and February that there could be a narrow margin of more synchronous data (less ΔT) between fast repeat ends of the transects (Fig. E1). They also indicate, what we have previously seen in the geostrophic velocities, that for the Jan, Feb and Mar missions the cross transect patterns have some similarity within the mission but are different for each mission (Fig E1 and Fig. E2). For example in January (Fig. E1) the areas of higher change in ΔT are dominated by the NC, in February (Fig. E2) stronger changes occur in the E, and in March (Fig. E2) the pattern of change is within deep vertical

structures across the transect (eddies). The data in May and June are not sufficient to define a pattern. The narrow margin when it occurs represents in time 1 - 1.5 days and in the W of the channel is mainly on the continental shelf.

This suggests there could be a period of synchronicity of order 1 - 1.5 days and that the presence of the margin and the size of the margin is dependant on the dynamics in the channel.

3.2 Coherence of structures along density surfaces.

Potential temperature and salinity were plotted on density surfaces rather than on the more usual isobars to look at coherence and consistency of structure. Specifically the location of WIW through time on specific isopycnals was investigated to see if there was a discernable coherence of structure associated with its appearance and evolution.

The plots of potential temperature and salinity on density surfaces indicate coherence with the picture seen in the geostrophic transports. For example in the canalesFeb2011 mission the intrusion of less dense and less saline water of more recent Atlantic origin appears the E of the channel (0.9 – 1.1°E) with a clear density distribution of Δt 28.5 - 28.75 not seen in the W, see Fig. 3. This intrusion appears in T4, 5 and 6 of the canalesJan2011 mission (not shown) and in June (not shown) as a strong salinity difference in the E of the channel (W ½ channel S 38.1 vs. E ½ the channel S 37.4), all of which is coincident with the pattern of the transports by water mass (Fig. E3 upper panel) derived from isobaric surfaces.

Plots of the location of WIW through time on density surfaces were also investigated, Fig. 4, WIW appears in late January/early February and is concentrated in the W of the channel, however by the end of February it can be seen across all the transect. In May the WIW Δt 29.2 is located on the shelf, which why we do not see it in the off-shelf deep channel transports. The plots do not indicate the temporal evolution of the eddy structures associated with WIW seen in plots of geostrophic velocity (not shown), however interestingly the signature of the WIW appears to increase in density over time.

3.3. INLA statistical model

r-INLA is a new toolkit for statistical analysis of environmental variables (Michela Cameletti et al., submitted) that Peter Challenor has successfully used for the analysis of sea level trends across the Mediterranean. INLA involves a Gaussian Field affected by a measurement error and a state process characterised by first order autoregressive dynamics and spatially correlated innovations. An effective estimation and spatial prediction strategy for the mode is developed through a SPDE (Stochastic Partial Differential Equations) approach and adopting an INLA (Integrated Nested Laplace Approximation) algorithm as a computationally efficient alternative. Results from analysis of the glider data should provide an indication of the correlation of the data in time and space, plus a model that could be used to predict and compare with the real data.

The INLA package was downloaded from www.r-inla.org, however getting r-INLA operational involved several initial challenges; including learning R, upgrading Mac OS X to 10.6.8 (Snow Leopard), and manipulating the densely sampled glider data into a suitable format for the model analysis. For the initial experiments vertical profiles of potential temperature were mapped to the Ibiza Channel transect line with an interpolated distance of 1 km in the horizontal and averaged to 10 m bins in the vertical and the time series was grouped into time steps of 6 h and 12 h.

Currently the program is running successfully for very small amounts of data, however to date we have not been able to compute a model for the whole dataset, despite increasing the computing power to 200 GB RAM. We are currently working on resolving how best to successfully run the r-INLA package for the whole glider dataset.

4.0 Summary

Thus far the results support the picture that high variability in transports, on 'weather' timescales (days), in the Ibiza Channel region is primarily due to the dynamics in the channel rather than aliasing or smearing of internal waves. There is good coherency between the picture presented by the transports (calculated from isobaric properties) and properties on the isopycnal surfaces, supporting the view that structures below 30 km wavelength can be resolved. From this analysis we cannot yet quantify with certainly the temporal or spatial scale of synchronicity within glider dataset, however glider sampling does not appear to be introducing a systematic bias across transects. From the difference

in potential temperature between consecutive transects interpolated to isopycnal surfaces a tentative timescale for synchronicity in the glider data of order of 1 – 1.5 days could be proposed, however this appears to be dependant on the type/frequency of the Ibiza Channel dynamics, perhaps results from the INLA statistical model may be able to resolve this further.

4.1 Next Steps

Work will continue between IMEDEA and NOCS to use the INLA model for the glider data. In addition, although the Rudnick et al. 2011 study used glider transects of length 500 – 1000 km (north of Hawaii between 22.8 an 34.5°N) to gain an inflection point for the wave spectra analysis between 30 – 50 km, in the Mediterranean (with a Rossby radius of order of 15 km) we may be able to determine a significant result from our transects of 80 km, therefore a wave spectra analysis will also be undertaken as part of the on going work.

5.0 Host Report from Dr. John Allen, NOCS

I can confirm that your work here on the STSM project, "Synchronicity in glider data" was completed successfully. As all good research projects should, this project has established some new ideas and it will form the baseline for further work, perhaps most specifically bringing a Bayesian statistical approach, using integrated nested Laplace approximations, to model the complex temporal and spatial data collection achieved by gliders. This I am sure will lead to a more complete and rigorous interpretation of this new method of data gathering.

6.0 References:

Håvard Rue, Sara Martino and Nicolas Chopin, Approximate Bayesian inference for latent Gaussian models by using integrated nested Laplace approximations. J. R. Statist. Soc. B

Michela Cameletti, Finn Lindgren, Daniel Simpson and Håvard Rue. Spatio-temporal modeling of particulate matter concentration through the SPDE approach. Submitted AStA Adv Stat Anal 2012

Rudnick, D.L. & Cole, S.T. (2011). On sampling the ocean using underwater gliders. J. Geophys. Res., Vol. 116, C08010.

7.0 Figures:

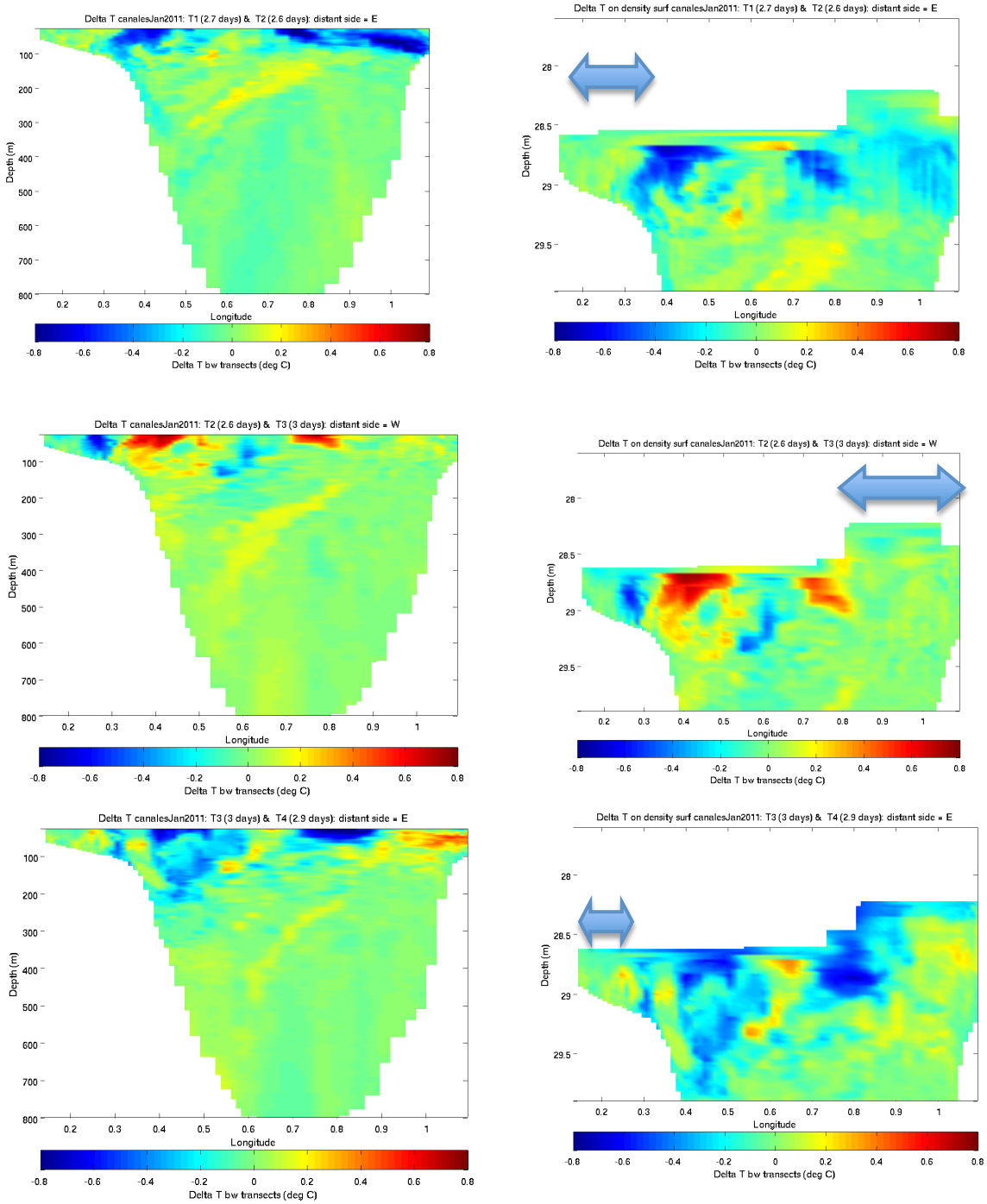

Figure E1. ΔT on isobars (left) and on isopycnals (right) from canalesJan2011.

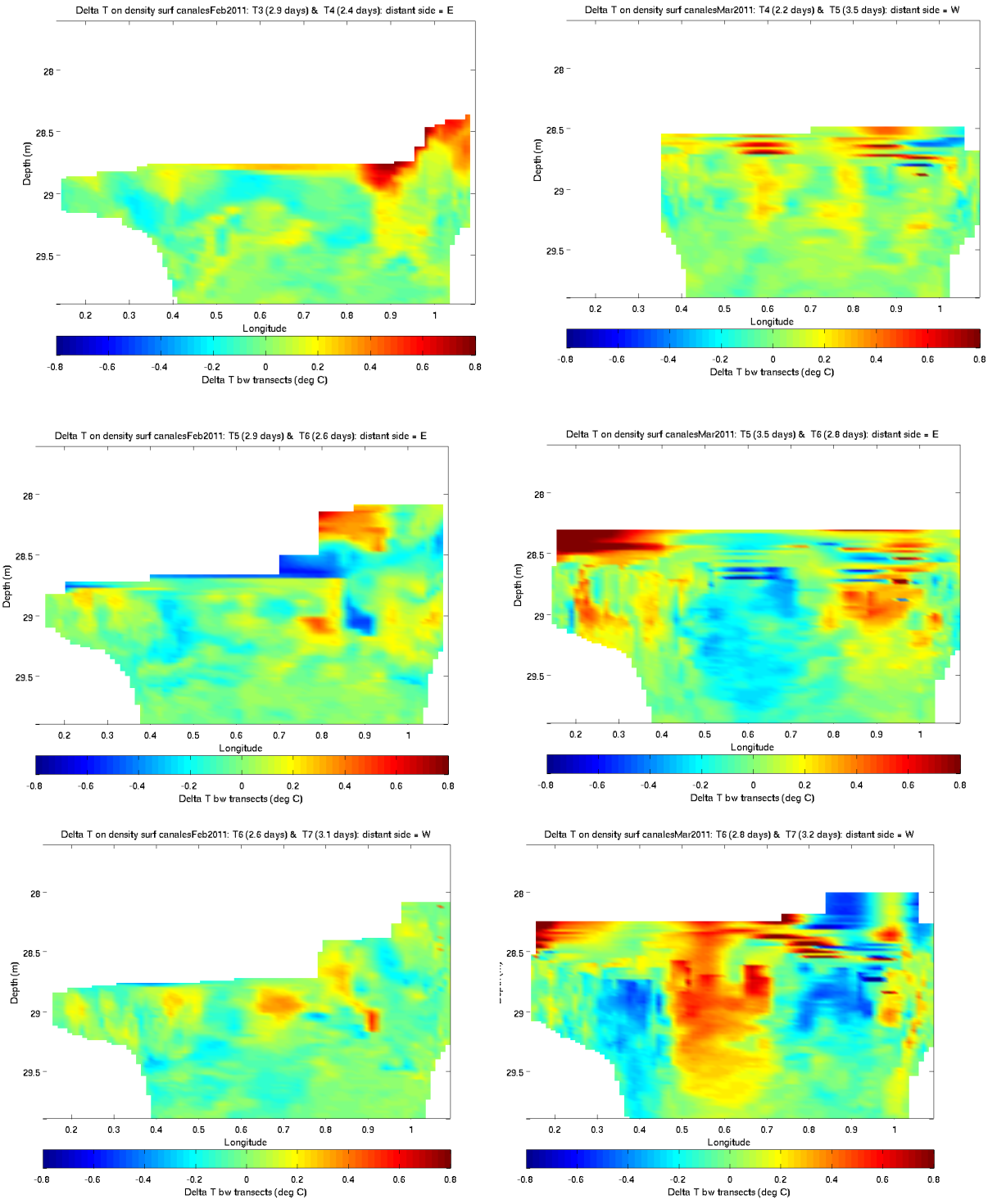

Figure E2. ΔT on isopycnals, canalesFeb2012 (left) and canalesMar2012 (right).

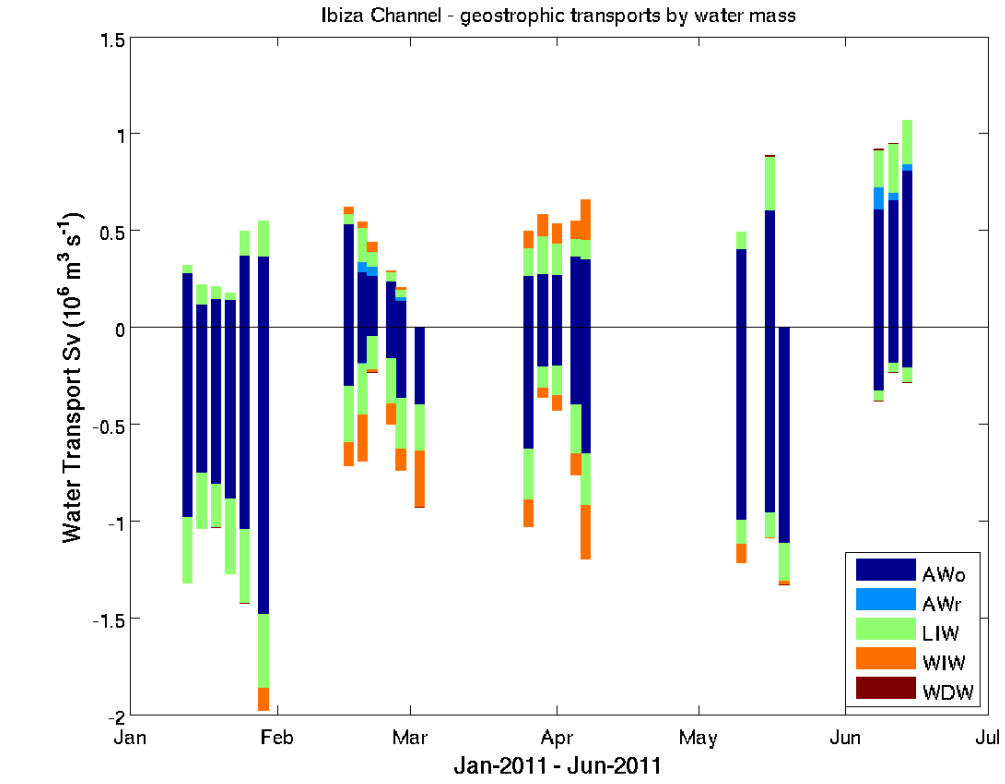

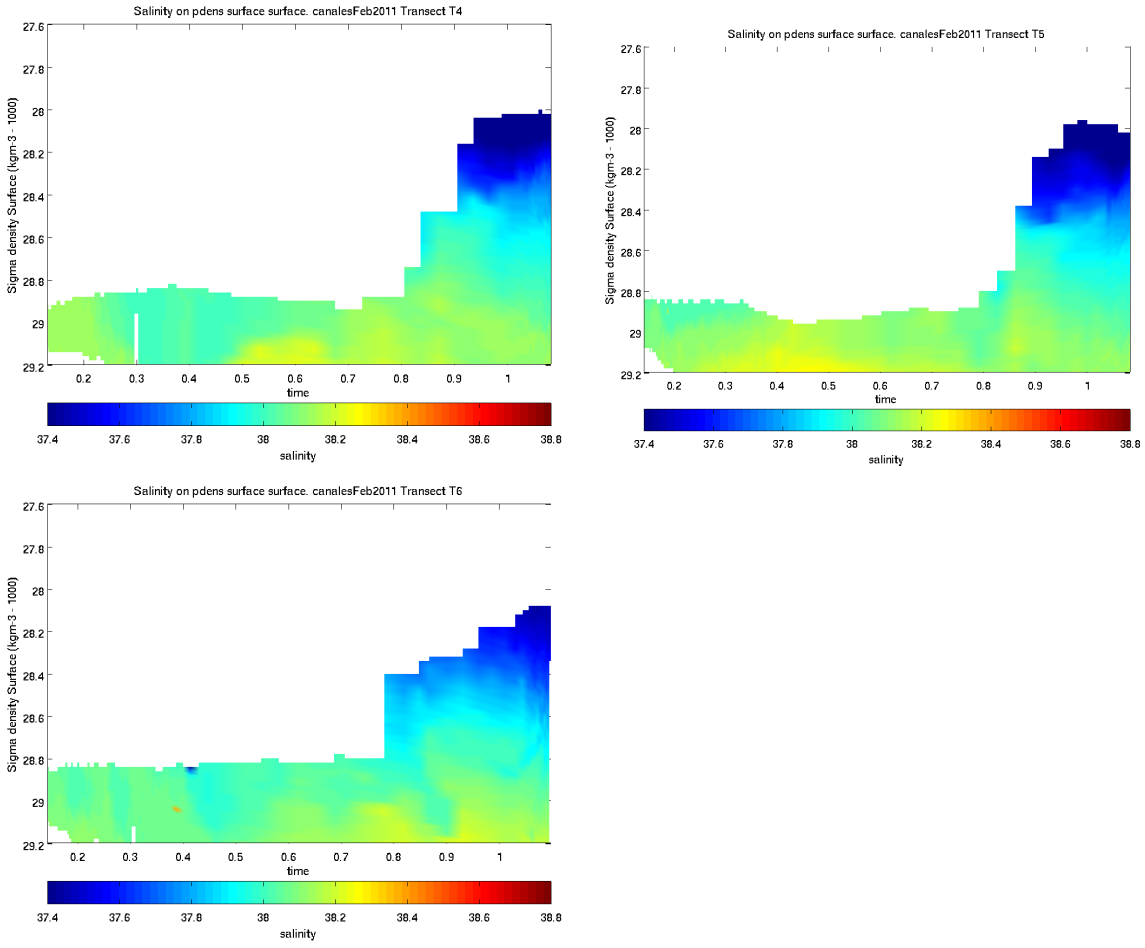

Figure E3. Salinity on density surfaces for canalesFeb2011.

Showing intrusion of the less saline more recent Atlantic water mass in the E of the channel.

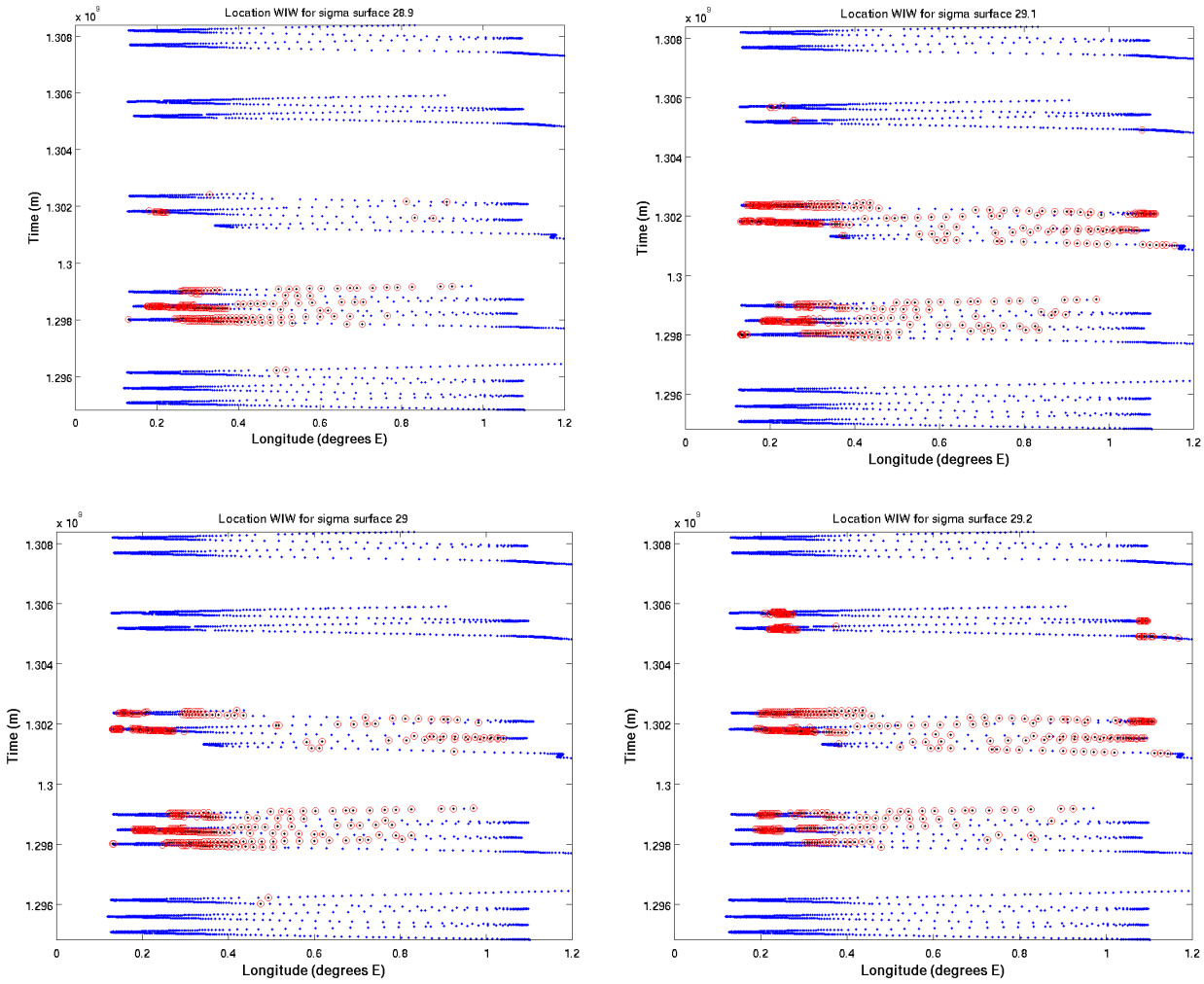

Figure E4. Plot of WIW location (red circles) through time on density surfaces.

Acknowledgements: The glider data was collected under the long-term monitoring program operated by SOCIB (Coastal Ocean Observing and Forecasting System of the Balearic Islands) and IMEDEA (CSIC-UIB). The research was funded by the ES0904 COST Action. Dr Yiannis Andrianakis for his help during the STSM and his on going support in getting the r-INLA package to work with our glider data.

Appendix F: Sensitivity test for vertical profile assumption in glider data

In many studies using glider data, including this one, glider profiles are assumed to be vertical during the initial processing when the glider flight path through the water column is a 'V'. This appendix tests if there is any difference visible in sections (θ, S, geostrophic velocity) or in the derived geostrophic transport if the glider data positions are mapped directly onto a 2D surface or are treated as vertical profiles. This provides insight into the error associated with the choice of basic processing methods for glider data, whereas other tests in Appendix B and C provide information on the errors associated with assumptions in the calculation of the geostrophic transport.

In this thesis the glider data are processed as follows:

1. GPS fixes (updated fixes only) are identified and latitude and longitude between are interpolated to the time base, assuming a linear flight path between the 'real' fixes. This linear flight path is an assumption as the glider may be advected in a non linear way by currents during the generally 6 hours between surfacing for GPS fix (Slocum gliders, for Seagliders the time is less and for Slocums can be greater if a new fix is not obtained). The pressure is filtered, using a Seabird standard filter (see Chapter 2), as per standard ship CTD processing protocols, which removes small fluctuations in pressure and aids profile identification (max. and min. depths). All sensor data is recovered, data without a timestamp is given an interpolated timestamp. Profiles are defined, outlying values of salinity are removed ($20 < S < 40$) and the salinity corrected (following the methods of Garau et al. 2010, as outlined in Chapter 2), providing salinity original and salinity corrected variables. Short transects or large gaps in the data are identified and these profiles are removed.
2. The profiles are assumed vertical and the mean latitude, longitude and time are taken to represent the profile and transects defined. Across transects short and surface profiles are filled (as detailed in Chapter 2) and the glider data is binned (5 m vertical and 2 km horizontal) and then interpolated onto the same regular grid (5 m vertical and 2 km horizontal).

3. Prior to the calculation of geostrophic velocity, the data is smoothed along the horizontal component of the gird with a moving average filter of 6 km (i.e. three data points). The data is also cropped to a standard bathymetry (see Chapter 2 for details).
4. Geostrophic velocity is then calculated using a reference level of zero velocity at the maximum common depth for each profile pair and the geostrophic transport calculated for each grid cell.

In this test the glider data positions, longitude and depth, are mapped directly onto a 2D grid across the IC using a 2D interpolation (hereafter 'glider V' method). The grid is the same as that used for transport calculations namely 5 m vertical and 2 km horizontal, and the latitude is assumed to be that of the standard transect line adopted for the processing of glider data. The 'glider V' to 2D method replaces the steps 2 and 3 outlined above, the standard process, following steps 2 and 3 is hereafter 'vertical profile' method.

The resultant plots of potential temperature, salinity and geostrophic velocity produced by both methods are shown below, figures F1, F2 and F3. The structure in potential temperature is almost identical in both cases, figure F1, the 'glider V' to 2D method has a 'web' of values in the west of the channel, caused by the method of interpolation (Delaunay triangulation) used to find the values at the grid points. This additional data is later cropped to the standard bathymetry at this latitude (step 4) and so plays no part in the calculation of geostrophic velocity. The structure depicted in salinity (figure F2) is also very similar, with only very minor differences visible. In figure F3 the pattern of geostrophic velocity across the channel is also shown, here subtle differences between the two sections can be detected, for example at ~8.5°E the shape of the base of the inflow current is subtly different and at ~6°E the core of the NC has more smoothed appearance for the 'glider V' to 2D interpolation. Overall the 'glider V' to 2D method provides perhaps a slightly smoother pattern in geostrophic velocity due to the method of interpolation.

In terms of derived transport values there is a difference of 2% in the calculated volume of flow northward and 4% in the transport southward between the two methods. These percentages can perhaps be taken as a guide as to the scale of error associated with the choice of basic processing methods. However they do not affect the new view of variability presented in Chapter 4 of this thesis or the new view of dynamics in the IC presented in Chapter 3.

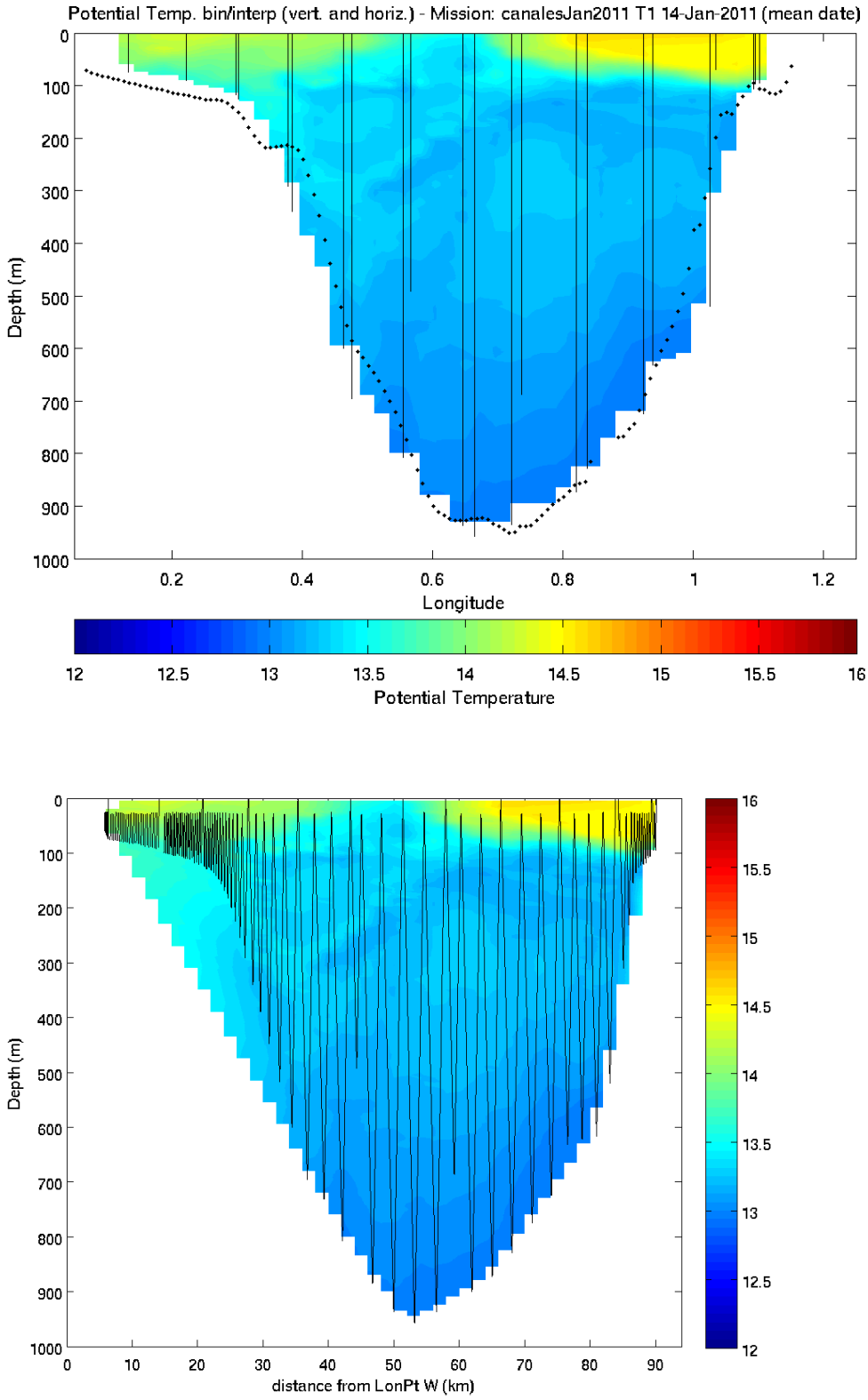

Figure F1. Comparison of potential temperature sections for T1 canalesJan2011.

Upper panel shows a section created using the 'vertical profile' method (steps 2 and 3 above) and the lower panel shows a section created using an interpolation directly from 'glider V' to 2D grid method (replacing for steps 2 and 3 above). For the upper panel ('vertical profile' method) the surfacing profiles are marked as black vertical lines and in the lower panel the 'glider Vs' method the glider flight path is marked in black.

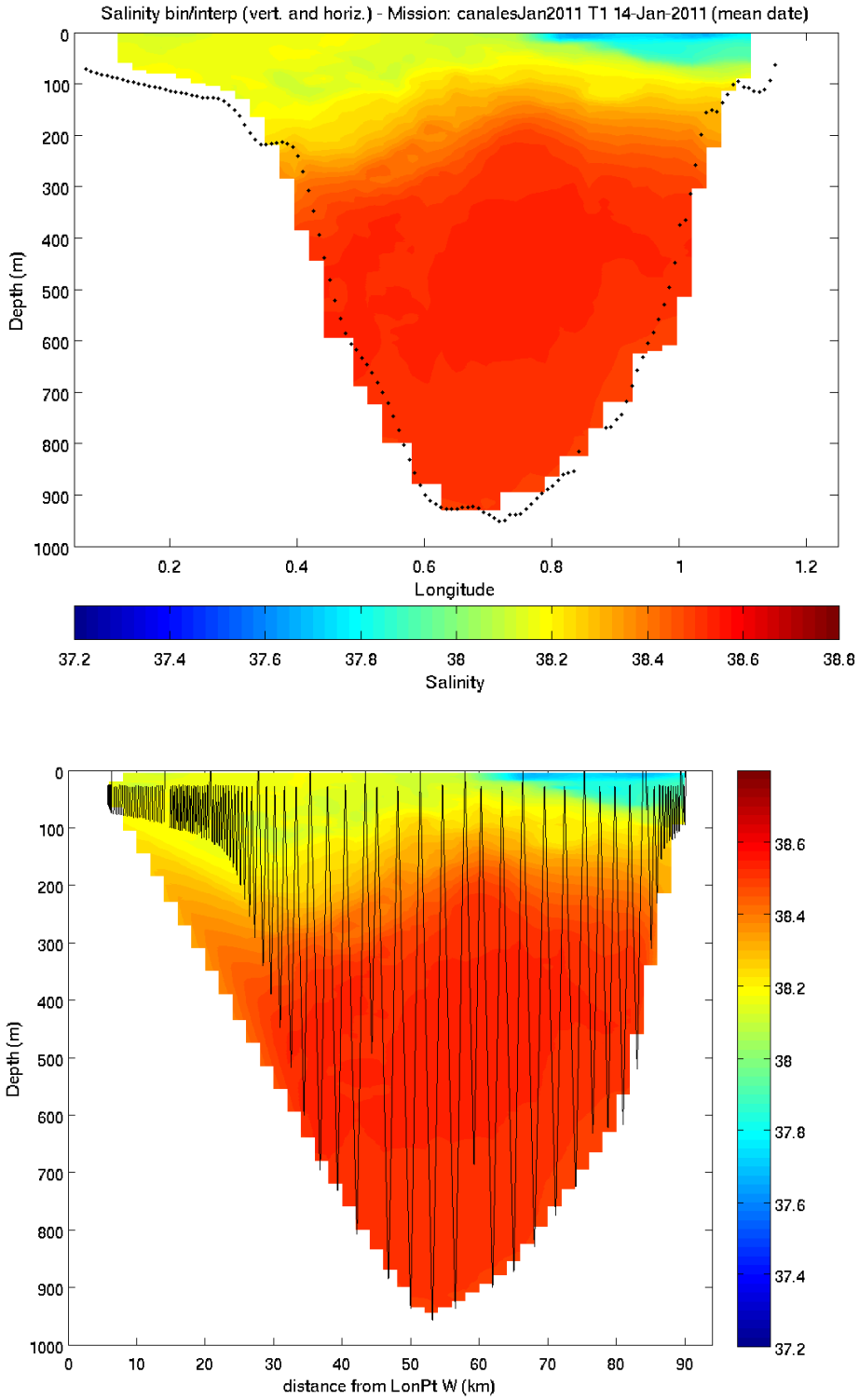

Figure F2. Comparison of sections of salinity for T1 canalesJan2011.

Upper panel shows a section created using the 'vertical profile' method (steps 2 and 3 above) and the lower panel shows a section created using an interpolation directly from 'glider Vs' to a 2D grid method (replacing for steps 2 and 3 above). For the lower panel the 'glider V' method the glider flight path is marked in black.

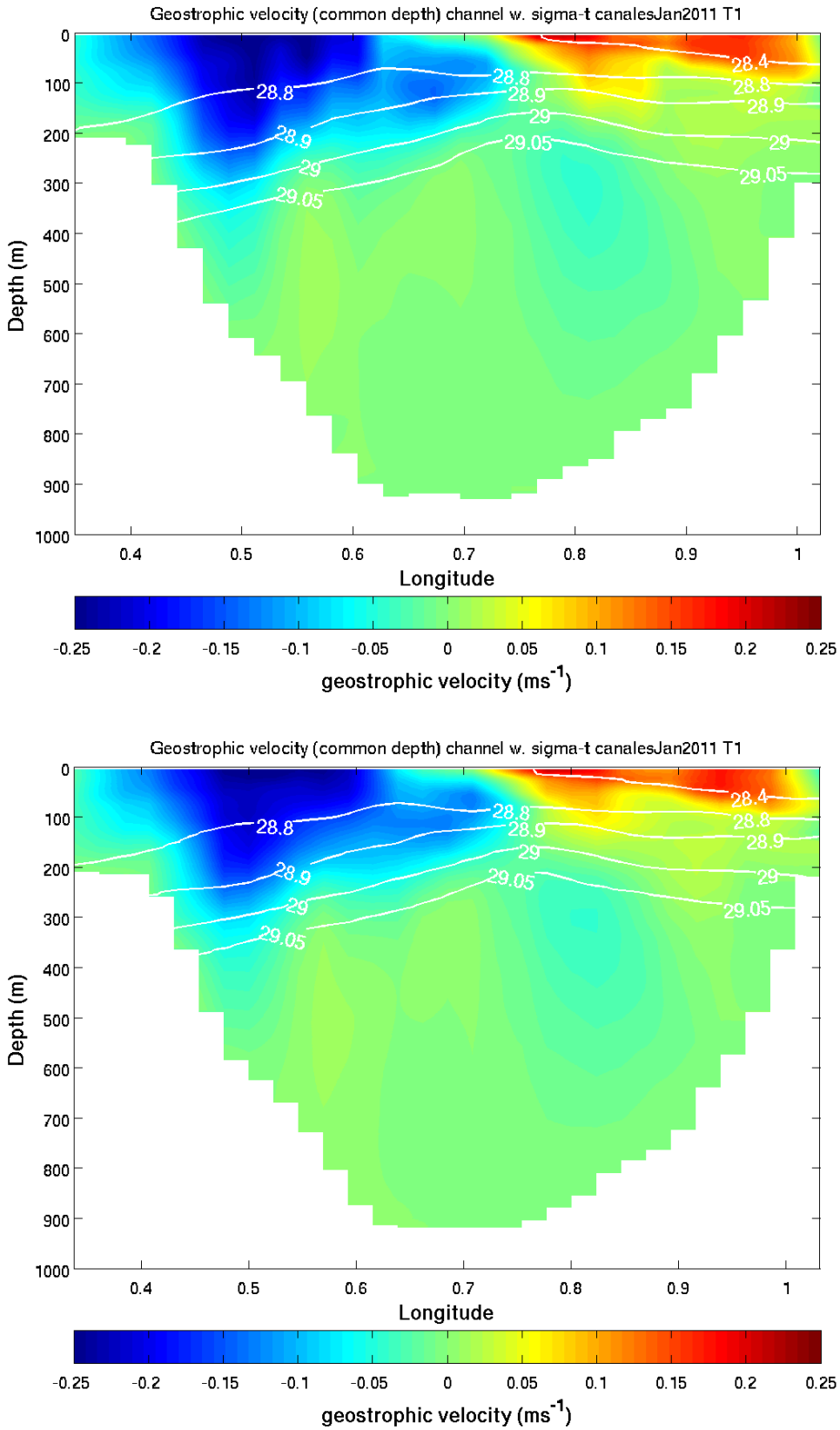

Figure F3. Comparison of sections of geostrophic velocity for T1 canalesJan2011.

Upper panel shows a section created using the 'vertical profile' method (steps 2 and 3 above) and the lower panel shows a section created using an interpolation directly from 'glider V' to a 2D grid method (replacing for steps 2 and 3 above).

In summary the 'glider V' to 2D method provides a neat solution to interpolating glider data that does not affect the results, but in encapsulating this in one step does run the risk of missing some of the detail or anomalies that might be seen when viewing the data first as profiles and then assessing the horizontal interpolation. The results do suggest that as long as sensible decisions are made, the glider data are not unduly sensitive to details in processing methods.

Appendix G: Mallorca Channel sections

This section contains sections of geostrophic velocity (gv), potential temperature (θ) and salinity for transects across the MC, as discussed in Chapter 3. For all figures the transect numbers are as marked in the bottom left corner of the section with the mean date of transect, the geostrophic velocities northward are positive and southward are negative, and selected isopycnals are marked on the geostrophic velocity sections in white.

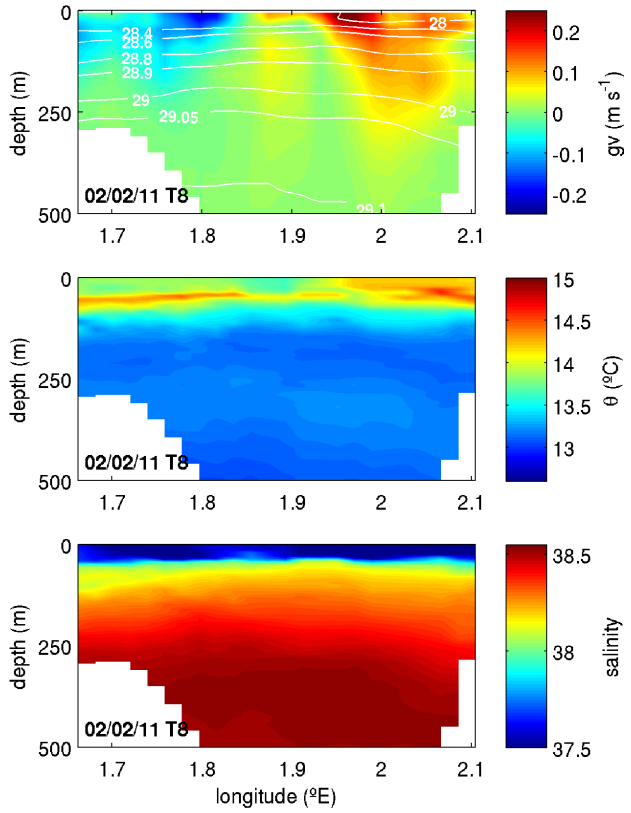

Figure G1. Sections of geostrophic velocity (gv), potential temperature (θ) and salinity for canalesJan2011.

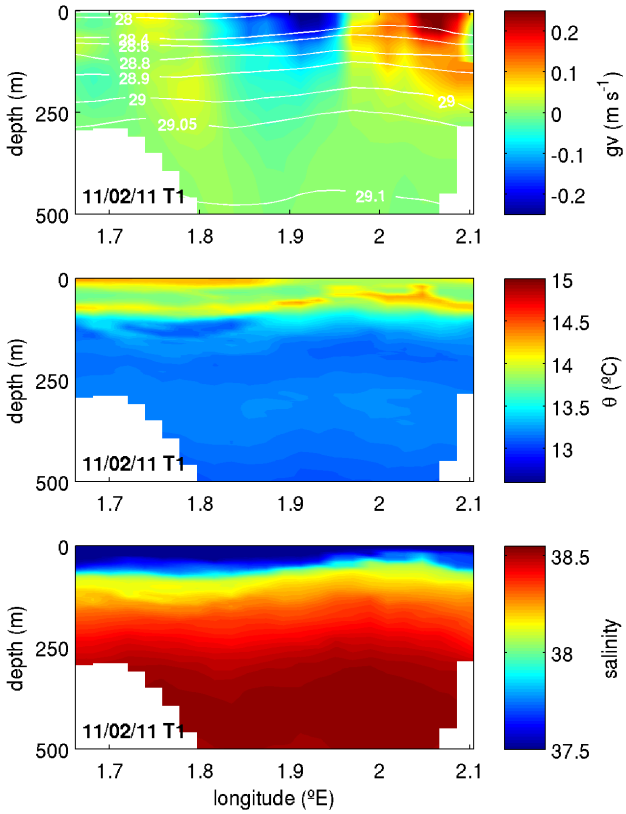

Figure G2. Sections of geostrophic velocity (gv), potential temperature (θ) and salinity for canalesFeb2011.

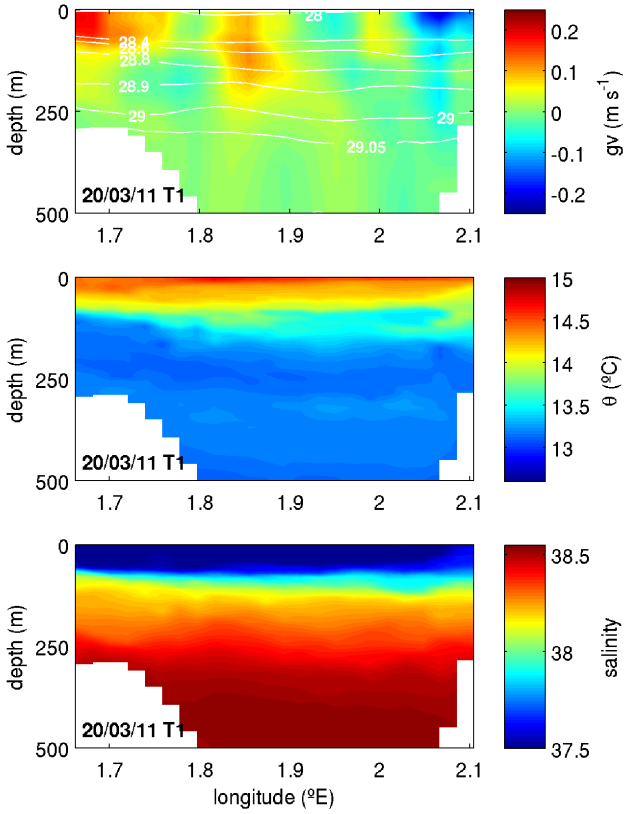

Figure G3. Sections of geostrophic velocity (gv), potential temperature (θ) and salinity for canalesMar2011.

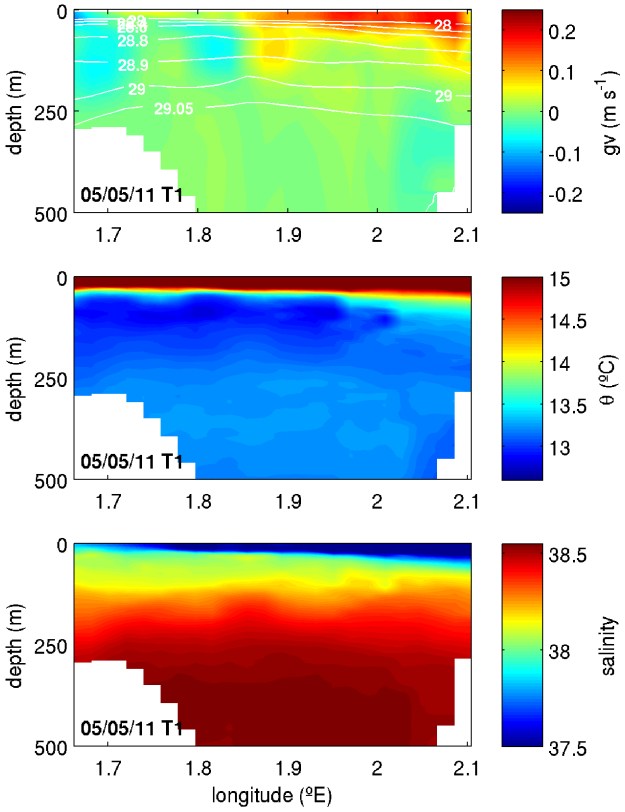

Figure G4. Sections of geostrophic velocity (gv), potential temperature (θ) and salinity for canalesMay2011.

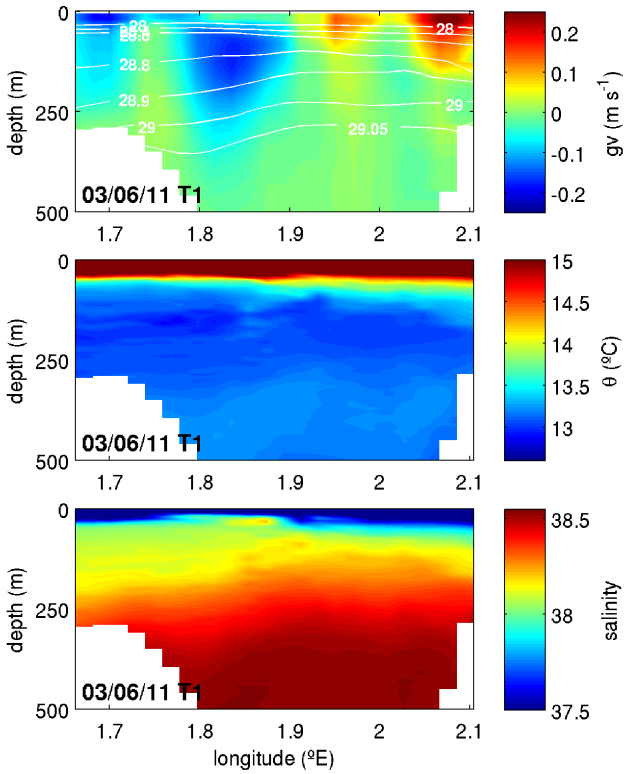

Figure G5. Sections of geostrophic velocity (gv), potential temperature (θ) and salinity for canalesJun2011.

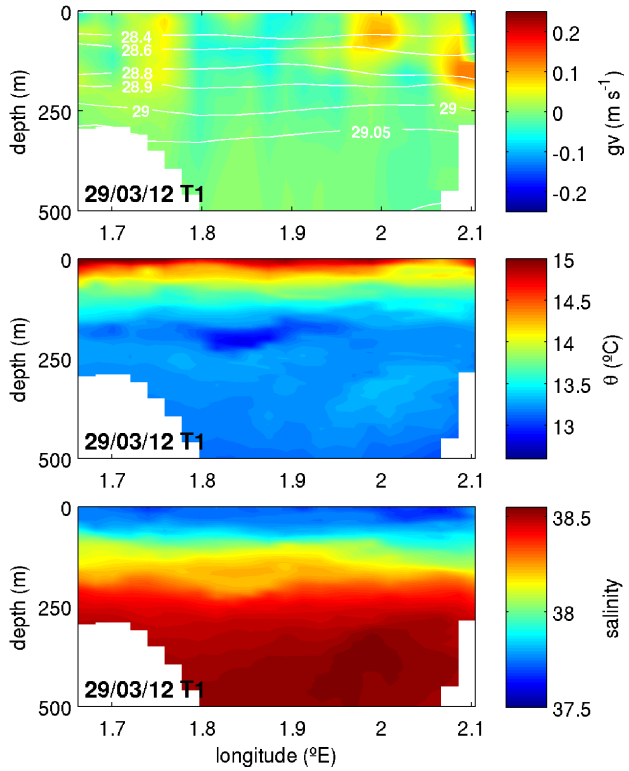

Figure G6. Sections of geostrophic velocity (gv), potential temperature (θ) and salinity for canalesMar2012.

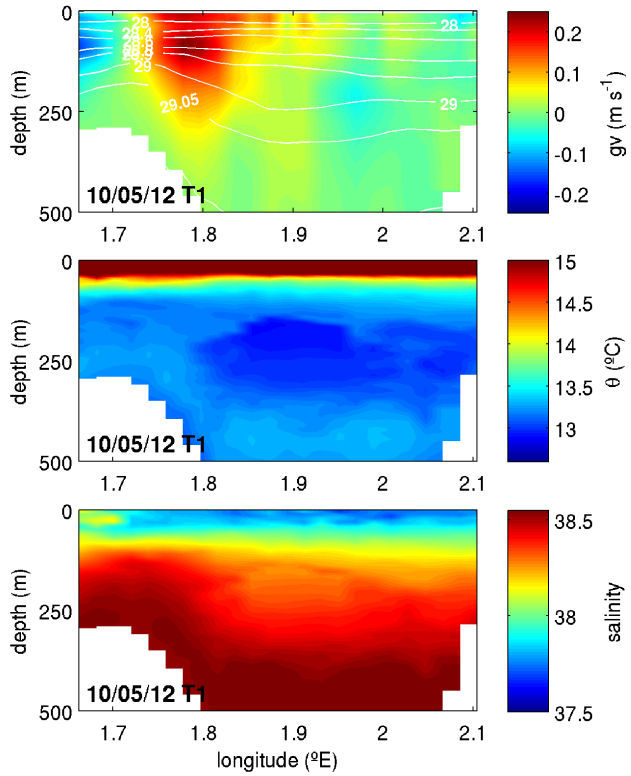

Figure G7. Sections of geostrophic velocity (gv), potential temperature (θ) and salinity for canalesMay2012.

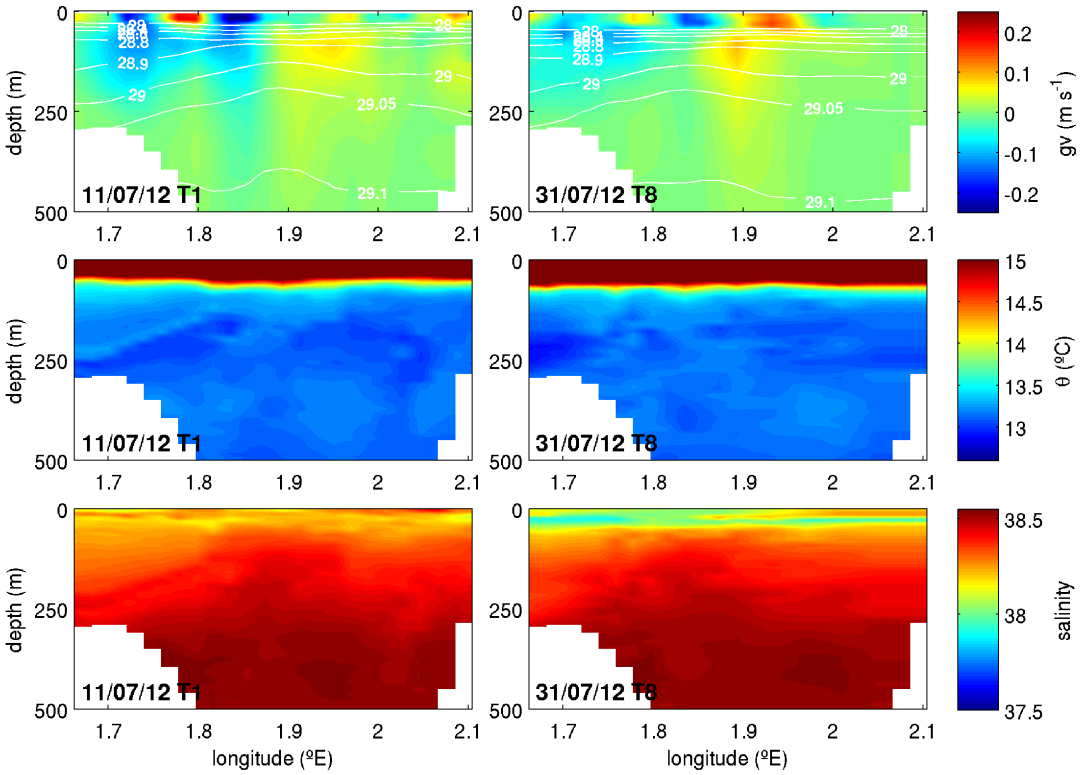

Figure G8. Sections of geostrophic velocity (gv), potential temperature (θ) and salinity for canalesJul2012.

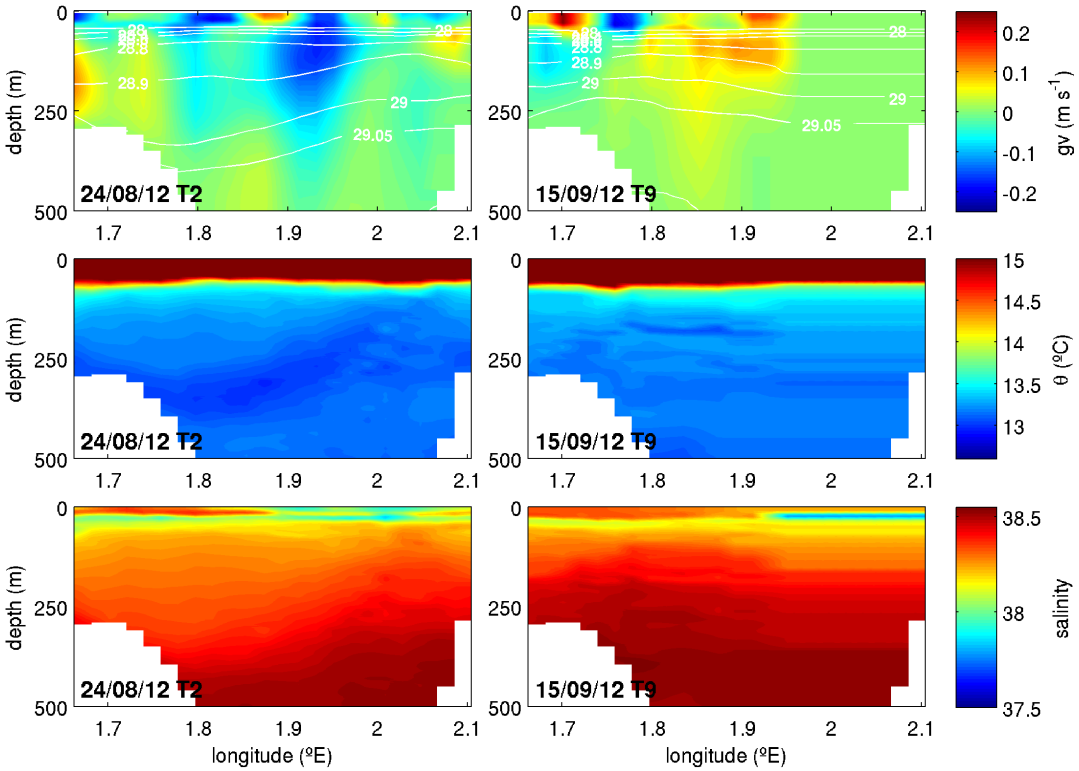

Figure G9. Sections of geostrophic velocity (gv), potential temperature (θ) and salinity for canalesAug2012.

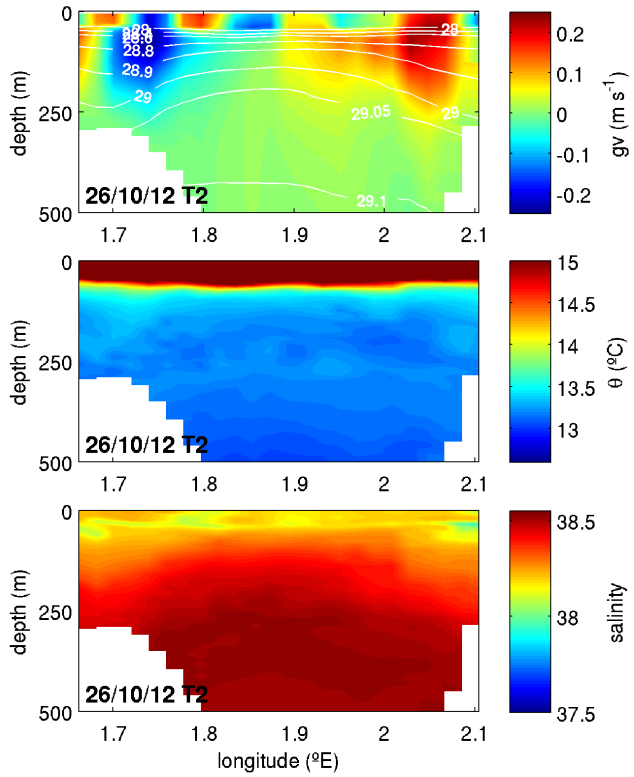

Figure G10. Sections of geostrophic velocity (gv), potential temperature (θ) and salinity for canalesOct2012.

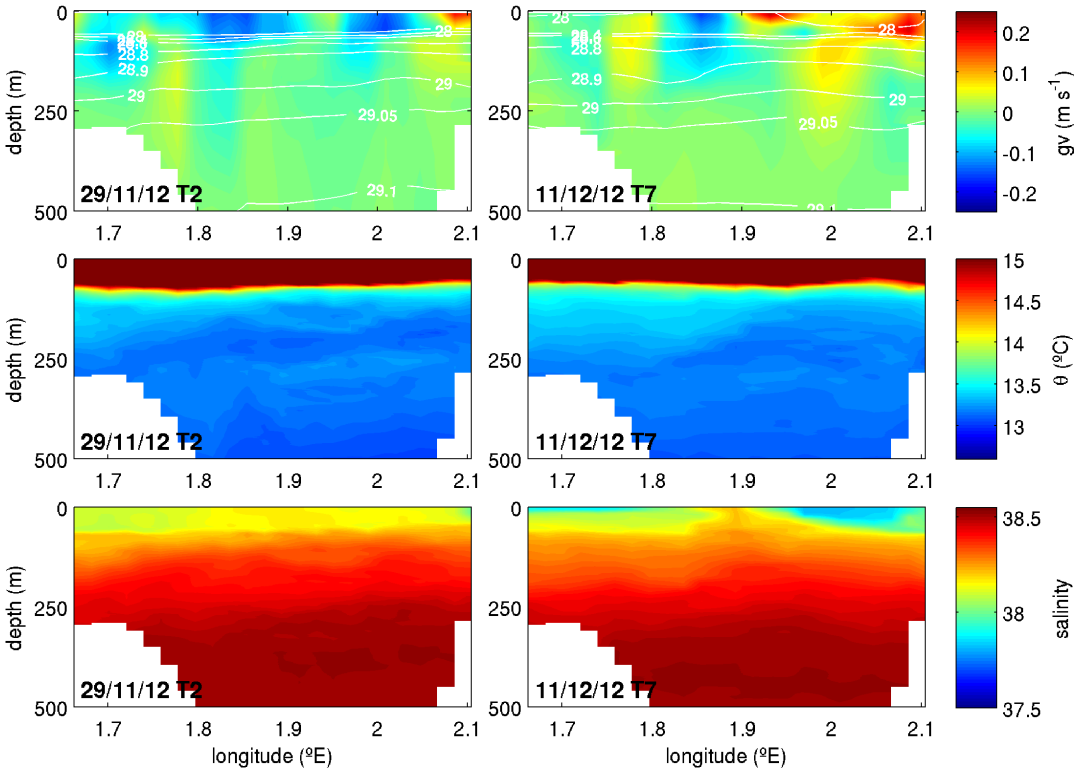

Figure G11. Sections of geostrophic velocity (gv), potential temperature (θ) and salinity for canalesNov2012.

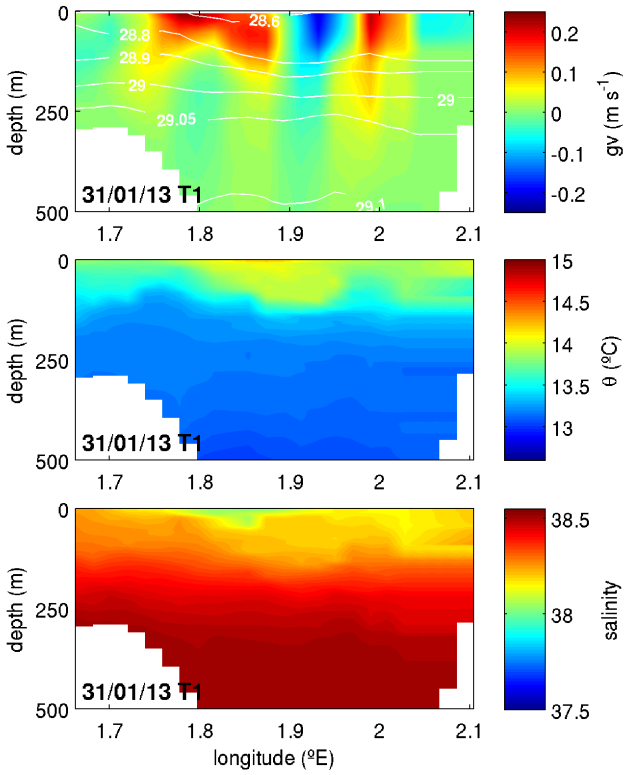

Figure G12. Sections of geostrophic velocity (gv), potential temperature (θ) and salinity for canalesJan2013.

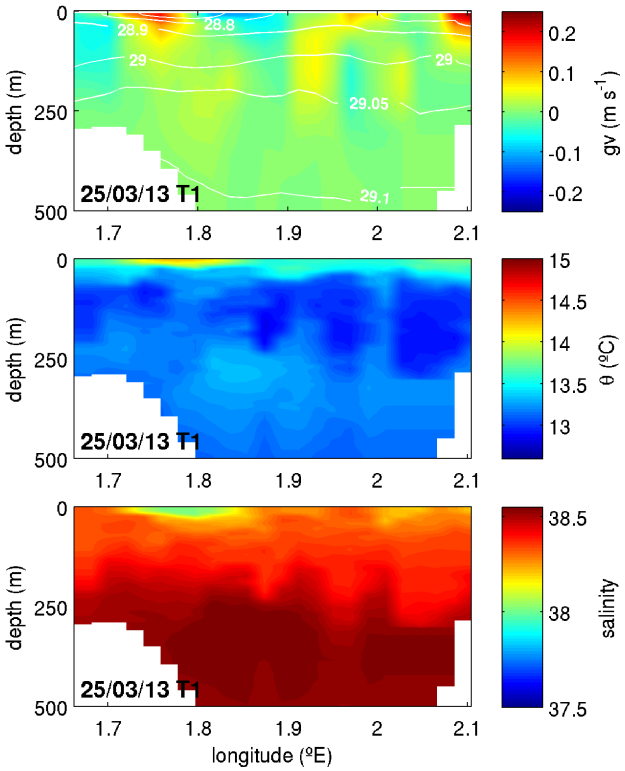

Figure G13. Sections of geostrophic velocity (gv), potential temperature (θ) and salinity for canalesMar2013.

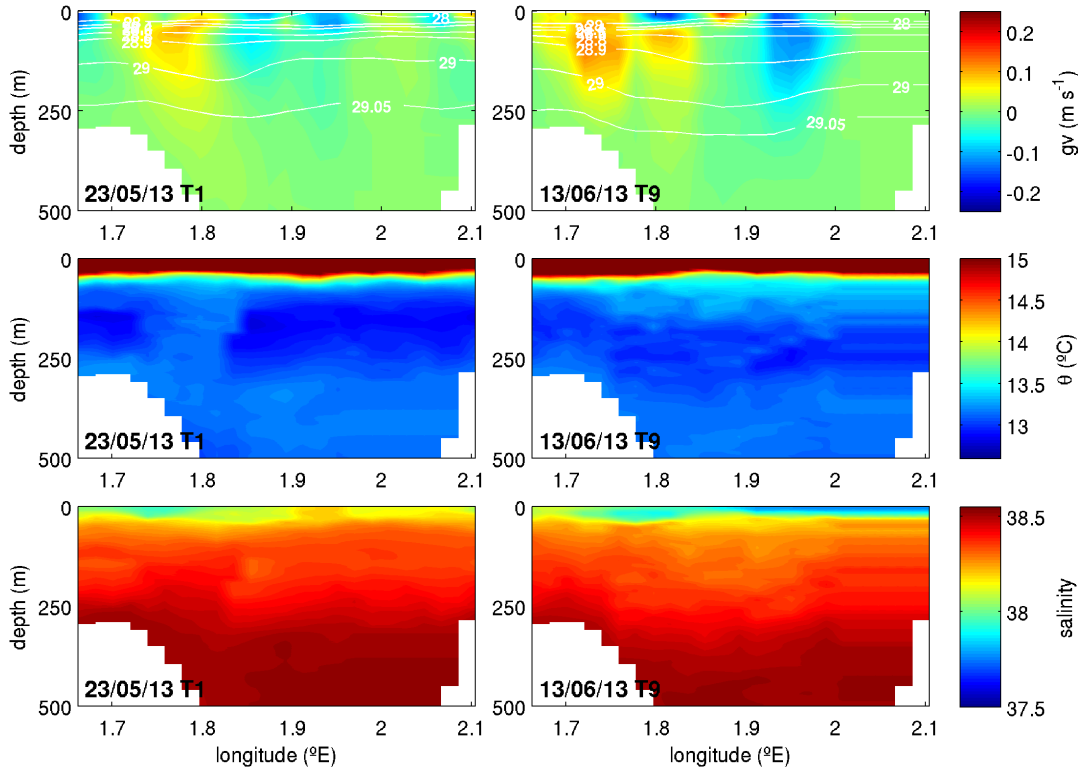

Figure G14. Sections of geostrophic velocity (gv), potential temperature (θ) and salinity for canalesMay2013.

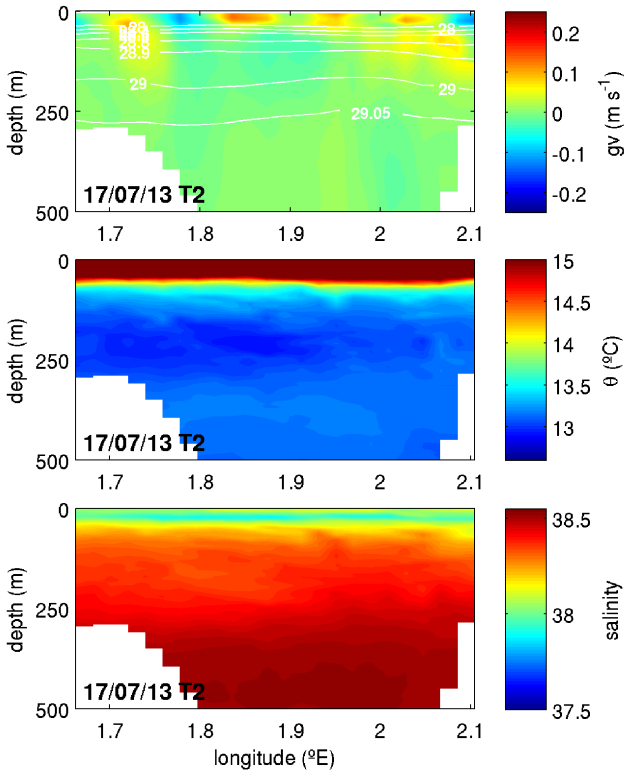

Figure G15. Sections of geostrophic velocity (gv), potential temperature (θ) and salinity for canalesJul2013.

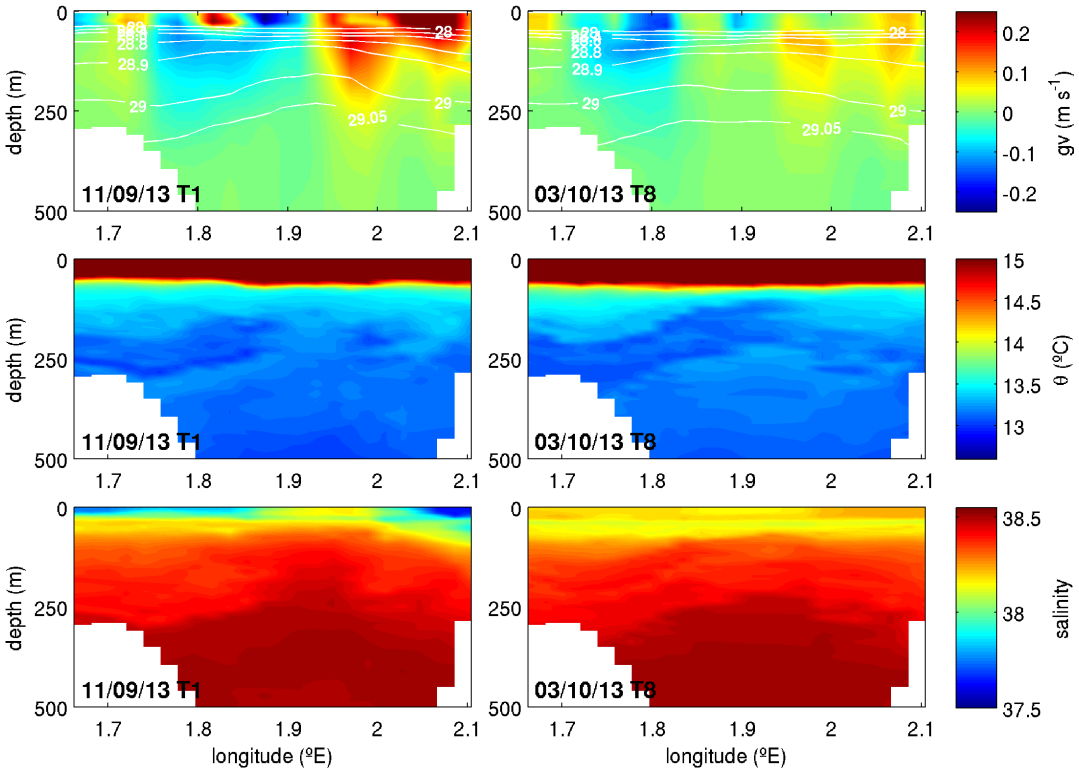

Figure G16. Sections of geostrophic velocity (gv), potential temperature (θ) and salinity for canalesSep2013.

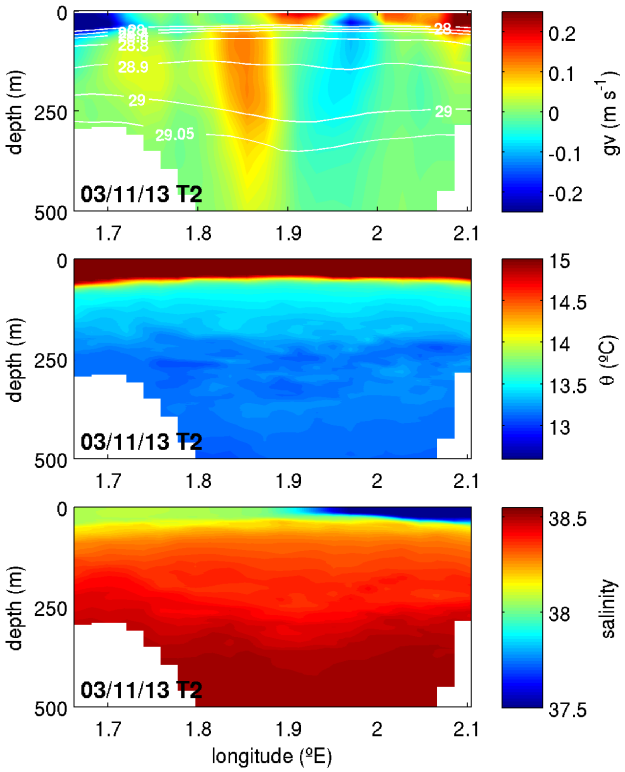

Figure G17. Sections of geostrophic velocity (gv), potential temperature (θ) and salinity for canalesNov2013.

Appendix H: Interannual mean velocity section

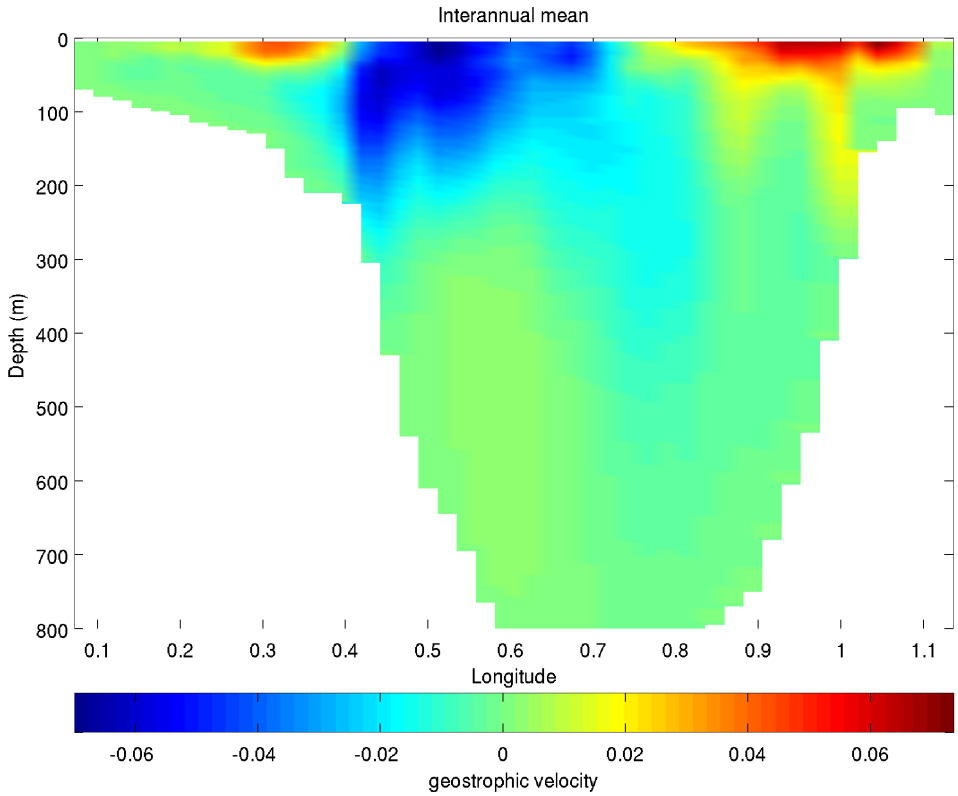

Figure H1. Inter annual mean geostrophic velocity across the Ibiza Channel.

The interannual mean pattern of geostrophic velocity is the component that is removed before the EOF analysis is performed on the remaining velocity field to analyse the temporal variability of dominant spatial patterns. This is then added to the EOF, multiplied by appropriate amplitudes, in order to provide a representation of the pattern of the geostrophic velocity field in the IC for that EOF and amplitude (see figs. 46a, 46b, 46c and 46d, lower panels).

Appendix I: SOCIB Glider Facility costs

Detailed in the table below are the operational costs for the SOCIB glider Facility, as originally submitted to EU FP7 Project JERICO* and more recently EU FP7 Project GROOM**.

SOCIB	2011*	2012**	2013**
Investment			
purchase of gliders	600,000	-	-
purchase of sensors	1,500		-
glider infrastructure (e.g. pressure chamber)	30,000	6,820	495
glider equipment (e.g. tools, R&D, launch)	6,000	3,000	486
safety equipment	500	3,127	-
Total investment	**638,000**	**12,947**	**981**
Operations			
Variable			
batteries	22,000	22,000	25,585
consumables other (e.g. cables)	600	-	-
Iridium	10,000	12,129	12,584
communications other (Argos, mobile)	500	500	1,000
spare parts for repair or upgrade etc.	5,000	1,295	-
calibration (outsourced)	5,000	-	12,000
vessel costs (e.g. hire, fuel)	6,000	6,000	5,600
transportation of equipment	2,000	2,000	3,600
waste disposal/service from institute	-	-	-
subtotal	**51,100**	**43,924**	**60,369**
Fixed			
Glider loss insurance	-	-	19,000
Shipping insurance			-
Liability insurance			-
Other insurance			-
subtotal	**-**	**-**	**19,000**
Other			3,748
Total Operations	**51,100**	**43,924**	**83,117**
Personnel			
SOCIB Glider Facility	66,500	70,000	70,000
SOCIB ETD	13,000	8,750	8,750
SOCIB Data Centre Facility	6,500	27,708	33,542
CSIC in-kind	6,500	37,500	37,500
travel personnel	1,800	6,000	6,200
training personnel	-		15,532
Total Personnel	**94,300**	**149,958**	**171,524**
TOTAL OPERATIONS & PERSONNEL	**145,400**	**193,882**	**254,641**
Indirect cost/overhead estimate			
20%	29,080	38,776	50,928
TOTAL INVESTMENT	**638,000**	**12,947**	**981**
TOTAL COSTS (inc. OVERHEAD)	**174,480**	**232,659**	**305,569**

Table I1. Investments and costs for the SOCIB Glider Facility, 2011 to 2013.

List of references

Alemany, F., Quintanilla, L., Velez-Belchí, P., García, A., Cortés, D., Rodríguez, J.M., Fernández de Puelles, M.L., González-Pola, C. and López-Jurado J.L. (2010). Characterization of the spawning habitat of Atlantic bluefin tuna and related species in the Balearic Sea (western Mediterranean), Prog. Oceanogr., 86, 21–38.

Allen, A.T., Painter, S.C. and Rixen, M. (2008). Eddy transport of Western Mediterranean Intermediate Water to the Alboran Sea, J. Geophys. Res., Vol. 113, C04024

Astraldi, M., Balopoulos S., Candela J., Font J., Gacic M., Gasparini G., Manca B., Theocharis A., and Tintoré J. (1999). The role of straits and channels in understanding the characteristics of Mediterranean circulation. Prog. Oceanogr., 44, 65-108.

Baird, M.E. and Ridgway, K.R. (2012). The southward transport of sub-mesoscale lenses of Bass Strait Water in the centre of anti-cyclonic mesoscale eddies. Geophys. Res. Lett., Vol. 39, L02603.

Balbín, R., López-Jurado, J.L., Flexas, M.M., Reglero, P., Vélez-Velchí, P., González-Pola, C., Rodríguez, J.M., García, A. and Alemany, F. (2014). Interannual variability of the early summer circulation around the Balearic Islands: Driving factors and potential effects on the marine ecosystem. J. Mar. Syst. 138, 70–81. doi: 10.1016/j.jmarsys.2013.07.004.

Becker, J. J., Sandwell, D. T., Smith, W. H. F., Braud, J., Binder, B., Depner, J., Fabre, D., Factor, J., Ingalls, S., Kim, S-H., Ladner, R., Marks, K., Nelson, S., Pharaoh, A., Trimmer, R., Von Rosenberg, J., Wallace, G. and Weatherall, P.(2009). 'Global Bathymetry and Elevation Data at 30 Arc Seconds Resolution: SRTM30_PLUS', Marine Geodesy, 32:4, 355-371.

Bergamasco, A. and Malanotte-Rizzoli, P. (2010). The circulation of the Mediterranean Sea: a historical review of experimental investigations. Advances in Oceanography and Limnology 1, 1,11–28.

Bethoux, J.P., Durrieu de Madron, X., Nyffeler, F., and Taillez, D. (2002). Deep water in the western Mediterranean: peculiar 1999 and 2000 characteristics, shelf formation hypothesis, variability since 1970 and geochemuical inferences. J. Mar. Systems, 33-34, 117-131.

Beuvier, J., Béranger, K., Lebeaupin, C., Brossier, Somot, S., Sevault, F., Drillet, Y., Bourdallé-Badie, R., Ferry, N., and Lyard F. (2012), Spreading of the Western Mediterranean Deep Water after winter 2005: Time scales and deep cyclone transport, J. Geophys. Res., 117, C07022.

Bianchi, C.N. and Morri, C. (2000). Marine Biodiversity of the Mediterranean Sea: Situation, Problems and prospects for Future Research. Mar. Pollut. Bull., Vol. 40, No. 5, pp 367 – 376.

Birol, F., Cancet, M., and Estournel, C. (2010). Aspects of the seasonal variability of the Northern Current (NW Mediterranean Sea) observed by altimetry Journal of Marine Systems 81 (297–311)

Bryden, H.L., King, B.A., McCarthy, G.D. and McDonagh, E.L. (2014) Impact of a 30% reduction in Atlantic meridional overturning during 2009-2010. Ocean Science, 10, (4), 683-691. (doi:10.5194/os-10-683-2014).

Bryden, H.L., Robinson, C., and Griffiths, G. (2012) A strategy for UK marine science for the next 20 years. Philosophical Transactions of The Royal Society A Mathematical Physical and Engineering Sciences, 370, (1980), 5455-5456. (doi:10.1098/rsta.2012.0403).

Bryden, H.L., Longworth, H.R., and Cunningham, S.A. (2005). Slowing of the Atlantic meridional overturning circulation at 25°N. Nature, 438, 655.

Bosse. A., Testor. P., Beguery. L., Bernardet. K., and Taillandier, V. (2013). Survey of submesoscale structures at the margin of the Northern Current in the North Western Mediterranean Sea using Gliders: observations and diagnostics, EGU General Assembly Conference Abstracts 15, 11138

Bouffard J., Renault L., Ruiz S., Pascual A., Dufau C., and Tintoré J. (2012). Sub-surface small scale eddy dynamics from multi-sensor observations and modelling, Prog. in Oceanog., Volume 106, pages 62–79.

Canals, M., Puig, P., de Madron, X. D., Heussner, S., Palanques, A., and Fabres, J. (2006). Flushing submarine canyons, Nature, 444, 355–357.

Candela, J.: Mediterranean water and the global circulation, in: Ocean Circulation

Candela, J. (2001). Chapter 5.7. Mediterranean water and global circulation. In J.C. Gerold Siedler and J. Gould, editors, Ocean Circulation and Climate Observing and Modelling the Global Ocean, volume 77 of International Geophysics, pages 419 – XLVIII. Academic Press.

Castelao, R., Glenn, S., Schofield, O., Chant, R., Wilkin, J., and Kohut, J. (2008), Seasonal evolution of hydrographic fields in the central Middle Atlantic Bight from glider observations, Geophys. Res. Lett., 35, L03617.

Castellon, A., Font, J. and Garcia, E. (1990). The Liguro-Provençal-Catalan current (NW Mediterranean) observed by Doppler profiling in the Balearic Sea. Sci. Mar., 54(3): 269-276

Crépon, M., Wald, L., and Monget, J-M. (1982). Low-frequency waves in the Ligurian Sea during December 1977. Journal of Geophysical Research, 87, 595–600.

Conan, P. and Millot, C. (1995). Variability of the northern current off Marseilles, western Mediterranean Sea, from February to June 1992. Oceanol. Acta., 18(2), 193 – 205.

Cunningham, S.A., Kanzow, T., Rayner, D., Baringer, M.O., Johns, W.E., Marotzke J., Longworth, H.R., Grant E.M., Hirschi, J. J.-M., Beal, L.M., Meinen, C.S., and Bryden H.L. (2007). Temporal Variability of the Atlantic Meridional Overturning Circulation at 26.5°N, Science, 317 (5840), 935-938.

Delaney, J. and Barga, R. (2010). A 2020 Vision for Ocean Science, in The Fourth Paradigm: Data-Intensive Scientific Discovery by Tony Hey, Stewart Tansley, and Kristin Tolle. Redmond, WA: Microsoft Research, 2009.284pp. ISBN 978-0982544204.

Demirov, E. and Pinardi N. (2007). On the relationship between water mass pathways and eddy variability in the Western Mediterranean Sea. J. Geophys. Res., 112 C(2), 1-21.

D'Ortenzio, F. and Ribera d'Alcalà, M. (2009). On the trophic regimes of the Mediterranean Sea: a satellite analysis, Biogeosciences, 6, 139-148.

Durrieu de Madron, X., Zervakis, V., Theocharis, A., and Georgopoulos, D. (2005). Comments on "cascades of dense water around the World ocean". Prog. In Oceanog., 64, 83-90.

Fofonff, N.P., Hayes, S.P., and Millard, R.C. (1974). Whoi/brown ctd microprofiler: methods of calibration and data handling. Technical Report 64pp, Woods Hole Oceanographic Institution Tech.Rep.

Font, J., Puig, P., Salat, J., Palanques, A., and Emelianov, M. (2007). Sequence of hydrographic changes in NW Mediterranean deep water due to the exceptional winter of 2005. Sci. Mar. 71(2), 339-346.

Font, J. (1987). The path of Levantine Intermediate Water to the Alboran Sea, Deep Sea Research, Vol. 34, 10, 1745 – 1755.

Font, J. and Mirales, L. (1978). Circulacion geostrofica en el mar Catalan. Res. Exp. Cient. B/O Cornide, 7, 155-162.

Font, J., Millot, C., Salas, J., Juliá, A., and Chic, O. (1998a). The drift of Modified Atlantic Water from the Alboran Sea to the eastern Mediterranean. Sci. Mar., 62(3): 211-216.

Font, J., Salat, J. and Tintoré, J. (1988b). Permanent features of the circulation in the Catalan sea. Oceanol. Acta., Vol. sp. 9, 51-57.

Font, J., Salat, J. and Julia, A., (1990). Marine circulation along the Ebro continental margin. In: C.H. Nelson and A. Maldonado (Editors), The Ebro Continental Margin, Northwestern Mediterranean Sea. Mar. Geol., 95: 165-177.

Garau, B., Ruiz, S., Zhang, W.G., Pascual, A., Heslop, E., Kerfoot, J., and Tintoré, J. (2011). Thermal lag correction on slocum ctd glider data. J. Atmos. Oceanic Technol., 28, 1065–1071.

García, B., Tintoré, J., Pinot, J.M., Font, J. and Manriquez, M. (1994). Surface Circulation and Dynamics of the Balearic Sea, Seasonal and Interannual Variability of the Western Mediterranean Sea, Coastal and Estuarine Studies, Vol. 46, Pages 73-91.

García-Ladona, E., Castellón, A., Font, F. and Tintoré, J. (1995). The Balearic current volume transports in the Balearic basin, Oceanol. Acta., Vol. 19, No. 5.

García-Lafuente, J. M., López-Jurado, J. L., Cano-Lucaya, N., Vargas-Yañez, M., and Aguiar-Garcia, J. (1995). Circulation of water masses through the Ibiza Channel, Oceanol. Acta, 18(2), 245–254.

Gasparini, G.P., Zodiatis, G., Astraldi, M., Galli, C., and Sparnochia, S. (1999). Winter intermediate water lenses in the Ligurian Sea. J. Mar. Systems, 20, 319-332.

Glenn, S., Jones, C., Twardowski, M., Bowers, L., Kerfoot, J., Kohut, J., Webb, D. and Schofield, O. (2008). Glider observations of sediment resuspension in a Middle Atlantic Bight fall transition storm, Limnol. Oceanogr., 53(5, part2), 2180-2196. doi:10.4319/lo.2008.53.5_part_2.2180.

Gourdeau, L., Kessler, W.S., Davis, R.E., Sherman, J., Maes, C. and Kestenare E. (2008). Zonal Jets Entering the Coral Sea, J. Phys. Oceanogr. 38: 715-725.

Hall, M.M. and Bryden, H.L. (1982). Direct estimates and mechanisms of ocean heat transport. Deep-Sea Res., 29, 339-359.

Hátún H., Eriksen C.C., and Rhines P.B. (2007). Buoyant Eddies Entering the Labrador Sea Observed with Gliders and Altimetry. J. Phys. Oceanogr. 37: 2838-2854.

Herbaut, C., Mortier L., and Crépon M. (1997). A sensitivity study of the general circulation of the Western Mediterranean Sea. Part II: The response to atmospheric forcing. J. Phys. Oceanogr., 27, 2126.

Heslop, E.E., Ruiz, S., Allen, J., López-Jurado, J. L., Renault, L., and Tintoré, J. (2012), Autonomous underwater gliders monitoring variability at "choke points" in our ocean system: A case study in the Western Mediterranean Sea. Geophys. Res. Lett., 39, L20604.

Herbaut, C., Mortier L., and Crépon M. (1996). A sensitivity study of the general circulation of the Western Mediterranean Sea. Part I: The response to density forcing through the straits. J. Phys. Oceanogr., 26, 65-84.

Josey, S. A., Somot, S., and Tsimplis, M. (2011), Impacts of atmospheric modes of variability on Mediterranean Sea surface heat exchange, J. Geophys. Res., 116, C02032.

Josey, S.A. (2003). Changes in the heat and freshwater forcing of the eastern Mediterranean and their influence on deep-water formation, Journal of Geophysical Research 108(C7), 3237.

Kerfoot, J., Glenn, S., Kohut, J., Schofield, O., and Roarty, J.H. (2006). Correction for thermal lag effects in non-pumped temperature-conductivity sensors on the Slocum coastal electric glider. Ocean Sciences Meeting Supplementary, volume 87. Eos Trans. AGU.

Leaman, K. and Schott, F. (1991). Hydrographic structure of the convection regime in the Gulf of Lion: Winter 1987. J. Phys. Oceanogr., 21, 575-598.

López Garcia, M.J., Millot, C., Font, J., and García-Ladona, E. (1994). Surface Circulation variability in the Balearic Basin, J. Geophys. Res., Vol. 99, No. C2, pages 3285-3296.

López-Jurado, J.L, Aparicio-González, A., Babín, R., Alonso, J., Amengual, B., Jansá, J., García-Martínez, M., Moya, F., Serra, M., and Vargas-Yáñez, M. (2014). IBAMar DATABASE: 4 decades sampling on the Western Mediterranean Sea. Instituto Español de Oceanografía, http://doi.pangaea.de/10.1594/PANGAEA.831923 and http://www.ba.ieo.es/ibamar.

López-Jurado, J.L., Marcos, M., and Monserrat, S. (2008). Hydrographic conditions affecting two fishing grounds of Mallorca island (Western Mediterranean): during the IDEA Project (2003–2004). J. Marine Syst., 71, 303 – 315.

López-Jurado, J.L., Gonzalez-Pola, L.C., and Velez-Belch, P. (2005). Observation of an abrupt disruption of the long-term warming trend at the Balearic Sea, western Mediterranean Sea, in summer 2005, Geophysical Research Letters, 32fs, L24606.

López-Jurado, J.L., García-Lafuente, J., and Lacaya N. (1995). Hydrographic conditions of the Ibiza channel during November 1990, March 1991 and July 1992. Oceanol. Acta, 18,2, 235-243.

López-Jurado, J.L. and del Rio, G. (1994). Dinàmica asociadad a las masas de agua en el canal de Ibiza en noviembre de 1990 y marzo de 1991, Bol. Inst. Esp. Oceanogr., 10(1), 3–22.

López-Jurado, J.L. (1990). Masas de agua alrededor de las Islas Baleares. Bol. Inst. Esp. Oceanog., 6(2), 3-20.

Lueck, R.G. and Picklo, J.J. (1990). Thermal Inertia of Conductivity Cells: Observations with a Sea-Bird Cell. Journal of Atmospheric and Oceanic Technology, 7:756–768.

Macdonald, A., Candela, J., and Bryden, H.L. (1994). An estimate of the net heat transport through the Strait of Gibraltar, Coastal and Estuarine Studies, 46.

Martin, J.P., Lee, C.M., Eriksen, C., Ladd, C. and Kachel, N.B. (2009). Glider observations of kinematics in a Gulf of Alaska eddy, J. Geophys. Res. 114: C12021.

McCarthy, G., Frajka-Williams, E., Johns, W.E., Baringer, M.O., Meinen, C.S., Bryden, H.L.; Rayner, D., Duchez, A., Roberts, C.D., Cunningham, S.A. (2012). Observed Interannual Variability of the Atlantic Meridional Overturning Circulation at 26.5N. Geophysical Research Letters, 39, L19609. 10.1029/2012GL052933.

Melanotte-Rizzoli, P., Manca, B.B., Ribera d'Alcala, M., Theocharis, A., Brenner, S., Budillon, G., and Ozsoy, E., (1999). The Eastern Mediterranean in the 80s and in the 90s: the big transition in the intermediate and deep circulation. Dynamics of Atmosphere and Oceans 29 (2– 4), 365–395.

Malanotte-Rizzoli, P., Artale, V., Borzelli-Eusebi, G. L., Brenner, S., Civitarese, G., Crise, A., Font, J., Gacic, M., Kress, N., Marullo, S., Ozsoy, E., Ribera d'Alcalá, M., Roether, W., Schroeder, K., Sofianos, S., Tanhua, T., Theocharis, A., Alvarez, M., Ashkenazy, Y., Bergamasco, A., Cardin, V., Carniel, S., D'Ortenzio, F., Garcia-Ladona, E., Garcia-Lafuente, J. M., Gogou, A., Gregoire, M., Hainbucher, D., Kontoyannis, H., Kovacevic, V., Krasakapoulou, E., Krokos, G., Incarbona, A., Mazzocchi, M.G., Orlic, M., Pascual, A., Poulain, P.M., Rubino, A., Siokou-Frangou, J., Souvermezoglou, E., Sprovieri, M., Taupier-Letage, I., Tintoré, J., and Triantafyllou, G. (2013). Physical forcing and physical/biochemical variability of the Mediterranean Sea: a review of unresolved issues and directions for future research, Ocean Science Discussions, 10, 4, 1205--1280.

Marshall, J. and Schott, F. (1999). Open-ocean convection: Observations, theory and models. Rev. Geophys., 37, 1-64.

Martin, J.P., Lee, C.M., Eriksen, C.C., Ladd, C. and Kachel, N.B. (2009). Glider observations of kinematics in a Gulf of Alaska eddy. J. Geophys. Res., Vol. 114, C12021.

Masó, M. and Tintoré, J. (1991). Variability of the shelf water off the northeast Spanish coast, Mar. Syst., 1,441-450.

Mason, E. and Pascual, A. (2013). Multiscale variability in the Balearic Sea: An altimetric perspective, J. Geophys. Res. Oceans, 118, 3007–3025.

Myers, N., Mittermeier, R.A., Mittermeier, C.G., da Fonseca, G.A.B. and Kent., J. (2000). Biodiversity hotspots for conservation priorities. Nature 403, 853-858. doi:10.1038/35002501.

MEDAR Group (2002). MEDATLAS/2002 database. Mediterranean and Black Sea database of temperature salinity and biochemical parameters. Climatological Atlas. IFREMER Edition.

MEDOC group, (1970). Observation of formation of deep water in the Mediterranean sea, 1969. Nature, 227, Nº 5262, 1037-1040.

Meinen, C.S., Baringer, M.O., and Garcia R.F. (2010). Florida Current transport variability: An analysis of annual and longer-period signals. Deep-Sea Res. I, Vol. 57, 835–846.

Merckelbach, L. (2009). CTD measurements from glider Bellamite, RAPID 2008, National Oceanography Centre Southampton (Internal Report June 2009).

Merckelbach, L.M., Briggs, R.D., Smeed, D.A. and Griffiths, G. (2008). Current measurements from autonomous underwater gliders. IEEE/OES 9th Working Conference on Current Measurement Technology, Richardson, USA, Institute of Electrical and Electronics Engineers, 61 67.

Meredith, M.P., Woodworth, P.L., Chereskin, T.K., Marshall, D.P., Allison, L.C., Bigg, G.R., Donohue, K., Heywood, K.J., Hughes, C.W., Hibbert, A., Hogg, A.McC., Johnson, H.L., Jullion, L., King, B.A., Leach, H., Lenn, Y.D., Morales Maqueda, M.A., Munday, D.R., Naveira Garabato, A.C., Provost C, Sallée, J.B. and Sprintall, J. (2011). Sustained

monitoring of the Southern Ocean at Drake Passage: Past achievements and future priorities. Rev. Geophys, 49, RG4005.

Mertens, C. and Schott, F. (1998). Interannual variability of deep-water formation in the northwestern Mediterranean, Journal of Physical Oceanography, 28, 1410–1424.

Micheli, F., Halpern, B.S., Walbridge, S., Ciriaco, S., Ferretti, F., Fraschetti, S., Lewison, R., Nykjaer, L., and Rosenberg, A.A. (2013). Cumulative Human Impacts on Mediterranean and Black Sea Marine Ecosystems: Assessing Current Pressures and Opportunities, PLoS ONE 8(12): e79889. doi:10.1371/journal.pone.0079889.

Millot, C., and Taupier-Letage, I. (2005). Circulation in the Mediterranean Sea. Handbook of Environmental Chemistry, Vol. 5, Part K, 29 – 66. Springer-Verlag Berlin Heidelberg. http://dx.doi.org/10.1007/b107143, DOI 10.1007/b107143, ISBN 978-3-540-25018-0

Millot ,C. (1999). Circulation in the Western Mediterranean Sea. J. Mar. Sys. 20, 423 – 442.

Millot, C. (1987). Circulation in the Western Mediterranean. Oceanol. Acta., 10(2), 143-149.

Monserrat, S., López-Jurado, J.L., and Marcos, M. (2008). A mesoscale index to describe the regional circulation around the Balearic Islands. J. Marine Syst., 71, 413 – 420.

Morison, J., Andersen, R., Larson, N., D'Asaro, E., and Boyd, T. (1994). The Correction for thermal-lag effects in Sea-Bird CTD data. Journal of Atmospheric and Oceanic Technology, 11:1151–1164.

Mote, P., Brekke, L., Duffy, P., and Maurer, E. (2011). Guidelines for conducting Climate Scenarios, AGU EOS, Vol. 92, No. 31 p257-258.

Nature 497, 167–168 (09 May 2013). doi:10.1038/497167a.

Nature 509, 270–271 (15 May 2014) doi:10.1038/509270a

Ovchinnikov, L.M. (1966) Circulation in the surface and intermediate layers of the Mediterranean, Oceanology. 6, pp. 48–59.

Pascual A., Buongiorno Nardelli, B., Larnicol G., Emelianov M., and Gomis, D. (2002). A case of an intense anticyclonic eddy in the Balearic Sea (western Mediterranean), Journal of geophysical Research Vol. 107, No. C11, 3183.

Pelland, N.A., Eriksen, C.C., and Lee, C.M. (2013). Subthermocline eddies over the washington continental slope as observed by seagliders, 2003–09. J. Phys. Oceanogr., 43, 2025–2053.

Pinot, J.M., López-Jurado, J.L. and Riera, M. (2002). The CANALES experiment (1996 – 1998). Interannual, seasonal, and mesoscale variability of the circulation in the Balearic Channels. Prog. Oceanogr. 55, 335 – 370.

Pinot, J.M. and Ganachaud, A. (1999). The role of winter intermediate waters in the spring-summer circulation of the Balearic Sea, 1. Hydrography and invese box modelling, J. Geophys. Res., Vol. 104, No. C12, Pages 29,843 – 29,864.

Pinot, J.M., Tintoré, J. and Gomis, D. (1995). Quasi-synoptic variability in the Balearic Sea. Deep-Sea Res. Pt. I, Vol. 41, No. 5/6, pp. 897 – 914.

Pond, S. and Pickard, G. L. (1983). Introduction to dynamical oceanography. *Pergamon Press, Oxford.*

Poulain, P.JM., Menna, M. and Mauri, E. (2012). Surface geostrophic circulation of the Mediterranean Sea derived from drifter and satellite altimeter data, J.Phys.Oceanogr., 42(6), 973J990.

Rahmstorf, S. (2003). "The concept of the thermohaline circulation". Nature 421 (6924): 699.

Reglero, P., Ciannelli, L., Alvarez-Berastegui, D., Balbín, R., López-Jurado, J-L., and Alemany. F. (2012). Geographically and environmentally driven spawning distributions of tuna species in the western Mediterranean Sea, Mar Ecol Prog Ser, Vol. 463: 273–284. doi: 10.3354/meps09800.

Renault, L., Oguz, T., Pascual, A., Vizoso, G., and Tintoré, J. (2012). Surface circulation in the Alboran Sea (western Mediterranean) inferred from remotely sensed data, J. Geophys. Res., 117, C08009.

Rohling, E.J. and Bryden, H.L. (1992). Man-induced salinity and temperature increases in the western Mediterranean deep water. Journal of Geophysical Research, 97, 11191–11198.

Rossi, V., Ser-Giacomi, E., López, C., and Hernández-García, E. (2014). Hydrodynamic provinces and oceanic connectivity from a transport network help designing marine reserves, Geophys. Res. Lett., 41, 2883–2891, doi:10.1002/2014GL059540.

Rubio, A., Barnier, B., Jordá, G., Espino, M., and Marsaleix P. (2009). Origin and dynamics of mesoscale eddies in the Catalan Sea (NW Mediterranean): Insight from a numerical model study, J. Geophys. Res., 114, C06009.

Ruiz, J., Macías, D., Rincón, M.M., Pascual, A., Catalán, I.A., and Navarro, G., (2013). Recruiting at the Edge: Kinetic Energy Inhibits Anchovy Populations in the Western Mediterranean, PLoS ONE 8(2): e55523.

Ruiz, S., Pelegrí, J.L., Emelianov, M., Pascual, A. and Mason E. (2014). Geostrophic and ageostrophic circulation of a shallow anticyclonic eddy off Cape Bojador, J. Geophys. Res. Oceans, 119. doi:10.1002/2013JC009169.

Ruiz, S., Renault, L., Garau, B., and Tintoré J. (2012). Underwater glider observations and modeling of an abrupt mixing event in the upper ocean, Geophys. Res. Lett., 39, L01603.

Ruiz, S., Pascual, A., Garau, B., Pujol, I. and Tintoré, J. (2009). Vertical motion in the upper ocean from glider and altimetry data. Geophys. Res. Lett., L14607. doi:10.1029/2009GL038569

Rudnick, D.L. and Cole, S.T. (2011). On sampling the ocean using underwater gliders. J. Geophys. Res., Vol. 116, C08010.

Rudnick, D.L., Davis, R.E., Eriksen, C.C., Frantatoni, D.M. and Perry, M.J. (2004). Underwater gliders for Ocean Research, Mar. Technol. Soc. J., Vol. 38, 1, 38-59.

Sabatés, A., Olivar, M.P., Salat J., Palomera I. and Alemany F. (2007). Physical and biological processes controlling the distribution of fish larvae in the NW Mediterranean. Progress in Oceanog., Vol. 74, 355–376.

Salat, J., Puig, P., and Latasa M., (2010). Violent storms in the sea: Dense water formation episodes in the NW Mediterranean. Adv. Geosci., 26, 53-59. doi: 10.5194/adgeo-26-53-2010.

Salat, J. and Font, J. (1987). Water mass structure near and offshore the catalan Coast during the winters of 1982 and 1983. Ann. Geophys. (B Terr. Planet. Phys.), Vol. 5, No. 1, 49-54.

Salat, J., (1982). Formation d'eau profonde pres de la cote catalane au sud du 42º N. Croisiere "Caron 82": Premiers resultants. CIESM 28ª plenary assembly, Cannes.

Schaeffer, A., Molcard, A., Forget, P., Fraunié, P., and Garreau, P., (2011). Generation mechanisms for mesoscale eddies in the Gulf of Lion: radar observation and modelling, Ocean Dynamics, 61:1587–1609.

Schröeder, K., Josey, S., Herrmann, M., Grignon, L., Gasparini, G., and Bryden, H.L. (2010). Abrupt warming and salting of the Western Mediterranean Deep Water after 2005: atmospheric forcings and lateral advection, J. Geophys. Res., 60.

Schröeder, K., Ribotti , A., Borghini, M., Sorgente R., Perilli, A., and Gasparini G.P., (2008). An extensive western Mediterranean deep water renewal between 2004 and 2006, Geophysical Research Letters, 35, L1 8605.

Schröeder, K., Gasparini, G.P., Tangherlini, M., and Astraldi, M., (2006). Deep and intermediate water in the western Mediterranean under the influence of the Eastern Mediterranean Transient, Geophysical Research Letters, 33, L21607.

Send, U., Burkill, P., Gruber, N., Johnson, G.C., Körtzinger, A., Koslow, T., O'Dor, R., Rintoul S., Roemmich D., Wijffels S. (2010). "Towards an Integrated Observing System: In Situ Observations" in the Proceedings of OceanObs'09: Sustained Ocean Observations and Information for Society (Vol. 1), OceanObs09.pp.35, ESA Publication WPP-306.

Send, U., Fint, J., Krahmann, G., Millot, C., Rhein, M., and Tintoré, J. (1999). Recent advances in observing the physical oceanography of the western Mediterranean Sea. Prog. Oceanogr., Vol. 44, 37–64, 587, 591.

Send, U., and Marshall, J. (1995). Integral effects of deep convection. J. Phys. Oceanogr., 25, 855-872.

Shchepetkin, A.F. and McWilliams, J.C. (2005). The regional oceanic modelling system (ROMS): a split-explicit, free-surface, topography-following-coordinate oceanic model, Ocean Modelling, 9, 347–304.

Shchepetkin, A.F. and McWilliams, J.C. (2003). A method for computing horizontal pressure-gradient force in an ocean model with a non-aligned vertical coordinate. J. Geophys. Res., 108 (C3), 3090.

Smeed, D.A., McCarthy, G., Cunningham, S.A., Frajka-Williams, E., Rayner, D., Johns, W.E., Meinen, C.S., Baringer, M.O., Moat, B.I., Duchez, A., and Bryden, H.L. (2014). Observed decline of the Atlantic Meridional Overturning Circulation 2004–2012, Ocean Science, 10 (1). 29-38. 10.5194/os-10-29-2014.

Smith, R.O., Bryden, H.L., and Stansfield, K. (2007). Observations of new western Mediterranean deep water formation using ARGO floats 2004–2006, Ocean Science, 4, 133–149.

Sparnocchia, S., Picco, P., Manzella, G.M.R., Ribotti, A., Copello, S., and Brasey, P. (1995). Intermediate water formation in the Ligurian Sea. Oceanol. Acta 12, 151–162.

Sun, D.Z. and Frank, B. (2010). Climate Dynamics: Why Does Climate Vary? Geophys. Monogr. Ser., Vol. 189, viii + 216 pages.

Testor, P., Meyers, G., Pattiaratchi, C., Bachmayer, R., Hayes, D., Pouliquen, S., Petit de la Villeon, L., Carva, T., Ganachaud, A., Gourdeau, L., Mortier, L., Claustre, H., Taillandier, V., Lherminier, P., Terre, T., Visbeck, M., Karstensen, J., Krahmann, G., Alvarez, A., Rixen, M., Poulain, P.M., Osterhus, S., Tintoré, J., Ruiz, S., Garau, B., Smeed, D., Griffiths, G., Merckelbach, L., Sherwin, T., Schmid, C., Barth, J.A., Schofield, O., Glenn, S., Kohut, J., Perry, M.J., Eriksen, C., Send, U., Davis, R., Rudnick, D., Sherman, J., Jones, C., Webb, D., Lee, C., Owens B. (2010). Gliders as a Component of Future Observing Systems In: Proceedings of the "OceanObs'09: Sustained Ocean Observations and Information for

Society". Hall, J., Harrison, D.E. and Stammer, D. (eds); ESA Publication, 2. OceanObs'09, Venice, Italy.

Testor, P. and Gascard, J. (2008). Post-convection spreading phase in the Northwestern Mediterranean Sea. Deep Sea Res., 53, 869-893.

Testor, P. and Gascard, J. (2003). Large-Scale Spreading of Deep Waters in the Western Mediterranean Sea by Submesoscale Coherent Eddies, Am. Met. Soc., Vol 33, 75-87.

Theocharis A., Klein, B., Nittis K., and Roether W. (2002). Evolution and status of the Eastern Mediterranean Transient (1997–1999), Journal of Marine Systems, 33–34, 91– 116.

Theocharis, A., Georgopoulos, D., Karagevrekis, P., Iona, A., Perivoliotis, L., and Charalambidis, N. (1992). Aegean influence in the deep layers of the eastern Ionian Sea, Rapp.Com. International Mer Mediterr. 33, 235.

Tintoré, J., Vizoso, G., Casas, B., Ruiz, S., Heslop, E., Renault, L., Oguz, T., Garau, B., Pascual, A., Martínez-Ledesma, M., Gómez-Pujol, L., Álvarez-Ellacuría, A., Orfila, A., Alemany, F., Álvarez-Berastegui, D., Reglero, P., Massuti, E., Vélez-Belchí, P., Ruiz, J., Gómez, M., Álvarez, E., Manriquez M. (2012). SOCIB the impact of new marine infrastructures in understanding and forecasting the Mediterranean Sea. pp 99-118. In CIESM: Designing Med-SHIPS: a Program for repeated oceanographic surveys. N. 43 CIESM Workshops Monographs (F. Briand Ed.), 164 pages, Monaco.

Todd, R.E., Rudnick, D.L., Mazloff, M.R., Davis, R.E., and Cornuelle, B.D. (2011). Poleward flows in the southern California Current System: Glider observations and numerical simulation. J. Geophys. Res., Vol. 116, C02026.

Ulses, C., Estournel, C., Puig, P., Durrieu de Madron, X., and Marsaleix P. (2008). Dense shelf water cascading in the northwestern Mediterranean during the cold winter 2005: Quantification of the export through the Gulf of Lion and the Catalan margin, Geophys. Res. Lett., 35, L07610.

Vargas-Yáñez M., Zunino, P., Schröeder, K., López-Jurado, J.L., Plaza, F., Serra, M., Castro, C., García-Martínez, M.C., Moya, F., and Salat, J. (2012). Extreme Western Intermediate Water formation in winter 2010. Journal of Marine Systems, 105-108, 52-59.

Vignudelli., S., Gasparini, G. P., Astraldi, M., and Schiano, M. E. (1999). A possible influence of the North Atlantic Oscillation on the circulation of the Western Mediterranean Sea, Geophys. Res., Lett., Vol 26, No.5, Pages 623-626.

Wunsch C., (1996). The ocean circulation inverse problem, 442 pp., Cambridge Univ. Press, New York.

Wunsch C., (1978). The North Atlantic general circulation west of 50°W determined by inverse methods, Rev. Geophys., 17, 583-620.